University of L'Aquila


PhD thesis in Information and communication technologies - ICT

Cycle XXXIII

# Radio link modelling for co-design of wireless control systems in industrial automation

*Author:* Amal Alrish

*Tutor:* Prof. Fortunato Santucci

*Co-tutor:* Prof. Alessandro D'Innocenzo

2019-2020

# UNIVERSITÀ DEGLI STUDI DELL'AQUILA

**DIPARTIMENTO DI _____ Ingegneria e scienze dell'informazione e matematica _**


Dottorato di Ricerca in _ Information and communication technologies - ICT _

Curriculum _ Systems Engineering, telecommunications and HW/SW platforms__

_XXXIII_ ciclo

Titolo della tesi

__ Radio link modelling for co-design of wireless control systems in industrial automation__

SSD _ING-INF/03 TELECOMUNICAZIONI_


Dottoranda

Amal Alrish

| Coordinatore del corso | Tutor | Co-Tutor |
|---|---|---|
| Prof. Vittorio Cortellessa | Prof. Fortunato Santucci | Prof. Alessandro D'Innocenzo |


A.A. 2019/2020

# Acknowledgments

Finally, three years of PhD finished, and my graduation day is in the horizon after so many struggles. I still can't believe it; it seems like yesterday when I started studying here. These years past in a blink of an eye, I will miss all people I met during this period!

First and foremost, praises and thanks to Allah, the Almighty, for His showers and blessings through my PhD to complete the research successfully.

I want to thank my family for supporting me in my life choices and always believing in me and never gave up. My mission in life is to make you proud, I can't thank you enough for all the love, prayers, caring and sacrifices for educating and preparing me for the future.

I would like to express my gratitude and appreciation for my supervisor professor Fortunato Santucci and my co-tutor professor Alessandro D'Innocenzo whose guidance, support and encouragement have been invaluable throughout this study. Without their precious support it would not be possible to conduct this research.

From the bottom of my heart, I would like to say big thank you for Dr. Claudia Rinaldi and Dr. Yuriy Zacchia Lun for their dedicated support, guidance, understanding and help throughout my project.

A very special gratitude goes out to all the Department faculty colleagues for their help, support and standing my endless questions.

A big thank you goes to the kindest and most caring friends I met during my studies, Shafaq and Anna. You were my companions in the struggles and the crying, forever grateful for your friendships, help and all the laughter and tears shared!

My sincere thanks also go to professor Carlo Fischione, who provided me an opportunity to join his team as intern, and who gave access to the laboratory and research facilities.

I place on record, my sense of gratitude to one and all, who directly or indirectly, have lent their hand in this venture.

I want to dedicate this thesis to all the girls in engineering! Do not give up, if you fall seven times, stand up eight times. Don't let the misogynist and life circumstances bring you down, you all are great and special!

Thank you again!

# Declaration

This thesis has been composed by myself and the presented work is my own one with collaboration of Dr. Yuriy Zacchia Lun from IMT Lucca and Dr. Claudia Rinaldi form the university of L'Aquila and under the guidance of my university supervisors Fortunato Santucci and Alessandro D'Innocenzo. Moreover, Chapter 2 is based on [1]. Chapters 3 and 4 use the framework of [1] and they are applied in [2]. Chapter 5 is the application of the model and includes the results published in [3]. All the aforementioned scientific papers were co-authored with my supervisors.

# Contents

# List of Figures

# List of Tables

# List of Abbreviations

| | |
|---|---|
| **ACKs** | **A**cknowledgments |
| **AM** | **A**dditive **M**anufacturing |
| **AR** | **A**ugmented **R**eality |
| **BDS** | **B**aseband **D**ata **S**ignal |
| **BER** | **B**it **E**rror **R**ate |
| **CCA** | **C**lear **C**hannel **A**ssessment |
| **CSMA/CA** | **C**arrier **S**ense **M**ultiple **A**ccess with **C**ollision **A**voidance |
| **CPSs** | **C**yber-**P**hysical **S**ystems |
| **DT** | **D**igital **T**ransformation |
| **DSSS** | **D**irect **S**equence **S**pread **S**pectrum |
| **ECUs** | **E**lectronic **C**ontrol **U**nits |
| **FSPL** | **F**ree-**S**pace **P**ath **L**oss |
| **IoT** | **I**nternet **o**f **T**hings |
| **LQI** | **L**ink **Q**uality **I**ndicator |
| **LQMs** | **L**ink **Q**uality **M**etrics |
| **MC** | **M**arkov **C**hain |
| **MJLS** | **M**arkov **J**ump **L**inear **S**ystem |
| **NCS** | **N**etworked **C**ontrol **S**ystem |
| **NRZ** | **N**on-**R**eturn-to-**Z**ero |
| **OQPSK** | **O**ffset **Q**uadrature **P**hase **S**hift **K**eying |

| | |
|---|---|
| **PCE** | **P**ower **C**ontrol **E**rror |
| **PER** | **P**acket **E**rror **R**ate |
| **PHY** | **P**hysical **L**ayer |
| **PL** | **P**ath **L**oss |
| **PN** | **P**seudo-random **N**oise |
| **PPDU** | **P**hysical **P**rotocol **D**ata **U**nit |
| **PSD** | **P**ower *S*pectral **D**ensity |
| **RF** | **R**adio **F**requency |
| **Rx** | **R**eceiver |
| **SINR** | **S**ignal-to-**I**nterferernce-plus-**N**oise **R**atio |
| **SoI** | **S**ignal **o**f **I**nterest |
| **TPM** | **T**ransition **P**robability **M**atrix |
| **TSCH** | **T**ime **S**lotted **C**hannel **H**opping |
| **Tx** | **T**ransmitter |
| **URLLC** | **U**ltra-**R**eliable **L**ow **L**atency **C**ommunication |
| **WNCSs** | **W**ireless **N**etworked **C**ontrol **S**ystems |

# Summary

Wireless networked control systems (WNCSs) alter dramatically the interaction between the control systems and the physical processes such as cyber-physical systems (CPSs), and Internet-of-things (IoT). WNCSs are becoming a fundamental infrastructure technology for critical control systems in automotive electrical systems, building management systems, and industrial automation. They bring in some new merits, such as low cost, reduced system wiring, simple system diagnosis and maintenance, and increased system agility. Therefore, they have become an interesting area in the research community. They are systems consisting of physically distributed smart agents, (sensors, actuators and controllers), that can sense the environment, act on it, and communicate with one another through a wireless communication network to achieve a common goal.

In order to cope with the automation-specific needs for quantifiably reliable, timely and efficient communication, the joint tuning of the critical interactive variables like sampling period, message delay, message dropout and network energy consumption is required, especially in the perspective of the fifth generation (5G) ultra-reliable low latency communication (URLLC). Since every radio link of a typical industrial site is affected by harsh propagation (path loss and fading) and interference, this thesis focuses on the modeling of a process that governs the message dropout, while taking into account complex interactions among several critical interactive system variables. In particular, we present a general framework for deriving an accurate radio link model (that is applicable to all data dropping links to and from a remote controller and/or state estimator), and then fix our attention on a link

between the controller and actuator, to show that having a rigorous link model is essential for solving a wireless networked control problem. In order to convey the results to a broad audience, our presentation of the control problem is based on a state feedback, i.e. we make an idealistic assumption that all the system state variables are measured and sent to a controller over an error free link. While WNCSs are becoming increasingly popular in several application domains, they are still used only occasionally in current control loops in the process industry: the lack of analytic methods for quantifying real-time performance in WNCSs has seriously hindered their adoption in industrial automation. That is why nowadays the WNCSs design must explicitly deal with interdependencies between control and communication variables, motivating a cyber-physical co-design approach that integrates wireless networks models and control algorithms.

Thus, we tackle the aforementioned problem by presenting a WNCSs modeling framework that accounts for both a detailed description of the wireless link and control plant characteristics. This provides useful insights onto the challenges of performance analysis and related design approach for WNCSs. As such challenges are well explained by considering wireless industrial control protocols, we focus on the common protocols used for wireless industrial automation, i.e. WirelessHART, ISA-100.11a, IEEE 802.15.4e. Therefore, the main contribution of this thesis is the following:

- Building the framework of our accurate analytic model of the communication link used in industrial control applications that accounts for the channel imperfections. Therefore, this model considers both channel and control dynamics. The proposed analytic model is derived by taking into account multiple interferers and physical phenomena characterizing a communication link.

- Addressing the modeling and design challenges by focusing on WirelessHART radio link affected by path loss, shadowing, power residual control and persistent interference.

- Working on the derivation of SINR according to IEEE 802.15.4 PHY layer standard using a symbol-level matching followed by decoding and considering the characteristics of the Pseudo-Noise (PN) sequences, which can be summa-

rized by the Hamming distances between them.

- Introducing link quality metrics (LQMs) representing a powerful tool that is capable to easily evaluate and validate finite-state channel models to be used in the WNCSs applications. Moreover, in order to adequately characterize the channel model proposed so far in terms of LQMs, the probability of packet errors is derived.

- Applying our model and test its applicability on an inverted pendulum on a cart. We show on a case study that our model allows us to improve the stability and thus the overall control performance of a closed loop system.

- Extending the application to other protocols such as ISA-100.11a and IEEE 802.15.4e and presenting a detailed parametric study of the wireless communication model under the influence of a persistent interferer as a function of various parameters.

# Abstract

Wireless networked control systems (WNCSs) are receiving ever growing attention from both researchers and practitioners thanks to the introduction and wide spreading of the concepts of the IoT (Internet of things) and 5G (fifth generation of cellular mobile communications). The main advantage of WNCSs is given by the full exploitation of a wireless communication for sensors, actuators, and control data, thus eliminating the cost and time-consuming problems arising by cabled connections implementation. This aspect clearly represents an enabling technology for industrial automation in the context of Industry 4.0, that can exploit the benefits offered by a WNCS such as ease of maintenance and installation, low costs, large flexibility, and possible enhancement of safety. On the other hand, WNCSs for industrial automation face unique challenges. Indeed, data exchange exploits a medium characterized by dynamically changing conditions due to interference, and time varying fading. This deficiency makes it challenging for WNCSs to meet the stringent reliable and low latency constraints of industrial control applications especially in the case of multi-hop communication over mesh networks. The design of WNCSs is a challenging task since it must consider these imperfections by integrating wireless networks models and control algorithms thus implementing the cyberphysical co-design approach. Moreover, in order to cope with the automation-specific needs for quantifiable reliable, timely and efficient communication, the interdependences between control and communication protocols and systems, must be taken into account to guarantee the joint tuning of the critical interactive variables. Furthermore, the lack of analytic methods for achieving real-time performance in WNCSs hinders

their adoption in control systems. Therefore, this thesis aims at filling this gap by tackling the problem of deriving an accurate analytic communication link model that accounts for the aforementioned imperfections. The thesis addresses the modelling and design challenge by focusing on different wireless standards like IEEE 802.15.4, WirelessHART, ISA-100.11a and IEEE 804.15.4e, which are networking protocol stacks of wide interest for wireless industrial automation. Specifically, since the aforementioned standards share the same physical layer, we first develop and validate a Markov link model that abstracts the wireless standard radio link subject to channel impairments and interference. The link quality metrics introduced in the theoretical framework are validated in order to enable the accurate representation of the average and extreme behaviour of the radio link. By adopting these metrics, it is straightforward to handle a consistent finite-state abstraction. Based on such a model, we then derive a stationary Markov jump linear system model that captures the dynamics of a control loop closed over the radio link. Subsequently, we show that our modelling framework allows to discover and manage the challenging subtleties arising from bursty behaviour. A relevant theoretical outcome consists in designing a controller that guarantees stability and improves control performance of the closed-loop system, where other approaches based on a simplified channel model fail. An extensive parametric analysis has been done on the model with the variation of different parameters.

Chapter 1

# Introduction

This chapter presents an overall description of the thesis and introduces its aims and objectives. The main topic of this thesis lies within the domain of wireless networked control systems (WNCSs) as an enabling technology for Industry 4.0. WNCSs are control systems wherein the control loops are closed through a wireless communication network. In particular, critical control systems, for example industrial automation systems, building automation systems and avionics control systems, fundamentally deploy WNCSs as an essential infrastructure technology benefiting from their advantages starting from the reduction of deployment, maintenance costs, possible improvement of safety and large flexibility. Since WNCSs establish the connections between the systems' elements wirelessly, the imperfections of these channels, for example the packet losses and varying transmission delays and sampling intervals, may affect the control performance of these systems which might lead to instability [16]. Therefore, the design of WNCSs is a challenging task since it must handle the inter-dependencies between control and communication variables, which motivates the cyber-physical co-design approach that integrates wireless networks models and control algorithms [17]. The lack of analytical methods for achieving real-time performance in WNCSs hinders their adoption in control systems. [17]. We analyzed several studies, rigorously selected from hundreds of potentially relevant works, and have found that, surprisingly, very few papers consider communication aspects or imperfections, and attempt to provide non-trivial mathematical models of communication protocols. Motivated by this result, we had a deeper look into

the statistical characteristics of the communication channels, and how they are modeled in wireless networked control systems. In the next sections of the introductory chapter, we first present the general domain of our work, i.e., Industry 4, Internet of things (IoT) and WNCSs with their advantages and particular challenges; later on we focus in our work on one flaw of the communication channel which is the packet losses. Then, we present the state of the art of the packet dropouts models in WNCSs literature. Lastly, we state our contribution explicitly and outline the technical part of the thesis.

## 1.1 Industry 4.0

The term "Industry 4.0" refers to that stage in the evolution of the concept of industry, which follows the previous three major phases, known as industrial revolutions. Throughout history, three moments of great change in industrial production have been identified, which called industrial revolutions, due to the large amount of innovation and transformation compared to the technologies used previously. Figure 1.1 shows the transformation history of manufacturing until arriving to the fourth industrial revolution.

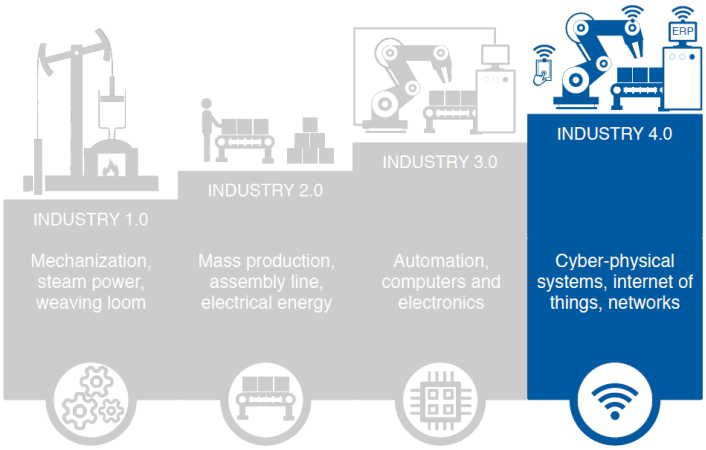


Figure 1.1: The industrial revolution history

In the early 70s, in the most developed west countries, information technology and electronics changed the factories: automation and mechanization entered all stages of industrial production in a widespread manner, generating further effi-

ciency. From 2011 to today we talk about the fourth industrial revolution: we use the term Industry 4.0 to describe all new technologies adopted by new smart factories [18]. The general context of Industry 4.0 is implemented in factories through what is called "Digital Transformation" (DT) [4]. One of the major drivers of this transformation is the interest in the customer's wishes and needs: the market demand has changed where it has evolved towards greater customization by combining the benefits of standard production systems with the needs of peculiarities and quantities. Today, the context in which companies operate is characterized by an ever-increasing complexity, which affects the product, the production process, the final customer: the system as a whole. Prices, quantities, and product cycles are increasingly volatile, they are leaner and more flexible structures are needed in order to be able to respond to requests quickly and effectively.

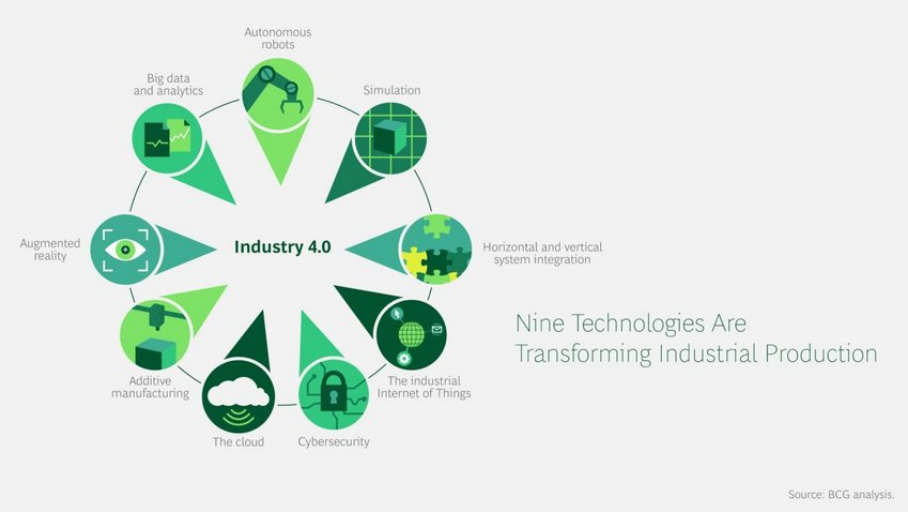


Figure 1.2: Nine enabling technologies of the fourth industrial revolution [4]

It is based on different technologies that are ***de facto*** agglomerated together by mechanical pioneers, essential clients, framework integrators [19]. According to Boston Consulting Group (BCG) the building block of the fourth industrial revolution consist of nine technologies as it is shown in the Figure 1.2. One important technology is Internet of Things (IOT) which is a term that encapsulates trends and technologies that could rewrite the rules of manufacturing and production [20]. In the next section we will have a general idea of its components.

## 1.2 Internet of Things (IoT) and Cyber Physical System (CPS)

IoT is the acronym of Internet of Things which is used to indicate all those objects or devices that are connected to a system via the internet, which receives the enormous amount of information they produce. Its aim is processing and communicating the information again to people or other objects. Therefore, there are four components of IOT [21]:

- Sensors: they are the devices which collect different degrees of complexities data from the surrounding environment.
- Connectivity: the collected data in the sensors are sent through various transport mediums to the cloud. These mediums could be cellular networks, Bluetooth, Wifi, etc.
- Data Processing: when the collected data gets to the cloud, the software performs processing on the obtained data.
- User Interface: the results of the previous processing will be shown, for example, as a triggering alarm or a text message on the user phone.

Consequently, an infinite network of connections between objects is created, which influence and cooperate with each other in order to make both the production process and our simple everyday life easier and easier, since they are products that could be present in everyday life.

In addition, according to [22], Cyber Physical System (CPS) has provided a prominent basis to build advanced industrial systems and applications by integrating innovative functionalities through Internet of Things (IoT) and Web of Things (WoB) to enable connection of the operations of the physical reality with computing and communication infrastructures. They are physical and engineered systems whose operations are monitored, coordinated, controlled, and integrated by a computing and communication core. Figure 1.3 illustrates the core building blocks i.e., three main components, that constitute the CPSs. They are computation, control and communication which need to be able to collaborate to deliver the correct and

expected functionality [23]. Just as the internet transformed how humans interact with one another, cyber-physical systems will transform how we interact with the physical world around us.

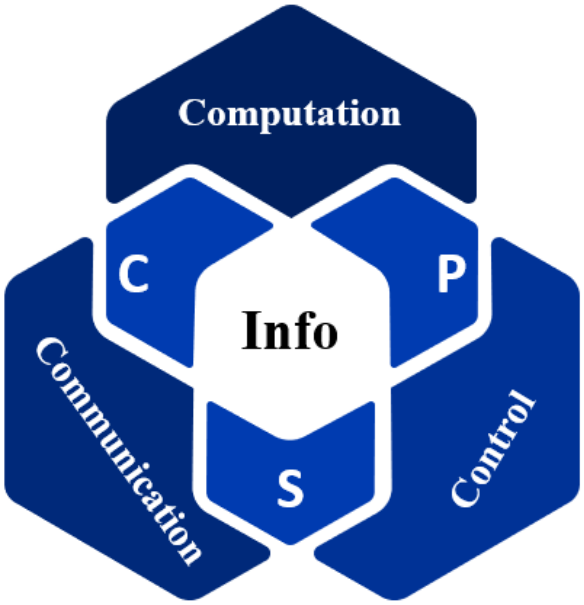


Figure 1.3: Three main components of Cyber Physical Systems CPSs

The theoretical foundation for design and analysis of the dynamical behavior of CPSs is constituted by the Wireless Networked Control Systems (WNCSs). Therefore, WNCSs find ever-growing adoption in industrial automation comprising one enabling part of the fourth industrial revolution Industry 4.0 as we will see in the next section.

## 1.3 WNCS

WNCSs have seen a notable wide spreading in the last decade which is even speeding up with the most recent concepts of Internet of things (IoT) and cyber-physical systems (CPSs). A WNCS, as reported in Figure 1.4, is composed by a Wireless Sensor Network (WSN), that is built on the physical plant, in charge of sensing, sampling, and transmitting data to a control system. The main advantage of WNCSs is given by the full utilization of a wireless communication for sensors, actuators and control data, thus reducing the cost and time-consuming problems arising by

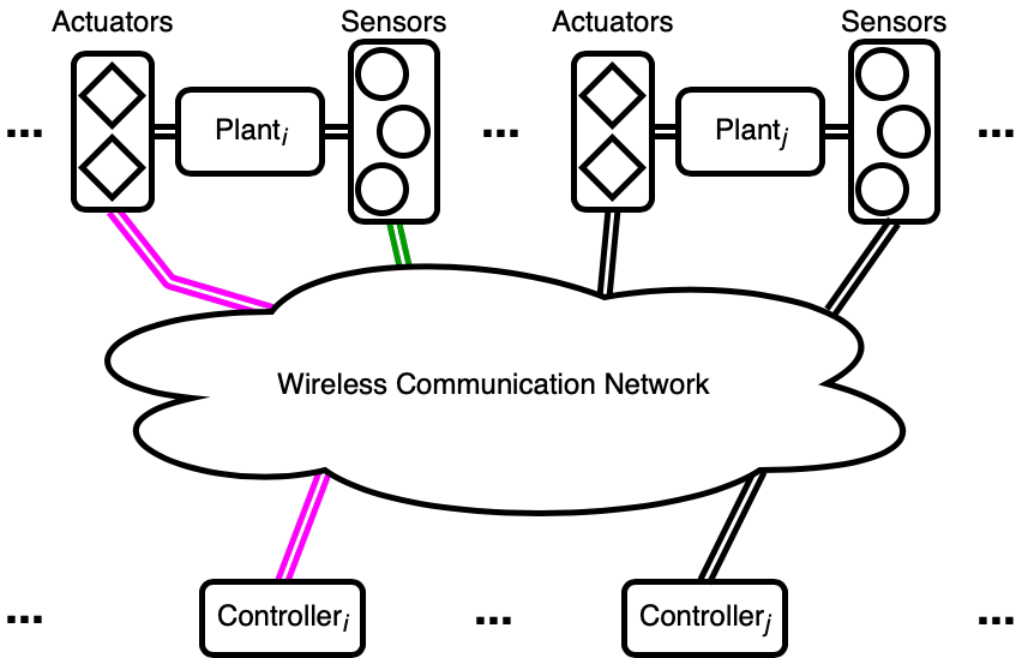


Figure 1.4: Example of a WNCS.

cabled connections implementation. This aspect represents an enabling technology for industrial automation in the context of Industry 4.0 [24], that can exploit the benefits offered by a WNCSs such as ease of maintenance and installation in places where cabling is impossible, low costs, large flexibility, and possible enhancement of safety. On the other hand, WNCSs for industrial automation face unique challenges that should be solved, and we present some of them as follows.

## 1.4 Challenges of WNCSs

Even though WNCSs are becoming a crucial infrastructure technology for critical control systems and various industrial automation systems, due to their several aforementioned advantages, they face different challenges. The main challenge is the joint designing of the communication and control systems taking into account the inter-dependencies between control and communication variables, which motivates the cyber-physical co-design approach that integrates wireless networks models and control algorithms [17]. In particular, in order to cope with the automation-

specific needs for quantifiable reliable, timely and efficient communication, the interdependences between control and communication protocols and systems, have to be considered to guarantee the joint tuning of the critical interactive variables like sampling period, message delay, message dropout and network energy consumption [5], [25], especially in the perspective of the fifth generation (5G) Ultra-Reliable Low Latency Communication (URLLC). This motivates complex cyber-physical coupled design approach. For example, sampling the dynamics of a physical system should be taken in certain time instants. The system's variables are measured at specific rate, which is called the update rate, that has to be proportional to the sampling rate. The smaller the update rate the closer I get to the continuous dynamics of the physical system. However, the wireless industrial standard has limitations on the update rate. For instance, WirelessHART uses Publish data message [9, p. 248] in order to send and receive the control system information, where the update period is $0.1s$. From the wireless standard perspective, the smaller the update rate, the more stringent constraints we have on receiving packets via channels which use WirelessHART standard. Similarly, some control systems need strict requirements which might be infeasible to meet in the communication section. For example, Networked Control Systems (NCSs) [26] impose a strict admissible number of consecutive message dropouts. On the other hand, the imperfections in the wireless system might lead to a larger number of consecutive packet burst. Therefore, the update rate and the maximum allowable number of consecutive dropouts are some of the joint parameters that ought to be set carefully in order to meet both channel and control dynamics requirements.

It is worth saying that increasing the degree of interaction might lead to control performance improvements however at the expense of increasing the design complexity and as a result causing crucial scalability and tractability issues [5]. Thus, a trade-off in the joint design should be taken into account. For instance, applying adaptive sampling period might be beneficial to track fast dynamical systems. On the other hand, it will increase the level of complexity if we have slow dynamical systems. Therefore, it is fundamental to evaluate the degree and cost of the joint design for control and communication systems.

Other technological concerns in WNCSs are the energy efficiency of WNCSs' devices and diversity techniques. In particular, since the battery life time of the

sensors and actuators is limited we might need to shut down the whole system for battery replacement and system maintenance. To cope with this bottleneck, several energy efficient technologies are used like energy harvesting. Using these technologies might impose additional constraints that ought to be taken into account in the joint design approach. In addition, in order to achieve ultra-reliable and low latency communication, different diversity techniques have been used in WNCSs. These techniques force the network designers to formulate again the joint design approach to re-balance the control cost and network lifetime.

As mentioned previously, from the automatic control perspective, the wireless links are intended as the means to convey information among sensors, actuators, and computational units of WNCSs. Data exchange exploits a medium characterized by dynamically changing conditions due to interference, multipath fading and shadowing, [27, 28, 29, 30].

Within this complex background, a convenient element for optimal control algorithms development, would be given by the availability of a channel modeling framework that is flexible enough to adapt to the control application properties (e.g., packet length) that has to be built on it and to the communication protocol that is chosen for the wireless links. This model of the wireless channel needs also to rigorously represent the various imperfections of this kind of communication (i.e., multipath fading, shadowing and interference).

The lack of analytic methods for quantifying real-time performance in WNCSs has seriously hindered their adoption in industrial automation [17], thus they are still used only occasionally in current control loops in the process industry [28]. That is why, as said before, nowadays the WNCSs design must explicitly deal with interdependencies between control and communication variables, motivating a cyber-physical co-design approach that integrates wireless network models and control algorithms [17], [5]. We focus in this thesis on facing this challenge and filling the gap by deriving an accurate analytic model that accounts for different channel phenomena. In the next section, we will address the state of the art of the packet losses models for WNCSs.

## 1.5 Literature review of the state-of-the-art

Fading and interference effects are typically abstracted in terms of frame/packet losses, that are modeled either as stochastic or deterministic phenomena [31]. The deterministic models proposed so far specify packet losses in terms of time averages or worst-case bounds on the number of consecutive dropouts (see e.g. [32]). On the flip side, a vast amount of research considers stochastic models which assume memoryless packet drops, so that dropouts are realizations of a Bernoulli process (see e.g. [33, 34, 35]). More in details, in [33] the basis of a new control theory which takes into account the effect of packet loss on the feedback loop is proposed. Moreover, Linear Quadratic Gaussian (LQG) problem, which seeks to find an optimal control that minimize the packet drops, is analyzed under two classes of protocols which are TCP-like UDP-like protocols. For TCP-like protocols, there is a critical threshold of packet reception probabilities under which the optimal controller cannot achieve stability. In addition, LQG is a linear function of estimate state. On the other hand, for UDP-like protocols the LQG optimal control problem is a much more complex and it is not linear. In [34] an algorithm which achieve the minimum mean square error the estimator can compute is proposed. Packet drops are assumed to be distributed according to Bernoulli distribution. A strategy for each node to update its state to be a linear combination of states of its neighbors is proposed in [35]. Therefore, a procedure to set the linear combinations each node has to apply in order to obtain stability of the plant could be introduced. Links in the networks are modeled as independent Bernoulli process with a certain probability of packet loss.

Pangung et others [5] has done an extensive survey of WNCSs. They have mentioned some references in which packet dropouts are modeled as Bernoulli process [36, 37]. A closed form expression of expected estimator performance as a function of sampling interval, system dynamics, MAC delay and packet loss probability is derived in [36]. Their objective was to minimize the mean square distortion of state estimation in the case of combined delay and packet loss probability. The mean square error is derived under Bernoulli process of packet loss as a function of sampling reception and delay distribution. A scheduling algorithm to improve end to end reliability on MAC layer by increasing the number of packet transmissions

according to the link characteristics is proposed in [37]. In this paper, authors assumed Bernoulli process for successful received packets. However, they did not take into consideration the packet length, rate and the transmitted power.

Bernoulli process is an idealization which facilitate the mathematical tractability. However, it neglects higher order statistics such as variance and autocovariance etc. Therefore, sometimes the abstraction model is too coarse, so it disregards some important dynamics. An intuitive example, consider having Gaussian distributions characterized by the same mean and different variance. All of them can be abstracted by Bernoulli process with probability of successful outcome equals to the mean of the Gaussian distributions. Clearly, this abstraction neglects the dynamics entailed by variance or other higher order statistics.

The works that consider more general (bursty) packet losses use a Transition Probability Matrix (TPM) of a stationary Markov chain (see e.g. the finite-state Markov modeling of multipath-induced fading channels in [38] and references therein) to describe the stochastic process that rules packet dropouts (see [33, 39, 40, 41]). In these works WNCSs with dropped (missing) packets are modeled as time-homogeneous Markov Jump Linear Systems (MJLSs). It is noteworthy that most of the aforementioned works dealing with bursty packet losses (i.e., [39] and the references from [33]) tackle the problem of the stationary continuous state estimation, thus assuming the instantaneous availability of the jump variable. Such an assumption does not hold true for the networked control problem, where the operational modes are observed by controller via Acknowledgments (ACKs). These ACKs are available only after the current decision on the gain to apply has been made and sent through the link, since the actual success of the transmission is not known in advance. The work [40] solves the problem of the optimal linear quadratic regulation of MJLSs with one time-step delayed mode observations, but it does not explore whether the provided solution effectively stabilizes a closed-loop system: this problem was recently solved in [41].

However, the models of packet losses assumed in automatic control literature are not consistently derived according to detailed channel models developed by the communications community and are typically oriented to oversimplify the actual behavior of the wireless link. Moreover, to the best of our knowledge, also the number of Markov channel models that take into account the physical characteristics

of the channel is still limited. As a result, the cyber-physical systems co-design approach is difficult to apply directly in this context.

The work [42] provided a comprehensive overview of the characterization of the wireless channels used in networked control and robotic systems. These wireless channels can be modeled in three dynamics which are path loss, shadow fading and small-scale fading. The survey covers probabilistic models which are the results of analyzing empirical data over years. Nevertheless, it did not consider the interference as a key factor that affects significantly the received signal.

Some works like [43] modeled the unslotted CSMA/CA algorithm used in IEEE 802.15.4 using a new approach called Event Chains Computation (ECC) which is based on the concept that the output of CSMA/CA algorithm can be considered as a chain of occurred events in the network. It reduces the complexity yet with accepted loss of accuracy and reduces the time to derive the performance metrics. However, this method is limited by a certain threshold under which all the probability of the considered chain of events must occur. Other works like [44] has implemented a lab setting which represents a channel emulation of point-to-point link for industrial Wireless Sensor Network (WSN) at the top of 802.15.4 standard. They tested the physical layer imperfection to evaluate the Packet error Rate (PER) and the distribution of Packet Error Burst (PEB) as metrics to evaluate the reliability. Nevertheless, this work depends on an empirical setting and their authors did not provide an explicit formula which describes the channel imperfections. Other works which are based on measurements acquired from an industrial environment are [45] and [46]. The work [45], based on extensive measurements campaigns in three different factory buildings, modeled the fading characteristics according to the movement of the transceivers. In particular, they modeled the fading properties as Rayleigh or close to Rayleigh when the transceivers are mobile whereas when they are at fixed locations they described the fading characteristics by a mixture of gamma, compound gamma log-normal distribution or a combination of them. On the other hand, authors in [46] performed a thorough analysis of noise power estimation techniques in terms of their stability, accuracy and complexity and proposed an algorithm for noise sample separation. Both [45] and [46] lack deriving a descriptive equation which abstract the link behaviour in a harsh industrial environment. Another interesting issue about the error correction in Wireless Network

Sensors (WNS) was proposed in [47]. The authors of [47] proposed a novel strategy to strengthen the physical layer of IEEE 802.15.4 and boost the error correction capability.

The works [48, 49] proposed an analytic model for concurrent transmissions over the wireless network. Authors in [48] derived a closed-form of the receiver bit decision variable for an arbitrary number of colliding signals and constellations of power ratios, time offsets, and carrier phase offsets. They instantiated their model with Minimum Phase Keying (MSK) modulation used for 2.45 GHz PHY layer of IEEE 802.15.4 standard that uses Direct Sequence Spread Spectrum (DSSS) with identical codes for all participants. They validated their model by an experimental study of packet reception under collisions. However, they did not consider the behavior of the code used by the standard which is pseudo noise sequence in the case of IEEE 802.15.4 IEEE 802.15.4 standard 2.45 GHz band [12].

The work [50], on the flip side, took into consideration this behavior by presenting an analytic model for the impact of concurrent transmission on the performance in terms of chips, symbol, and packet error probability of IEEE 802.15.4 systems. The authors of [50] analyzed mathematically the effect of the interferer on packet reception and obtain curves used to get physical models for network simulators. However, they assumed the existence of strong transmitted power or choosing the optimum link from transmitter to receiver. Using such assumptions would make the interference the dominant phenomenon in the environment. Therefore, on one hand, they neglect the noise to obtain these models. On the other hand, they consider its effect to validate the model by comparing it with experimental results. Nevertheless, they did not consider explicitly the effect of the physical imperfections like path loss, shadow fading and small-scale fading. Moreover, they did not take into account the interference signal which arrives at the receiver before the signal of the interest. In other words, they just assumed the case when the interferer signal arrives at the receiver after the SoI with a certain delay.

The works [51, 52] filled partially the previous gap by deriving an analytic model of chip, bit, symbol and packet error probability in IEEE802.15.4 networks under the influence of AWGN, multipath fading and co-channel interference between two hidden nodes. They validated their results using Mote Carlo simulation on the physical layer and empirical measurements. However, they did not derive explicitly

the expression of the signal to interference plus noise ratio which describes the rate of information transfer in network. Moreover, the effect of each imperfection of the channel, which are AWGN, multipath fading, interference and dispreading of the code, on the packet error rate is separately considered i.e., they did not provide one expression of the packet error probability which takes into account the aforementioned phenomena . Furthermore, this work lacked a better approach to a real channel. This approach can better characterize the channel by representing the combination of the phenomena which affect the transmitted signal during its way towards the receiver.

We fill this gap by providing an accurate and analytic model for industrial control that accounts for all physical phenomena. This model will be based on Markovian chains which describe in an efficient way the characteristics of the system and therefore they can be solved by mathematical methods. Consequently, our model would better represent the channel statistics improving the performance of the overall system.

In order to provide a first modeling framework, this thesis focuses on short range communication protocols previously presented and in particular on the first two layers of the protocol stack. For this reason appendix B reports the main functionalities and parameters that characterize each communication protocol under analysis, showing that there are plenty of commonalities to be represented by the same model due to the previously described motivations on the development of such standards moving from the common PHY offered by IEEE 802.15.4 (see Table 1.1, where CSMA/CA stands for Carrier Sense Multiple Access with Collision Avoidance, DSSS stands for Direct Sequence Spread Spectrum, and TSCH stands for Time Slotted Channel Hopping).

Thus, we tackle the aforementioned problem by presenting a WNCSs modeling framework that accounts for both a detailed description of the wireless link and control plant characteristics, i.e. the modeling of a process that governs the message dropout, while taking into account complex interactions among several critical interactive system variables from [5], as represented in Fig. 1.5. This provides useful insights onto the challenges of performance analysis and related design approach for WNCSs.

As such challenges are well explained by considering wireless industrial control

Table 1.1: Comparison of wireless standards, from [5].

| | Physical Layer | Medium Access Control |
|---|---|---|
| IEEE 802.15.4 | DSSS | CSMA/CA |
| WirelessHART | IEEE 802.15.4 PHY | IEEE 802.15.4 MAC |
| ISA-100.11a | IEEE 802.15.4 PHY | IEEE 802.15.4 MAC |
| IEEE 802.15.4e | IEEE 802.15.4 PHY | TSCH, LLDN, DSME |

protocols, we focus on the common properties of the PHY and MAC layers of the mostly used protocols for wireless industrial automation, i.e. WirelessHART [53, 9], ISA-100.11a [10], IEEE 802.15.4e [54].

On the other hand, the availability of detailed and rigorous model of the wireless channel is a desired property for the control community, as long as its abstraction is flexible enough to adapt to the communication protocol.

A first desired property of the abstraction of wireless channel is its flexibility in representing, by changing few parameters, both short range and long range communication protocols. In the particular tackled context of industrial automation, the most frequently adopted communication protocols that are currently allowing the spreading of the Industry 4.0 paradigm, are WirelessHART [53, 9], ISA-100.11a [10], IEEE 802.15.4e [54] for short range communication and 802.11 ah [55], NB-IoT [56], LTE-M [57], Sigfox [58] and LORA [59] for medium and long range communication. Table 1.2 shows different types of communications.

WirelessHART was born as an extension of the widely used HART communication protocol and it is considered to be the first open standard for WSNs specific targeted for industrial automation, [60]. It adopts the IEEE 802.15.4 at 2.4 GHz physical layer, while adding its own Data-Link (DLL), Network (NL) and Application Layer (AL). It is based on a centrally managed mesh network and TDMA communication with a fixed slot size (10 ms) is used for energy saving of sensors. Other functionalities include channel blacklisting and channel hopping that are provided as means for interference and channel impairments reduction.

ISA-100.11a is the major competitor of WirelessHART and many similar features exist between the two communication standards, [61]. Indeed, ISA-100.11a is based on the IEEE 802.15.4 physical layer and its MAC layer assumes TDMA communica-

Table 1.2: Some communication protocols used for industrial control applications.

| Type of communication protocols | Type of Spectrum | Some examples of these protocols | | |
|---|---|---|---|---|
| Protocols for short range communication | Licensed | WirelessHART | ISA-100.11a | 802.15.4e |
| | | [53, 9] | [10] | [54] |
| Protocols for medium and long range communication | Licensed | 802.11 ah | NB-IoT | LTE-M |
| | | [55] | [56] | [57] |
| | Unlicensed | LORA | Sigfox | |
| | | [59] | [58] | |

tion but with a configurable slot size on a superframe base. Channel blacklisting and three options for channel hopping are also described. On the other hand, it does not provide for backward compatibility with other industrial standards, focusing instead on improving flexibility and adaptability.

IEEE 802.15.4e is the last released standard, in 2012, for industrial applications and it was conceived for addressing the emerging needs of embedded (industrial) applications that the IEEE 802.15.4 was not able to satisfy, [15]. IEEE 802.15.4e could be considered as an extension of IEEE 802.15.4-2006, it thus preserves backward compatibility since all the extensions are marked by the bits/bytes that were defined as reserved in 2006 version. In particular, within the three major MAC modes defined, the one known as Time Slotted Channel Hopping (TSCH) basically comprises all the main features of WirelessHART DLL, thus for instance TDMA with a fixed time slot length of 10 ms.

Various works have been done in recent years for short range industrial protocols comparison, both theoretical and experimental one. In [8], analogies and differences between WirelessHART and ISA-100.11a are analyzed in detail. The author pointed out that the most significant difference is given by the application layer that is HART-based for WirelessHART, while ISA-100.11a only allows for, but does not define, application protocols for flexibility purposes. This is particularly meaningful in the focus of the current thesis because it requires special attention while looking for a common model representing various communication protocols. Authors in [62] present a comparison between WirelessHART and IEEE 802.15.4e, underling that the latter has been explicitly developed for including functionalities of the older WirelessHART. It is worth noting that IEEEE 802.15.4e was released in 2012, while WirelessHART is only compliant to IEEE 802.15.4-2006 (even if it is built on the

top of IEEE 802.15.4-2003). The relevant difference is that IEEE 802.15.4e defines various MAC layers, where the TSCH replicates WirelessHART main functionalities, but it leaves undefined the upper layers, thus it is missing the main element of WirelessHART that is: the network manager.

On the other hand, as previously stated, medium and long range communication for M2M communication can be achieved through licensed spectrum protocols, for example,( 802.11ah, NB-IoT, and LTE-M ) and unlicensed spectrum protocols like LoRa and Sigfox as it is shown in Table 1.2. The former standard defines PHY and DLL layers: it is an amendment to the IEEE 802.11 family, where the communication range has been extended from the typical few tens of meters of traditional WiFi to a few hundred meters. The main advantage is given by the exploitation of frequencies below 1GHz (sub 1 GHz WLAN) in order to reduce the significant interference at 2.4 GHz. Use cases scenarios include smart grid, smart farming and surveillance are shown in ([63] Tables 4 and 5). LoRa, [59], allows the coverage of hundreds of square kilometers with a single gateway, it allows for the development of Low Power Wide Area Networks (LPWAN) since it is designed to guarantee transmission of small amounts of data over long distances few times per hour, thus offering multi-year battery lifetime for involved devices, [64]. Sigfox [58] share the same aim as LoRa, for what concern the allowance for LPWAN with wider coverage area, lower cost radio modules, smaller amount of data and slower with respect to LoRa. Nevertheless, Sigfox has some key challenges regarding the mobility, deployment, and less link budget going from base station to endpoints than going up (i.e., from endpoints to base stations).

Narrow Band- Internet of things (NB-IoT) has been released by 3GPP ($3^{rd}$ Generation Partnership Project) at the basis of LTE building blocks and higher protocol layer to meet the demanding requirement of extended coverage and ultra-low device complexity [56]. Similarly, LTE-Machine Type Communication (MTC), (LTE-M) depends on the infrastructure of LTE network. However, it is optimized for higher bandwidth and mobile connections, including voice, with respect to NB-IoT. While NB-IoT are designed for low data rate where small delays are fine, LTE-M has higher throughput with lower latency and battery use is optimized accordingly. Both technologies support LPWAN which improves battery life of devices and enhance the connectivity between them.

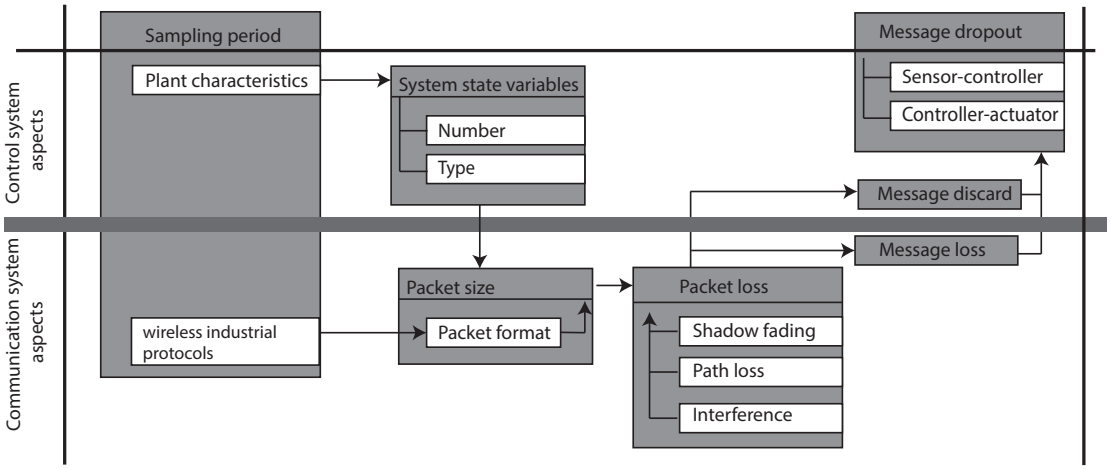


Figure 1.5: Dependencies between critical system variables, [5].

It is worth mentioning that, in the last decade, machine learning has been a key tool to solve a vast amount of engineering complex problems yet in an effective and quick way. In particular, a deep reinforcement learning could solve the scheduling issues and resources allocating [65] and references therein (see e.g., [66, 67, 68, 69, 70] for scheduling problem and [71, 72] for resource allocation). Moreover, in [65] wireless fading conditions are considered. Specifically, authors of [65] leverage actor-critic reinforcement learning algorithms to propose a model-free approach to design allocation and control policies that take into account not only plant states and resource constraints but also fading conditions of the wireless network. The proposed policies depend on the current estimates of the state of control plants and wireless fading conditions. It outperforms other solutions that depends on current estimates by its ability to balance control and communication metrics while distributing resources among the plants. Although the reinforcement learning has many advantages it still needs a lot of computation and loads of data especially in the case of solving complex problems like representing the multidimensional real channel phenomena. In the next section, we will report the research methodology we used in this project.

## 1.6 Research methodology

This research started with a literature review, with the goal of identifying and adopting the general research problem to be addressed. The study included the literature surveying the overall state of WNCS benefits and challenges. At this point, the lack of an accurate analytic model which accounts for various channel phenomena was defined as one of the most prominent challenges and it was adopted as the general research problem to be addressed in this research. Then, a literature review is carried out, stressing the importance of proper communication models in communication and control co-design, and capturing most of the relevant work in the area, both from the control and wireless perspective.

The next step was to define the approach to be taken, i.e. the solution space. The problem of channel modelling can be addressed in several ways, and it was decided to approach the problem on the PHY layer, for two reasons. The first reason is based on the fact that the radio environment is the main compromising factor to communication imperfections, and it makes an immediate impact on the PHY layer. The second reason is related to the concept of layering in communication networks, where lower layers provide services to upper layers in the stack. In that respect, the PHY layer, together with Data link layer (DLL), plays a central role in several important issues in communication networks (e.g. reliability), because no routing or transport-layer protocols can reach their full potential without link-level reliability. Since most of the scientific work in the literature has been focused on the DLL, it was decided to concentrate on the PHY layer deriving the proposed model and planning to build up a more generic one considering the DLL in the future.

After setting the research scope, we build a general framework of an accurate analytic model for an interfered control protocol system. This model accounts for various physical phenomena affecting signal transmission - such as noise, path loss, shadow and multipath fading, and interference. At this point, it was necessary to study related scientific literature of different models of the aforementioned imperfections. The goal of the second literature study was to investigate the existing approaches to various phenomena models and understand the suitable ones for our case. As a result, we set the model for each phenomenon and justify the reason of

choosing it.

Motivated by the notion that challenges in co-design and analysis of WNCSs are best explained by considering wireless industrial control protocols, it was decided to choose WirelessHART protocols as the basis for our proposed model. In particular, an explicit analytic model for the interfererd WirelessHART link is derived. Meanwhile, several research gaps were identified in the related scientific literature, which paved the way for understanding how to fill them and obtain a more precise model.

After deriving the four steps proposed model, we base on some assumptions to obtain a simplified yet realistic version of the model. Moreover, we chose a control plant, which is the inverted pendulum on a cart, to show the importance of our model and examine its relevancy using simulation methods. Furthermore, after generalizing the model to cover other standards and to show the relative importance of the design parameters, an extensive parametric analysis of the wireless link model subject to a persistent interferer was conducted.

The last stage of the research process was the recapitulation of research questions, in order to verify that the research objective has been reached. Finally, the directives for future work were outlined. In the next section, we will present the agenda of the thesis with our contribution in each chapter.

## 1.7 Contributions and Outlines of the thesis

This section gives an outline of the thesis and the major contribution. The focus of this thesis is on

### 1.7.1 Chapter 2: The Proposed Model for an Interfered Control Protocol System

We work on a systematic derivation of an accurate Markov channel model suitable to represent any industrial communication protocol. Our first contribution is to build the framework of our accurate analytic model of the communication link used in industrial control applications that accounts for the channel imperfections. Therefore, this model considers both channel and control dynamics. The proposed analytic model is derived by taking into account multiple interferers and physical

phenomena characterizing a communication link. We report the wireless channel imperfections that might affect the packet loss and the most important models which abstract each one of them. The proposed model consists in four steps. These steps demonstrate explicitly how to derive the aforementioned model.

This chapter is based on the following paper which won the 15th IEEE International WFCS (Workshop on Factory Communication Systems) best work in progress paper award:

- A. Alrish, Y. Zacchia Lun, A. D'Innocenzo, and F. Santucci, "Work in progress: Systematic derivation of accurate analytic Markov channel models for industrial control," in IEEE Int. Workshop Factory Commun. Syst. (WFCS), May 2019, pp. 1-4.

### 1.7.2 Chapter 3: The Scenario and Explicit Analytic Model for the Interfered WirelessHART Link

Since the challenges in analysis and co-design of wireless networked control systems are well highlighted by considering wireless industrial control protocols. In this perspective, our second contribution is to address the modeling and design challenges by focusing on WirelessHART radio link affected by path loss, shadowing, power residual control and persistent interference. As a first step, we follow in this chapter the framework model proposed in chapter 2 by addressing the scenario of the model. Then, the explicit analytic model of SINR is extensively derived. In particular, an important contribution of this thesis is working on the derivation of SINR according to IEEE 802.15.4 PHY layer standard using a symbol-level matching followed by decoding and considering the characteristics of the Pseudo-Noise (PN) sequences, which can be summarized by the Hamming distances between them. This expression will express the received signal subject to the aforementioned imperfections of the link.

### 1.7.3 Chapter 4: The Implicit Analytic and Finite-state Markov Model for the Interfered WirelessHART Link

After having SINR equation, we find a tractable representation of the explicit analytic model of SINR by approximating it using moment matching. An important contribution is introducing link quality metrics (LQMs) representing a powerful tool that is capable to easily evaluate and validate finite-state channel models to be used in the WNCSs applications. In other words, LQMs permit us to assess how good a finite-state representation of the radio link is. In order to adequately characterize the channel model proposed so far in terms of LQMs, the probability of packet errors is derived. We show on a numerical case study how these metrics are essential for an easy discovering of some pitfalls related to both the choice of the method of partitioning of the range of signal-to-interference-plus-noise ratio (SINR) and the computation of transition probabilities between operational modes of the Markov channel. By adopting the LQMs, it is straightforward to derive a finite state abstraction that has the corresponding Markovian LQMs. The derivation of chapter 3 and 4 is used in a journal paper that is going to be submitted soon.

- Y. Zacchia Lun, A. Alrish, C. Rinaldi, A. D'Innocenzo, and F. Santucci, "Accurate radio link modeling and its impact on wireless networked control systems design," 2021, the paper will be submitted soon to IEEE Transactions on Control Systems Technology.

### 1.7.4 Chapter 5: Applying the model

To demonstrate the applicability of our model on different protocols and in different scenarios, we derive a simpler version of our model to apply it on a WNCSs. We choose WirelessHART as a wireless industrial control protocol subject to several imperfections in a harsh environment. Therefore, a further contribution is to apply our model and test its applicability on an inverted pendulum on a cart. We show on a case study that our model allows us to improve the stability and thus the overall control performance of a closed loop system. The results of the case study is published in the following INFOCOM paper

- Y. Zacchia Lun, C. Rinaldi, A. Alrish, A. D'Innocenzo, and F. Santucci, "On the impact of accurate radio link modeling on the performance of WirelessHART control networks," in IEEE INFOCOM 2020 - IEEE Conference on Computer Communications, 2020, pp. 2430-2439.

Moreover, an additional contribution is extending the application to other protocols such as ISA-100.11a and IEEE 802.15.4e and presenting a detailed parametric study of the wireless connection model under the influence of a persistent interferer as a function of various different parameters. A discussion on the proposed model limitations is carried on in this chapter which paved the way to further future work.

### 1.7.5 Chapter 6: Conclusion and Future work

In this chapter, we conclude the main part of the thesis, and we survey the main contributions and results which can be improved or extended further. Our future work will be focusing on a more generic scenario including multiple devices belonging to other networks. Therefore, we will model the presence of devices which interfere a certain link as a binary random process that represents their activity status (ON-OFF). Moreover, we are planning to apply the forward error correction (FEC) which improves the reliability by making the transmitter send redundant data which allows the receiver to recognize just the part of the data that contains no errors. Furthermore, we will analyze the impact of the quantization method used in dividing the range of SINR on the LQMs that are indicators of the channel performance.

### 1.7.6 Appendix A

In appendix A, we present the proofs of the derived equations in chapters 3 and 4. Specifically, we give an extensive proof of Signal-to-interference-and-noise-Ratio (SINR) equation's components. We explain the stochastic analysis of the Hamming distance between the useful signal and the interferer signal at the receiver.

### 1.7.7 Appendix B

We present, in appendix B, an overview of the used industrial standards (WirelessHART, ISA-100.11a, IEEE 802.15.4e). In particular, we go through the most

crucial features of the physical and Data link layers of the aforementioned standards that we employed in our research where we address their parameters used in the numerical cases and an explanation of some special computed parameters. For example, the structure of the protocol data unit (PDU) of each one of them.

Chapter 2

# The Proposed Model for an Interfered Control Protocol System

As mentioned in chapter 1, we are aiming, in our work, at addressing the gap of the lack of analytic models which represent the real channel. In particular, we derive an accurate and analytic model of the communication link used in industrial control applications that accounts for several physical phenomena. Such a model would better represent the channel statistics and help to enhance the overall system performance. In the next section, we will set up the main proposed model we rely on in our project.

We use a bottom-up modeling approach based on analytic description of the radio propagation environment which characterizes the industrial site geometry and degree of motion around communication nodes and determines physical phenomena and range of values for the channel model parameters.

Therefore, the proposed model is a sort of process which consists of four stages. These stages explain how we could derive the model that represents the link with all the imperfections. Figure 2.1 illustrates the block diagram of the process that allows to derive the channel model subject to several physical phenomena due to various neighboring networks. It composed of the following steps/blocks [1].

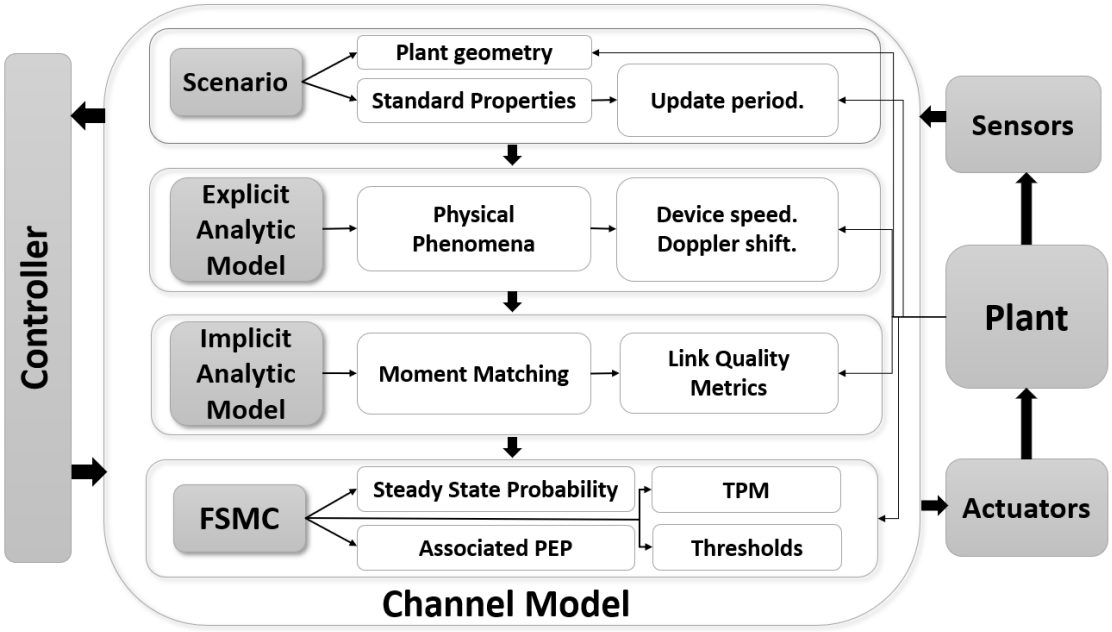


Figure 2.1: The block diagram of the channel model of a WNCS

## 2.1 Scenario

The first step in developing a precise model of the wireless link is done through considering a thorough analysis of the communication scenario [1]. As mentioned previously, the challenges in analysis and co-design of WNCSs are best explained by considering wireless industrial control protocols. WirelessHART and ISA-100.11a standards have been used widely for control and monitoring applications adopted in the previous years [73].

Since most of the physical systems evolve in terms of continuous time but are often governed by discrete controllers, its substantial to transfer to the discrete domain by sampling the dynamics of the system. The samples should be taken at specific time instants. The update rate is how often we may measure the systems variables through sensors and send control commands to actuators. This update rate should be proportional to the sampling rate chosen according to the dynamics of the system. However, each standard has some restrictions on the sampling rate. For example, WirelessHART has limitation on the update rate. WirelessHART uses

Publish data messages [9, p. 268] in order to convey the control system data. Its application layer protocol supports publishing at cyclical process data with update period starting from 0.1 s to 3600 s. Whereas ISA-100.11a support values for the update period from 1/32 ms increments up to 3600 s. It is worth noting that the shorter is the update rate, the more stringent constraints we have on receiving packets via WirelessHART link. Thus, the update rate is a joint parameter that needs to be set carefully in order to meet both channel and control dynamics requirements.

Moreover, a realistic scenario in industrial environment must handle the impact of other networks presence at the same ambient, where multiple transmitters and multiple receivers are taken into account. Therefore, one receiver might or might not have one or more interferers depending on the standard and the application. Thus, in general, an accurate analytic model should account for multiple interferers aside from physical phenomena characterizing a communication channel.

## 2.2 Explicit analytic model

The second step is to derive an explicit equation that represents the transmitted signal subject to different channel imperfections [1]. In our model, transmitted signals are assumed to be affected by noise, path loss, shadow fading, multipath fading, and interference. In the next subsections, we discuss how we could model each phenomenon of them.

### 2.2.1 Noise

Noise is unwanted random undesirable signal which affects the communication channel. Measures are usually taken to reduce it, though it cannot be totally eliminated. It causes different effects for example it limits the operating range of the systems and affects the sensitivity of the receiver, and it can be classified into two types. The first one is the external noise which could be subdivided into three types atmospheric, extraterrestrial, and industrial noises. This type cannot be reduced unless we change the location of the receiver or the whole system. The second type of the noise is the internal noise which may be put into four categories thermal or white, shot, transit time and miscellaneous internal noises. Since this type can be evaluated

mathematically and can be reduced to a great extent by proper designs, we tackle this type. Specifically, the internal noise can be considered as a sum of random process which tend to follow normal distribution according to the central theorem [74]. It could be modeled as Added White Gaussian Noise (AWGN) which follows the Gaussian distribution with zero mean and has noise power spectral density $N_0$. Thus, the signal to noise ratio which represents the ratio between the signal and noise powers $S$, $N$ respectively, can be expressed as

$$SNR == \frac{S}{N} = \frac{B_R . E_b}{N_0 . B_W} \tag{2.1}$$

where $B_R$ is the bit rate, $E_b$ is the energy per bit, and $B_W$ is the channel bandwidth. The ratio $\frac{E_b}{N_0}$ represents the normalized SNR. This ratio is used to evaluate the error rate of various modulation schemes without taking into account the bandwidth. In our work, we use AWGN in order to model the noise which follow Gaussian distribution with zero mean.

### 2.2.2 Path loss (PL)

Path loss is one of the mechanism which cause the attenuation between the transmitter (Tx) and the receiver (Rx) due to the obstacles. We model the PL in order to describe this attenuation between Tx and RX as a function of the distance that separates them and other parameters. Therefore, PL models are used to compute the unwanted reduction of the power of a radio signal as it propagates away from the transmitter. They are mathematical tools used by engineers and researchers to design and optimize the wireless links according to the environment and used standards. For instance, WirelessHART is based on IEEE 802.15.4-2006 standard, as we will see later in 3, which for 2.4 GHz center frequency uses a two segments function with a path loss exponent of 2 for the first 8 m and then a path loss exponent of 3.3 thereafter.

Many path loss models have been addressed in the literature. The models could be generally categorized to three types of models empirical, deterministic, and stochastic models [75]. Empirical models which just rely on the measurements and observations whereas deterministic models are based using electromagnetic laws that govern the propagation channel to estimate the received signal power. No ran-

domness is involved in the development of future states of the deterministic systems. On the other hand, stochastic models have the advantages of demanding the least information and power to produce the estimation. However, they are considered the least accurate out of them. They aim at estimating the probability density function by using series of random variables. Some examples will be mentioned in the following:

#### 2.2.2.1 Free-space path loss (FSPL)

FSPL model is used to predict the strength of a radio-frequency (RF) signal at a particular distance. It is considered a good approximation when the propagation of the RF signal is in the free space and not obstructed by any obstacles or reflectors [76]. However, it is not accurate for general communication environment. We can calculate this path loss in dB by the following equation:

$$FSPL = 20\,log10(d) \;+\; 20\,log_{10}(f) \;+\; 20\,log_{10}(\frac{4\pi}{c}) - G_{Tx} - G_{Rx}, \qquad (2.2)$$

where $d$ is the distance between Rx and Tx in km, $f$ is the frequency of the signal in MHz, $G_{Tx}, G_{Rx}$ is the overall Tx gain including the feeder losses and the overall Rx gain including the feeder losses, respectively in dBi.

#### 2.2.2.2 Ray tracing path loss model

It is a deterministic model used when the transmitter and the receiver are in line of sight (LOS). When there are obstacles between the transmitter and the receiver, the received signal would have two components. The first one is the direct LOS component while the second one is the additional copies of the transmitted signal as a result of the refection, diffraction, or scattering of the main signal. These copies are called the multipath component and could be attenuated in power, delayed in time, and/or shifted in frequency [6]. When it is considered just one reflected path, the model is called two-ray model. Figure 2.2 illustrates this model where $d$ is the distance between the transmitter and the receiver, $G_a, G_b, G_c, G_d$ are transmit and receive antenna field radiation patterns in the LOS direction and Non line of sight (NLOS) direction, respectively. $h_t, h_r$ is the height of the transmitter and the height of the receiver, respectively. The received signal power would be:

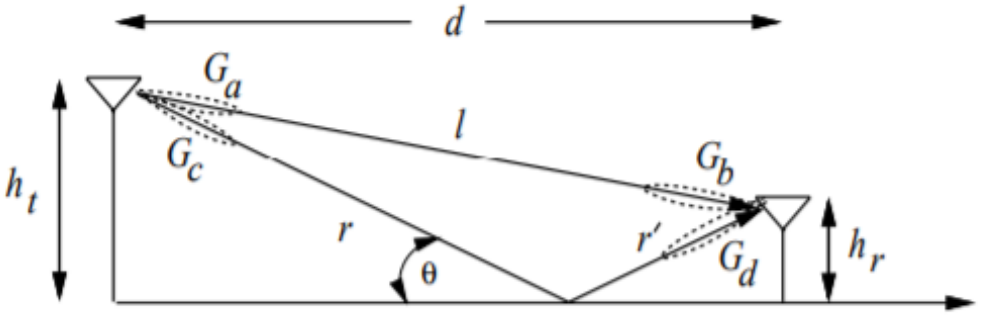


Figure 2.2: Tow ray model [6].

$$P_r(dBm) = P_t\,(dBm) \;+\; 10\,log_{10}(G_l) \;+\; 20\,log_{10}(h_t h_r) \;-\; 40\,log_{10}(d), \tag{2.3}$$

where $P_r, P_t$ are the received signal power and the transmitted signal power respectively. $G_l$ is the product of the transmit and receive antenna field radiation patterns in the LOS direction i.e $G_a\,G_b$. It is worth saying that both Friis free space and two-ray ground reflection model predict the received power as a deterministic function of distance.

#### 2.2.2.3 simplified path loss model

There is always a trade-off between the accuracy and complexity of the considered path loss model. In general, a complex ray tracing PL model or empirical models could accomplish a high accurate PL model representing the channel in the underlying environment. However, wireless communication designers tend commonly to approximate the characteristics of the wireless link and simplify the PL model [6]. Therefore, many of them use the simplified PL model which has the following equation:

$$P_r(dBm) = P_t\,(dBm) \;+ K\,(dB) \;-\; 10\,n\;log_{10}\left(\frac{d}{d_0}\right), \tag{2.4}$$

Such that $d > d_0$, where $d$ is the distance between the transmitter and the receiver, $d_0$ is the reference distance for the far-field antenna, $K$ is a constant which is determined according to the average attenuation of the channel and the antenna characteristics and sometimes is set to free space PL at distance $d_0$, $n$ is the path loss exponent

Table 2.1: Typical path loss exponent, from [6].

| Environment | Range of $n$ |
|---|---|
| Urban macrocells | 3.7-6.5 |
| Urban microcells | 2.7-3.5 |
| Office Building (same floor) | 1.6-3.5 |
| Office Building (multiple floors) | 2-6 |
| Store | 1.8-2.2 |
| Factory | 1.6-3.3 |
| Home | 3 |

which has different values according to the environment [6]. Table 2.1 reports the typical PL exponents for this model.

#### 2.2.2.4 Empirical Models

As mentioned previously, free space, two ray, and simplified PL models are not accurate enough to predict total PL of the signal in a certain environment. On the other hand, Empirical models, which are based on extensive measurements and observations of the received signal with respect to other parameter like the TX-RX distance and the signal frequency, can estimate more accurate models representing the channel. Various experimental PL models are addressed in the literature and some of them will be mentioned in the following:

1. Okumura Model: This model is widely used for [77]

   - large urban areas up to 100 km.
   - a range of frequencies form 150 MHz to 1920 MHz.
   - a range of base station antenna heights $h_{te}$ from 30 m to 1000 m.
   - a range of mobile antenna heights $h_{re}$ up to 3 m.

   Okumura chose a quasi-smooth terrain, fixed the $h_{te}$ to 200 m, $h_{re}$ to 3 m, calculated the free-space propagation loss $L_F$ and its relative median attenuation

$A_{mu}$ as a function of frequency $f$ and distance $d$, by developing a set of curves. Consequently, the median of the path loss $L_{50}(dB)$

$$L_{50}(dB) \;=\; L_F \;+ A_{mu}(f,d) \;-\; G(h_{te}) \;-\; G(h_{re}) \;-\; G_{AREA}, \tag{2.5}$$

where $G(h_{te}), G(h_{re})$ are the base station antenna and mobile height gain factor respectively, and $G_{AREA}$ is the gain associated to the environment type.

2. Hata Model: This model formulates the Okumura model using the same parameters for a range of frequencies (150-1500) MHz in order to obtain a closed form expression without resorting to empirical curves [77]. Consequently, the median of the path loss $L_{50}(dB)$

$$\begin{aligned} L_{50}(dB) \;=\; 69.55 \;+\; 26.16\, log_{10}(fc) \;-\; 13.82\, log_{10}(h_{te}) \\ -\; a(h_{re}) + (44.9 \;-\; 6.55\, log_{10}(h_{te}))\, log_{10}(d), \end{aligned} \tag{2.6}$$

$a(h_{re})$ is a sort of correction factor for the effective height of the mobile antenna which varies according to the underlying environment [77].

3. COST231 Extension to Hata Model: This model is widely used for the prediction of the PL in mobile communication networks. It is an extension of Hata model to 2 GHz developed by European cooperative for scientific and technical research (EUROCOST). The main equation of this model is expressed as:

$$\begin{aligned} L_{50,urban}(dB) \;=\; 46.3 \;+\; 33.9\, log_{10}(f_c) \;-\; 13.82\, log_{10}(h_t) \\ -\; a(hr) \;+\; (44.9 \;-\; 6.55\, log_{10}(h_t))\, log_{10}(d) \;+\; CM, \end{aligned} \tag{2.7}$$

where $a(h_{re})$ has the same value as in equation 2.6, $CM = 0\,dB$ for suburban or open environment, and $3\,dB$ in urban environments.

In our scenario the path loss, $\varsigma$, is modeled as in the standard [12, p. 274] for 2.4 GHz by two segments equations which we will address later.

$$\varsigma(d_i) = \begin{cases} 40.2 + 20\log_{10}(d_i) & \text{if } d \leq 8\ , \\ 58.3 + 33\log_{10}(\frac{d_i}{8}) & \text{otherwise,} \end{cases} \tag{2.8}$$

where $d_i$ is the distance between the transmitter (Tx) $i$ and the reference receiver (Rx).

### 2.2.3 Shadow fading

Shadowing feature is a significant portion of wireless communication; therefore it is important to incorporate this feature in our geometric stochastic model. It accounts for the variation in the local mean power at a given distance due to blockage from obstacles on the propagation path between the transmitter and the receiver. It depends on the size, number, and the material of these obstacles. Many models have been developed to try and predict this value. Some of these models are site-dependent and require a huge deal of information about the environment near and between the transmitter and receiver. An example of these models is the ray-tracing technique for indoor and outdoor environment which requires a lot of information including for example the positions of the transmitter and the receiver and the materials of which the building are composed etc. Others are more statistically based and try to predict the nature of the propagation loss from some small number of parameters of the radio system and the type of environment in which it is operating [78]. For example the class of slope-intercept models which treat the propagation loss as a combination of deterministic and statistic components. The deterministic component represents the previously mentioned path loss and it is a distance related component which could be written as:

$$L_p(dB) = \alpha + \beta \, log_{10}(d), \tag{2.9}$$

where d is the distance between the transmitter and the receiver and $\alpha, \beta$ are parameters determined from the empirical measurements as follows. First, the multipath effects are averaged out at different locations in the channel by averaging the measurements of the received signal power over several wavelength. Then, the power measurements are plotted as a function of the log of the distance between the receiver and the transmitter. Then, a linear least squares fit is made to the data where its slope determines $\beta$ and its intercept with the transmit power and antenna gains determines $\alpha$. The statistical component is determined by removing the linear least squares fit from the measured data then examining the residuals which follow approximately a Gaussian distribution with a zero mean and a standard deviation of about 8 dB[78]. Moreover, many empirical propagation models indicate that the average received signal power, in outdoor or indoor propagation channels, decreases

logarithmically with distance [79]. Hence, the shadow fading component follows a log-normal distribution.

Therefore, the most common model for random variations due to blockage from objects is log-normal shadowing [80], which has been investigated for indoor environments in [81, 82]. Moreover, under the assumption of constant path loss (PL) the shadow fading is proven to have lognormal distribution in [83]. The authors of [83] presented an additive model as a physical basis of the shadow fading. The shadowing correlation properties can be modeled as in [84]. They are described with correlation standard deviation, the typical decay distance, and the device speed. Therefore, the speed of the movement of the system or some parts of it will affect the channel model. Hence, this speed is considered as a joint parameter that has to be set carefully by WNCSs designers.

On the other hand, some works like [85] models the shadow fading in satellite and terrestrial channels by gamma distribution which facilitate the analytical computation of the average symbol error rate. Moreover, in [86] shadow fading is modeled as a Gaussian random variable with zero mean and a certain standard deviation. It is computed as the difference in dB between the data points obtain from 24 measurements at a certain distance in different frequencies and predicted PL at the that distance.

5G requirements of high reliability and low latency has imposed certain constraints on the model abstracting the channel. In particular, there is a need for novel accurate models which are appropriate to the high spectrum bands used in 5G which could be up to 100 GHz. Therefore, the work [87] and references therein presented an overview of shadow fading models in 5G urban macrocells networks.

Sometimes the shadow fading in indoor environments could be resulted from the reflection of the human body. Hence, the work [88] investigated the shadowed fading in indoor off body communications channels at 5.8 GHz. The authors assumed that the power of the reflected and LOS components is affected by significant variations that follow the gamma distribution.

Since we do not have any experimental settings we tend to use the common log-normal shadowing model which has been proven to describe wireless phenomenon in indoor scenario [78] and the results of the measurements in industrial environment show that the shadow fading conforms to the lognormal distribution [89], [90].

### 2.2.4 Multipath fading

Figure 2.3 shows the difference between path loss, shadow fading and small-scale fading which is independent from the distance between the transmitter and the receiver and occurs on a spatial scales $\lambda/2$.

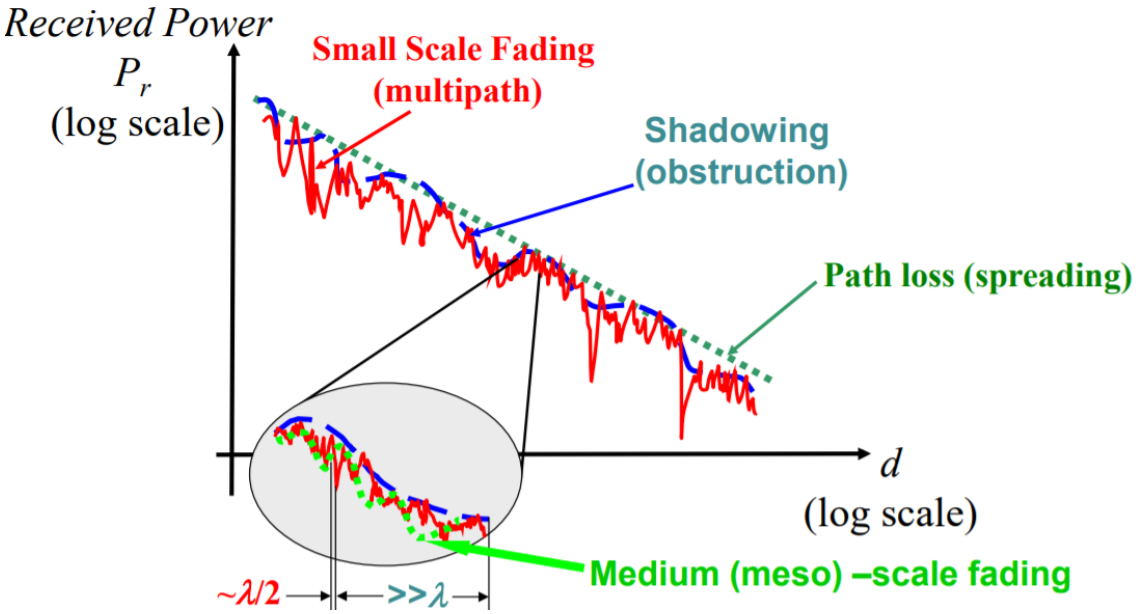


Figure 2.3: The degradation of the received signal because of different phenomena [7].

Multipath fading occurs in any environment where there is a multipath propagation and the paths change for some reason. Multipath fading changes not only the strengths of involved signals but also their phases, as the path lengths change. Therefore, when the system (or any of its parts) is moving, its velocity causes a shift in the frequency of the signal transmitted along each signal path making the so-called Doppler frequency. Thus, the Doppler frequency is also a collaborative parameter that affects both channel and control dynamics. The general wireless channel model must take into account the multipath fading that can be modeled through Rician or Nakagami distribution based on the characteristics of the channel that interconnect the network. In particular, when the signal arrives at the receiver by several paths and at least one of these paths typically a Line of Sight (LOS) or some strong reflection signal is much stronger than the others, the multipath fading

is models as Rician fading [91]. The probability density function (pdf) is given by

$$P_{Ric}(r) = \frac{r}{\sigma^2} + e^{-\frac{r^2+Am^2}{2\,\sigma^2}}\, I_0(\frac{x\,r}{\sigma^2}) \qquad r \geq 0, \tag{2.10}$$

where $r$ is the signal amplitude, $\sigma^2$ is the variance of the in phase and quadrature phase components, $I_0$ is the zero order modified Bessel function of the first kind and $Am$ is the LOS amplitude. Moreover, Rician distribution is often featured by K parameter which represents the ratio between the strength of the LOS path and the strength of other scattered paths and is given by

$$K = \frac{Am^2}{2\,\sigma^2}, \tag{2.11}$$

When K is zero meaning that there is no LOS path between the transmitter and the receiver, we get a special case of Rician which is Rayleigh fading. The received signal will be in this case the sum of the reflected and scattered multipath components and the pdf will be written as follows

$$P_{Ray}(r) = \frac{r}{\sigma^2} + e^{-\frac{r^2}{2\,\sigma^2}} \qquad r \geq 0, \tag{2.12}$$

When K factor is huge, so the only existing component is the LOS and as a result the channel is modeled as a AWGN channel.

Nakagami fading has been found to match up the measurements of signals in several scenarios particularly in indoor ones. The pdf of Nakagami distribution is given by

$$P_{Nak}(r) = \frac{2}{\Gamma(m)} + (\frac{m}{\omega})^2 r^{2m-1}\, e^{\frac{-m}{\omega}r^2} \qquad m > 0.5\ \omega > 0, \tag{2.13}$$

where m is the shape parameter and $\omega$ is the spread parameter. When $m = 1$ and $\omega = 2\sigma^2$ Nakagami fading will be similar to Rayleigh fading and as we increase m we will move away from Rayleigh case to Rician one.

It's worth to remember that multipath fading can be subdivided into two types. The first is based on the multipath delay spread which can be divided into two other types of fading according to the relation between the time of the modulated symbol $T_s$ and the maximum excess time delay $T_{max}$ of the multipath components or the relation between the channel coherent bandwidth $f_0$ and the signal bandwidth $W$. In particular, if the received multipath components exceed the symbol's time

i.e $T_{max} > T_s$ or $f_0 < W$ the fading is called frequency selective fading which causes the Inter-Symbol Interference (ISI). On the other hand, the fading is non-selective (flat) fading if the maximum excess delay time is less than the symbol time i.e., all the received multipath components arrive within the symbol $T_{max} < T_s$ or $f_0 > W$ [91]. For example, if we have WirelessHART as a Wireless Industrial Control Protocol (WICP) used in a certain WNCS which is based on IEEE802.15.4, the symbol duration is $0.5\mu s$. Thus, when the path difference is less than $150m$ the channel exhibits non-selective (flat) fading while if it's greater then the channel induced ISI and the receiver experience selective fading. The second type of dividing multipath fading is based on the doppler spread where it could be divided into two other types according to the relation between channel coherence time $T_{co}$ and the symbol period, $T_s$. If $T_{co} < T_s$ i.e., the change rate of the channel is higher than the symbol period then the channel experience fast fading. Whereas it is slow fading if the $T_{co} > T_s$ meaning that the object inside the scenario is moving slowly [74].

In indoor environment the received signal is composed of much larger number of rays than in outdoor environment. The reason for that is the horizontal rays undergo multiple reflections which bounce off the walls and furniture and the vertical rays could reflect off the ceiling and pavement too. In addition, it is worth saying that the difference between small scale and large-scale fading is not that observable as in the case of outdoor environment. For this reason, Doppler spectrum can be modeled as flat. Moreover, since the velocity of the indoor devices is relatively slow comparing with its velocity in outdoor some models are developed according to the location whether it is shadowed to the transmitter or it is LOS [78]. Hence, log-normal fading could be used, in this scenario, as an accepted model to describe the small scale fading. Furthermore, we underline that in some industrial settings typical for WNCSs applications, multipath fading is not an issue since highly absorbing environments often eliminate multipath propagation [92]. Thus, some channel models may neglect it or they suppose to compensate the multipath fading by the power control when it is available [80].

### 2.2.5 Interference

In industrial applications there is a need of some kind of emergence between different Wireless Industrial Control Protocols (WICPs) like WirelessHART and ISA-100.11a [93]. This leads to the requirements of the coexistence of several wireless networks which operates in proximity in a shared environment. We say that several devices can coexist in one system if one system can achieve their objective in a shared environment whether the other devices belonging to other systems use the same standard or not [94]. Thus, as the useful signal travels along a channel between its source and receiver, it might happen that unwanted signals, whether they are generated by devices using the same communication standard or by coexistence devices (i.e. using different standards), could be added to the useful signal and modify it in a disruptive manner. Therefore, at any given instant, a channel occupied by the signal of interest may or may not be interfered by one or more neighboring devices belonging to other networks. These devices can affect the signal of interest in different levels according to different characteristics regarding, for example, the standard they are following, their output power, their distance from the transmitter etc. To address the case of coexistence devices one might use a CCA (clear channel assessment) mechanism, if available and appropriate. In particular, CCA provides an optional coexistence feature targeting other protocols and modulation standards, but it cannot address the case of users of different neighboring networks based on the same protocol. In such a case, even frequency hopping spread spectrum technique cannot provide immunity to interference (due to a limited number of available channels).

Let's assume that the transmitter uses IEEE 802.15.4 standard. This standard and protocols which are built based on it are used for short range communication as stated in chapter 1. They provide reliable communication for limited power and moderate throughput applications. Their output power is around 0 dB with 50m range. IEEE 802.15.4 devices operate in an open ISM-band. The band 2.4 GHz is used in the whole world which offer the large number of non-overlapping 16 channels. Each of these channels has a large 2 MHz bandwidth which provides 250 kbps and the separation between them is 5 MHz.

If we have, for instance, at the same environment devices belong to other sys-

tems using IEEE 802.11 b/g. This standard provides the basis for wireless networks products which use WiFi brands and uses unlicensed 2.4 GHz as one of the possible operating frequencies. Therefore, it could affect the standard IEEE 802.15.4. However, it uses 14 channels with 22 bandwidth and a separation of 5 MHz between the channels. The output power is around 20 dB operate within 100m range and it is significantly larger than the output power of IEEE 802.15.4. Therefore, IEEE 802.11 b/g networks with their large duty cycle and high output power which operate in the same environment and the same range of IEEE 802.15.4 networks can extremely affect the latter networks especially if they use the same carrier frequency [94]. In contrast, since IEEE 802.15.4 networks have low output power compared to IEEE 802.11 b/g, they have a small impact on the channels of IEEE 802.11 b/g. For a satisfactory IEEE 802.15.4 performance, it is recommended to organize the channel by providing radio gaps between them. For instance, there must be 7 MHz frequency offset from IEEE 802.11 b/g channels [95]. In case of unavoidable overlapping of operation at the same channels it is counseled to separate the IEEE 802.15.4 devices from IEEE 802.11 devices by 8 to 10m.

Bluetooth standard is widely used for exchanging data between devices which are located at short distance using different ISM-band. One of these band is 2.4 GHz in which 79 channels are defined. Each channel has a 1 MHz bandwidth and 1 MHz is the separation between the channels. It uses slow frequency hopping scheme to transmit each packet on one of the 79 channels. It performs 1600 hop per second with adaptive frequency hopping (AFH). The output power varies according to the devices' classes. For example, class 1 has the maximum permitted power 20 dBm while it is 4 dBm for class 2. Bluetooth devices can have some effect on IEEE 802.15.4 devices yet this effect is much less than IEEE 802.11 one. In order to cope with it and achieve a good performance and thus a good Packet Reception Rate (PRR), a separation of 2m can be applied between the devices [94].

Since the microwave ovens leak some of their microwaves which operate at the same frequency as IEEE 802.15.4, it could be a source of an interference [94]. To overcome this impact a separation of 1m is provided.

It is worth mentioning that IEEE 802.15.4 standard gets benefits of some of its characteristics and applies some mechanisms in order to avoid the interference and guarantee a high reliable communication. For instance, using Direct Sequence

Spread Spectrum (DSSS) helps to guarantee a good PRR. Moreover, devices check the channel state before it transmits to send the data on the least affected one. Furthermore, if packets are lost because of different imperfections in the link, IEEE 802.15.4 provides a retransmission mechanism and thus increasing the PRR.

The presence of devices which interfere a certain link can be modeled in different ways. In spread spectrum systems, it is possible to model the interference as an additive value $I_{int}$ to the thermal noise $N_0$. In particular, in order to model the Wireless Local Area Network (WLAN) interferer signal the work [96] modeled it as a band limited AWGN. However, the work [97] modeled the Bluetooth signal as a partial band jammer to Zigbee user.

Interference could also modeled as a binary random process that represents their activity status (ON-OFF). This time-varying behavior is a distinctive characteristic of the channel affected by multiple intermittent interferences. Such behavior can be encompassed, as said previously, by the signal-to-interference-plus noise ratio (SINR), which is the power of a certain signal of interest divided by the sum of the interference power (from all the other interfering signals) and the power of some background noise. Typically, the bit error rate (BER) is a function of SINR, so following the basic characteristics of the underlying protocol (e.g., the frame length, modulation, symbol rate), SINR and PER could be derived as a function of their features. In particular, the PER is always a function of BER which is in turn a function of SINR. The relation between PER and BER depends on whether any forward error correction (FEC) method is implemented in a protocol or not. FEC improves the reliability by making the transmitter send redundant data which allows the receiver to recognize just the part of the data that contains no errors [98]. As a result, the receiver has the ability to detect a limited number of errors that may occur anywhere in the message, and often to correct these errors at the cost of a fixed, higher forward channel bandwidth. In the case of no FEC, even one erroneous bit leads to a corrupted data packet.

## 2.3 Summary

In this chapter, we described the general block diagram of our proposed model and explained the steps of the process in details. We listed the considered phenomena and gave a brief background of the possible models considered in the literature of each one of them. We stated the models considered in this thesis for each imperfection and justified the reason behind that. In the next chapter, we will investigate the first two steps of our model i.e., setting up the scenario and deriving explicitly the analytic model of SINR to obtain a closed-form representation of the signal subject to different possible imperfections in the link.

Chapter 3

# The Scenario and Explicit Analytic Model for the Interfered WirelessHART Link

As mentioned previously in chapter 2, the WNCSs used in industrial automation face many challenges. The main challenge in designing WNCSs according to packets is

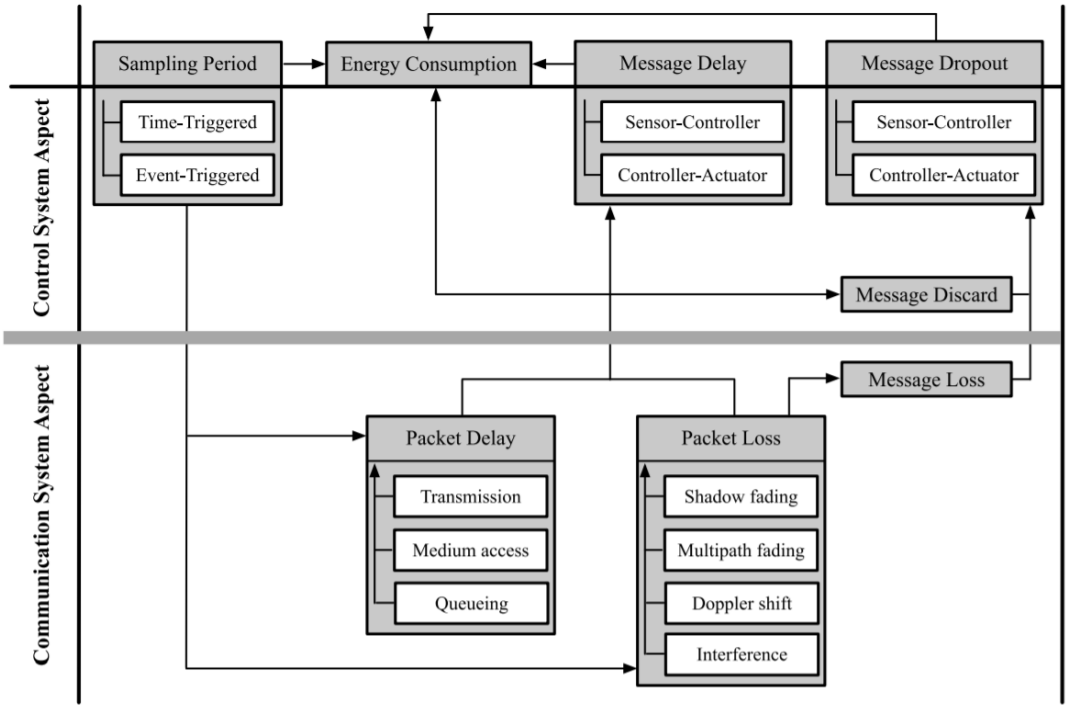


Figure 3.1: Complex interaction between critical system variables [5]

the joint design of communication and control systems. The challenges in co-design and analysis of WNCSs are best explained by considering wireless industrial control protocols. As a first step, we will start with WirelessHART protocol. Figure 3.1 in [5] presents the dependencies between different critical system variables. We focus in our work on time-triggered sampling period and message dropouts caused by shadow fading, interference, path loss and residual power control error and we get Figure 3.2 [3].

The sampling period is determined by the number and type of the system state variables and by the industrial communication standard. In [3] we have started with WirelessHART standard. The WirelessHART network is composed of access points connected to a plant automation host through gateways implemented or connected to a network manager and security manager as it is shown in Figure 3.3. We use a progressive modeling approach described in section 2 which is based on analytic characterization of the channel including analyzing the plant geometry, the degree of motion and the physical phenomena characterizing the channel. WirelessHART standard has some constraints that reduce the degree of freedom of the model. The network supports both stared and mesh network technology. The direct connection to the access points is used by the devices with stringent requirements on latency found in factory automation.

## 3.1 Scenario of the WirelessHART network

The first step in developing our model is to study and analyze the communication scenario. The description of each radio link can be obtained from an extensive measurement campaign in the existing industrial site, or it can be derived analytically by considering the geometry of the (actual or possible) propagation environment, the degree of motion around the communicating nodes and the relevant physical phenomena involved. We follow the latter approach not only because it is not restrained to any particular industrial site, enabling technological feasibility and robustness analyses before committing to time-consuming expensive measurement campaigns, but also because the empirical data obtained from any measurement campaign can be used to calibrate the theoretical model. We consider a scenario

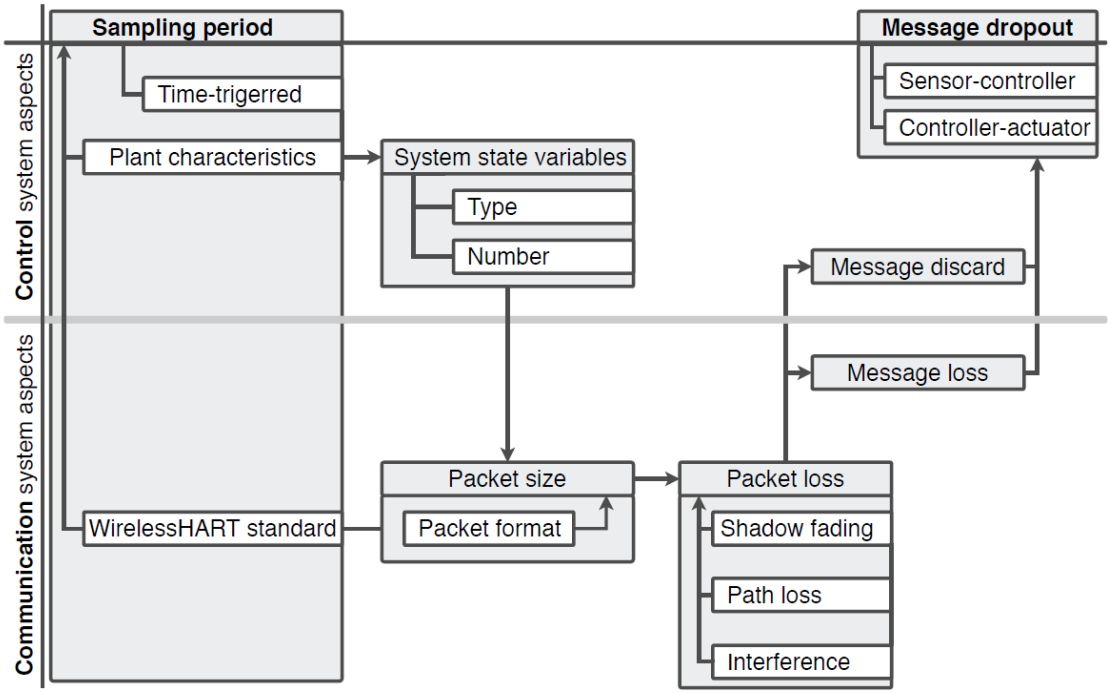


Figure 3.2: Dependencies between critical system variables using WirelessHART standard.

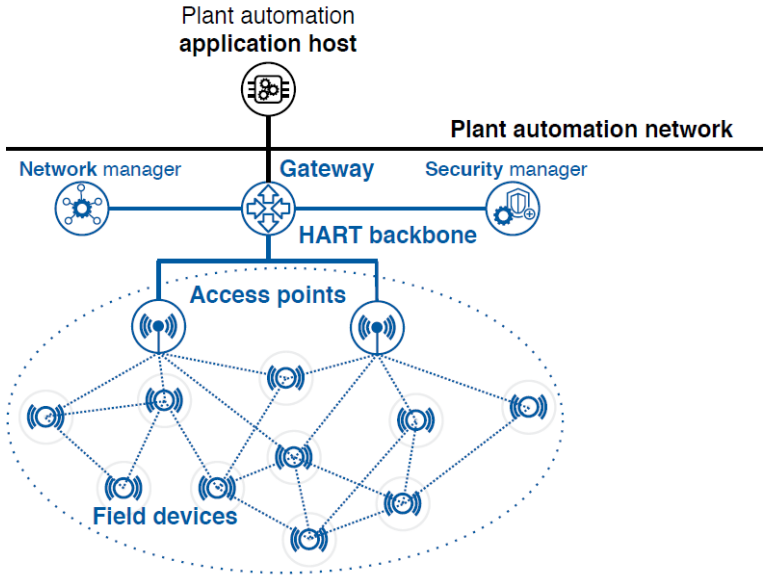


Figure 3.3: The WirelessHART network.

where there are two adjacent wireless networks, and we focus on a single communication link between access point and the device that is interfered by a device from another WirelessHART network. The underlying scenario is illustrated in Figure 3.4. In such a scenario the clear channel assessment (CCA) mode, provided in the

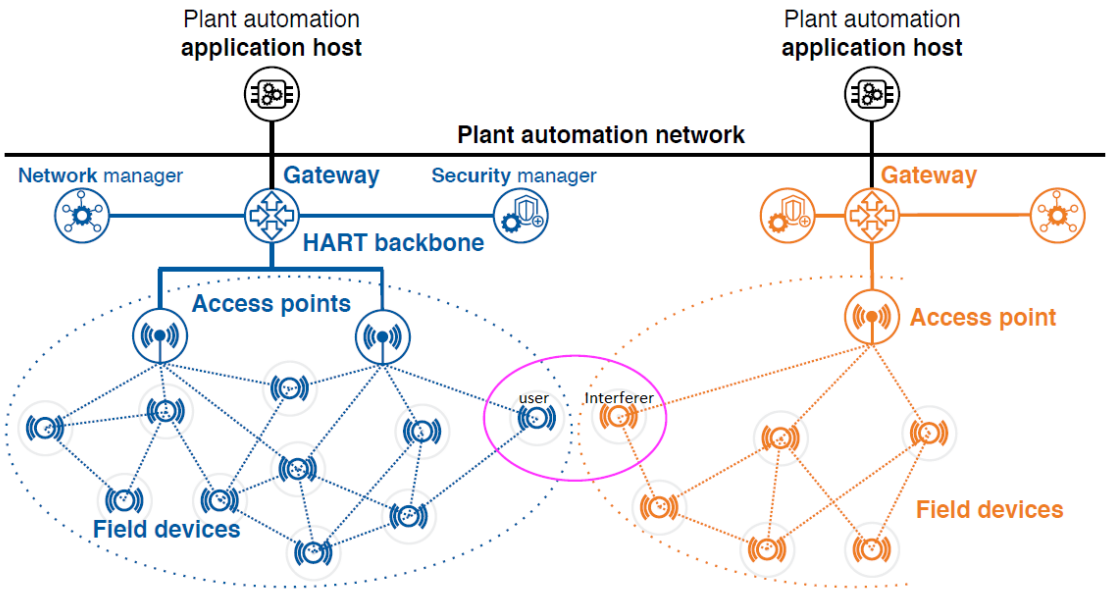


Figure 3.4: The underlying scenario.

standard ([12, p. 66]), will not help since CCA mechanism is an optional co-existence feature targeting protocols and modulation standards different from WirelessHART. Therefore, it cannot address the case of users of different neighboring WirelessHART networks characterized by the same channel hopping sequence (which is the worst possible scenario that also accounts for malicious behaviors such as deliberate jamming) [3].

In our theoretical analysis, we use the bottom-up modeling approach, where we characterize the propagation environment starting from the physical layer (PHY) of the OSI model. We assume that all the transmitted signals $\mathcal{X}(t)$ use the offset quadrature phase-shift keying direct-sequence spread spectrum (OQPSK-DSSS) modulation with half-sine pulse shaping filter [99]. This assumption is required by IEEE 802.15.4 2450 MHz DSSS physical layer, which is common to all the consid-

ered industrial wireless communication standards. The index $i$ represents the source index. $i = 0$ indicates the desired signal or the reference generating the signal of interest (SoI), while $i = 1$ refers to the interference signal. Then the next step of our modeling framework is to derive an explicit equation that represents the transmitted signal subject to the aforesaid channel imperfections and interference.

## 3.2 Explicit Analytic Model of SINR

We discuss in this subsection the system model aiming to derive the analytic expression of SINR as a function of the physical phenomena, model parameters and the design constraints. This expression enables technological feasibility and robustness analysis before committing to time-consuming expensive measurement campaigns. It describes the wide-sense stationary stochastic process.

### 3.2.1 Sender Model

We instantiate our model with the OQPSK modulation applied at the chip level as described in IEEE 802.15.4 standard, being aware that OQPSK with sinusoidal pulse shaping is equivalent to MSK, [100]. We follow the notation of Proakis and Salehi in [100]: the OQPSK modulation with half sine pulse shaping is a two dimensional signal with unit basis functions expressed as

$$\phi_I(t) = \sqrt{\frac{2}{T_c}} \cos(w_c t) \tag{3.1}$$

$$\phi_Q(t) = \sqrt{\frac{2}{T_c}} \sin(w_c t), \tag{3.2}$$

where $w_c/2\pi$ is the carrier frequency. The modulation has as an input a chip sequence $a_{i,\ell,\hat{m}}$, where $\hat{m} \in (0, 1, ....31)$ is the chip index, and $\ell \in (0, 1, n_{s,i} - 1)$ is the position of 16-ary symbol, where $n_{s,i}$ is the number of 16-ary MSK symbols in the relevant PPDU transporting the data message of the $i^{th}$ source. Each symbol $S_{i,\ell}$ is encoded via one of 16 pseudo random noise (PN) sequences which are defined by IEEE 802.15.4 standard. Even-indexed chips are modulated onto the in-phase (I) carrier, while odd-indexed chips are modulated onto quadrature (Q) carrier, NRZ

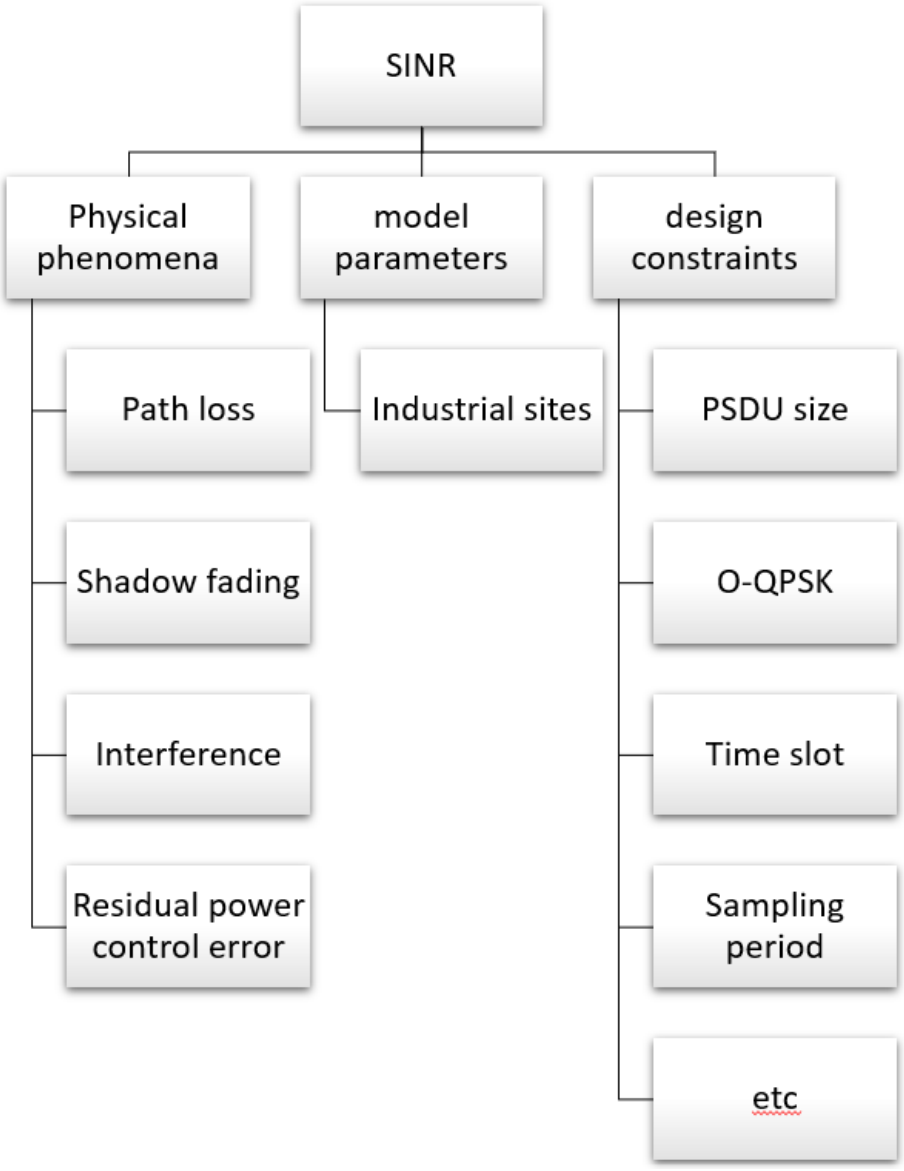


Figure 3.5: Factors that affect SINR function.

encoded chips are given as follows:

$$\hat{b}_{I,i,\ell,m} = 2a_{i,\ell,2m} - 1 \tag{3.3}$$

$$\hat{b}_{Q,i,\ell,m} = 2a_{i,\ell,2m+1} - 1, \tag{3.4}$$

where $m \in (0, 1, ...15)$. We assume that the receiver is fully synchronized to the signal of interest (SoI), i.e., the SoI is received without any time offset and all possible interferers have relative offsets as in [48].

The signal that encodes the data of $\ell^{th}$ symbol of PHY protocol data unit (PPDU) can be written as

$$\mathcal{X}_{0,\ell}(t) = b_{I,0}(t)\, \cos(w_p t)\phi_I(t) - b_{Q,0}(t)\, \sin(w_p t)\, \phi_Q(t), \tag{3.5}$$

where $b_{j,i}(t)$ is the baseband data signal (BDS) on the I-phase (when $j = I$) or quadrature $j = Q$ component of the signal, and $w_p$ is the angular frequency of baseband pulses. If we denote by $n_b$ the PPDU size in bits, by $n_o$ the respective size in octets (bytes), so that

$$n_{s,i} = 2n_o = \frac{n_b}{4}, \tag{3.6}$$

we can express any realization of a chip level BDS as

$$b_{I,i}(t) = \sum\nolimits_{m=0}^{15} \hat{b}_{I,i,l,m}\, h_{T_c}\left(\frac{t\, -\, 2\,(m\, +\, 32l)\, T_c}{2T_c}\right), \tag{3.7}$$

$$b_{Q,i}(t) = \sum\nolimits_{m=0}^{15} \hat{b}_{Q,i,l,m}\, h_{T_c}\left(\frac{t\, -\, (2\,(m\, +\, 32l) + 1)\, T_c}{2T_c}\right), \tag{3.8}$$

where $\hat{b}_{I,i,l,m}, \hat{b}_{Q,i,l,m} \in \pm 1 \,\forall\, i, l, m$ , $T_c$ is the inverse of the chip rate (which is nominally 2.0 Mchip/s), and $h_{T_c}(t)$ is unite pulse described as follows,

$$h_{T_c}(t) = \begin{cases} 1 & \text{if } 0 < t < 1\ , \\ \frac{1}{2} & \text{if } t = 0 \quad \text{or} \quad t = 1, \\ 0 & \text{otherwise,} \end{cases} \tag{3.9}$$

The encoding of the octet 00111100, or 3C in the hexadecimal notation, is illustrated in Figure 3.6 as an example of a chip level BDS obtained from 3.7 and 3.9. The

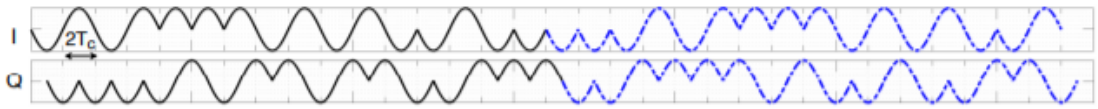


Figure 3.6: Sample baseband chip sequences with half-sine pulse shaping.

signal in solid black line represents symbol C, while the signal in dashed blue line encodes symbol 3 (the least significant bits are encoded and transmitted first). The Q-phase chips are delayed by $T_c$ with respect to I-phase chips.

An asynchronized interferer is characterized by a constant (at least for the duration of PPDU) time offset $\tau_i$, and carrier phase offset $\phi_{c,i}$. Thus, $\forall i > 0$

$$\begin{aligned}\mathcal{X}(t, \tau_i, \phi_{c_i}) = \sqrt{\frac{2}{T_c}}\Big[&b_{I,i}(t-\tau_i)\,\cos(w_p(t-\tau_i))\,\cos(w_c t - \phi_{c_i}) \\ &- b_{Q,i}(t-\tau_i)\,\sin(w_p(t-\tau_i))\,\sin(w_c t - \phi_{c_i})\Big].\end{aligned} \tag{3.10}$$

### 3.2.2 Channel Model

We use the additive collision channel whose output is the input of the receiver. The radio propagation environment that affects the transmitted signals can be described analytically as follows. We assume that all the transmitted signals $\mathcal{X}_i(t)$ are, as it is indicated in chapter 2, affected by path loss, shadow fading, random delays, and residual power fluctuations left by power control. It is worth noting that, although power control is not provided in all the considered standards, this functionality is here modeled for the sake of generality. The effect of multipath fading is supposed to be compensated by the aforementioned power control when available, or it is neglected [80]. This last assumption is also justified by the fact that in industrial setting highly absorbing environments may eliminate multipath propagation [101].

The path loss, $\varsigma$, is modeled as in the standard [12, p. 274] for 2.4 GHz:

$$\varsigma(d_i) = \begin{cases} 40.2 + 20\log_{10}(d_i) & \text{if } d \leq 8\ , \\ 58.3 + 33\log_{10}(\frac{d_i}{8}) & \text{otherwise,} \end{cases} \tag{3.11}$$

where $d_i$ is the distance between the transmitter (Tx) of the signal $\mathcal{X}_i(t)$ and the reference receiver (Rx). The path loss coefficient used in our model is:

$$\alpha_i = 10^{\frac{-\varsigma(d_i)}{10}}, \tag{3.12}$$

The shadowing is expressed by its log-normal model [80], which has been investigated for indoor environments in [81, 82]. According to this model, the shadow fading contribution to the received signal $\mathcal{Y}_i(t)$ is expressed by the term $\beta_i(t)$, that has a normal distribution with zero mean, variance $\sigma^2_{\beta_i}$, and squared exponential correlation function

$$c_{\beta_i}(\tau) = \sigma^2_{\beta_i} e^{-\frac{1}{2}\left(\frac{v_i \tau}{\delta_i}\right)^2}. \tag{3.13}$$

where $\delta_i$ denotes the typical decorrelation decay distance and $v_i$ indicates the field device speed, if it is mobile [102], or the speed of the moving reflectors in the propagation environment. The residual power control error (PCE) is also defined by a log-normal process, so that the related term $e_i(t)$ has a zero-mean normal distribution with variance $\sigma^2_{e_i}$ and autocovariance

$$c_{\xi_i}(\tau) = \sigma^2_{\xi_i} e^{-\frac{1}{2}\left(\frac{\tau}{\tau_{\xi_i}}\right)^2}, \tag{3.14}$$

where $\tau_{\xi_i}$ is the decorrelation time within which the PCE is significant [103], and

$$\sigma_{\xi_i} = \left(\frac{\ln(10)}{10}\right) \sigma_{e_i}, \tag{3.15}$$

Therefore, the signal received by the reference user is then

$$\mathcal{Y}(t) = \sum\nolimits_{i=0}^{1} c_i(t)\, \mathcal{X}_i(t) + \mathcal{W}(t), \tag{3.16}$$

where i = 0, 1 refers to the desired and interference signals as mentioned previously, $\mathcal{W}(t)$ is the additive white Gaussian noise (AWGN) that has a two-sided power spectral density (PSD) $\frac{N_0}{2}$, and $c_i(t)$ is a positive real-valued factor that accounts for the signal amplification $\sqrt{E_{c,i}}$ by the sender, where $E_{c,i}$ is the chip energy of the device, path loss, shadow fading introduced by the channel, and possible residual power fluctuations left by power control. It's worth mentioning that $c_i(t)$ is modeled as correlated random process whose realizations are constant for a duration of a

signal that transports one PPDU. If we denote by $T_s$ the inverse of the symbol rate (which is 62.5 ksymbol/s), then the duration of the signals of interest is $n_s T_s$. Since for the IEEE 802.15.4 2450 MHz DSSS PHY the maximal size of the PPDU is 133 octets, this duration lasts at most 4.256 ms. $c_i(t)$ can be expressed as

$$c_i(t) = \sqrt{E_{c,i}}\ \varsigma_i e^{\frac{\chi_i(t)}{2}} = \hat{c}_{i,t}, \tag{3.17}$$

where $\chi_i(t) = \xi_i(t) + \beta_i(t)$ is the contribution of correlated shadow fading and power control error (PCE) which are constant during the transmission interval and $\hat{c}_{i,t}$ is the value of $c_i(t)$ at the time $t$.

In order to understand the components of $\mathcal{Y}(t)$ let's have one example assuming that $\mathcal{Y}_i(t) = c_i(t)\,\mathcal{X}_i(t)$ and, for the sake of clarity and following the proposed scenario, we assume the existence of one interferer. This interferer starts the transmission at $\tau_1 = -42.66T_c$ seconds before the reference user and the interferer PPDU is two bytes larger i.e $n_{s,1} = n_{s_0} + 4$ as it is illustrated in Figure 3.7.

In the lower part of the figure, we see that at the PPDU (frame) level there is a misalignment of one symbol and at the symbol level there is a misalignment of 5 chips whereas at the chip level there is a misalignment of $\hat{\tau_1} = \frac{2}{3}T_c$. Thus, we can write

$$\tau_1 = \tau_{1,f} + \tau_{1,s} + \hat{\tau_1}, \tag{3.18}$$

where $\tau_{1,f}, \tau_{1,s}, \hat{\tau_1}$ are the misalignments at the frame, symbol, and chip level respectively.

This shows that at the symbol level $S_{0,\ell}$ is affected by two symbols $S_{1,\ell'}$ and $S_{1,\ell'+1}$, while at the chip level, each chip $\hat{b}_{j,0,\ell,m}$ is affected by two chips on I and Q components. From the Figure 3.7 we see that a chip of the SoI may be affected by chips belonging to two symbols. For example, $\hat{b}_{I,0,1,10}$ is received at the same time $\hat{b}_{I,1,2,15}$ and $\hat{b}_{I,1,3,0}$ and as $\hat{b}_{Q,1,2,15}$ and $\hat{b}_{Q,1,3,0}$ as it is depicted in Figure 3.7.

Even assuming that the symbols in the interfering signal are equiprobable, we still need to account for every pair of symbols, all admissible misalignment $\tau_{1,s}$ at the symbol level while taking the chip level time offset $\hat{\tau_1}$ as a parameter. Specifically, under the equiprobable assumption, if the interferer is active for the whole frame PPDU duration we consider:

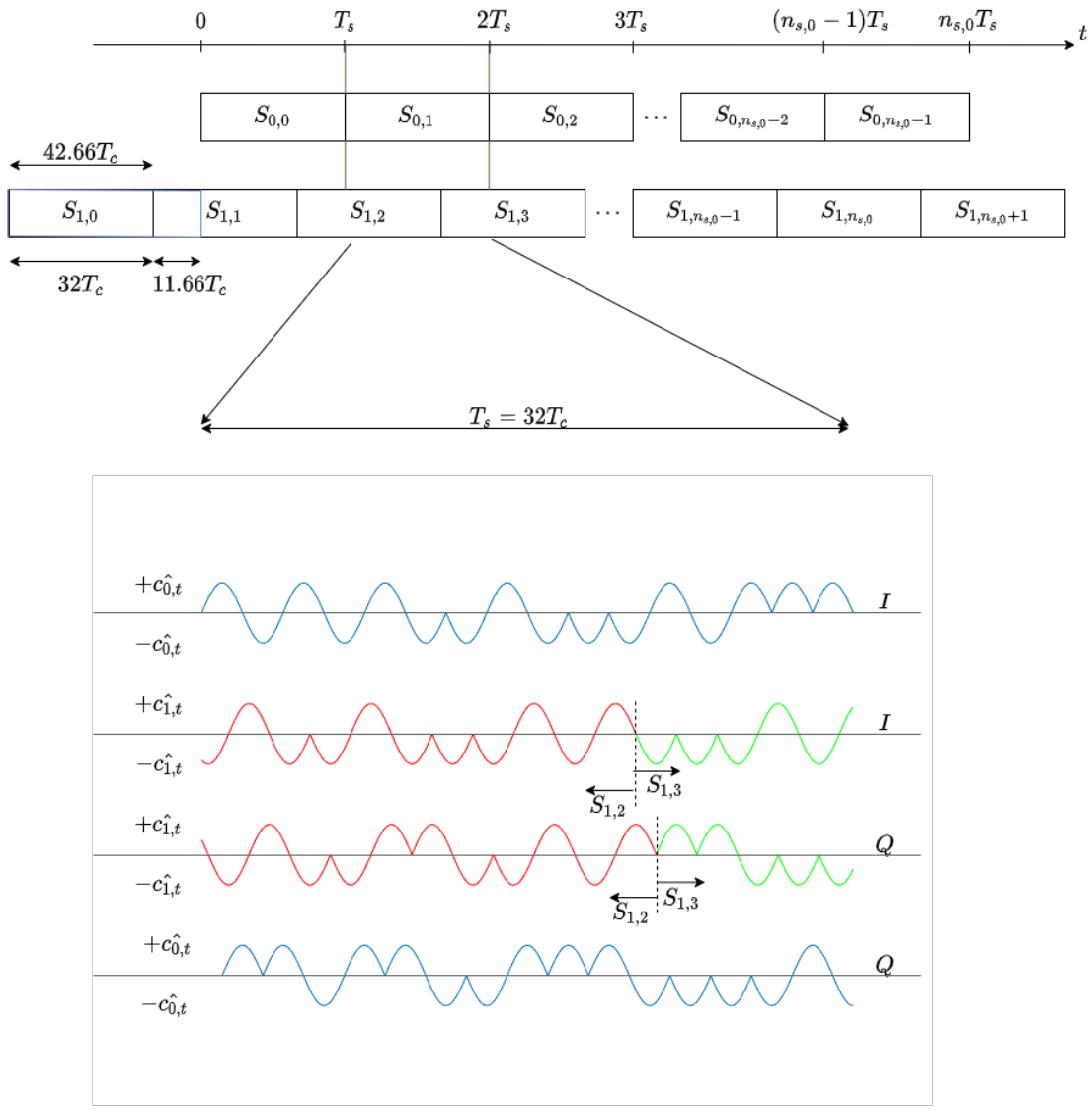


Figure 3.7: Example of the components of $\mathcal{Y}(t)$ and the time offset between them.

- $\hat{\tau}_1 \in (0, 2T_c)$ is a chip level time offset.
- $\tau_{1,s} = 2T_c\, n_{\tau_1}$ is a symbol time offset so that $n_{\tau_1} \in (0, 1, .....15)$ indicates misalignment in chips thus

$$\tau_1 = \tau_{1,s} + \hat{\tau}_1, \tag{3.19}$$

Notably $\tau_1 \in (0, 32T_c) = (0, T_s)$.

We also need to underline that $T_c = \tau^*$ is a threshold for which there is a perfect alignment of the In-phase component of the interfering signal with its Q-phase component of the SoI so that for $n_{\tau_1} = 0$ we have
if $\hat{\tau}_1 < \tau^*$, the interfering chips have the same indices on both I and Q components, if $\hat{\tau}_1 > \tau^*$ these indices will be misaligned by 1 (See Figure (3) in [48]). This concept will be explained with more details in the following subsection.

Therefore, in order to obtain a stochastic characterization of a single interferer there are $(16 \cdot 2)$ cases to consider for each couple of 16-ary symbols. It is worth noting that there is an important property in IEEE 802.15.4 standard 2.45 GHz band, PN sequences that

$$\sum\nolimits_{m=0}^{15} \hat{b}_{j,i,\ell,m} = 0 \ \forall j, i, \ell \tag{3.20}$$

$$\sum\nolimits_{\ell=0}^{15} \hat{b}_{j,i,\ell,m} = 0 \ \forall j, i, m, \tag{3.21}$$

where $\ell$ indicates distinct 16-ary symbols, i.e the sum of NRZ encoded chips with the same position ($m$ is fixed) over all 16 PN sequences is always zero. The second fact ensures that the expected value of the contribution of the interferer is always null when the symbols are equiprobable. We provide the stochastic analysis of the cross-product of I and Q components with time offset of IEEE 802.15.4 2.45 GHz band PN sequences in the next subsection (particularly in paragraph 3.2.3.1.2).

### 3.2.3 Receiver Model

We assume that the receiver has a good phase estimate of the carrier, so that a coherent demodulator can decompose the received signal into its I and Q components (see e.g. [104] for a detailed discussion of the OQPSK-DSSS demodulation, and [105] as an example of the architecture of a dual mode IEEE 802.15.4 receiver that includes

a QPSK demodulator chain). This is equivalent to using an optimal soft decision decoding as in [100, p. 424-448] (section 7.4). The optimal receiver is realized by the use of couple of filters (or cross correlations) matched to the OQPSK waveforms used to transmit each pair of chips in the codeword, followed by the decoder that forms the 16 decision variables corresponding to 16 codewords as in Figure 3.8 which illustrates the structure of the matched filter receiver with 16 correlators. The basis functions are $\phi_I^*(T_s - t), = \cos(w_p t)\,\phi_I(t)$ and $\phi_Q^*(T_s - t) = \sin(w_p t)\,\phi_Q(t)$ where the output signal can be written as in [100]

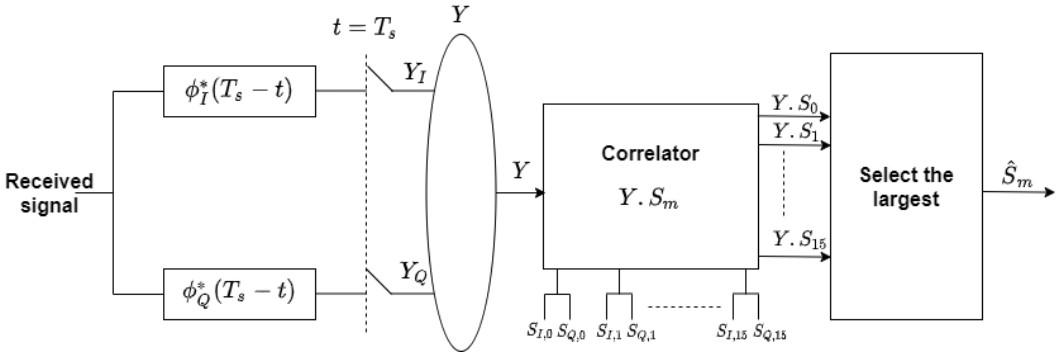


Figure 3.8: The structure of the matched filter receiver with 16 correlators.

$$\hat{S}_m = \underset{1 \le m \le M=16}{argmax}\ Y.S_m \tag{3.22}$$

where

$$\begin{aligned} S_m(t) = &\mathcal{X}_{\ell,m}(t) = b_{I,\ell,m}(t)\,\phi_I^*(T_s - t) - b_{Q,\ell,m}(t)\,\phi_Q^*(T_s - t), \\ &= b_{I,m}(t)\,cos(w_p t)\phi_I(t) - b_{Q,m}(t)\,sin(w_p t)\,\phi_Q(t), \end{aligned} \tag{3.23}$$

where $\mathcal{X}_{\ell,m}$ represents the transmitted symbol $S_m$ which has the index $\ell$ in the PPDU. It is worth saying that we assume the signals are equiprobable and have equal energy.

From 3.16, by the linearity of integration, we have

$$Y_j = \sum\nolimits_{i=0}^{1} Y_{j,i} + W_j, \tag{3.24}$$

where $Y_j(t)$, $Y_{j,i}(t)$, and $W_j(t)$ are the in-phase or quadrature components of $\mathcal{Y}(t)$, $\mathcal{Y}_i(t)$, and $\mathcal{W}(t)$ , respectively. Without loss of generality, as we said above, we assume a synchronized received signal of the useful reference $\tau_0 = 0$. Following the

approach similar to the one in [106], the outputs of the coherent correlation receiver matched filter to a realization of BDS $b_{j,0}(t)$ and sampled at $T_s$ are

$$Y_{I,\ell} = \int_0^{T_s} \mathcal{Y}(t)\,\phi_I(t)\,\sum_{m=0}^{15} \hat{b}_{I,i,l,m}\,h_{T_c}\left(\frac{t\;-\;2\,(m\;+\;32l)\,T_c}{2T_c}\right)\cos(w_p t)dt, \tag{3.25}$$

$$Y_{Q,\ell} = \int_0^{T_s} \mathcal{Y}(t)\,\phi_Q(t)\,\sum_{m=0}^{15} \hat{b}_{Q,i,l,m}\,h_{T_c}\left(\frac{t\;-\;(2\,(m\;+\;32l)+1)\,T_c}{2T_c}\right)\sin(w_p t)dt, \tag{3.26}$$

Now after having the output lets derive SINR expression.

#### 3.2.3.1 SINR derivation

We define the signal-to-interference-plus-noise ratio as the ratio between the expected value to the standard deviation of the received signal

$$\gamma = \frac{E[Y]}{\sigma[Y]}, \tag{3.27}$$

where $Y = \sqrt{Y_{I,\ell}^2 + Y_{Q,\ell}^2}$. Therefore, we need to derive the explicit expressions of its components. Thus, (3.25) can be written as

$$\begin{aligned} Y_{I,\ell} = \int_0^{T_s} \Big(c_0(t)\,\mathcal{X}_0(t) + c_1(t)\,\mathcal{X}_1(t) + \mathcal{W}(t)\Big)\sqrt{\frac{2}{T_c}}\cos(w_c t)\cdot \\ \sum_{m=0}^{15} \hat{b}_{I,i,l,m}\,h_{T_c}\left(\frac{t\;-\;2\,(m\;+\;32l)\,T_c}{2T_c}\right) cos(w_p(t))dt, \\ = Y_{I,0,\ell} + Y_{I,1,\ell} + W_{I,\ell}, \end{aligned} \tag{3.28}$$

where we have

$$\begin{aligned} Y_{I,0,\ell} = \sqrt{\frac{2}{T_c}}\sum_{m=0}^{15}\hat{c}_{0,t}\int_0^{T_s} \mathcal{X}_0(t)\;\cos(w_c t)\,cos(w_p t)\cdot \\ \hat{b}_{I,0,l,m}\,h_{T_c}\left(\frac{t\;-\;2\,(m\;+\;32l)\,T_c}{2T_c}\right)dt, \end{aligned} \tag{3.29}$$

$$Y_{I,1,\ell} = \sqrt{\frac{2}{T_c}} \sum_{m=0}^{15} \hat{c}_{1,t} \int_0^{T_s} \mathcal{X}_1(t)\, \cos(w_c t)\, cos(w_p t) \cdot \hat{b}_{I,0,l,m}\, h_{T_c}\left(\frac{t\, -\, 2\,(m\, +\, 32l)\, T_c}{2T_c}\right) dt, \tag{3.30}$$

$$W_{I,\ell} = \sqrt{\frac{2}{T_c}} \sum_{m=0}^{15} \int_0^{T_s} \mathcal{W}(t)\, \cos(w_c t)\, cos(w_p t) \cdot \hat{b}_{I,0,l,m}\, h_{T_c}\left(\frac{t\, -\, 2\,(m\, +\, 32l)\, T_c}{2T_c}\right) dt, \tag{3.31}$$

In the same manner equation (3.26) can be expressed as

$$\begin{aligned} Y_{Q,\ell} = \sum_{m=0}^{15} \int_0^{T_s} \Big(c_0(t)\, \mathcal{X}_0(t) + c_1(t)\, \mathcal{X}_1(t) + \mathcal{W}(t)\Big) \sqrt{\frac{2}{T_c}} \sin(w_c t) \cdot \\ \hat{b}_{Q,i,l,m}\, h_{T_c}\left(\frac{t\, -\, (2\,(m\, +\, 32l) + 1)\, T_c}{2T_c}\right) \sin(w_p t) dt, \\ = Y_{Q,0,\ell} + Y_{Q,1,\ell} + W_{Q,\ell}, \end{aligned} \tag{3.32}$$

where we have

$$Y_{Q,0,\ell} = \sqrt{\frac{2}{T_c}} \sum_{m=0}^{15} \hat{c}_{0,t} \int_0^{T_s} \mathcal{X}_0(t)\, \sin(w_c t)\, \sin(w_p t) \cdot \hat{b}_{Q,0,l,m\cdot}\, h_{T_c}\left(\frac{t\, -\, (2\,(m\, +\, 32l) + 1)\, T_c}{2T_c}\right) dt, \tag{3.33}$$

$$Y_{Q,1,\ell} = \sqrt{\frac{2}{T_c}} \sum_{m=0}^{15} \hat{c}_{1,t} \int_0^{T_s} \mathcal{X}_1(t)\, \sin(w_c t)\, \sin(w_p t) \cdot \hat{b}_{Q,0,l,m}\, h_{T_c}\left(\frac{t\, -\, (2\,(m\, +\, 32l) + 1)\, T_c}{2T_c}\right) dt, \tag{3.34}$$

$$W_{Q,\ell} = \sqrt{\frac{2}{T_c}} \sum_{m=0}^{15} \int_0^{T_s} \mathcal{W}(t)\, \sin(w_c t)\, \sin(w_p t) \cdot \hat{b}_{Q,0,l,m}\, h_{T_c}\left(\frac{t\, -\, (2\,(m\, +\, 32l) + 1)\, T_c}{2T_c}\right) dt, \tag{3.35}$$

Since $W(t)$ is the AWGN with two sided power spectral density (PSD) $\frac{N_0}{2}$, we have $E[W(t)] = 0 \Rightarrow E[W_{I,\ell,m}] = E[W_{Q,\ell,m}] = 0$. After some algebra shown in appendix A

we get

$$\begin{aligned}\sigma^2[W_{I,\ell}] &= E[W_{I,\ell}^2] - E^2[W_{I,\ell}] = E[W_{I,\ell,m}^2] \\ &= \frac{2}{T_c}\int_0^{T_s}\int_0^{T_s} E[w(t_1)w(t_2)]\cos(w_c t_1)\cos(w_p t_1)\cdot \\ &\qquad \sum_{m=0}^{15}\hat{b}_{I,0,l,m}^2\,\cos(w_c t_2)\cos(w_p t_2)\,dt_1 dt_2 \\ &= \frac{N_0 T_s}{4Tc},\end{aligned}$$

In the same manner we compute the variance of the quadrature phase and we get

$$\begin{aligned}\sigma^2[W_{Q,\ell}] &= E[W_{Q,\ell}^2] - E^2[W_{Q,\ell}] = E[W_{Q,\ell,m}^2] \\ &= \frac{2}{T_c}\int_0^{T_s}\int_0^{T_s} E[w(t_1)w(t_2)]\sin(w_c t_1)\sin(w_p t_1)\cdot \\ &\qquad \sum_{m=0}^{15}\hat{b}_{Q,0,l,m}^2\,\sin(w_c t_2)\sin(w_p t_2)\,dt_1 dt_2 \\ &\approx \frac{N_0 T_s}{4Tc},\end{aligned}$$

Therefore, the variance of the noise can be expressed as

$$\begin{aligned}\sigma^2[W_\ell(t)] &= \sigma^2[W_{I,\ell}] + \sigma^2[W_{Q,\ell}] \\ &\approx \frac{N_0 T_s}{4Tc} + \frac{N_0 T_s}{4Tc} \approx \frac{N_0 T_s}{2Tc} \approx 16N_0\,,\end{aligned}$$

Now let's compute the received SoI components starting from the in-phase component in (3.29) since the received signal is assumed to be synchronized with the transmitted one so we obtain

$$\begin{aligned}Y_{I,0,\ell} = \sqrt{\frac{2}{T_c}}\hat{c}_{0,t}\sum_{m=0}^{15}\int_{2\,(m+32l)\,T_c}^{2\,(m+32l+1)T_c} \mathcal{X}_0(t)\,\cos(w_c t)\,cos(w_p t)\cdot \\ \hat{b}_{I,0,l,m}\,h_{T_c}\left(\frac{t\,-\,2\,(m\,+\,32l)\,T_c}{2T_c}\right)dt,\end{aligned} \tag{3.36}$$

We notice that within the interval $[2\,(m\,+\,32l)\,T_c,\,2\,(m\,+1\,+32l)\,T_c]$ we have that

$$\begin{aligned}\mathcal{X}_{0,\ell}(t) = \sqrt{\frac{2}{T_c}}\Bigg[ &\sum_{m=0}^{15} \hat{b}_{I,0,l,m} h_{T_c}\left(\frac{t\,-\,2\,(m\,+\,32l)\,T_c}{2T_c}\right)\cos(w_c t)\,\cos(w_p t) \\ &-\sin(w_c t)\,\sin(w_p t)\left(\sum_{m=0}^{15}\hat{b}_{Q,0,l,m}\,h_{T_c}\left(\frac{t\,-\,(2(m\,+\,32l)+1)\,T_c}{2T_c}\right)\right. \\ &\left.+\sum_{m=0}^{15}\hat{b}_{Q,0,l,m-1}\,h_{T_c}\left(\frac{t\,-\,(2(m\,+\,32l)-1)\,T_c}{2T_c}\right)\right)\Bigg],\end{aligned} \tag{3.37}$$

After substituting the right-hand-side of the $\mathcal{X}_0(t)$ in $Y_{I,0,\ell,m}$, by linearity of integration and taking into account the definition of $h(t)$ we obtain

$$\begin{aligned}Y_{I,0,\ell} = \frac{2}{T_c}\hat{c}_{0,t}\sum_{m=0}^{15}\Bigg(&\int_{2\,(m+32l)\,T_c}^{2\,(m+32l\,+1)T_c}\hat{b}_{I,0,l,m}^2\,\cos^2(w_c t)\,cos^2(w_p t)dt \\ &-\int_{2\,(m+32l)\,T_c}^{(2\,(m+32l)\,+1)T_c}\hat{b}_{I,0,l,m}\hat{b}_{Q,0,l,m-1}\sin(w_c t)\cos(w_c t)\sin(w_p t)\cos(w_p t)dt \\ &-\int_{(2\,(m+32l)\,+1)T_c}^{2\,(m+32l\,+1)T_c}\hat{b}_{I,0,l,m}\hat{b}_{Q,0,l,m}\sin(w_c t)\cos(w_c t)\sin(w_p t)\cos(w_p t)dt,\Bigg) \\ &=\ 16\,\hat{c}_{0,t}\,,\end{aligned} \tag{3.38}$$

The proof of the equations of this chapter can be found in appendix A. Clearly, this implies that $E[Y_{I,0,\ell}] = 16\,\hat{c}_{0,t}$ and $\sigma^2[Y_{I,0,\ell}] = 0$. It is worth mentioning that for $m = 0\,\&\,\ell \neq 0$ we have $\hat{b}_{j,i,\ell,m-1} = \hat{b}_{j,i,\ell-1,15}$, and for $m = 0\,\&\,\ell = 0$ we state that $\hat{b}_{j,I,0,-1} = 0$

The quadrature part of the received SoI can be derived in the same way so we can get

$$\begin{aligned}Y_{Q,0,\ell} = \sqrt{\frac{2}{T_c}}\hat{c}_{0,t}\sum_{m=0}^{15}\int_{(2\,(m+32l)\,+1)T_c}^{2\,(m+32l\,+1)T_c+T_c}&\mathcal{X}_0(t)\,\sin(w_c t)\,\sin(w_p t)\,\hat{b}_{Q,0,\ell,m}\cdot \\ &h_{T_c}\left(\frac{t\,-\,(2\,(m\,+\,32l)\,+1)T_c}{2T_c}\right)dt,\end{aligned} \tag{3.39}$$

$\mathcal{X}_{0,\ell}(t)$ can be expressed in the interval $[(2\,(m\,+\,32l)+1)\,T_c,\,2\,(m\,+1\,+32l)\,T_c+T_c]$ as

$$\begin{aligned}\mathcal{X}_{0,\ell}(t) = \sqrt{\frac{2}{T_c}}\Bigg[ & \sum_{m=0}^{15} \hat{b}_{Q,0,l,m} h_{T_c}\left(\frac{t\,-\,(2\,(m\,+\,32l)+1)\,T_c}{2T_c}\right)\sin(w_c t)\,\sin(w_p t) \\ & -\cos(w_c t)\,\cos(w_p t)\,\left(\sum_{m=0}^{15}\hat{b}_{I,0,l,m}\,h_{T_c}\left(\frac{t\,-\,2(m\,+\,32l)\,T_c}{2T_c}\right)\right. \\ & \left.+\sum_{m=0}^{15}\hat{b}_{Q,0,l,m+1}\,h_{T_c}\left(\frac{t\,-\,2(m\,+\,32l+1)\,T_c}{2T_c}\right)\right)\Bigg]\,dt,\end{aligned} \tag{3.40}$$

Thus, we can write

$$\begin{aligned}Y_{Q,0,\ell} = \frac{2}{T_c}\hat{c}_{0,t}\sum_{m=0}^{15}\Bigg(&\int_{(2\,(m+32l)+1)\,T_c}^{2\,(m+32l+1)T_c+T_c}\hat{b}^2_{Q,0,l,m}\,\sin^2(w_c t)\,\sin^2(w_p t)dt \\ &-\int_{(2\,(m+32l)+1)\,T_c}^{2\,(m+32l+1)T_c}\hat{b}_{Q,0,l,m}\hat{b}_{I,0,l,m}\sin(w_c t)\cos(w_c t)\sin(w_p t)\cos(w_p t)dt \\ &-\int_{2\,(m+32l+1)T_c}^{2\,(m+32l+1)T_c+T_c}\hat{b}_{Q,0,l,m}\hat{b}_{I,0,l,m+1}\sin(w_c t)\cos(w_c t)\sin(w_p t)\cos(w_p t)dt,\Bigg) = \\ &= \boxed{16\,\hat{c}_{0,t}}\,,\end{aligned} \tag{3.41}$$

Thus, the received SoI can be written as

$$Y_0 = \sqrt{Y^2_{I,0,\ell} + Y^2_{Q,0,\ell}} = 16\,\sqrt{2}\,\hat{c}_{0,t}. \tag{3.42}$$

Now let's compute the interferer's components starting from equation (3.30) to get the I-phase component and substituting the asynchronized interferer signal (3.10)

in it and assuming that $i = 1$ to refer to the interferer, we obtain:

$$
\begin{aligned}
Y_{I,1,\ell}/n_{\tau_1} = \sqrt{\frac{2}{T_c}}\sqrt{\frac{2}{T_c}}\hat{c}_{1,t}\int_0^{T_s} \Big[ & b_{I,1}(t-\tau_1)\,\cos(w_p(t-\tau_1))\,\cos(w_c t-\phi_{c_1}) \\
& - b_{Q,1}(t-\tau_1)\,\sin(w_p(t-\tau_1))\,\sin(w_c t-\phi_{c_1})\Big]\,\cos(w_c t)\,cos(w_p(t))\cdot \\
& \sum_{m=0}^{15}\,\hat{b}_{I,0,l,m} h_{T_c}\left(\frac{t\,-\,2\,(m\,+\,32l)\,T_c}{2T_c}\right)dt = \\
& = \frac{2}{T_c}\hat{c}_{1,t}\int_0^{T_s}\Bigg[ b_{I,1}(t-\tau_1)\,\cos(w_c t)\cos(w_c t-\phi_{c_1})\cos(w_p(t))\cdot \\
& \cos(w_p(t-\tau_1))\sum_{m=0}^{15}\,\hat{b}_{I,0,l,m}\,h_{T_c}\left(\frac{t\,-\,2\,(m\,+\,32l)\,T_c}{2T_c}\right)\Bigg] - \\
& - \Bigg[ b_{Q,1}(t-\tau_1)\,\cos(w_c t)\sin(w_c t-\phi_{c_1})\cos(w_p(t))\sin(w_p(t-\tau_1))\,. \\
& \sum_{m=0}^{15}\hat{b}_{I,0,l,m}\,h_{T_c}\left(\frac{t\,-\,2\,(m\,+\,32l)\,T_c}{2T_c}\right)\Bigg]dt,
\end{aligned}
\tag{3.43}
$$

It is worth mentioning that the carrier phase offset is hard to control because of oscillators drifts and other phase changes during transmission, [79]. Thus, we consider $\phi_{c_1}$ i.i.d. uniform which could be any value from the range $[0, 2\pi]$ for each packet unless stated otherwise. On the other hand, we consider the time offset $\tau_1$ is constant for all the packets because experimental work shows that this timing can be precisely controlled. For instance, Elsas et all in [107] use a setup which offers precise control over the timing offset between the SoI and the interferer signal. Glossy [108], which is about a novel flooding architecture for wireless sensor networks, achieves a timing precision of 500 ns over 8 hops with 96 probability, and Wang et al. [109] proposed practical techniques to effectively compensate propagation and radio processing delays.

The value of the integration in equation (3.43) varies according to the value of the time offset $\tau_1$ as in (3.19). We will consider different values of $n_{\tau,1} \in \{0, 1, 2...15\}$ and $\hat{\tau_1} \in \{0, ...2Tc\}$. Figure 3.9 shows the cases we consider for the value of $\hat{\tau_1}$ where $\tau_1 = 2\,T_c\,n_{\tau_1} + \hat{\tau_1}$ as mentioned previously.

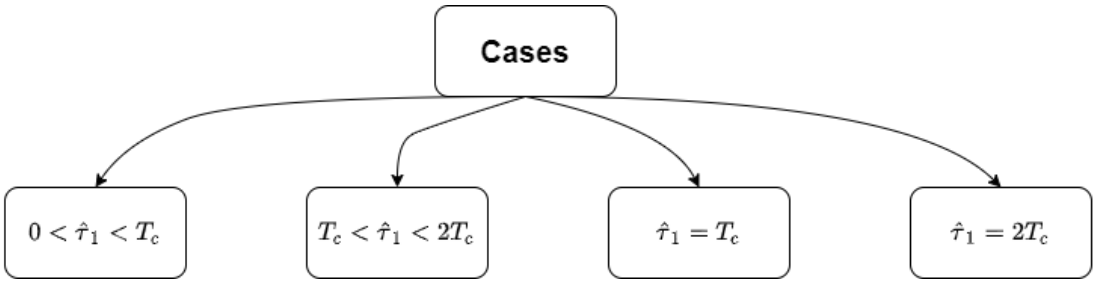


Figure 3.9: Considered cases of the value of $\hat{\tau}_1$.

**3.2.3.1.1 Case 1** $0 < \hat{\tau}_1 < T_c$ We will start with the first case having $n_{\tau_1} = 0$ as it is illustrated in Figure 3.10. For the sake of simplicity of the computation, we call the first part of equation (3.43), $A_1$, and the second part $B_1$ so $Y_{I,1,\ell}/n_{\tau_1} = \frac{2}{T_c}\hat{c}_{1,t}(A_1 - B_1)$. Let's first compute $A_1$.

$$A_1 = \int_0^{T_s} \left[ b_{I,1}(t-\tau_1)\, \cos(w_c t)\cos(w_c t - \phi_{c_1})\cos(w_p(t))\cos(w_p(t-\tau_1)) \cdot \sum_{m=0}^{15} \hat{b}_{I,0,l,m}\, h_{T_c}\left(\frac{t - 2\,(m + 32l)\,T_c}{2T_c}\right)\right] dt, \tag{3.44}$$

After standard mathematical manipulations we can write

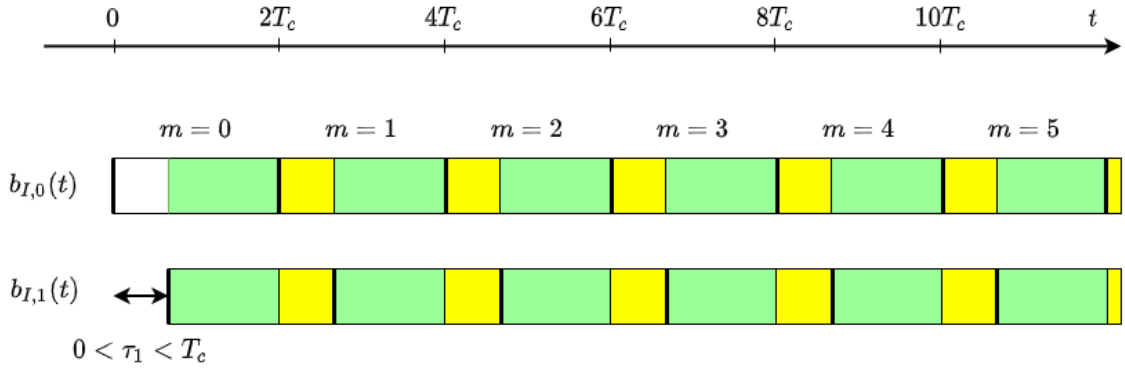


Figure 3.10: An illustration of the reception of the I-phase component of both the SoI and the interferer when $n_{\tau_1} = 0$, $0 < \hat{\tau}_1 < T_c$.

$$A_1 = \int_0^{T_s} \Bigg[ b_{I,1}(t-\tau_1)\,\frac{1}{2}\Big(\cos(\phi_{c_1}) + \cos(2w_c t + \phi_{c_1})\Big)\cdot \\ \frac{1}{2}\Big(\cos(\phi_p) + \cos(2w_p t + \phi_p)\Big)\sum_{m=0}^{15} \hat{b}_{I,0,l,m}\, h_{T_c}\left(\frac{t\ -\ 2\,(m\ +\ 32l)\,T_c}{2T_c}\right)\Bigg] dt, \tag{3.45}$$

where $\phi_p = w_p\,\tau_1$ is the pulse phase offset caused by $\tau_1$. We apply perfect low-pass filtering to filter out high-frequency components $2w_c t$ as in [48] and assuming that carrier phase, time delay and the data symbols are independent as in [106] so we can write

$$A_1 = \frac{1}{4}\cos(\phi_{c_1}) \int_0^{T_s} \Bigg[ \left(\cos(\phi_p) + \cos(2w_p t + \phi_p)\right) b_{I,1}(t-\tau_1)\cdot \\ \sum_{m=0}^{15} \hat{b}_{I,0,l,m}\, h_{T_c}\left(\frac{t\ -\ 2\,(m\ +\ 32l)\,T_c}{2T_c}\right)\Bigg] dt, \tag{3.46}$$

If we consider the function $f(t,\tau_1) = \Bigg[\left(\cos(\phi_p) + \cos(2w_p t + \phi_p)\right) b_{I,1}(t-\tau_1) \sum_{m=0}^{15} \hat{b}_{I,0,l,m}\, h_{T_c}\left(\frac{t-2\,(m+32l)\,T_c}{2T_c}\right)\Bigg]$, and divide the range of the integration, because of linearity, to several ranges whose summation equals to one symbol so we obtain

$$A_1 = \frac{1}{4}\cos(\phi_{c_1})\Bigg[\int_0^{\hat{\tau}_1} f(t,\tau_1)dt + \int_{\hat{\tau}_1}^{2T_c} f(t,\tau_1)dt + \int_{2T_c}^{2T_c+\hat{\tau}_1} f(t,\tau_1)dt + \\ \int_{2T_c+\hat{\tau}_1}^{4T_c} f(t,\tau_1)dt + \int_{4T_c}^{4T_c+\hat{\tau}_1} f(t,\tau_1)dt + \ldots\ldots\ldots \int_{30T_c+\hat{\tau}_1}^{32T_c} f(t,\tau_1)dt\Bigg], \tag{3.47}$$

In order to analyze the product $\sum_{m=0}^{15}\ \hat{b}_{I,0,l,m}\ h_{T_c}\left(\frac{t-2\,(m+32l)\,T_c}{2T_c}\right)\ \hat{b}_{I,1,l,m}\cdot h_{T_c}\left(\frac{t-\tau_1-2\,(m+32l)\,T_c}{2T_c}\right)$ we need to consider the characteristics of the PN sequences defined by IEEE 802.15.4 standard 2.45 GHz band, which can be summarized by the Hamming distances between them. The next subsection will explain these characteristics.

**3.2.3.1.2 Stochastic Analysis of the cross-product of I and Q components with time offset of IEEE 802.15.4 2.45 GHz band PN sequences** . While

Table 3.1: Chip sequences used in the 2.4 GHz PHY of IEEE 802.15.4 [12].

| Symbol | Bits | PN sequences |
|---|---|---|
| 0 | 0000 | 1 1 0 1 1 0 0 1 1 1 0 0 0 0 1 1 0 1 0 1 0 0 1 0 0 0 1 0 1 1 1 0 |
| 1 | 0001 | 1 1 1 0 1 1 0 1 1 1 0 1 1 1 0 0 0 0 1 1 0 1 0 1 0 0 1 0 0 0 1 0 |
| 2 | 0010 | 0 0 1 0 1 1 1 0 1 1 0 1 1 0 0 1 1 1 0 0 0 0 1 1 0 1 0 1 0 0 1 0 |
| 3 | 0011 | 0 0 1 0 0 0 1 0 1 1 1 0 1 1 0 1 1 0 0 1 1 1 0 0 0 0 1 1 0 1 0 1 |
| 4 | 0100 | 0 1 0 1 0 0 1 0 0 0 1 0 1 1 1 0 1 1 0 1 1 0 0 1 1 1 0 0 0 0 1 1 |
| 5 | 0101 | 0 0 1 1 0 1 0 1 0 0 1 0 0 0 1 0 1 1 1 0 1 1 0 1 1 0 0 1 1 1 0 0 |
| 6 | 0110 | 1 1 0 0 0 0 1 1 0 1 0 1 0 0 1 0 0 0 1 0 1 1 1 0 1 1 0 1 1 0 0 1 |
| 7 | 0111 | 1 0 0 1 1 1 0 0 0 0 1 1 0 1 0 1 0 0 1 0 0 0 1 0 1 1 1 0 1 1 0 1 |
| 8 | 1000 | 1 0 0 0 1 1 0 0 1 0 0 1 0 1 1 0 0 0 0 0 0 1 1 1 0 1 1 1 1 0 1 1 |
| 9 | 1001 | 1 0 1 1 1 0 0 0 1 1 0 0 1 0 0 1 0 1 1 0 0 0 0 0 0 1 1 1 0 1 1 1 |
| 10 | 1010 | 0 1 1 1 1 0 1 1 1 0 0 0 1 1 0 0 1 0 0 1 0 1 1 0 0 0 0 0 0 1 1 1 |
| 11 | 1011 | 0 1 1 1 0 1 1 1 1 0 1 1 1 0 0 0 1 1 0 0 1 0 0 1 0 1 1 0 0 0 0 0 |
| 12 | 1100 | 0 0 0 0 0 1 1 1 0 1 1 1 1 0 1 1 1 0 0 0 1 1 0 0 1 0 0 1 0 1 1 0 |
| 13 | 1101 | 0 1 1 0 0 0 0 0 0 1 1 1 0 1 1 1 1 0 1 1 1 0 0 0 1 1 0 0 1 0 0 1 |
| 14 | 1110 | 1 0 0 1 0 1 1 0 0 0 0 0 0 1 1 1 0 1 1 1 1 0 1 1 1 0 0 0 1 1 0 0 |
| 15 | 1111 | 1 1 0 0 1 0 0 1 0 1 1 0 0 0 0 0 0 1 1 1 0 1 1 1 1 0 1 1 1 0 0 0 |

Wilhelm et all in [48] did not consider the behavior of the code, we take into account the properties of the chipping (PN) sequences defined in IEEE 802.15.4 standard 2.45 GHz band [12]. This means that 4 bit groups are first spread to 32 chips sequences before they are transmitted in $b_{j,0,\ell,m}$ and $b_{j,1,\ell,m}$. The PN sequences are given in Table 3.1. Then, the even-indexed chips (i.e. $c_0, c_2$, etc.) are modulated onto the I-phase (I) carrier and the odd-indexed chips (i.e. $c_1, c_3$, etc.) are modulated onto the quadrature-phase (Q) carrier. In general, the misalignment with respect to the SoI could be positive or negative so $n_{\tau,1} \in \{-15, -14, ...., 0, 1, 2, .....15\}$. Clearly, when it is positive so it indicates a delay while it indicates an anticipation when it is negative. When $n_{\tau,1} \neq 0$ a 16 array symbol is always affected by two interfering symbols, the first one is affecting the first $\|n_{\tau,1}\|$ by its last chips, while the second is affecting the remaining $16 - n_{\tau,1}$ by its first chips. For example, if we assume that $n_{\tau,1} = -1$ so the interferer is one chip ahead as it is illustrated in Figure 3.11 while when $n_{\tau,1} = 1$ the scenario is symmetric to the previous one as it is shown in Figure 3.12. Let's consider that the symbol of the SoI is $S_{0,0}$ and $n_{\tau_1} = 1$, the value of Hamming distance between the first $n_{\tau_1} = 1$ chip and the last chip of the previous

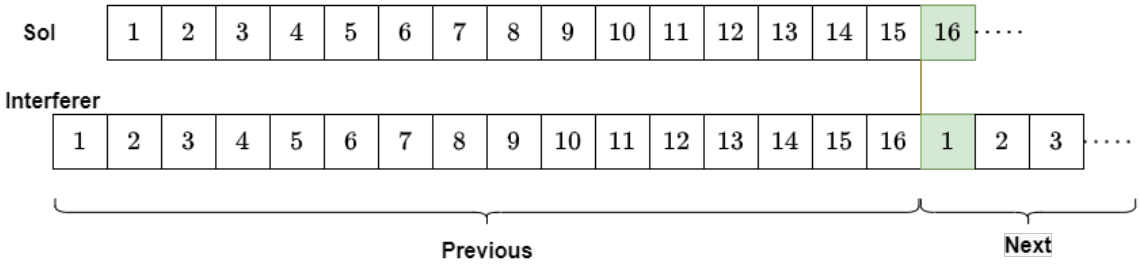


Figure 3.11: An illustration of the time offset between the SoI and the interferer when $n_{\tau,i} = -1$ .

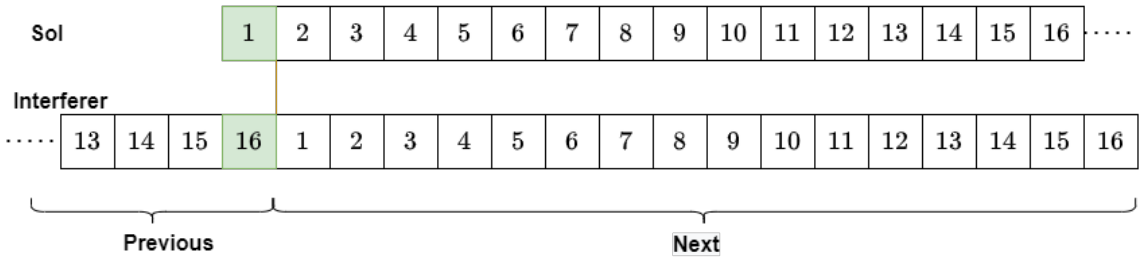


Figure 3.12: An illustration of the time offset between the SoI and the interferer when $n_{\tau,i} = 1$ .

Table 3.2: Hamming distances when $n_{\tau,1} = 0, 1$.

| $n_{\tau,1}$ | $HD$ | Hamming distances | | | | | | | | | | | | | | | |
|---|---|---|---|---|---|---|---|---|---|---|---|---|---|---|---|---|---|
| 0 | $HD_0$ | 0 | 6 | 8 | 12 | 12 | 12 | 8 | 6 | 0 | 6 | 8 | 12 | 12 | 12 | 8 | 6 |
| 1 | $HD_2$ | 0 | 0 | 0 | 1 | 0 | 1 | 1 | 1 | 0 | 0 | 1 | 1 | 0 | 1 | 1 | 1 |
| | $HD_1$ | 10 | 8 | 8 | 5 | 6 | 7 | 7 | 9 | 10 | 8 | 8 | 5 | 6 | 7 | 7 | 9 |

interfering symbol, which could be any admissible sequence value j $\in$ (0, 15), equals to

$$HD_{prev}(n_{\tau_1}) = \Big[d_H\left(S_0, S_{prev}(\mathrm{j}, n_{\tau_1})\right) \text{ for } (\mathrm{j} = 0, \ldots, 15)\Big] = HD_2, \tag{3.48}$$

where $d_H(.\,,.)$ is the Hamming distance between two sequences indicated between brackets. Similarly, the Hamming distance between the last $16 - n_{\tau_1}$ of the SoI and the first $16 - \|n_{\tau_1}\|$ chips of the next interfering symbol is

$$HD_{Next}(n_{\tau_1}) = \Big[d_H\left(S_0, S_{Next}(\mathrm{i}, n_{\tau_1})\right) \text{ for } (\mathrm{i} = 0, \ldots, 15)\Big] = HD_1, \tag{3.49}$$

It is worth noting that we might obtain the same scenario when $n_{\tau,1} = -15$ and likewise the scenario when $n_{\tau,1} = -1$ is similar to the one when $n_{\tau,1} = 15$. In this case, when $n_{\tau_1} = 1$, the Hamming distance forms a 16 by 16 matrix $HD_{n\tau_1}(\mathrm{i}, \mathrm{j})$ whose elements are the summation of $HD_1, HD_2$ for all the admissible value of (i, j). When $n_{\tau_1} = 0$, i.e when there is no misalignment between the symbols, the Hamming distance is indicated with $HD_0$. The values of these Hamming distances can be summarized in the Table 3.2. Therefore, all possible considered Hamming distances have values within the range $[0, 16]$ and are obtained as

$$(HD_n(\mathrm{i}, \mathrm{j})|n_{\tau,1}) = \sum_{\mathrm{i}=1}^{16} \sum_{\mathrm{j}=1}^{16} \left[(HD_1(\mathrm{i})|n_{\tau,1}) + (HD_2(\mathrm{j})|n_{\tau,1})\right], \tag{3.50}$$

where $HD_n(\mathrm{i}, \mathrm{j})|n_{\tau,1}$ is the matrix $HD_n$ knowing that the misalignment is $n_{\tau_1}$. An example for this matrix is the following matrix where $n_{\tau_1} = 1$.

$HD_n(\mathrm{i}, \mathrm{j})|1 =$

$$= \begin{bmatrix}
10 & 10 & 10 & 11 & 10 & 11 & 11 & 11 & 10 & 10 & 10 & 11 & 10 & 11 & 11 & 11 \\
8 & 8 & 8 & 9 & 8 & 9 & 9 & 9 & 8 & 8 & 8 & 9 & 8 & 9 & 9 & 9 \\
8 & 8 & 8 & 9 & 8 & 9 & 9 & 9 & 8 & 8 & 8 & 9 & 8 & 9 & 9 & 9 \\
5 & 5 & 5 & 6 & 5 & 6 & 6 & 6 & 5 & 5 & 5 & 6 & 5 & 6 & 6 & 6 \\
6 & 6 & 6 & 7 & 6 & 7 & 7 & 7 & 6 & 6 & 6 & 7 & 6 & 7 & 7 & 7 \\
7 & 7 & 7 & 8 & 7 & 8 & 8 & 8 & 7 & 7 & 7 & 8 & 7 & 8 & 8 & 8 \\
7 & 7 & 7 & 8 & 7 & 8 & 8 & 8 & 7 & 7 & 7 & 8 & 7 & 8 & 8 & 8 \\
9 & 9 & 9 & 10 & 9 & 10 & 10 & 10 & 9 & 9 & 9 & 10 & 9 & 10 & 10 & 10 \\
10 & 10 & 10 & 11 & 10 & 11 & 11 & 11 & 10 & 10 & 10 & 11 & 10 & 11 & 11 & 11 \\
8 & 8 & 8 & 9 & 8 & 9 & 9 & 9 & 8 & 8 & 8 & 9 & 8 & 9 & 9 & 9 \\
8 & 8 & 8 & 9 & 8 & 9 & 9 & 9 & 8 & 8 & 8 & 9 & 8 & 9 & 9 & 9 \\
5 & 5 & 5 & 6 & 5 & 6 & 6 & 6 & 5 & 5 & 5 & 6 & 5 & 6 & 6 & 6 \\
6 & 6 & 6 & 7 & 6 & 7 & 7 & 7 & 6 & 6 & 6 & 7 & 6 & 7 & 7 & 7 \\
7 & 7 & 7 & 8 & 7 & 8 & 8 & 8 & 7 & 7 & 7 & 8 & 7 & 8 & 8 & 8 \\
7 & 7 & 7 & 8 & 7 & 8 & 8 & 8 & 7 & 7 & 7 & 8 & 7 & 8 & 8 & 8 \\
9 & 9 & 9 & 10 & 9 & 10 & 10 & 10 & 9 & 9 & 9 & 10 & 9 & 10 & 10 & 10
\end{bmatrix}$$

The probability of this matrix is $P(HD_{n\tau_1}) = \frac{1}{256}$ under the assumption that interfering symbols are equiprobable. Considering the multiplicities of the values $HD_2(\mathrm{j})|n_{\tau_1}, HD_1(\mathrm{i})|n_{\tau_1}$, we obtain for $n_{\tau_1} = 1$: Let $\nu_{n\tau_1}$ be a value of $HD_n(\mathrm{i},\mathrm{j})|n_{\tau_1}$ for any admissible i, j and $m_{n\tau_1}$ be its multiplicity. Similarly, let $\nu_{n\tau_1,Prev}$, $\nu_{n\tau_1,Next}$, $m_{n\tau_1,Prev}$, $m_{n\tau_1,Next}$ are the values and multiplicities of $H_{prev}(\mathrm{j})/n_{\tau_1}, H_{Next}(\mathrm{i})/n_{\tau_1}$ respectively so we have

$$\begin{array}{rclcrcl}
\nu_{n\tau_1,Prev} & = & \{0,1\} & & \nu_{n\tau_1,Next} & = & \{5,6,7,8,9,10\} \\
m_{n\tau_1,Prev} & = & \{8,8\} & & m_{n\tau_1,Prev} & = & \{2,2,4,4,2,2\}
\end{array}$$

$\Rightarrow$

$$\begin{array}{rcl}
\nu_{n\tau_1} & = & \{5,6,7,8,9,10,11\} \\
m_{n\tau_1} & = & \{16,32,48,64,48,32,16\}
\end{array}$$

The proof is reported in appendix A.

We define a random variable called $k_{j_0,j_1,n_{\tau_1}}$, which is a random variable that depends on the symbols transmitted by the interferer at a given instant, where $j_0$ is the (I) or (Q) component of the SoI and $j_1$ is the (I) or (Q) component of the

interferer. This random variable is characterized by the following parameters

$$\begin{cases} P(HD_{n_{\tau_1}}) & = \frac{1}{256} \\ \nu_{n_{\tau_1}} & = \{5,6,7,8,9,10,11\} \\ m_{n_{\tau_1}} & = \{16,32,48,64,48,32,16\}, \end{cases} \tag{3.51}$$

Since the product of the chips of the SoI and interfering chips $\hat{b}_{j,0,l,m} \cdot \hat{b}_{j,1,l,m} \in \{\pm 1\}$ where

$$\begin{cases} \hat{b}_{j,0,l,m} \cdot \hat{b}_{j,1,l,m} & = +1 \quad \text{for } (16 - \nu_{n_{\tau_1}}) \text{ cases}, \\ \hat{b}_{j,0,l,m} \cdot \hat{b}_{j,1,l,m} & = -1 \quad \text{for } 16(\nu_{n_{\tau_1}}) \text{ cases}, \end{cases} \tag{3.52}$$

the value of the random variable $k_{j_0,j_1,n_{\tau_1}}$ can be defined as

$$\begin{aligned} k_{j_0,j_1,n_{\tau_1}} &= (16 - \nu_{n_{\tau_1}}) - \nu_{n_{\tau_1}} \\ &= 16 - 2\nu_{n_{\tau_1}}, \end{aligned} \tag{3.53}$$

Therefore, the expected values and the variances can be found accordingly

$$E[k_{j_0,j_1,n_{\tau_1}}] = \sum_i \frac{1}{256}(16 - 2\nu_{n_{\tau_1}}(i)) * m_{n_{\tau_1}}(i), \tag{3.54}$$

for our example $E[k_{I,I,1}] = E[k_{I,I,0}] = 0$ and we proof in appendix A that $E[k_{j_0,j_1,n_{\tau_1}}]$= $0 \ \forall \ j_0, j_1, n_{\tau_1}$. The variance can be written as

$$\begin{aligned} \sigma^2[k_{j_0,j_1,n_{\tau_1}}] &= E[k^2_{j_0,j_1,n_{\tau_1}}] - E^2[k_{j_0,j_1,n_{\tau_1}}] \\ &= \sum_i \frac{1}{256}(16 - 2\nu_{n_{\tau_1}}(i))^2 * m_{n_{\tau_1}}(i), \end{aligned} \tag{3.55}$$

For our example $\sigma^2[k_{I,I,0}] = 60$, $\sigma^2[k_{I,I,1}] = 10$.

Coming back to equation (3.47), $\int_0^{\hat{\tau}_1} f(t, \hat{\tau}_1)dt = 0$ since in the range of integral $b_{I,1}(t) = 0$ so based on the stochastic analysis and noting that the unit pulses $h_{T_c}\left(\frac{t - 2\,(m+32l)\,T_c}{2T_c}\right)$,

$h_{T_c}\left(\frac{t-\tau_1-2\,(m+32l)\,T_c}{2T_c}\right)$ are constant 1 in the integration intervals we can write

$$A_1 = \frac{1}{4}\cos(\phi_{c_1})\sum_{m=0}^{15}\left[k_{I,I,0}\int_{2mT_c+\hat{\tau}_1}^{(m+1)2T_c}\cos(\phi_p)+\cos(2w_pt-\phi_p)dt+\right.$$
$$\left.k_{I,I,1}\int_{2mT_c}^{2mT_c+\hat{\tau}_1}\cos(\phi_p)+\cos(2w_pt-\phi_p)dt\right],$$
$$=\frac{1}{4}\cos(\phi_{c_1})\left[\cos(\phi_p)\Big(k_{I,I,0}(2T_c-\hat{\tau}_1)+k_{I,I,1}(\hat{\tau}_1)\Big)+\frac{\sin(\phi_p)}{w_p}\Big(-k_{I,I,0}+k_{I,I,1}\Big)\right] \tag{3.56}$$

The proof is available in the appendix A.

The second part of (3.43) is B1

$$B_1 = \int_0^{T_s}\left[b_{Q,1}(t-\tau_1)\,\cos(w_ct)\sin(w_ct-\phi_{c_1})\cos(w_p(t))\sin(w_p(t-\tau_1))\cdot\right.$$
$$\left.\sum_{m=0}^{15}\hat{b}_{I,0,l,m}\,h_{T_c}\left(\frac{t\,-\,2\,(m\,+\,32l)\,T_c}{2T_c}\right)\right]dt \tag{3.57}$$

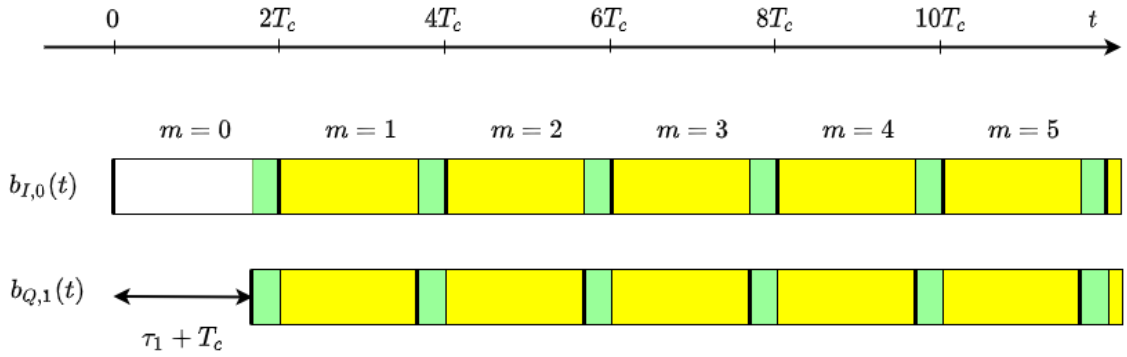


Figure 3.13: An illustration of the reception of the I-phase component of SoI and Quadrature component of the interferer when $n_{\tau_1}=0, 0<\hat{\tau}_1<T_c$.

Following the same approach of deriving the value of $A_1$ we can write $B_1$ as

$$\begin{aligned} B_1 &= \frac{1}{2}\sin(\phi_{c_1})\sum_{m=0}^{15}\Bigg[k_{I,Q,0}\int_{(2m+1)T_c+\hat{\tau}_1}^{(m+1)2T_c}\sin(w_p t-\phi_p)\cos(w_p t)dt+ \\ &\qquad + k_{I,Q,1}\int_{2mT_c}^{(2m+1)T_c+\hat{\tau}_1}\sin(w_p t-\phi_p)\cos(w_p t)dt\Bigg], \\ &= \frac{1}{4}\sin(\phi_{c_1})\Bigg[-\sin(\phi_p)\Big(k_{I,Q,0}(T_c-\hat{\tau}_1)+k_{I,Q,1}(T_c+\hat{\tau}_1)\Big)+ \\ &\qquad + \frac{\cos(\phi_p)}{w_p}\Big(-k_{I,Q,0}+k_{I,Q,1}\Big)\Bigg], \end{aligned} \tag{3.58}$$

After substituting the A1 and B1 equation (3.43) we can write

$$\begin{aligned} Y_{I,1,\ell}/(0,0<\hat{\tau}_1<T_c) = \frac{\hat{c}_{1,t}}{2T_c}\Bigg[ &\cos(\phi_{c_1})\Big(\cos(\phi_p)\left(k_{I,I,0}(2T_c-\hat{\tau}_1)+k_{I,I,1}(\hat{\tau}_1)\right)+ \\ &\frac{\sin(\phi_p)}{w_p}\left(-k_{I,I,0}+k_{I,I,1}\right)\Big)-\sin(\phi_{c_1})\cdot \\ &\Big(-\sin(\phi_p)\left(k_{I,Q,0}(T_c-\hat{\tau}_1)+k_{I,Q,1}(T_c+\hat{\tau}_1)\right)+ \\ &+\frac{\cos(\phi_p)}{w_p}\left(-k_{I,Q,0}+k_{I,Q,1}\right)\Big)\Bigg]. \end{aligned} \tag{3.59}$$

Consequently, we generalize the last equation for all $m$ values so we get

$$\begin{aligned} Y_{I,1,\ell}/(n_{\tau_1},0<\hat{\tau}_1<T_c) = \frac{\hat{c}_{1,t}}{2T_c}\Bigg[ &\cos(\phi_{c_1})\Big(\cos(\phi_p)\Big(k_{I,I,n_{\tau_1}}(2T_c-\hat{\tau}_1)+ \\ &+k_{I,I,n_{\tau_1}+1}(\hat{\tau}_1)\Big)\frac{\sin(\phi_p)}{w_p}\left(-k_{I,I,n_{\tau_1}}+k_{I,I,n_{\tau_1}+1}\right)\Big)- \\ &-\sin(\phi_{c_1})\Big(-\sin(\phi_p)\Big(k_{I,Q,n_{\tau_1}}(T_c-\hat{\tau}_1)+\Big)+ \\ &+k_{I,Q,n_{\tau_1}+1}(T_c+\hat{\tau}_1)+\frac{\cos(\phi_p)}{w_p}\left(-k_{I,Q,n_{\tau_1}}+k_{I,Q,n_{\tau_1}+1}\right)\Big)\Bigg]. \end{aligned} \tag{3.60}$$

The quadrature component of the interferer's received signal (3.34) after substituting

the asynchronized interferer signal (3.10) can be written as

$$
\begin{aligned}
Y_{Q,1,\ell}/(n_{\tau_1}, 0 < \hat{\tau_1} < T_c) = \sqrt{\frac{2}{T_c}}\sqrt{\frac{2}{T_c}}\hat{c}_{1,t}\int_0^{T_s} \Big[ & b_{I,i}(t-\tau_1)\,\cos(w_p(t-\tau_1))\cdot \\
& \cos(w_c t - \phi_{c_1}) - b_{Q,1}(t-\tau_1)\,\sin(w_p(t-\tau_1))\cdot \\
& \sin(w_c t - \phi_{c_1})\Big]\sin(w_c t)\sin(w_p(t))\sum_{m=0}^{15}\hat{b}_{Q,0,l,m}\cdot \\
& h_{T_c}\left(\frac{t\,-\,(2\,(m\,+\,32l)+1)\,T_c}{2T_c}\right)dt = \\
= \frac{2}{T_c}\hat{c}_{1,t}\int_0^{T_s}\Bigg[ & b_{I,1}(t-\tau_1)\,\sin(w_c t)\cos(w_c t - \phi_{c_1})\sin(w_p(t))\cdot \\
& \cos(w_p(t-\tau_1))\sum_{m=0}^{15}\hat{b}_{Q,0,l,m}\,h_{T_c}\left(\frac{t\,-\,(2\,(m\,+\,32l)+1)\,T_c}{2T_c}\right)\Bigg] - \\
\Bigg[ & b_{Q,1}(t-\tau_1)\,\sin(w_c t)\sin(w_c t - \phi_{c_1})\sin(w_p(t))\cdot \\
& \sin(w_p(t-\tau_1))\sum_{m=0}^{15}\hat{b}_{Q,0,l,m}\,h_{T_c}\left(\frac{t\,-\,(2\,(m\,+\,32l)+1)\,T_c}{2T_c}\right)\Bigg]dt,
\end{aligned}
\tag{3.61}
$$

Here we call the first part of the (3.61) as $C_1$ and the second as $D_1$. Figure 3.14 represents $C_1$

$$
\begin{aligned}
C_1 = \int_0^{Ts}\Bigg[ & b_{I,1}(t-\tau_1)\,\sin(w_c t)\cos(w_c t - \phi_{c_1})\sin(w_p(t))\cos(w_p(t-\tau_1))\cdot \\
& \sum_{m=0}^{15}\hat{b}_{Q,0,l,m}\,h_{T_c}\left(\frac{t\,-\,(2\,(m\,+\,32l)+1)\,T_c}{2T_c}\right)\Bigg]dt,
\end{aligned}
\tag{3.62}
$$

and could be computed in the same way A1 and B1 was computed so we get

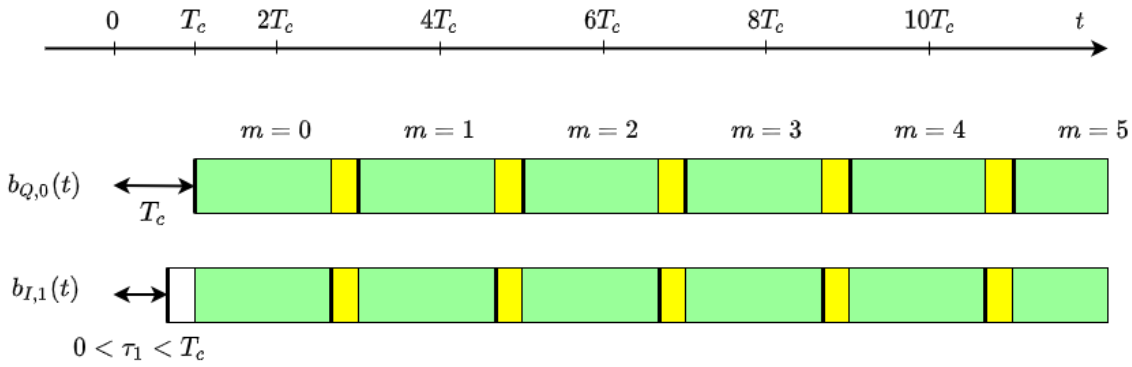


Figure 3.14: An illustration of the reception of the quadrature component of SoI and in-phase component of the interferer when $n_{\tau_1} = 0, 0 < \hat{\tau_1} < T_c$.

$$\begin{aligned} C_1 &= \frac{-1}{2}\sin(\phi_{c_1})\sum_{m=0}^{15}\Bigg[k_{Q,I,0}\int_{(2m+1)T_c}^{(m+1)2T_c+\hat{\tau}_1}\sin(w_p t)\cos(w_p t-\phi_p)dt+ \\ &\qquad + k_{Q,I,-1}\int_{(m+1)2T_c+\hat{\tau}_1}^{(2m+3)T_c}\sin(w_p t)\cos(w_p t-\phi_p)dt\Bigg], \\ &= \frac{-1}{4}\sin(\phi_{c_1})\Bigg[\sin(\phi_p)\Big(k_{Q,I,-1}(T_c-\hat{\tau}_1)+k_{Q,I,0}(T_c+\hat{\tau}_1)\Big)+ \\ &\qquad + \frac{\cos(\phi_p)}{w_p}\Big(k_{Q,I,-1}-k_{Q,I,0}\Big)\Bigg], \end{aligned} \tag{3.63}$$

The second part of (3.61) is $D_1$ which is illustrated in Figure 3.15.

$$\begin{aligned} D_1 = \int_0^{Ts}\Bigg[&b_{Q,1}(t-\tau_1)\,\sin(w_c t)\sin(w_c t-\phi_{c_1})\sin(w_p(t))\sin(w_p(t-\tau_1))\cdot \\ &\sum_{m=0}^{15}\hat{b}_{Q,0,l,m}\,h_{T_c}\left(\frac{t\;-\;(2\,(m\;+\;32l)+1)\,T_c}{2T_c}\right)\Bigg]dt, \end{aligned} \tag{3.64}$$

After some Algebra shown in appendix A we get

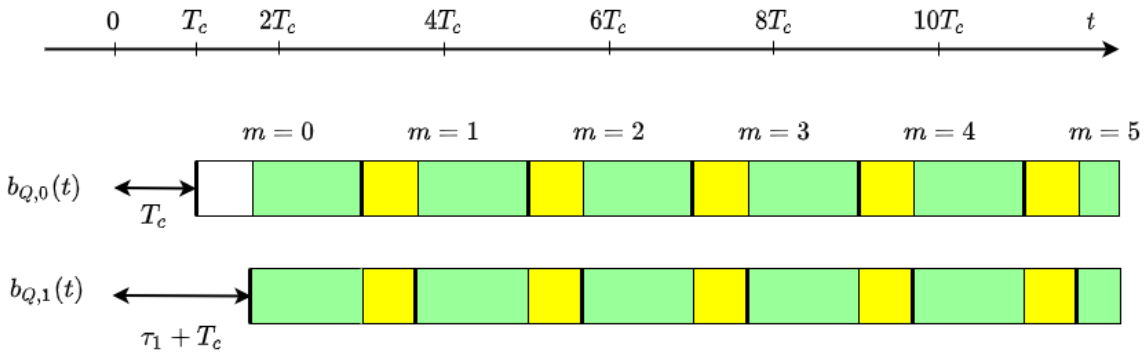


Figure 3.15: An illustration of the reception of the Quadrature component of both SoI and the interferer when $n_{\tau_1} = 0, 0 < \hat{\tau}_1 < T_c$.

$$
\begin{aligned}
D_1 = \frac{1}{2}\cos(\phi_{c_1}) \sum_{m=0}^{15} \Bigg[ & k_{Q,Q,0} \int_{(2m+1)T_c+\hat{\tau}_1}^{(2m+3)T_c} \sin(w_p t)\sin(2w_p t - \phi_p)dt + \\
& k_{Q,Q,1} \int_{(2m+1)T_c}^{(2m+1)T_c+\hat{\tau}_1} \sin(w_p t)\sin(2w_p t - \phi_p)dt \Bigg], \\
= \frac{1}{4}\cos(\phi_{c_1}) \Bigg[ & \cos(\phi_p)\Big(k_{Q,Q,0}(2T_c - \hat{\tau}_1) + k_{Q,Q,1}(\hat{\tau}_1)\Big) + \\
& + \frac{\sin(\phi_p)}{w_p}\Big( - k_{Q,Q,0} + k_{Q,Q,1}\Big)\Bigg].
\end{aligned}
\tag{3.65}
$$

Therefore (3.61) can then be written

$$
\begin{aligned}
Y_{Q,1,\ell}/(0, 0 < \hat{\tau}_1 < T_c) = \frac{\hat{c}_{1,t}}{2T_c}\Bigg[ & - \sin(\phi_{c_1})\Bigg( \sin(\phi_p)\Big(k_{Q,I,-1}(T_c - \hat{\tau}_1) + \\
& + k_{Q,I,0}(T_c + \hat{\tau}_1)\Big) + \frac{\cos(\phi_p)}{w_p}\Big(k_{Q,I,-1} + k_{Q,I,0}\Big)\Bigg) - \\
& - \cos(\phi_{c_1})\Bigg( \cos(\phi_p)\Big(k_{Q,Q,0}(2T_c - \hat{\tau}_1) + \\
& + k_{Q,Q,1}(\hat{\tau}_1)\Big) + \frac{\sin(\phi_p)}{w_p}\Big( - k_{Q,Q,0} + k_{Q,Q,1}\Big)\Bigg)\Bigg].
\end{aligned}
\tag{3.66}
$$

By generalizing the previous procedure to cover all the values of $n_{\tau_1}$ we obtain

$$Y_{Q,1,\ell}/(n_{\tau_1}, 0 < \hat{\tau}_1 < T_c) = \frac{\hat{c}_{1,t}}{2T_c}\Bigg[ - \sin(\phi_{c_1})\Bigg( \sin(\phi_p)\Big(k_{Q,I,n_{\tau_1-1}}(T_c - \hat{\tau}_1) + \\ + k_{Q,I,n_{\tau_1}}(T_c + \hat{\tau}_1)\Big) + \frac{\cos(\phi_p)}{w_p}\Big(k_{Q,I,n_{\tau_1-1}} + k_{Q,I,n_{\tau_1}}\Big)\Bigg) - \\ - \cos(\phi_{c_1})\Bigg( \cos(\phi_p)\Big(k_{Q,Q,n_{\tau_1}}(2T_c - \hat{\tau}_1) + \\ + k_{Q,Q,n_{\tau_1+1}}(\hat{\tau}_1)\Big) + \frac{\sin(\phi_p)}{w_p}\Big( - k_{Q,Q,n_{\tau_1}} + k_{Q,Q,n_{\tau_1+1}}\Big)\Bigg)\Bigg]. \tag{3.67}$$

We can prove that $E[Y_1/n_{\tau_1}] = 0$ (see appendix A). Therefore, the variance of the received interferer's signal in this case would be:

$$\begin{aligned} \sigma^2(Y_1/(n_{\tau_1}, 0 < \hat{\tau}_1 < T_c) &= E[Y_1^2/n_{\tau_1}] - E^2[Y_1/n_{\tau_1}] = E[Y_1^2/n_{\tau_1}] = \\ &= E[Y_{I,1,\ell}^2 + Y_{Q,1,\ell}^2] = E[Y_{I,1,\ell}^2] + E[Y_{I,1,\ell}^2] \\ &= \frac{\hat{c}_{1,t}^2}{4T_c^2}\, E[\mathcal{Z}(\phi_{c_1}, n_{\tau_1}, \hat{\tau}_1)], \end{aligned} \tag{3.68}$$

where $\mathcal{Z}(\phi_{c_1}, n_{\tau_1}, 0 < \hat{\tau}_1 < T_c) = \Big(A_1^2 - 2A_1B_1 + B_1^2 + C_1^2 - 2C_1D_1 + D_1^2\Big)$, which is a function related to the phase offset and the time offset and because of linearity its expected value can be obtain as

$$E[\mathcal{Z}(\phi_{c_1}, n_{\tau_1}, 0 < \hat{\tau}_1 < T_c)] = E[A_1^2] + E[-2A_1B_1] + E[B_1^2] + E[C_1^2] + E[-2C_1D_1] + E[D_1^2], \tag{3.69}$$

We can prove, as in appendix A that $E[\cos^2(\phi_{c_1})] = E[\sin^2(\phi_{c_1})] = \frac{1}{2}$, assuming that the carrier phase $\phi_{c_1}$ is uniformly distributed over its respective range $[0, 2\pi]$, as we said previously, and the time offset is a constant during the period of PPDU

transmission. Thus, we can write

$$E[\mathcal{Z}(\phi_{c_1}, n_{\tau_1}, 0 < \hat{\tau}_1 < T_c)] = \Bigg[\frac{1}{16}\,\frac{1}{2}\Bigg(\Bigg(\cos^2(\phi_p)\,\Big((2T_c - \hat{\tau}_1)^2\,E[k^2_{I,I,n_{\tau_1}}] + (\hat{\tau}_1)^2\cdot$$

$$E[k^2_{I,I,n_{\tau_1+1}}] + 2\,\hat{\tau}_1\,(2T_c - \hat{\tau}_1)\,E[k_{I,I,n_{\tau_1}}k_{I,I,n_{\tau_1+1}}]\Big)\Bigg) + \Bigg(\frac{\sin^2(\phi_p)}{w_p^2}\Big(E[k^2_{I,I,n_{\tau_1}}]+$$

$$E[k^2_{I,I,n_{\tau_1+1}}] - 2E[k_{I,I,n_{\tau_1}}k_{I,I,n_{\tau_1+1}}]\Big)\Bigg) + \Bigg(\frac{\sin(2\phi_p)}{w_p}\,\Big((-2T_c + \hat{\tau}_1)\cdot$$

$$E[k^2_{I,I,n_{\tau_1}}] + \,\hat{\tau}_1 E[k^2_{I,I,n_{\tau_1+1}}] + 2(T_c - \hat{\tau}_1)E[k_{I,I,n_{\tau_1}}k_{I,I,n_{\tau_1+1}}]\Big)\Bigg)\Bigg)\Bigg] +$$

$$+\Bigg[\frac{-1}{16}\,\sin(2\phi_{c_1})\,\Bigg(\frac{-1}{2}\sin(2\phi_p)\,\Bigg((2T_c - \hat{\tau}_1)(T_c - \hat{\tau}_1)E[k_{I,I,n_{\tau_1}}k_{I,Q,n_{\tau_1}}]+$$

$$(2T_c - \hat{\tau}_1)(T_c + \hat{\tau}_1)\;E[k_{I,I,n_{\tau_1}}k_{I,Q,n_{\tau_1+1}}] + \hat{\tau}_1(T_c - \hat{\tau}_1)E[k_{I,I,n_{\tau_1+1}}k_{I,Q,n_{\tau_1}}]+$$

$$\hat{\tau}_1(T_c + \hat{\tau}_1)E[k_{I,I,n_{\tau_1+1}}k_{I,Q,n_{\tau_1+1}}]\Bigg) + \frac{\cos^2(\phi_p)}{w_p}\,\Bigg((-2T_c + \hat{\tau}_1)\cdot$$

$$E[k_{I,I,n_{\tau_1}}k_{I,Q,n_{\tau_1}}] + (2T_c - \hat{\tau}_1)E[k_{I,I,n_{\tau_1}}k_{I,Q,n_{\tau_1+1}}] - \hat{\tau}_1 E[k_{I,I,n_{\tau_1+1}}k_{I,Q,n_{\tau_1}}]+$$

$$+\,\hat{\tau}_1 E[k_{I,I,n_{\tau_1+1}}k_{I,Q,n_{\tau_1+1}}]\Bigg) - \frac{\sin^2(\phi_p)}{w_p}\,\Bigg((-T_c + \hat{\tau}_1)E[k_{I,I,n_{\tau_1}}k_{I,Q,n_{\tau_1}}]-$$

$$-\,(T_c + \hat{\tau}_1)E[k_{I,I,n_{\tau_1}}k_{I,Q,n_{\tau_1+1}}] + (T_c - \hat{\tau}_1)E[k_{I,I,n_{\tau_1+1}}k_{I,Q,n_{\tau_1}}]+$$

$$(T_c + \hat{\tau}_1)E[k_{I,I,n_{\tau_1+1}}k_{I,Q,n_{\tau_1}+1}]\Bigg) + \frac{\sin(2\phi_p)}{2w_p^2}\,\Bigg(E[k_{I,I,n_{\tau_1}}k_{I,Q,n_{\tau_1}}]-$$

$$-\,E[k_{I,I,n_{\tau_1}}k_{I,Q,n_{\tau_1+1}}] - E[k_{I,I,n_{\tau_1+1}}k_{I,Q,n_{\tau_1}}] + E[k_{I,I,n_{\tau_1+1}}k_{I,Q,n_{\tau_1+1}}]\Bigg)\Bigg)\Bigg] +$$

$$+\Bigg[\frac{1}{16}\,\frac{1}{2}\Bigg(\Bigg(\sin^2(\phi_p)\,\Big((T_c - \hat{\tau}_1)^2\,E[k^2_{I,Q,n_{\tau_1}}] + (T_c + \hat{\tau}_1)^2E[k^2_{I,Q,n_{\tau_1+1}}]+$$

$$+\,2\,(T_c - \hat{\tau}_1)\,(T_c + \hat{\tau}_1)\,E[k_{I,Q,n_{\tau_1}}k_{I,Q,n_{\tau_1+1}}]\Big)\Bigg) + \Bigg(\frac{\cos^2(\phi_p)}{w_p^2}\,\Big(E[k^2_{I,Q,n_{\tau_1}}]+$$

$$E[k^2_{I,Q,n_{\tau_1+1}}] - 2E[k_{I,Q,n_{\tau_1}}k_{I,Q,n_{\tau_1+1}}]\Big)\Bigg) + \Bigg(\frac{-\sin(2\phi_p)}{w_p}\,\Big((-T_c + \hat{\tau}_1)\cdot$$

$$E[k^2_{I,Q,n_{\tau_1}}] + \,(T_c + \hat{\tau}_1)E[k^2_{I,Q,n_{\tau_1+1}}] - 2\hat{\tau}_1 E[k_{I,Q,n_{\tau_1}}k_{I,Q,n_{\tau_1+1}}]\Big)\Bigg)\Bigg)+$$

$$+\left[\frac{1}{16}\,\frac{1}{2}\left(\left(\sin^2(\phi_p)\left((T_c-\hat{\tau}_1)^2\,E[k^2_{Q,I,n_{\tau_1-1}}]+(T_c+\hat{\tau}_1)^2E[k^2_{Q,I,n_{\tau_1}}]+\right.\right.\right.$$

$$\left.+2\,(T_c-\hat{\tau}_1)\,(T_c+\hat{\tau}_1)\,E[k_{Q,I,n_{\tau_1-1}}k_{Q,I,n_{\tau_1}}]\right)\Big)+\left(\frac{\cos^2(\phi_p)}{w_p^2}\left(E[k^2_{Q,I,n_{\tau_1}-1}]+\right.$$

$$\left.+E[k^2_{Q,I,n_{\tau_1}}]-2E[k_{Q,I,n_{\tau_1-1}}k_{Q,I,n_{\tau_1}}]\right)\Big)+\left(\frac{\sin(2\phi_p)}{w_p}\left((T_c-\hat{\tau}_1)\cdot\right.\right.$$

$$\left.\left.\left.E[k^2_{Q,I,n_{\tau_1-1}}]-\,(T_c+\hat{\tau}_1)E[k^2_{Q,I,n_{\tau_1}}]+2(\hat{\tau}_1)\,E[k_{Q,I,n_{\tau_1-1}}k_{Q,I,n_{\tau_1}}]\right)\Big)\Big)\Big)\right]+$$

$$+\left[\frac{1}{16}\,\sin(2\phi_{c_1})\left(\frac{1}{2}\sin(2\phi_p)\left((T_c-\hat{\tau}_1)(2T_c-\hat{\tau}_1)E[k_{Q,I,n_{\tau_1-1}}k_{Q,Q,n_{\tau_1}}]+\right.\right.\right.$$

$$(T_c-\hat{\tau}_1)(\hat{\tau}_1)\;E[k_{Q,I,n_{\tau_1-1}}k_{Q,Q,n_{\tau_1+1}}]+(T_c+\hat{\tau}_1)(2T_c-\hat{\tau}_1)E[k_{Q,I,n_{\tau_1}}k_{Q,Q,n_{\tau_1}}]+$$

$$\left.\hat{\tau}_1(T_c+\hat{\tau}_1)E[k_{Q,I,n_{\tau_1}}k_{Q,Q,n_{\tau_1+1}}]\right)+\frac{\sin^2(\phi_p)}{w_p}\left((-T_c+\hat{\tau}_1)E[k_{Q,I,n_{\tau_1-1}}k_{Q,Q,n_{\tau_1}}]+\right.$$

$$+(T_c-\hat{\tau}_1)E[k_{Q,I,n_{\tau_1-1}}k_{Q,Q,n_{\tau_1+1}}]-(T_c+\hat{\tau}_1)E[k_{Q,I,n_{\tau_1}}k_{Q,Q,n_{\tau_1}}]+$$

$$\left.(T_c+\hat{\tau}_1)\;E[k_{Q,I,n_{\tau_1}}k_{Q,Q,n_{\tau_1+1}}]\right)+\frac{\cos^2(\phi_p)}{w_p}\left((2T_c-\hat{\tau}_1)E[k_{Q,I,n_{\tau_1-1}}k_{Q,Q,n_{\tau_1}}]\right.$$

$$+(\hat{\tau}_1)E[k_{Q,I,n_{\tau_1-1}}k_{Q,Q,n_{\tau_1+1}}]-(2T_c-\hat{\tau}_1)E[k_{Q,I,n_{\tau_1}}k_{Q,Q,n_{\tau_1}}]-$$

$$\left.(\hat{\tau}_1)E[k_{Q,I,n_{\tau_1}}k_{Q,Q,n_{\tau_1+1}}]\right)+\frac{\sin(2\phi_p)}{2w_p^2}\left(-E[k_{Q,I,n_{\tau_1-1}}k_{Q,Q,n_{\tau_1}}]+\right.$$

$$\left.\left.+E[k_{Q,I,n_{\tau_1-1}}k_{Q,Q,n_{\tau_1+1}}]+E[k_{Q,I,n_{\tau_1}}k_{Q,Q,n_{\tau_1}}]-E[k_{Q,I,n_{\tau_1}}k_{Q,Q,n_{\tau_1+1}}]\right)\right)\Big)\Big]+$$

$$+\left[\frac{1}{16}\,\frac{1}{2}\left(\left(\cos^2(\phi_p)\left((2T_c-\hat{\tau}_1)^2\,E[k^2_{Q,Q,n_{\tau_1}}]+(\hat{\tau}_1)^2E[k^2_{Q,Q,n_{\tau_1+1}}]+\right.\right.\right.$$

$$\left.+2\,(2T_c-\hat{\tau}_1)\,(\hat{\tau}_1)\,E[k_{Q,Q,n_{\tau_1}}k_{Q,Q,n_{\tau_1+1}}]\right)\Big)+\left(\frac{\sin^2(\phi_p)}{w_p^2}\left(E[k^2_{Q,Q,n_{\tau_1}}]+\right.$$

$$\left.E[k^2_{Q,Q,n_{\tau_1+1}}]-2E[k_{Q,Q,n_{\tau_1}}k_{Q,Q,n_{\tau_1+1}}]\right)\Big)+\left(\frac{\sin(2\phi_p)}{w_p}\left((-2T_c+\hat{\tau}_1)\cdot\right.\right.$$

$$\left.\left.\left.E[k^2_{Q,Q,n_{\tau_1}}]+\,(\hat{\tau}_1)E[k^2_{Q,Q,n_{\tau_1+1}}]+2(T_c-\hat{\tau}_1)E[k_{Q,Q,n_{\tau_1}}k_{Q,Q,n_{\tau_1+1}}]\right)\Big)\Big)\Big)\right], \tag{3.70}$$

Let's now discover how I and Q components of the received interfering signal change if the $T_c < \hat{\tau}_1 < 2T_c$.

**3.2.3.1.3 Case 2** $T_c < \hat{\tau}_1 < 2T_c$ We apply the same line of reasoning of the previous case, i.e when $0 < \hat{\tau}_1 < T_c$. For the sake of distinction, we call the parts of the I and Q components by $A_2, B_2, C_2, D_2$. We start with A2 which is illustrated in Figure 3.16 and its

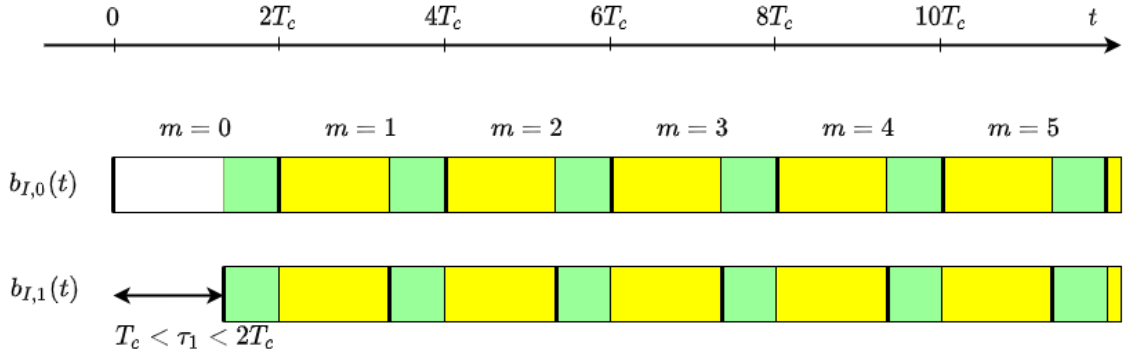


Figure 3.16: An illustration of the reception of the I-phase component of both SoI and the interferer when $n_{\tau_1} = 0, T_c < \hat{\tau}_1 < 2T_c$.

$$A_2 = \frac{1}{2}\cos(\phi_{c_1}) \sum_{m=0}^{15} \Bigg[ k_{I,I,0} \int_{2mT_c+\hat{\tau}_1}^{(m+1)2T_c} \cos(w_p t)\cos(w_p t - \phi_p)dt + k_{I,I,1} \int_{2mT_c}^{2mT_c+\hat{\tau}_1} \cos(w_p t)\cos(w_p t - \phi_p)dt \Bigg],$$

$$= \frac{1}{4}\cos(\phi_{c_1}) \Bigg[ \cos(\phi_p)\Big(k_{I,I,0}(2T_c - \hat{\tau}_1) + k_{I,I,1}(\hat{\tau}_1)\Big) + \frac{\sin(\phi_p)}{w_p}\Big( - k_{I,I,0} + k_{I,I,1}\Big)\Bigg] \tag{3.71}$$

We notice that it has the same value of $A_1$. Figure 3.17 shows the second part of the I-phase component of the received interfering signal $B_2$. We realize that the interferer's chips misaligned the SoI chips by 1 or 2 chips. Thus, it is different form the previous case $B_1$ where the misalignment is 0 or 1. I use the green color to indicate no misalignment, yellow color to show a misalignment of 1, and a red color

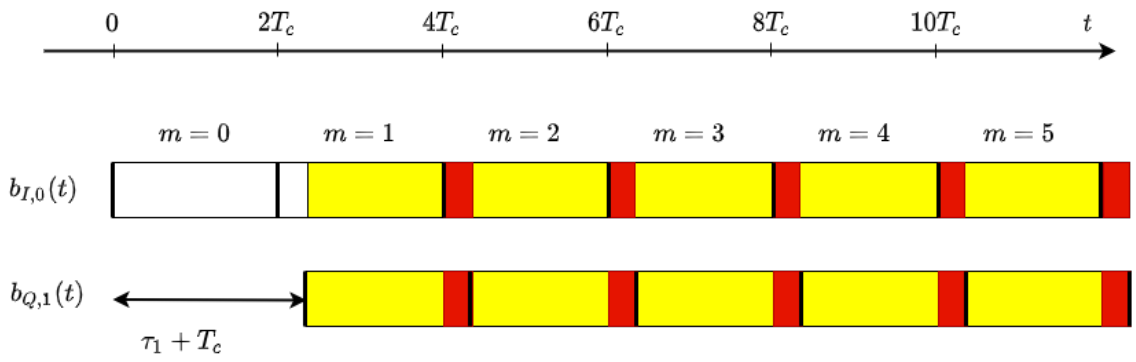


Figure 3.17: An illustration of the reception of the I-phase component of the SoI and the quadrature component of the interferer when $n_{\tau_1} = 0, T_c < \hat{\tau}_1 < 2T_c$.

to denote a misalignment of 2. The value of $B_2$ could be written as

$$\begin{aligned} B_2 = \frac{1}{2}\sin(\phi_{c_1}) \sum_{m=0}^{15} \Bigg[ & k_{I,Q,1} \int_{(2m-1)T_c+\hat{\tau}_1}^{(m+1)2T_c} \sin(w_p t - \phi_p)\cos(w_p t)dt + \\ & + k_{I,Q,2} \int_{2mT_c}^{(2m-1)T_c+\hat{\tau}_1} \sin(w_p t - \phi_p)\cos(w_p t)dt \Bigg], \\ = \frac{1}{4}\sin(\phi_{c_1}) \Bigg[ & -\sin(\phi_p)\Big(k_{I,Q,1}(3T_c - \hat{\tau}_1) + k_{I,Q,2}(-T_c + \hat{\tau}_1)\Big) + \\ & + \frac{\cos(\phi_p)}{w_p}\Big(-k_{I,Q,1} + k_{I,Q,2}\Big)\Bigg], \end{aligned} \tag{3.72}$$

Therefore, in this case, the I phase component of the received interferer signal is written as $Y_{I,1,\ell} = \frac{2\hat{c}_{1,t}}{T_c}(A_2 - B_2)$ so

$$\begin{aligned} Y_{I,1,\ell}/(0, T_c < \hat{\tau}_1 < 2T_c) = \frac{\hat{c}_{1,t}}{2T_c} \Bigg[ & \cos(\phi_{c_1})\Big(\cos(\phi_p)\left(k_{I,I,0}(2T_c - \hat{\tau}_1) + k_{I,I,1}(\hat{\tau}_1)\right) + \\ & \frac{\sin(\phi_p)}{w_p}\left(-k_{I,I,0} + k_{I,I,1}\right)\Big) - \sin(\phi_{c_1}) \cdot \\ & \Big(-\sin(\phi_p)\left(k_{I,Q,1}(3T_c - \hat{\tau}_1) + k_{I,Q,2}(-T_c + \hat{\tau}_1)\right) + \\ & + \frac{\cos(\phi_p)}{w_p}\left(-k_{I,Q,1} + k_{I,Q,2}\right)\Big)\Bigg]. \end{aligned} \tag{3.73}$$

Therefore, $Y_{I,1,\ell,m}$ can be written as

$$Y_{I,1,\ell}/(n_{\tau_1}, T_c < \hat{\tau}_1 < 2T_c) = \frac{\hat{c}_{1,t}}{2T_c}\Bigg[\cos(\phi_{c_1})\Big(\cos(\phi_p)\Big(k_{I,I,n_{\tau_1}}(2T_c - \hat{\tau}_1) + \\ + k_{I,I,n_{\tau_1+1}}(\hat{\tau}_1)\Big) + \frac{\sin(\phi_p)}{w_p}\left(-k_{I,I,n_{\tau_1}} + k_{I,I,n_{\tau_1+1}}\right)\Big) - \\ - \sin(\phi_{c_1})\Big(-\sin(\phi_p)\Big(k_{I,Q,n_{\tau_1+1}}(3T_c - \hat{\tau}_1) + k_{I,Q,n_{\tau_1+2}}. \\ (-T_c + \hat{\tau}_1)\Big) + \frac{\cos(\phi_p)}{w_p}\left(-k_{I,Q,n_{\tau_1+1}} + k_{I,Q,n_{\tau_1+2}}\right)\Big)\Bigg]. \tag{3.74}$$

The Q component of the received interferer signal is written as $Y_{Q,1,\ell} = \frac{2\hat{c}_{1,t}}{T_c}(C_2 - D_2)$, where $C_2$ is the part of $Y_{Q,1,\ell,m}$ which represents the product of the Q component of the received SoI and the I component of the received interferer signal and $D_2$ is the second part of $Y_{Q,1,\ell,m}$ representing the product of the Q component of both received signal of the SoI and the interferer. Figure 3.18 shows how the Q-phase and I-phase of the transmitter and the interferer respectively are correlated. Equation (3.75) reported the value of $C_2$.

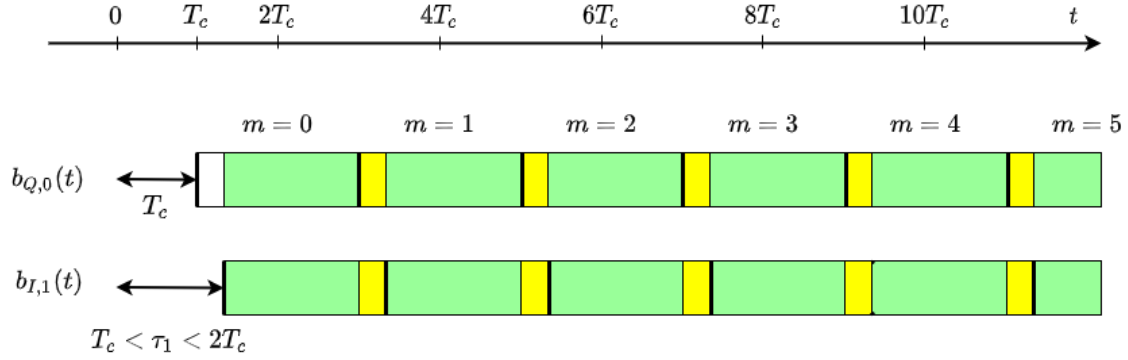


Figure 3.18: An illustration of the reception of the Quadrature component of the SoI and the I-phase component of the interferer when $n_{\tau_1} = 0, T_c < \hat{\tau}_1 < 2T_c$.

$$
\begin{aligned}
C_2 &= \frac{-1}{2}\sin(\phi_{c_1})\sum_{m=0}^{15}\Bigg[k_{Q,I,0}\int_{2mT_c+\hat{\tau}_1}^{(2m+3)T_c}\sin(w_pt)\cos(w_pt-\phi_p)dt+ \\
&\qquad + k_{Q,I,1}\int_{(2m+1)T_c}^{2mT_c+\hat{\tau}_1}\sin(w_pt)\cos(w_pt-\phi_p)dt\Bigg], \\
&= \frac{-1}{4}\sin(\phi_{c_1})\Bigg[\sin(\phi_p)\Big(k_{Q,I,0}(3T_c-\hat{\tau}_1)+k_{Q,I,1}(-T_c+\hat{\tau}_1)\Big)+ \\
&\qquad + \frac{\cos(\phi_p)}{w_p}\Big(k_{Q,I,0}-k_{Q,I,1}\Big)\Bigg],
\end{aligned}
\tag{3.75}
$$

Now Figure 3.19 describes the reception of the Q component of both the SoI and the interferer, and (3.76) reports its value.

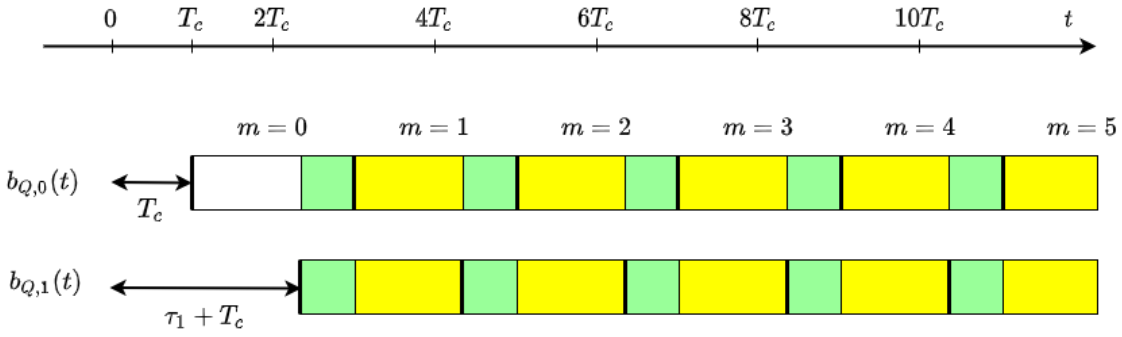


Figure 3.19: An illustration of the reception of the Quadrature component of both SoI and the interferer when $n_{\tau_1}=0, T_c<\hat{\tau}_1<2T_c$.

$$
\begin{aligned}
D_2 &= \frac{1}{2}\cos(\phi_{c_1})\sum_{m=0}^{15}\Bigg[k_{Q,Q,0}\int_{(2m+1)T_c+\hat{\tau}_1}^{(2m+3)T_c}\sin(w_pt)\sin(w_pt-\phi_p)dt+ \\
&\qquad k_{Q,Q,1}\int_{(2m+1)T_c}^{(2m+1)T_c+\hat{\tau}_1}\sin(w_pt)\sin(w_pt-\phi_p)dt\Bigg], \\
&= \frac{1}{4}\cos(\phi_{c_1})\Bigg[\cos(\phi_p)\Big(k_{Q,Q,0}(2T_c-\hat{\tau}_1)+k_{Q,Q,1}(\hat{\tau}_1)\Big)+ \\
&\qquad + \frac{\sin(\phi_p)}{w_p}\Big(-k_{Q,Q,0}+k_{Q,Q,1}\Big)\Bigg]
\end{aligned}
\tag{3.76}
$$

Therefore, the Q component of the interferer's received signal is

$$Y_{Q,1,\ell}/(0, T_c < \hat{\tau}_1 < 2T_c) = \frac{\hat{c}_{1,t}}{2T_c}\Bigg[ - \sin(\phi_{c_1})\Bigg( \sin(\phi_p)\Big(k_{Q,I,0}(3T_c - \hat{\tau}_1) + \\ + k_{Q,I,1}(-T_c + \hat{\tau}_1)\Big) + \frac{\cos(\phi_p)}{w_p}\Big(k_{Q,I,0} - k_{Q,I,1}\Big)\Bigg) - \\ - \cos(\phi_{c_1})\Bigg( \cos(\phi_p)\Big(k_{Q,Q,0}(2T_c - \hat{\tau}_1) + k_{Q,Q,1}(\hat{\tau}_1)\Big) + \\ + \frac{\sin(\phi_p)}{w_p}\Big( - k_{Q,Q,0} + k_{Q,Q,1}\Big)\Bigg)\Bigg]. \tag{3.77}$$

Thus, for any value of $n_{\tau_1}$ we obtain

$$Y_{Q,1,\ell}/(n_{\tau_1}, T_c < \hat{\tau}_1 < 2T_c) = \frac{\hat{c}_{1,t}}{2T_c}\Bigg[ - \sin(\phi_{c_1})\Bigg( \sin(\phi_p)\Big(k_{Q,I,n_{\tau_1}}(3T_c - \hat{\tau}_1) + \\ + k_{Q,I,n_{\tau_1}+1}(-T_c + \hat{\tau}_1)\Big) + \frac{\cos(\phi_p)}{w_p}\Big(k_{Q,I,n_{\tau_1}} - k_{Q,I,n_{\tau_1}+1}\Big)\Bigg) - \\ - \cos(\phi_{c_1})\Bigg( \cos(\phi_p)\Big(k_{Q,Q,n_{\tau_1}}(2T_c - \hat{\tau}_1) + k_{Q,Q,n_{\tau_1}+1}(\hat{\tau}_1)\Big) + \\ + \frac{\sin(\phi_p)}{w_p}\Big( - k_{Q,Q,n_{\tau_1}} + k_{Q,Q,n_{\tau_1}+1}\Big)\Bigg)\Bigg]. \tag{3.78}$$

The variance in this case is computed as in the previous case

$$\sigma^2(Y_1/(n_{\tau_1}, T_c < \hat{\tau}_1 < 2T_c)) = \frac{\hat{c}_{1,t}^2}{4T_c^2}\, E[\mathcal{Z}(\phi_{c_1}, n_{\tau_1}, T_c < \hat{\tau}_1 < 2T_c)], \tag{3.79}$$

where $\mathcal{Z}(\phi_{c_1}, n_{\tau_1}, T_c < \hat{\tau}_1 < 2T_c) = \Big(A_2^2 - 2A_2B_2 + B_2^2 + C_2^2 - 2C_2D_2 + D_2^2\Big)$with an expected value obtained as

$$E[\mathcal{Z}(\phi_{c_1}, n_{\tau_1}, T_c < \hat{\tau}_1 < 2T_c)] = E[A_2^2] + E[-2A_2B_2] + E[B_2^2] + E[C_2^2] + E[-2C_2D_2] + E[D_2^2] \tag{3.80}$$

$$E[\mathcal{Z}(\phi_{c_1}, n_{\tau_1}, T_c < \hat{\tau}_1 < 2T_c)] = \Bigg[\frac{1}{16}\,\frac{1}{2}\Bigg(\Bigg(\cos^2(\phi_p)\,\Big((2T_c - \hat{\tau}_1)^2\,E[k^2_{I,I,n_{\tau_1}}] + (\hat{\tau}_1)^2\cdot$$

$$E[k^2_{I,I,n_{\tau_1+1}}] + 2\,\hat{\tau}_1\,(2T_c - \hat{\tau}_1)\,E[k_{I,I,n_{\tau_1}}k_{I,I,n_{\tau_1+1}}]\Big)\Bigg) + \Bigg(\frac{\sin^2(\phi_p)}{w_p^2}\,\Big(E[k^2_{I,I,n_{\tau_1}}]+$$

$$E[k^2_{I,I,n_{\tau_1+1}}] - 2E[k_{I,I,n_{\tau_1}}k_{I,I,n_{\tau_1+1}}]\Big)\Bigg) + \Bigg(\frac{\sin(2\phi_p)}{w_p}\,\Big((-2T_c + \hat{\tau}_1)\cdot$$

$$E[k^2_{I,I,n_{\tau_1}}] + \hat{\tau}_1 E[k^2_{I,I,n_{\tau_1+1}}] + 2(T_c - \hat{\tau}_1)E[k_{I,I,n_{\tau_1}}k_{I,I,n_{\tau_1+1}}]\Big)\Bigg)\Bigg)\Bigg] +$$

$$+\Bigg[\frac{-1}{16}\,\sin(2\phi_{c_1})\,\Bigg(\frac{-1}{2}\sin(2\phi_p)\,\Bigg((2T_c - \hat{\tau}_1)(3T_c - \hat{\tau}_1)E[k_{I,I,n_{\tau_1}}k_{I,Q,n_{\tau_1+1}}]+$$

$$(2T_c - \hat{\tau}_1)(-T_c + \hat{\tau}_1)\;E[k_{I,I,n_{\tau_1}}k_{I,Q,n_{\tau_1+2}}] + \hat{\tau}_1(3T_c - \hat{\tau}_1)E[k_{I,I,n_{\tau_1+1}}k_{I,Q,n_{\tau_1+1}}]+$$

$$\hat{\tau}_1(-T_c + \hat{\tau}_1)E[k_{I,I,n_{\tau_1+1}}k_{I,Q,n_{\tau_1+2}}]\Bigg) + \frac{\cos^2(\phi_p)}{w_p}\,\Bigg((-2T_c + \hat{\tau}_1)\cdot$$

$$E[k_{I,I,n_{\tau_1}}k_{I,Q,n_{\tau_1+1}}] + (2T_c - \hat{\tau}_1)E[k_{I,I,n_{\tau_1}}k_{I,Q,n_{\tau_1+2}}] - \hat{\tau}_1 E[k_{I,I,n_{\tau_1+1}}k_{I,Q,n_{\tau_1+1}}]+$$

$$+\,\hat{\tau}_1 E[k_{I,I,n_{\tau_1+1}}k_{I,Q,n_{\tau_1+2}}]\Bigg) - \frac{\sin^2(\phi_p)}{w_p}\,\Bigg((-3T_c + \hat{\tau}_1)E[k_{I,I,n_{\tau_1}}k_{I,Q,n_{\tau_1+1}}]-$$

$$-\,(-T_c + \hat{\tau}_1)E[k_{I,I,n_{\tau_1}}k_{I,Q,n_{\tau_1+2}}] + (3T_c - \hat{\tau}_1)E[k_{I,I,n_{\tau_1+1}}k_{I,Q,n_{\tau_1+1}}]+$$

$$(-T_c + \hat{\tau}_1)E[k_{I,I,n_{\tau_1+1}}k_{I,Q,n_{\tau_1}+2}]\Bigg) + \frac{\sin(2\phi_p)}{2w_p^2}\,\Bigg(E[k_{I,I,n_{\tau_1}}k_{I,Q,n_{\tau_1+1}}]-$$

$$-\,E[k_{I,I,n_{\tau_1}}k_{I,Q,n_{\tau_1+2}}] - E[k_{I,I,n_{\tau_1+1}}k_{I,Q,n_{\tau_1+1}}] + E[k_{I,I,n_{\tau_1+1}}k_{I,Q,n_{\tau_1+2}}]\Bigg)\Bigg)\Bigg] +$$

$$+\Bigg[\frac{1}{16}\,\frac{1}{2}\Bigg(\Bigg(\sin^2(\phi_p)\,\Big((3T_c - \hat{\tau}_1)^2\,E[k^2_{I,Q,n_{\tau_1+1}}] + (-T_c + \hat{\tau}_1)^2E[k^2_{I,Q,n_{\tau_1+2}}]+$$

$$+\,2\,(3T_c - \hat{\tau}_1)\,(-T_c + \hat{\tau}_1)\,E[k_{I,Q,n_{\tau_1+1}}k_{I,Q,n_{\tau_1+2}}]\Big)\Bigg) + \Bigg(\frac{\cos^2(\phi_p)}{w_p^2}\,\Big(E[k^2_{I,Q,n_{\tau_1+1}}]+$$

$$+\,E[k^2_{I,Q,n_{\tau_1+2}}] - 2E[k_{I,Q,n_{\tau_1+1}}k_{I,Q,n_{\tau_1+2}}]\Big)\Bigg) - \Bigg(\frac{\sin(2\phi_p)}{w_p}\,\Big((-3T_c + \hat{\tau}_1)E[k^2_{I,Q,n_{\tau_1+1}}]+$$

$$+\;(-T_c + \hat{\tau}_1)E[k^2_{I,Q,n_{\tau_1+2}}] + 2\,(2T_c - \hat{\tau}_1)\,E[k_{I,Q,n_{\tau_1+1}}k_{I,Q,n_{\tau_1+2}}]\Big)\Bigg)\Bigg)\Bigg] +$$

$$
+\left[\frac{1}{16}\,\frac{1}{2}\left(\left(\sin^2(\phi_p)\left((3T_c-\hat{\tau}_1)^2\,E[k^2_{Q,I,n_{\tau_1}}]+(-T_c+\hat{\tau}_1)^2E[k^2_{Q,I,n_{\tau_1+1}}]+\right.\right.\right.\right.
$$

$$
\left.+\,2\,(3T_c-\hat{\tau}_1)\,(-T_c+\hat{\tau}_1)\,E[k_{Q,I,n_{\tau_1}}k_{Q,I,n_{\tau_1+1}}]\right)\Bigg)+\left(\frac{\cos^2(\phi_p)}{w_p^2}\left(E[k^2_{Q,I,n_{\tau_1}}]+\right.\right.
$$

$$
\left.\left.+\,E[k^2_{Q,I,n_{\tau_1+1}}]-2E[k_{Q,I,n_{\tau_1}}k_{Q,I,n_{\tau_1+1}}]\right)\right)+\left(\frac{\sin(2\phi_p)}{w_p}\left((3T_c-\hat{\tau}_1)E[k^2_{Q,I,n_{\tau_1}}]-\right.\right.
$$

$$
\left.\left.\left.\left.-\;(-T_c+\hat{\tau}_1)E[k^2_{Q,I,n_{\tau_1+1}}]-2\,(2T_c-\hat{\tau}_1)\,E[k_{Q,I,n_{\tau_1}}k_{Q,I,n_{\tau_1+1}}]\right)\right)\right)\right]+
$$

$$
+\left[\frac{1}{16}\,\sin(2\phi_{c_1})\left(\frac{1}{2}\sin(2\phi_p)\left((3T_c-\hat{\tau}_1)(2T_c-\hat{\tau}_1)E[k_{Q,I,n_{\tau_1}}k_{Q,Q,n_{\tau_1}}]+\right.\right.\right.
$$

$$
(3T_c-\hat{\tau}_1)(\hat{\tau}_1)\;E[k_{Q,I,n_{\tau_1}}k_{Q,Q,n_{\tau_1+1}}]+(-T_c+\hat{\tau}_1)(2T_c-\hat{\tau}_1)E[k_{Q,I,n_{\tau_1+1}}k_{Q,Q,n_{\tau_1}}]+
$$

$$
\left.\hat{\tau}_1(-T_c+\hat{\tau}_1)E[k_{Q,I,n_{\tau_1+1}}k_{Q,Q,n_{\tau_1+1}}]\right)+\frac{\sin^2(\phi_p)}{w_p}\left((-3T_c+\hat{\tau}_1)E[k_{Q,I,n_{\tau_1}}k_{Q,Q,n_{\tau_1}}]+\right.
$$

$$
+\,(3T_c-\hat{\tau}_1)E[k_{Q,I,n_{\tau_1}}k_{Q,Q,n_{\tau_1+1}}]-(-T_c+\hat{\tau}_1)E[k_{Q,I,n_{\tau_1+1}}k_{Q,Q,n_{\tau_1}}]+
$$

$$
\left.(-T_c+\hat{\tau}_1)\;E[k_{Q,I,n_{\tau_1+1}}k_{Q,Q,n_{\tau_1+1}}]\right)+\frac{\cos^2(\phi_p)}{w_p}\left((2T_c-\hat{\tau}_1)E[k_{Q,I,n_{\tau_1}}k_{Q,Q,n_{\tau_1}}]\right.
$$

$$
+\,(\hat{\tau}_1)E[k_{Q,I,n_{\tau_1}}k_{Q,Q,n_{\tau_1+1}}]-(2T_c-\hat{\tau}_1)E[k_{Q,I,n_{\tau_1+1}}k_{Q,Q,n_{\tau_1}}]-(\hat{\tau}_1)\cdot
$$

$$
E[k_{Q,I,n_{\tau_1+1}}k_{Q,Q,n_{\tau_1+1}}]\Bigg)+\frac{\sin(2\phi_p)}{2w_p^2}\Bigg(-E[k_{Q,I,n_{\tau_1}}k_{Q,Q,n_{\tau_1}}]+E[k_{Q,I,n_{\tau_1}}k_{Q,Q,n_{\tau_1+1}}]
$$

$$
\left.\left.\left.+\,E[k_{Q,I,n_{\tau_1+1}}k_{Q,Q,n_{\tau_1}}]-E[k_{Q,I,n_{\tau_1+1}}k_{Q,Q,n_{\tau_1+1}}]\right)\right)\right]+
$$

$$
+\left[\frac{1}{16}\,\frac{1}{2}\left(\left(\cos^2(\phi_p)\left((2T_c-\hat{\tau}_1)^2\,E[k^2_{Q,Q,n_{\tau_1}}]+(\hat{\tau}_1)^2E[k^2_{Q,Q,n_{\tau_1+1}}]+\right.\right.\right.\right.
$$

$$
\left.+\,2\,(2T_c-\hat{\tau}_1)\,(\hat{\tau}_1)\,E[k_{Q,Q,n_{\tau_1}}k_{Q,Q,n_{\tau_1+1}}]\right)\Bigg)+\left(\frac{\sin^2(\phi_p)}{w_p^2}\left(E[k^2_{Q,Q,n_{\tau_1}}]+\right.\right.
$$

$$
E[k^2_{Q,Q,n_{\tau_1+1}}]-2E[k_{Q,Q,n_{\tau_1}}k_{Q,Q,n_{\tau_1+1}}]\Big)\Bigg)+\left(\frac{\sin(2\phi_p)}{w_p}\left((-2T_c+\hat{\tau}_1)\cdot\right.\right.
$$

$$
\left.\left.\left.E[k^2_{Q,Q,n_{\tau_1}}]+\;(\hat{\tau}_1)E[k^2_{Q,Q,n_{\tau_1+1}}]+2\,(T_c-\hat{\tau}_1)E[k_{Q,Q,n_{\tau_1}}k_{Q,Q,n_{\tau_1+1}}]\right)\right)\right)\right],
\tag{3.81}
$$

**3.2.3.1.4 Case 3** $\hat{\tau}_1 = T_c$ Following the same line of reasoning to get the I-phase and the Q phase in this case and assuming that $n_{\tau_1} = 0$ we get Figures 3.20, 3.21 which represent the illustration of the reception of both I components of SoI and the interferer and the reception of I component of SoI and Q component of the interferer respectively. Thus, the I component of the received interferer signal is $Y_{I,1,\ell} = \frac{2\,\hat{c}_{1,t}}{T_c}\,(A_3 - B_3)$, where

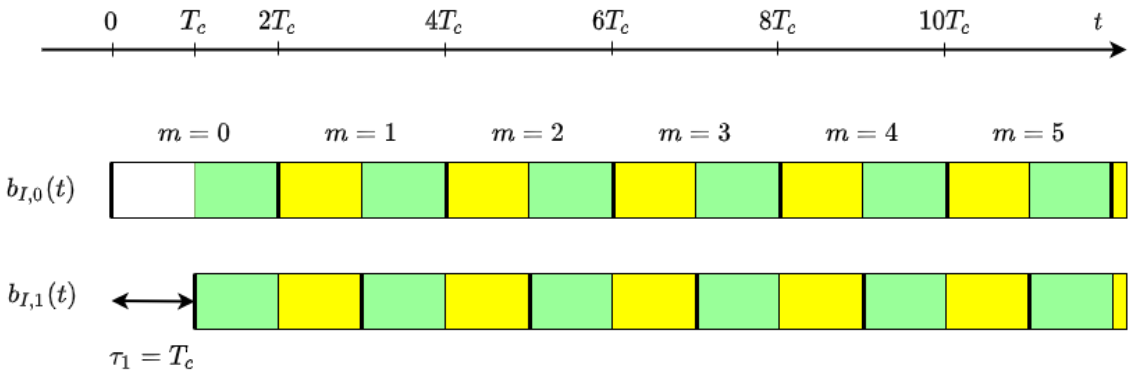


Figure 3.20: An illustration of the reception of the I-phase component of both SoI and the interferer when $n_{\tau_1} = 0, \hat{\tau}_1 = T_c$.

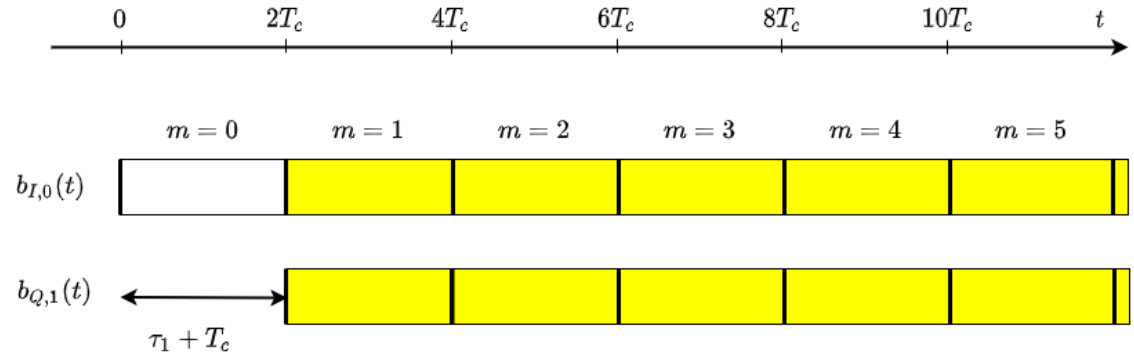


Figure 3.21: An illustration of the reception of the I-phase component of SoI and Quadrature component of the interferer when $n_{\tau_1} = 0, \hat{\tau}_1 = T_c$.

$$A_3 = \frac{1}{4}\cos(\phi_{c_1})\Bigg[\cos(\phi_p)\,(T_c)\Big(k_{I,I,n_{\tau_1}} + k_{I,I,n_{\tau_1+1}}\Big) + \frac{\sin(\phi_p)}{w_p}\Big(-k_{I,I,n_{\tau_1}} + k_{I,I,n_{\tau_1+1}}\Big)\Bigg] \tag{3.82}$$

$$B_3 = \frac{1}{4}\sin(\phi_{c_1})\Bigg[ -\sin(\phi_p)\,(2Tc)\,k_{I,I,n_{\tau_1+1}}\Bigg], \tag{3.83}$$

Thus, we obtain

$$\begin{aligned} Y_{I,1,\ell}/(n_{\tau_1}, \hat{\tau}_1 = T_c) = \frac{\hat{c}_{1,t}}{2T_c}\Bigg[ \cos(\phi_{c_1})\Bigg( \cos(\phi_p)\Big(k_{I,I,n_{\tau_1}} + k_{I,I,n_{\tau_1+1}}\Big) + \\ \frac{\sin(\phi_p)}{w_p}\Big( -k_{I,I,n_{\tau_1}} + k_{I,I,n_{\tau_1+1}}\Big)\Bigg) - \\ -\sin(\phi_{c_1})\Bigg( -\sin(\phi_p)\,(2Tc)\,k_{I,I,n_{\tau_1+1}}\Bigg)\Bigg]. \end{aligned} \tag{3.84}$$

Figures 3.22, 3.23 represent the illustration of the reception of Q component of SoI and I component of the interferer and the reception of both Q components of SoI and the interferer respectively. Thus, the Q component of the received interferer signal is $Y_{Q,1,\ell} = \frac{2\hat{c}_{1,t}}{T_c}(C_3 - D_3)$, where

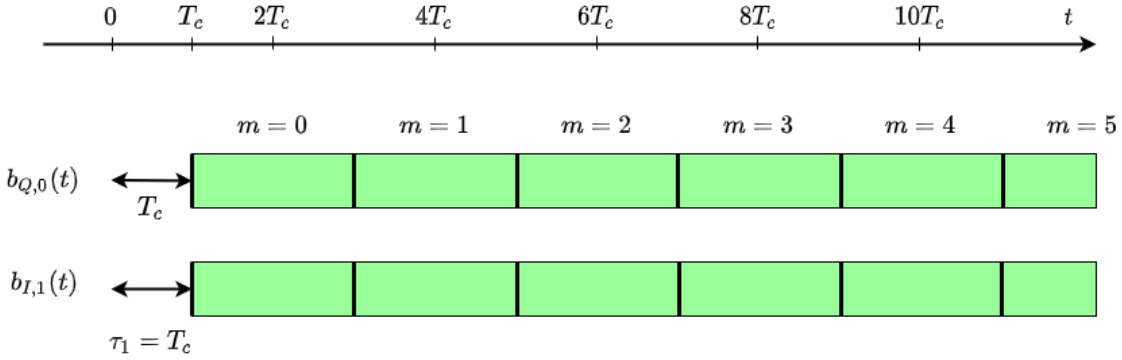


Figure 3.22: An illustration of the reception of the Quadrature component of SoI and I-phase component of the interferer when $n_{\tau_1} = 0, \hat{\tau}_1 = T_c$.

$$C_3 = \frac{-1}{4}\sin(\phi_{c_1})\Bigg[\sin(\phi_p)\,(2Tc)\,k_{Q,I,n_{\tau_1}}\Bigg], \tag{3.85}$$

$$\begin{aligned} D_3 = \frac{1}{4}\cos(\phi_{c_1})\Bigg[\cos(\phi_p)\,(T_c)\Big(k_{Q,Q,n_{\tau_1}} + k_{Q,Q,n_{\tau_1+1}}\Big) + \\ \frac{\sin(\phi_p)}{w_p}\Big( -k_{Q,Q,n_{\tau_1}} + k_{Q,Q,n_{\tau_1+1}}\Big)\Bigg] \end{aligned} \tag{3.86}$$

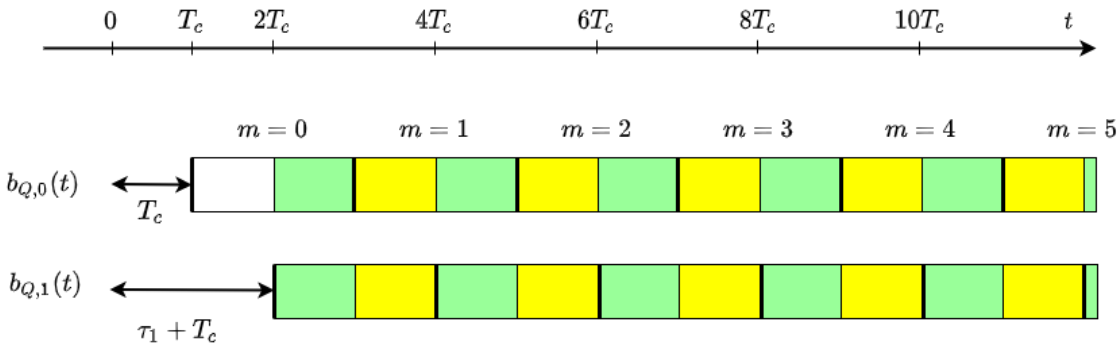


Figure 3.23: An illustration of the reception of the Quadrature component of both SoI and the interferer when $n_{\tau_1} = 0, \hat{\tau}_1 = T_c$.

$$Y_{Q,1,\ell}/(n_{\tau_1}, \hat{\tau}_1 = T_c) = \frac{\hat{c}_{1,t}}{2T_c}\Bigg[ - \sin(\phi_{c_1})\Bigg( \sin(\phi_p)\,(2Tc)\,k_{Q,I,n_{\tau_1}}\Bigg) - \\ - \cos(\phi_{c_1})\Bigg( \cos(\phi_p)\,(T_c)\Big(k_{Q,Q,n_{\tau_1}} + k_{Q,Q,n_{\tau_1}+1}\Big) + \\ \frac{\sin(\phi_p)}{w_p}\Big( - k_{Q,Q,n_{\tau_1}} + k_{Q,Q,n_{\tau_1}+1}\Big)\Bigg)\Bigg]. \tag{3.87}$$

Consequently, the variance in this case is computed as follows

$$\sigma^2(Y_1/(n_{\tau_1}, \hat{\tau}_1 = T_c)) = \frac{\hat{c}_{1,t}^2}{4T_c^2}\, E[\mathcal{Z}(\phi_{c_1}, n_{\tau_1}, \hat{\tau}_1 = T_c)], \tag{3.88}$$

where $\mathcal{Z}(\phi_{c_1}, n_{\tau_1}, \hat{\tau}_1 = T_c) = \Big(A_3^2 - 2A_3B_3 + B_3^2 + C_3^2 - 2C_3D_3 + D_3^2\Big)$, and its expected value, because of linearity can be expressed as

$$E[\mathcal{Z}(\phi_{c_1}, n_{\tau_1}, \hat{\tau}_1 = T_c)] = E[A_3^2] + E[-2A_3B_3] + E[B_3^2] + E[C_3^2] + E[-2C_3D_3] + E[D_3^2] \tag{3.89}$$

$$E[\mathcal{Z}(\phi_{c_1}, n_{\tau_1}, \hat{\tau}_1 = T_c)] = \Bigg[\frac{1}{16}\frac{1}{2}\Bigg(\Bigg(\cos^2(\phi_p)\,(T_c)^2\,\Big(E[k^2_{I,I,n_{\tau_1}}] + E[k^2_{I,I,n_{\tau_1+1}}] + 2\;E[k_{I,I,n_{\tau_1}}k_{I,I,n_{\tau_1+1}}]\Big)\Bigg) + \Bigg(\frac{\sin^2(\phi_p)}{w_p^2}\Big(E[k^2_{I,I,n_{\tau_1}}] + E[k^2_{I,I,n_{\tau_1+1}}] - 2E[k_{I,I,n_{\tau_1}}k_{I,I,n_{\tau_1+1}}]\Big)\Bigg) + \Bigg(\frac{\sin(2\phi_p)}{w_p}\,(T_c)\Big(-E[k^2_{I,I,n_{\tau_1}}] + E[k^2_{I,I,n_{\tau_1+1}}]\Big)\Bigg)\Bigg)\Bigg] +$$

$$+\Bigg[\frac{-1}{16}\sin(2\phi_{c_1})\Bigg(\frac{-1}{2}\sin(2\phi_p)\,(2T_c^2)\,\Big(E[k_{I,I,n_{\tau_1}}k_{I,Q,n_{\tau_1+1}}] + E[k_{I,I,n_{\tau_1+1}}k_{I,Q,n_{\tau_1+1}}]\Big) - \frac{\sin^2(\phi_p)}{w_p}\,(2T_c)\Big(-E[k_{I,I,n_{\tau_1}}k_{I,Q,n_{\tau_1+1}}] + E[k_{I,I,n_{\tau_1+1}}k_{I,Q,n_{\tau_1+1}}]\Big)\Bigg)\Bigg] + \Bigg[\frac{1}{16}\frac{1}{2}\Bigg(\sin^2(\phi_p)\,(4T_c^2)E[k^2_{I,Q,n_{\tau_1+1}}]\Bigg)\Bigg] +$$

$$+\Bigg[\frac{1}{16}\frac{1}{2}\Bigg(\sin^2(\phi_p)\,(4T_c^2)E[k^2_{Q,I,n_{\tau_1}}]\Bigg)\Bigg] + \Bigg[\frac{1}{16}\sin(2\phi_{c_1})\Bigg(\frac{1}{2}\sin(2\phi_p)\,(2T_c^2)\cdot\Bigg(E[k_{Q,I,n_{\tau_1}}k_{Q,Q,n_{\tau_1}}] + E[k_{Q,I,n_{\tau_1}}k_{Q,Q,n_{\tau_1+1}}]\Bigg) + \frac{\sin^2(\phi_p)}{w_p}\,(2T_c)\cdot\Bigg(-E[k_{Q,I,n_{\tau_1}}k_{Q,Q,n_{\tau_1}}] + E[k_{Q,I,n_{\tau_1}}k_{Q,Q,n_{\tau_1+1}}]\Bigg)\Bigg)\Bigg] + \Bigg[\frac{1}{16}\frac{1}{2}\Bigg(\Bigg(\cos^2(\phi_p)\,(T_c^2)\cdot\Big(E[k^2_{Q,Q,n_{\tau_1}}] + E[k^2_{Q,Q,n_{\tau_1+1}}] + 2\;E[k_{Q,Q,n_{\tau_1}}k_{Q,Q,n_{\tau_1+1}}]\Big)\Bigg) + \Bigg(\frac{\sin^2(\phi_p)}{w_p^2}\Big(E[k^2_{Q,Q,n_{\tau_1}}] + E[k^2_{Q,Q,n_{\tau_1+1}}] - 2E[k_{Q,Q,n_{\tau_1}}k_{Q,Q,n_{\tau_1+1}}]\Big)\Bigg) + \Bigg(\frac{\sin(2\phi_p)}{w_p}\,(T_c)\Big(-E[k^2_{Q,Q,n_{\tau_1}}] + E[k^2_{Q,Q,n_{\tau_1+1}}]\Big)\Bigg)\Bigg)\Bigg]. \tag{3.90}$$

**3.2.3.1.5 Case 4** $\hat{\tau}_1 = 2T_c$ For this last case we repeat the same steps with the same assumptions so we get Figure 3.24, 3.25, 3.26, and 3.27 which are the reception demonstration of the products of $(I_0, I_1)$, $(I_0, Q_1)$, $(Q_0, I_1)$ and $(Q_0, Q_1)$ of the SoI and the interferer respectively. Therefore, the I-phase and the quadrature

phase components of the interferer's received signal would be $Y_{I,1,\ell} = \frac{2\,\hat{c}_{1,t}}{T_c}\,(A_4 - B_4)$ and $Y_{Q,1,\ell} = \frac{2\,\hat{c}_{1,t}}{T_c}\,(C_4 - D_4)$ respectively.

$$A_4 = \frac{1}{4}\cos(\phi_{c_1})\Bigg[\cos(\phi_p)\,(2Tc)\,k_{I,I,n_{\tau_1+1}}\Bigg], \tag{3.91}$$

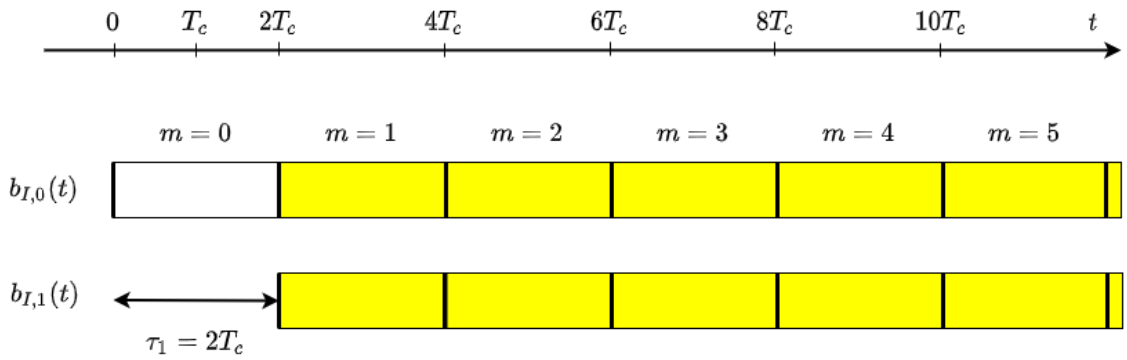


Figure 3.24: An illustration of the reception of the I-phase component of both SoI and the interferer when $n_{\tau_1} = 0, \hat{\tau}_1 = 2T_c$.

$$B_4 = \frac{1}{4}\sin(\phi_{c_1})\Bigg[-\sin(\phi_p)\,(T_c)\Big(k_{I,Q,n_{\tau_1+1}} + k_{I,Q,n_{\tau_1+2}}\Big) + \frac{\cos(\phi_p)}{w_p}\Big(-k_{I,Q,n_{\tau_1+1}} + k_{I,Q,n_{\tau_1+2}}\Big)\Bigg] \tag{3.92}$$

$$Y_{I,1,\ell}/(n_{\tau_1}, \hat{\tau}_1 = 2T_c) = \frac{\hat{c}_{1,t}}{2T_c}\Bigg[\cos(\phi_{c_1})\Bigg(\cos(\phi_p)\,(2Tc)\,k_{I,I,n_{\tau_1+1}}\Bigg) - \sin(\phi_{c_1}).\Bigg(-\sin(\phi_p)\,(T_c)\Big(k_{I,Q,n_{\tau_1+1}} + k_{I,Q,n_{\tau_1+2}}\Big) + \frac{\cos(\phi_p)}{w_p}\Big(-k_{I,Q,n_{\tau_1+1}} + k_{I,Q,n_{\tau_1+2}}\Big)\Bigg)\Bigg]. \tag{3.93}$$

$$C_4 = \frac{-1}{4}\sin(\phi_{c_1})\Bigg[\sin(\phi_p)\,(T_c)\Big(k_{Q,I,n_{\tau_1}} + k_{Q,I,n_{\tau_1+1}}\Big) + \frac{\cos(\phi_p)}{w_p}\Big(k_{Q,I,n_{\tau_1}} - k_{Q,I,n_{\tau_1+1}}\Big)\Bigg] \tag{3.94}$$

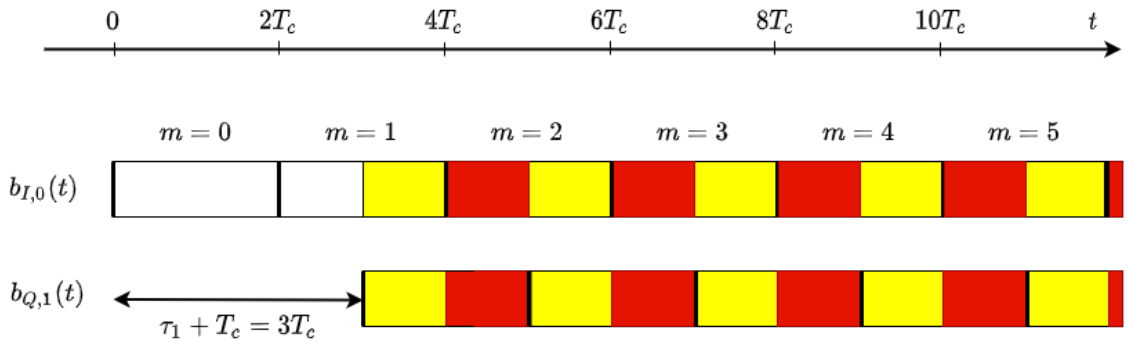


Figure 3.25: An illustration of the reception of the I-phase component of SoI and Quadrature component of the interferer when $n_{\tau_1} = 0, \hat{\tau}_1 = 2T_c$.

$$D_4 = \frac{1}{4}\cos(\phi_{c_1})\left[\cos(\phi_p)\,(2Tc)\,k_{Q,Q,n_{\tau_1+1}}\right], \tag{3.95}$$

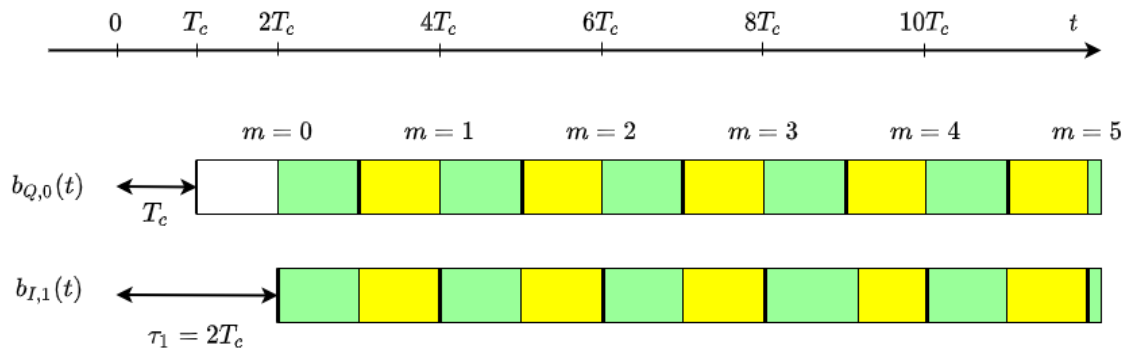


Figure 3.26: An illustration of the reception of the Quadrature component of SoI and I-phase component of the interferer when $n_{\tau_1} = 0, \hat{\tau}_1 = 2T_c$.

$$\begin{aligned} Y_{Q,1,\ell}/(n_{\tau_1}, \hat{\tau}_1 = 2T_c) = \frac{\hat{c}_{1,t}}{2T_c}\Bigg[\sin(\phi_{c_1})\Bigg(\sin(\phi_p)\,(T_c)\Big(k_{Q,I,n_{\tau_1}} + k_{Q,I,n_{\tau_1+1}}\Big) + \\ + \frac{\cos(\phi_p)}{w_p}\Big(k_{Q,I,n_{\tau_1}} - k_{Q,I,n_{\tau_1+1}}\Big)\Bigg) - \cos(\phi_{c_1}). \\ \Bigg(\cos(\phi_p)\,(2Tc)\,k_{Q,Q,n_{\tau_1+1}}\Bigg)\Bigg]. \end{aligned} \tag{3.96}$$

Consequently, the variance in this case is computed as follows

$$\sigma^2(Y_1/(n_{\tau_1}, \hat{\tau}_1 = 2T_c)) = \frac{\hat{c}_{1,t}^2}{4T_c^2}\,E[\mathcal{Z}(\phi_{c_1}, n_{\tau_1}, \hat{\tau}_1 = 2T_c)], \tag{3.97}$$

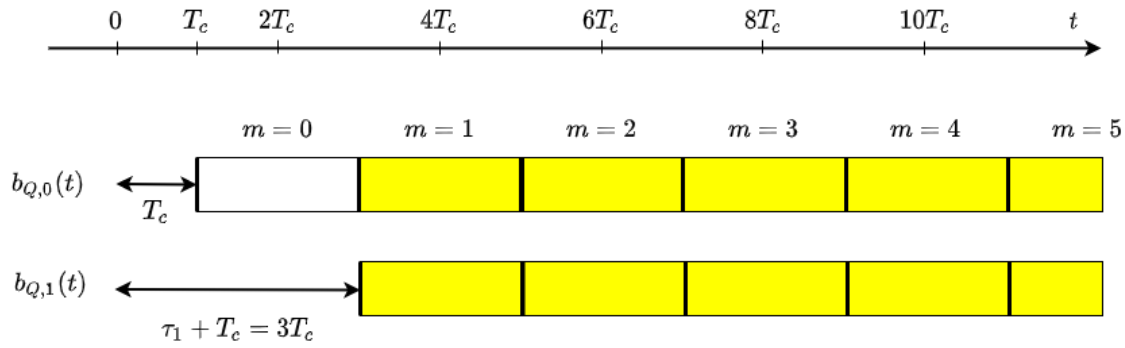


Figure 3.27: An illustration of the reception of the Quadrature component of both SoI and the interferer when $n_{\tau_1} = 0, \hat{\tau}_1 = 2T_c$.

where $\mathcal{Z}(\phi_{c_1}, n_{\tau_1}, \hat{\tau}_1 = 2T_c) = \Big(A_4^2 - 2A_4B_4 + B_4^2 + C_4^2 - 2C_4D_4 + D_4^2\Big)$and assuming the linearity its expected value can be written as

$$E[\mathcal{Z}(\phi_{c_1}, n_{\tau_1}, \hat{\tau}_1 = 2T_c)] = E[A_4^2] + E[-2A_4B_4] + E[B_4^2] + E[C_4^2] + E[-2C_4D_4] + E[D_4^2] \tag{3.98}$$

$$E[\mathcal{Z}(\phi_{c_1}, n_{\tau_1}, \hat{\tau}_1 = 2T_c)] = \left[\frac{1}{16}\frac{1}{2}\left(\cos^2(\phi_p)\,(4T_c^2)E[k^2_{I,I,n_{\tau_1+1}}]\right)\right] + \left[\frac{-1}{16}\sin(2\phi_{c_1})\cdot\right.$$
$$\left(\frac{-1}{2}\sin(2\phi_p)\,(2T_c^2)\,\Big(E[k_{I,I,n_{\tau_1+1}}k_{I,Q,n_{\tau_1+1}}]E[k_{I,I,n_{\tau_1+1}}k_{I,Q,n_{\tau_1+2}}]\Big) + \frac{\cos^2(\phi_p)}{w_p}\cdot\right.$$
$$\left.\left.(2T_c)\Big(-E[k_{I,I,n_{\tau_1+1}}k_{I,Q,n_{\tau_1+1}}] + E[k_{I,I,n_{\tau_1+1}}k_{I,Q,n_{\tau_1+2}}]\Big)\right)\right] + \left[\frac{1}{16}\frac{1}{2}\Bigg(\Bigg(\sin^2(\phi_p)\cdot\right.$$
$$(T_c^2)\,\Big(E[k^2_{I,Q,n_{\tau_1+1}}] + E[k^2_{I,Q,n_{\tau_1+2}}] + 2\,E[k_{I,Q,n_{\tau_1+1}}k_{I,Q,n_{\tau_1+2}}]\Big)\Bigg) + \Bigg(\frac{\cos^2(\phi_p)}{w_p^2}\cdot$$
$$\Big(E[k^2_{I,Q,n_{\tau_1+1}}] + E[k^2_{I,Q,n_{\tau_1+2}}] - 2E[k_{I,Q,n_{\tau_1+1}}k_{I,Q,n_{\tau_1+2}}]\Big)\Bigg) - \Bigg(\frac{\sin(2\phi_p)}{w_p}(T_c)\cdot$$
$$\left.\left.\Big(-E[k^2_{I,Q,n_{\tau_1+1}}] + E[k^2_{I,Q,n_{\tau_1+2}}]\Big)\Bigg)\Bigg)\right] + \left[\frac{1}{16}\frac{1}{2}\Bigg(\Bigg(\sin^2(\phi_p)\,(T_c^2)\,\Big(E[k^2_{Q,I,n_{\tau_1}}] + \right.\right.$$
$$\left.\left.+ E[k^2_{Q,I,n_{\tau_1+1}}] + 2\,E[k_{Q,I,n_{\tau_1}}k_{Q,I,n_{\tau_1+1}}]\Big)\Bigg) + \Bigg(\frac{\cos^2(\phi_p)}{w_p^2}\Big(E[k^2_{Q,I,n_{\tau_1}}] + \right.$$

$$+ E[k^2_{Q,I,n_{\tau_1+1}}] - 2E[k_{Q,I,n_{\tau_1}} k_{Q,I,n_{\tau_1+1}}]\Big)\Big) + \left(\frac{\sin(2\phi_p)}{w_p}\,(T_c)\Big(\,E[k^2_{Q,I,n_{\tau_1}}]- \right.$$
$$\left. -\;E[k^2_{Q,I,n_{\tau_1+1}}]\Big)\Big)\Big)\right] + \left[\frac{1}{16}\,\frac{1}{2}\left(\cos^2(\phi_p)\,(4T_c^2)E[k^2_{Q,Q,n_{\tau_1+1}}]\right)\right]. \tag{3.99}$$

Now substituting the aforementioned values in SINR equation 3.27, and taking into account that $E[Y_{j,1,\ell}] = 0$ because $E[k_{j_0,j_1,n_{\tau_1}}] = 0\ \forall(j_0, j_1, n_{\tau_1})$ as it is proved in appendix A and $E[W_{j,\ell}] = 0$ we obtain

$$\begin{aligned}
\gamma\,(t, \phi_{c_1}, n_{\tau_1}, \hat{\tau}_1) \;&=\; \frac{E\left[\sqrt{Y^2_{I,\ell} + Y^2_{Q,\ell}}\right]}{\sqrt{16\,N_0 \;+ \frac{\hat{c}^2_{1,t}}{4T_c^2}\,E[\mathcal{Z}(\phi_{c_1}, n_{\tau_1}, \hat{\tau}_1)]}} = \\
&= \frac{E\left[\sqrt{Y^2_{I,0,\ell} + Y^2_{Q,0,\ell}}\right]}{\sqrt{16\,N_0 \;+ \frac{\hat{c}^2_{1,t}}{4T_c^2}\,E[\mathcal{Z}(\phi_{c_1}, n_{\tau_1}, \hat{\tau}_1)]}} = \\
&= \frac{16\,\sqrt{2}\;\hat{c}_{0,t}}{\sqrt{16\,N_0 \;+ \frac{\hat{c}^2_{1,t}}{4T_c^2}\,E[\mathcal{Z}(\phi_{c_1}, n_{\tau_1}, \hat{\tau}_1)]}} = \\
&= \sqrt{\frac{512\;\hat{c}^2_{0,t}}{16\,N_0 \;+ \frac{\hat{c}^2_{1,t}}{4T_c^2}\,E[\mathcal{Z}(\phi_{c_1}, n_{\tau_1}, \hat{\tau}_1)]}},
\end{aligned} \tag{3.100}$$

It is worth remarking that we assume that the symbol of the SoI is $S_0$ i.e the first sequence of the PN sequences. In addition, the importance of each parameter affecting the explicit analytic model of SINR is going to be discussed in Chapter 3 where a rigorous parametric analysis will be performed on a specific test case.

## 3.3 Summary

In this chapter, we derive explicitly the expression which represents the received signal subject to different channel imperfections, such as path loss, shadow fading and power residual error as a function of the time and phase offset. We assume four cases of the time offset and derived the corresponding interferer variance according to each case. The closed-form analytic expression of SINR evolves at the symbol

rate and encompasses the stochastic characteristics of the WirelessHART link for the considered scenario. It allows us to define some important quality metrics describing the lossy communication link, which will be explained in the next chapter. However, to define these quality metrics formally, we need to pay attention to the control-related data messages and not just to individual symbols.

In the next chapter, we will apply the last two steps of the proposed model i.e we are going to find a tractable representation of equation (3.100) and derive the corresponding consistent finite-state Markov link abstraction.

Chapter 4

# The Implicit Analytic and Finite-state Markov Model for the Interfered WirelessHART Link

In this chapter, we derive an easy handled representation of the analytic expression we got in chapter 3 which we call it implicit analytic model. Moreover, we derive the Finite-state Markov channel (FSMC), that is represented by the lower block of the channel model in Figure 2.1 to represent the behavior of the underlying protocol link.

## 4.1 Implicit analytic model of SINR

The following step of our modeling process is finding a tractable representation of the explicit analytic model of SINR 3.100. To perform that, we can approximate it with another random process, (e.g., log-normal process) and then apply moment matching approach to get the signal statistics as follows.

The SINR equation 3.100 (which will be denoted by $\Gamma$ in logarithmic scale, and by $\gamma$ when using the power value, $\Gamma \triangleq 10\log_{10}(\gamma)$ [dB]) conditioned to PCEs and shadowing. Following [110], the expression derived is a logarithmic scale and it is a square root of reciprocal weighted linear combination of correlated log-normal

process as depicted in equation 4.1.

$$\Gamma(t,\phi_{c_1},n_{\tau_1},\hat{\tau}_1) = 10\,log_{10}\left(a\,e^{-\chi_0(t)}) + b\,e^{\chi_1(t)-\chi_0(t))}\right)^{-\frac{1}{2}}, \tag{4.1}$$

There is no explicit closed form expression of the distribution of the weighted linear combination. There are different techniques to approximate the distribution as described in [111]. We use moment matching approximation described in [110] which extends Fenton-Wilkinsom approximation to the second order statistics and provides good accuracy on the tails of the probability density function. Therefore, we let $\Gamma(t,\phi_{c_1},n_{\tau_1},\hat{\tau}_1) \approx \mathrm{L}^{-1/2}(t,\phi_{c_1},n_{\tau_1},\hat{\tau}_1)$, where due to the properties of the random prcesses involved, $\mathrm{L}^{-1/2}(t,\phi_{c_1},n_{\tau_1},\hat{\tau}_1)$ is seen as a weighted sum of randomly correlated log-normal processes. This is valid also for $\mathrm{L}(t,\phi_{c_1},n_{\tau_1},\hat{\tau}_1)$, which could be expressed as

$$\mathrm{L}(t,\phi_{c_1},n_{\tau_1},\hat{\tau}_1) = \mathrm{D}e^{-\chi_0(t)} + \mathrm{B}(\phi_{c_1},n_{\tau_1},\hat{\tau}_1)\,e^{\chi_1(t)-\chi_0(t)}, \tag{4.2}$$

$$\mathrm{D} = \frac{N_0}{32\alpha_0^2 E_{c,0}}, \quad \mathrm{B}(\phi_{c_1},n_{\tau_1},\hat{\tau}_1) = \frac{E_{c,1}\,\alpha_1^2\,E[\mathcal{Z}(\phi_{c_1},n_{\tau_1},\hat{\tau}_1)]}{2048\,T_c^2\,E_{c,0}\,\alpha_0^2}. \tag{4.3}$$

So, we apply the moment matching technique [110] as follows. Let $Z(t,\phi_{c_1},n_{\tau_1},\hat{\tau}_1)$ be a Gaussian process with mean $\eta_Z$, variance $\sigma_Z^2$, and autocovariance $c_Z(\tau)$, such that $\mathrm{L}(t,\phi_{c_1},n_{\tau_1},\hat{\tau}_1) \approx e^{Z(t,\phi_{c_1},n_{\tau_1},\hat{\tau}_1)}$. Let $\mathrm{E}\{\cdot\}$ denote the mathematical expectation. Then

$$\begin{cases} \mathrm{M}_1 \;=\; \mathrm{E}\{\mathrm{L}(t,\phi_{c_1},n_{\tau_1},\hat{\tau}_1)\} \triangleq \mathrm{E}\{e^{Z(t,\phi_{c_1},n_{\tau_1},\hat{\tau}_1)}\} \;=\; e^{\eta_Z+\frac{1}{2}\sigma_Z^2}, \\ \mathrm{M}_2(\tau) \;=\; \mathrm{E}\{\mathrm{L}(t,\phi_{c_1},n_{\tau_1},\hat{\tau}_1)\mathrm{L}(t+\tau,\phi_{c_1},n_{\tau_1},\hat{\tau}_1)\} \triangleq \mathrm{E}\{e^{Z(t)+Z(t+\tau)}\} \\ \qquad\quad = e^{2\eta_Z+\sigma_Z^2+c_Z(\tau)}, \\ \mathrm{M}_2(0) \;=\; \mathrm{E}\{\mathrm{L}(t,\phi_{c_1},n_{\tau_1},\hat{\tau}_1)\mathrm{L}(t,\phi_{c_1},n_{\tau_1},\hat{\tau}_1)\} \triangleq e^{2\eta_Z+2\sigma_Z^2}. \end{cases} \tag{4.4}$$

Solving the equations defining $\mathrm{M}_1$, $\mathrm{M}_2(\tau)$ and $\mathrm{M}_2(0)$ in $\eta_Z$, $\sigma_Z^2$ and $c_Z(\tau)$ yields the following expressions:

$$\begin{cases} \eta_Z = 2\ln \mathrm{M}_1 - \frac{1}{2}\ln \mathrm{M}_2(0), \\ \sigma_Z^2 = \ln \mathrm{M}_2(0) - 2\ln \mathrm{M}_1, \\ c_Z(\tau) = \ln\left(\frac{\mathrm{M}_2(\tau)}{\mathrm{M}_1^2}\right). \end{cases} \tag{4.5}$$

Since $\xi_i(t)$ and $\beta_i(t)$ are zero mean independent processes,

$$\begin{cases} \mathrm{M}_1 = \mathrm{D}e^{\frac{1}{2}(\sigma^2_{\xi_0}+\sigma^2_{\beta_0})} + \mathrm{B}(\phi_{c_1}, n_{\tau_1}, \hat{\tau}_1)e^{\frac{1}{2}(\sigma^2_{\xi_1}+\sigma^2_{\beta_1}+\sigma^2_{\xi_0}+\sigma^2_{\beta_0})}, \\ \mathrm{M}_2(\tau) = e^{\sigma^2_{\chi_0}+c_{\chi_0}(\tau)}\Big[\mathrm{D}^2+2\mathrm{DB}(\phi_{c_1}, n_{\tau_1}, \hat{\tau}_1)e^{\frac{1}{2}\sigma^2_{\chi_1}}+\mathrm{B}^2(\phi_{c_1}, n_{\tau_1}, \hat{\tau}_1)e^{\sigma^2_{\chi_1}+c_{\chi_1}(\tau)}\Big], \end{cases}$$

where $c_{\chi_i}(\tau)=c_{\xi_i}(\tau)+c_{\beta_i}(\tau)$, $\sigma^2_{\chi_i}=\sigma^2_{\xi_i}+\sigma^2_{\beta_i}$, for $i=0,1$.
Given the relation between $Z(t, \phi_{c_1}, n_{\tau_1}, \hat{\tau}_1)$ and $\mathrm{L}(t, \phi_{c_1}, n_{\tau_1}, \hat{\tau}_1)$, few manipulations bring to

$$\Gamma(t, \phi_{c_1}, n_{\tau_1}, \hat{\tau}_1)=\kappa Z(t, \phi_{c_1}, n_{\tau_1}, \hat{\tau}_1) \quad \text{where} \quad \kappa=-\frac{5}{\ln 10}, \tag{4.6}$$

so that $\Gamma(t, \phi_{c_1}, n_{\tau_1}, \hat{\tau}_1)$ is a Gaussian process with mean, variance and autocovariance

$$\begin{cases} \eta_\Gamma=\kappa\eta_Z, \\ \sigma^2_\Gamma=\kappa^2\sigma^2_Z, \\ c_\Gamma(\tau)=\kappa^2 c_Z(\tau). \end{cases} \tag{4.7}$$

In the rest of this thesis, we will denote it by $\Gamma(t, \phi_{c_1}, n_{\tau_1}, \hat{\tau}_1) \sim \mathcal{N}(\eta_\Gamma, \sigma^2_\Gamma)$, if the relevant values of $c_\Gamma(\tau)$ will be given. The closed-form expression 4.7 evolves at the symbol rate and encompasses the stochastic characteristics of the WirelessHART link for the considered scenario. It allows us to define some important quality metrics describing the lossy communication link, which will be expounded in the next subsection. However, to define these quality metrics formally, we need to pay attention to the control-related data messages and not just to individual symbols. In networks based on IEEE 802.15.4 compatible hardware the SINR estimation is performed for each received packet during link quality indicator (LQI) measurement [12, p. 65]. The standard IEEE 802.15.4 maps 4 data bits in one data symbol, ([12], pag. 48), thus the number of symbols within a control-related frame is $(\ell_F/4)$, given that $\ell_F$ indicates the number of bits in the *frame*. Therefore, the estimated $\Gamma(t)$ refers to a block of $(\ell_F/4)$ symbols. WirelessHART-based WNCSs send data at a rate that is inversely proportional to the update period of the dedicated Publish data messages [9, p. 248]. Thus, between two control-related data transmissions the presented link has approximately $\ell_\mathrm{E}$ *evolutions* which could be expressed as

$$\ell_\mathrm{E}=\mathrm{round}\left(\frac{4T_u}{\ell_\mathrm{F}T_s}\right). \tag{4.8}$$

In general, we need to

$$\text{compute values of } c_\Gamma(\tau) \text{ for } \tau = k\ell_\text{E}+1,\ k\in\mathbb{N},$$

in order to evaluate the time correlations at the time scale of the control application.

### 4.1.1 Symbol Error Probability Computation

In order to properly characterize the channel model proposed so far in terms of link quality metrics, the probability of wrongly receiving a data packet has to be defined.

This metric can be derived moving from the symbol error probability ($R_s(x)$) which is a function of $x$ that is going to be described in the following. In particular, recalling that in IEEE 802.15.4 PHY each symbol is composed by 4 bits, by calling as $\ell_F$ the number of bits for each frame, then having 16-ary symbols implies:

$$R_p(x) = 1 - (1 - R_s(x))^{\frac{\ell_F}{4}} \tag{4.9}$$

The rest of this section will be devoted to the derivation of the expression of $R_s$ assuming coherent detection.

Basing on [100], performance characteristics of optimum receivers can be equivalently obtained by exploiting a *waveform channel model* or a *vector channel model*. This implies that the received signal can be expressed in one of the following ways:

$$y(t) = c(t)s_p(t) + n(t) \quad 1 \leq p \leq M \tag{4.10}$$

where $M$ is the modulation dimension, or in vectorial terms

$$\boldsymbol{y} = \boldsymbol{c} \cdot \boldsymbol{s}_m + \boldsymbol{n} \tag{4.11}$$

where all vectors are $N$ dimensional real vectors, given that $N$ is the dimension of the orthonormal basis set $\{\phi_j(t), 1 \leq j \leq N\}$ depending on the specific modulation used for transmission. For the specific PHY level considered in this thesis, assuming an OQPSK modulation, $N = 2$. The equivalence of the two models is proved in [100] for an AWGN channel, but it can be easily generalized for the current scenario.

The receiver observes the received vector and decides which message (or 4 bits symbol in the specific case) was transmitted. Indicating as $\hat{p}$ the message that the

receiver decided to have been transmitted and assuming equiprobable and equal energy symbols, following the reasoning in [100] the optimal detection rule is:

$$\hat{p} = \underset{1\leq p\leq M}{arg\ max}\ \boldsymbol{y}\cdot\boldsymbol{S}_p \tag{4.12}$$

$$\boldsymbol{y}\cdot\boldsymbol{S}_p =< \boldsymbol{y}, \boldsymbol{S}_p >= \sum_{j\in\{I,Q\}} y_j \cdot S^*_{p,j} = Y_p = Y_{I,p} + Y_{Q,p}$$

where $Y_{j,q,p}$ refers to the I or Q component of the $q$th transmitted symbol ($S_q$), matched to $S_p$.
The error probability for 16 equiprobable symbols can be written as:

$$P_e = \frac{1}{16}\sum_{p=1}^{16} P_{e|S_p} \quad \text{where}$$

$$P_{e|S_p} = \text{Prob}[y \notin D_p | S_p \text{ sent}] = \text{Prob}[Y_p < Y_{p'} \text{ for any } p' \neq p] \tag{4.13}$$

$D_p$ is the decision region associated to symbol $S_p$, so in general:

$$P_{e|S_p} = \sum_{\substack{1\leq p'\leq p\\ p'\neq p}} \int_{D_{p'}} p(\mathbf{y}|\mathbf{S}_p)d\mathbf{y} \tag{4.14}$$

Since decisions regions maybe complicated to define, the union bound for a general channel is assumed:

$$P_e \leq \frac{1}{M}\sum_{p=1}^{16}\sum_{\substack{1\leq p'\leq p\\ p'\neq p}} P_{p\to p'} \tag{4.15}$$

In this case $P_{p\to p'}$ is called pairwise error probability and it is the reason of the bound presence, as explained in [100], section 4.2.
Referring to equation (4.13), an explicit expression is derived in the following for $p = 0$ and $p' = 1$. The aim is thus to evaluate the $\text{Prob}(Y_0 < Y_1)$ whose argument $Y_0 < Y_1$ can be written as:

$$Y_{I,0,0} + Y_{I,\text{int},0} + W_{I,0} + Y_{Q,0,0} + Y_{Q,\text{int},0} + W_{Q,0} < Y_{I,0,1} + Y_{I,\text{int},1} + W_{I,1} + Y_{Q,0,1} + Y_{Q,\text{int},1} + W_{Q,1}$$

where $Y_{I,0,0}$ is the in-phase of the received SoI matched to $S_0$ and $Y_{I,int,0}$ is the in-phase of the received interferer signal matched to $S_0$ and so on. We remark that we use the notation *int* for the interferer instead of 1 to differentiate it from the notation of the sequences of the matched filters. We call $Y_{I,0,0} + Y_{Q,0,0} - Y_{I,0,1} - Y_{Q,0,1} = \Delta Y_{0,1}$ which depends on the Hamming distance between $S_0$ and $S_1$, thus we obtain:

$$\begin{aligned} \text{Prob}[Y_0 < Y_1] = \\ = \text{Prob}[Y_{I,\text{int},1} + Y_{Q,\text{int},1} - Y_{I,\text{int},0} - Y_{Q,\text{int},0} + \\ + W_{I,1} + W_{Q,1} - W_{I,0} - W_{Q,0} > \Delta Y_{0,1}] \end{aligned} \tag{4.16}$$

We call the total contribution coming from a generic interferer int as: $Y_{I,\text{int},1} + Y_{Q,\text{int},1} - Y_{I,\text{int},0} - Y_{Q,\text{int},0} = Y_{\text{int,tot},(1,0)}$

### 4.1.2 Noise components

We focus now on the noise components, moving from the generic expression for the noise at the output of the filter matched to $s_i$, that are a generalization of equations (3.31) and (3.35):

$$\begin{aligned} W_{I,\ell,i} = \sqrt{\frac{2}{T_c}} \sum_{m=0}^{15} \int_0^{T_s} \mathcal{W}(t)\ \cos(\omega_c t)\, cos(\omega_p t) \cdot \\ \hat{b}_{I,i,l,m}\, h_{T_c} \left( \frac{t\ -\ 2\,(m\ +\ 32l)\,T_c}{2T_c} \right) dt, \end{aligned} \tag{4.17}$$

$$\begin{aligned} W_{Q,\ell,i} = \sqrt{\frac{2}{T_c}} \sum_{m=0}^{15} \int_0^{T_s} \mathcal{W}(t)\ \sin(\omega_c t)\ \sin(\omega_p t) \cdot \\ \hat{b}_{Q,i,l,m}\, h_{T_c} \left( \frac{t\ -\ (2\,(m\ +\ 32l) + 1)\,T_c}{2T_c} \right) dt, \end{aligned} \tag{4.18}$$

Now, neglecting pedex $\ell$ for readability issue, $W_{j,i}$, now represents the $j$-th noise component at the receiver matched to $s_i$, for $j \in I, Q$ and $i = 0, \ldots 15$. For the specific case under analysis:

$$W_{I,0} = \sqrt{\frac{2}{T_c}} \sum_{m=0}^{15} \int_0^{T_s} \mathcal{W}(t) \cos(\omega_c t) \cos(\omega_p t) \hat{b}_{I,0,l,m} h_{T_c}(\cdot) dt$$

$$W_{I,1} = \sqrt{\frac{2}{T_c}} \sum_{m=0}^{15} \int_0^{T_s} \mathcal{W}(t) \cos(\omega_c t) \cos(\omega_p t) \hat{b}_{I,1,l,m} h_{T_c}(\cdot) dt$$

$$W_{Q,0} = \sqrt{\frac{2}{T_c}} \sum_{m=0}^{15} \int_0^{T_s} \mathcal{W}(t)\ \sin(w_c t)\ \sin(\omega_p t) \hat{b}_{Q,0,l,m}\, h_{T_c}(\cdot) dt$$

$$W_{Q,1} = \sqrt{\frac{2}{T_c}} \sum_{m=0}^{15} \int_0^{T_s} \mathcal{W}(t)\ \sin(w_c t)\ \sin(\omega_p t) \hat{b}_{Q,1,l,m}\, h_{T_c}(\cdot) dt$$

The noise terms in expression (4.16) can be coupled as follows:

$$\begin{aligned} &W_{I,1} - W_{I,0} = \\ &= \sqrt{\frac{2}{T_c}} \sum_{m=0}^{15} \left( \hat{b}_{I,1,l,m} - \hat{b}_{I,0,l,m} \right) \int_0^{T_s} \mathcal{W}(t) \cos(\omega_c t) \cos(\omega_p t) h_{T_c}(\cdot) dt \end{aligned} \tag{4.19}$$

Considering that $\sum_{m=0}^{15} \left( \hat{b}_{I,1,l,m} - \hat{b}_{I,0,l,m} \right) \neq 0$ only when chips of symbols 0 and 1 are different and assuming, without loss of generality, that NRZ encoded I or Q components of symbols $s_0$ and $s_1$ differ on the first $\mathrm{HD}(j,1,0)$ chips:

$$\sum_{m=0}^{15} \left( \hat{b}_{I,1,l,m} - \hat{b}_{I,0,l,m} \right) = \sum_{m=0}^{\mathrm{HD}(I,1,0)} \left( \hat{b}_{I,1,l,m} - \hat{b}_{I,0,l,m} \right)$$

$$W_{I,1} - W_{I,0} = \sum_{m=0}^{\mathrm{HD}(I,1,0)} \left( \hat{b}_{I,1,l,m} - \hat{b}_{I,0,l,m} \right) \cdot W_I$$

where $W_I = \sqrt{\frac{2}{T_c}} \int_0^{T_s} \mathcal{W}(t) \cos(\omega_c t) \cos(\omega_p t) h_{T_c}(\cdot) dt$, and coherently:

$$W_{Q,1} - W_{Q,0} = \sum_{m=0}^{\mathrm{HD}(Q,1,0)} \left( \hat{b}_{Q,1,l,m} - \hat{b}_{Q,0,l,m} \right) \cdot W_Q$$

Thus the probability we are looking for becomes:

$$\begin{aligned} \mathrm{Prob}[Y_0 < Y_1] = \\ &= \mathrm{Prob}[Y_{\mathrm{int,tot}} + \sum_{m=0}^{\mathrm{HD}(I,1,0)} \left( \hat{b}_{I,1,l,m} - \hat{b}_{I,0,l,m} \right) W_I \\ &+ \sum_{m=0}^{\mathrm{HD}(Q,1,0)} \left( \hat{b}_{Q,1,l,m} - \hat{b}_{Q,0,l,m} \right) W_Q > \Delta Y_{0,1}] \end{aligned} \tag{4.20}$$

### 4.1.3 Central limit theorem

In order to obtain a tractable distribution for the random variables involved in the right hand side of (4.20), the Central Limit Theorem is invoked. We recall that for independent random variables with Gaussian distributions i.e. $n_i \sim \mathcal{N}(\mu_i, \sigma_i^2)$, their linear combination $\sum_i a_i n_i + k$ can be approximated as $\mathcal{N}\left(\sum_i a_i\mu_i + k\sum_i (a_i\sigma_i)^2\right)$.

Thus applying the central limit theorem to the combination of random variables given by: $Y_{\text{int,tot}(0,1)} + \sum_{m=0}^{\text{HD}(I,1,0)} \left(\hat{b}_{I,1,l,m} - \hat{b}_{I,0,l,m}\right) W_I + \sum_{m=0}^{\text{HD}(Q,1,0)} \left(\hat{b}_{Q,1,l,m} - \hat{b}_{Q,0,l,m}\right) W_Q$, we obtain a Gaussian distribution with mean $\mu_{\text{all}}$ and variance $\sigma^2_{\text{all}}$ given by:

$$\mu_{\text{all}} = E\{Y_{\text{int,tot}(0,1)}\} \text{ because } \mu_{W_I} = \mu_{W_Q} = 0$$

$$\sigma^2_{\text{all}} = \text{Var}\left\{Y_{\text{int,tot}(0,1)}\right\} + \text{Var}\left\{\sum_{m=0}^{\text{HD}(I,1,0)} \left(\hat{b}_{I,1,l,m} - \hat{b}_{I,0,l,m}\right) W_I\right\}$$

$$+ \text{Var}\left\{\sum_{m=0}^{\text{HD}(Q,1,0)} \left(\hat{b}_{Q,1,l,m} - \hat{b}_{Q,0,l,m}\right) W_Q\right\}$$

We can write that

$$\text{Var}\left\{\sum_{m=0}^{\text{HD}(I,1,0)} \left(\hat{b}_{I,1,l,m} - \hat{b}_{I,0,l,m}\right) W_I\right\} =$$

$$= \sum_{m=0}^{\text{HD}(I,1,0)} \text{Var}\left\{\left(\hat{b}_{I,1,l,m} - \hat{b}_{I,0,l,m}\right) W_I\right\} =$$

$$= \sum_{m=0}^{\text{HD}(I,1,0)} \left(\hat{b}_{I,1,l,m} - \hat{b}_{I,0,l,m}\right)^2 \cdot 8N_0 =$$

$$= \sum_{m=0}^{\text{HD}(I,1,0)} 4 \cdot 8N_0 =$$

$$= \text{HD}(I,1,0) 4 \cdot 8N_0$$

where $(\hat{b}_{I,1,l,m} - \hat{b}_{I,0,l,m})^2 = 4$ because we are dealing with NRZ digits which may assume only values equal to $+1$ or $-1$. In the same manner, we get the variance of the quadrature part:

$$\text{Var}\left\{\sum_{m=0}^{\text{HD}(Q,1,0)} \left(\hat{b}_{Q,1,l,m} - \hat{b}_{Q,0,l,m}\right) W_Q\right\} = \text{HD}(Q,1,0) 4 \cdot 8N_0$$

Thus, we obtain

$$\begin{aligned}\mu_{\text{all}} &= E\{Y_{\text{int,tot}(0,1)}\} \\ \sigma^2_{\text{all}} &= \text{Var}\left\{Y_{\text{int,tot}(0,1)}\right\} + (\text{HD}(I,1,0) + \text{HD}(Q,1,0)) \cdot 4 \cdot 8N_0\end{aligned} \tag{4.21}$$

$$\begin{aligned}&\text{Prob}[Y_0 < Y_1] = \text{Prob}[N_{all} > \Delta Y_{0,1}] = \\ &= Q\left(\frac{\Delta Y_{0,1} - E[Y_{\text{int,tot}(0,1)}]}{\sqrt{\text{Var}\left\{Y_{\text{int,tot}(0,1)}\right\} + \text{HD}(I,1,0) \cdot 4 \cdot 8N_0 + \text{HD}(Q,1,0) \cdot 4 \cdot 8N_0}}\right)\end{aligned} \tag{4.22}$$

since $E\{Y_{\text{int,tot,}(0,1)}\} = 0$:

$$\text{Prob}[Y_0 < Y_1] = Q\left(\frac{\Delta Y_{0,1}}{\sqrt{\text{Var}\left\{Y_{\text{int,tot}(0,1)}\right\} + (\text{HD}(I,1,0) + \text{HD}(Q,1,0)) \cdot 4 \cdot 8N_0}}\right) \tag{4.23}$$

It is possible to show that:

$$\begin{aligned}\Delta Y_{0,1} &= \hat{c}_{0,t}\left(32 - (32 - 2\left(\text{HD}(I,0,1) + \text{HD}(Q,0,1)\right)\right) \\ &= 2\left(\text{HD}(I,0,1) + \text{HD}(Q,0,1)\right),\end{aligned} \tag{4.24}$$

Thus,

$$\begin{aligned}\text{Prob}[Y_0 < Y_1] &= Q\left(\frac{2\hat{c}_{0,t}\left(\text{HD}(I,0,1) + \text{HD}(Q,0,1)\right)}{\sqrt{\text{Var}\left\{Y_{\text{int,tot}(0,1)}\right\} + (\text{HD}(I,1,0) + \text{HD}(Q,1,0)) \cdot 4 \cdot 8N_0}}\right) = \\ &= Q\left(\frac{2\hat{c}_{0,t}\left(\text{HD}(0,1)\right)}{\sqrt{\text{Var}\left\{Y_{\text{int,tot}(0,1)}\right\} + (\text{HD}(1,0)) \cdot 4 \cdot 8N_0}}\right)\end{aligned} \tag{4.25}$$

where $(\text{HD}(I,0,1) + \text{HD}(Q,0,1)) = (\text{HD}(0,1))$ i.e $(\text{HD}(0,1))$ accounts for the summation between the Hamming distance between the in-phase parts of $(S_0, S_1)$ and the Hamming distance of the quadrature parts of $(S_0, S_1)$. Now, let's calculate the variance of $Y_{\text{int,tot}}$.

### 4.1.4 Variance of $Y_{\text{int,tot}(0,1)}$

The variance of the interferer might be written as follows

$$\text{Var}\Big[Y_{\text{int,tot}(0,1)}\Big] = \text{Var}\Big[Y_{I,int,1} + Y_{Q,int,1} - (Y_{I,int,0} + Y_{Q,int,0})\Big], \tag{4.26}$$

where $Y_{I,int,1}, Y_{Q,int,1}$ are the in-phase and quadrature phase of the received signal of the interferer matched to $S_1$ respectively, and $Y_{I,int,0}+Y_{Q,int,0}$ are the in-phase and quadrature phase of the received signal of the interferer matched to $S_0$ respectively. If we divide the received interferer signal to 4 parts as we have done in chapter 3, $(A_v, B_v, C_v, D_v)$, where $v \in (1,2,3,4)$ according to its case i.e according to the value $\hat{\tau_1}$, we can write

$$\begin{aligned}\mathrm{Var}\Big[Y_{\mathrm{int,tot}(0,1)}\Big] = \mathrm{Var}\Big[\frac{\hat{c}_{1,t}}{2\,T_c}\Big(\,(A_v|S_1\,-\,B_v|S_1) + (C_v|S_1\,-\,D_v|S_1) - \\ -\,(A_v|S_0\,-\,B_v|S_0) - (C_v|S_0\,-\,D_v|S_0)\,\Big)\Big],\end{aligned} \tag{4.27}$$

where $A_v|S_1$ is the first part of the In-phase received signal which corresponds to the integration of the product of the in-phase part of the interferer and the in-phase of the sequence $S_1$, $B_v|S_1$ is the second part of the received signal which corresponds to the integration of the product of in-phase part of the sequence $S_1$ and the Q-phase part of the interferer, $C_v|S_1$ is the first part of the Q-phase received signal which corresponds to the integration of the product of the Q-phase of the sequence $S_1$ with the in-phase part of the interferer, $D_v|S_1$ is the second part of the Q-phase received signal which corresponds to the integration of the product of the Q-phase of the sequence $S_1$ and the Q-phase part of the interferer. We know that the variance can be written as

$$\mathrm{Var}\Big[Y_{\mathrm{int,tot}(0,1)}\Big] = E\Big[\,\big(Y_{\mathrm{int,tot}(0,1)}\big)^2\,\Big] \,-\, \Big(E[Y_{\mathrm{int,tot}(0,1)}]\Big)^2, \tag{4.28}$$

However, $E[Y_{\mathrm{int,tot}(0,1)}] = 0$ so

$$\begin{aligned}\mathrm{Var}\Big[Y_{\mathrm{int,tot}(0,1)}\Big] &= E\Big[\,\big(Y_{\mathrm{int,tot}(0,1)}\big)^2\,\Big] \,= \\ &= \frac{\hat{c}_{1,t}^2}{4\,T_c^2}\,\Big[E[Y_{I,int,1}^2] + E[Y_{Q,int,1}^2] - E[Y_{I,int,0}^2] + E[Y_{Q,int,0}^2]\Big]\end{aligned} \tag{4.29}$$

$$\begin{aligned}\mathrm{Var}\Big[Y_{\mathrm{int,tot}(0,1)}\Big] = \frac{\hat{c}_{1,t}^2}{4\,T_c^2}\,\Big[\Big(E[A_v^2|S_1]\,-2\,E[A_v|S_1\,\cdot B_v|S_1]\,+E[B_v^2|S_1]+ \\ +\,E[C_v^2|S_1]\,-2\,E[C_v|S_1\,\cdot D_v|S_1]\,+E[D_v^2|S_1]\Big)- \\ -\,\Big(E[A_v^2|S_0]\,-2\,E[A_v|S_0\,\cdot B_v|S_0]\,+E[B_v^2|S_0]+ \\ +\,E[C_v^2|S_0]\,-2\,E[C_v|S_0\,\cdot D_v|S_0]\,+E[D_v^2|S_0]\Big)\Big]\end{aligned} \tag{4.30}$$

which could be written as

$$\mathrm{Var}\Big[Y_{\mathrm{int,tot}(0,1)}\Big] = \frac{\hat{c}_{1,t}^2}{4\,T_c^2}\,\Big[\Big(E[\mathcal{Z}(\phi_{c_1}, n_{\tau_1}, \hat{\tau_1})|S_1]\,-\,E[\mathcal{Z}(\phi_{c_1}, n_{\tau_1}, \hat{\tau_1})|S_0]\Big)\Big] \tag{4.31}$$

Therefore, if we want to generalize the equation to all other possible sequences $i = 1, \ldots, 15$ we can write

$$\mathrm{Var}\Big[Y_{\mathrm{int,tot}(0,i)}\Big] = \frac{\hat{c}_{1,t}^2}{4\,T_c^2}\,\Big[\Big(E[\mathcal{Z}(\phi_{c_1}, n_{\tau_1}, \hat{\tau}_1)|S_i]\;-\;E[\mathcal{Z}(\phi_{c_1}, n_{\tau_1}, \hat{\tau}_1)|S_0]\Big)\Big] \tag{4.32}$$

Thus,

$$\begin{aligned}\mathrm{Prob}[Y_0 < Y_i] &= Q\left(\frac{2\hat{c}_{0,t}\,(\mathrm{HD}(0,i))}{\sqrt{\mathrm{Var}\left\{Y_{\mathrm{int,tot}(0,i)}\right\} + 32N_0\mathrm{HD}(0,i)}}\right) = \\ &= Q\left(\frac{2\hat{c}_{0,t}\,(\mathrm{HD}(0,i))}{\sqrt{32N_0\mathrm{HD}(0,i)\;+\;\frac{\hat{c}_{1,t}^2}{4T_c^2}\,\Big[\Big(E[\mathcal{Z}(\phi_{c_1}, n_{\tau_1}, \hat{\tau}_1)|S_1]\;-\;E[\mathcal{Z}(\phi_{c_1}, n_{\tau_1}, \hat{\tau}_1)|S_i]\Big)\Big]}}\right)\end{aligned} \tag{4.33}$$

Basing on section 4.1.3, equation (4.33) is given by:

$$\mathrm{Prob}[Y_0 < Y_i] = Q\Big[\,(F(\phi_{c_1}, n_{\tau_1}, \hat{\tau}_1))^{-\frac{1}{2}}\,\Big], \tag{4.34}$$

where

$$F(\phi_{c_1}, n_{\tau_1}, \hat{\tau}_1) = \mathrm{D}^* e^{-\chi_0(t)} + \mathrm{B}^*(\phi_{c_1}, n_{\tau_1}, \hat{\tau}_1) e^{\chi_1(t)-\chi_0(t)}, \tag{4.35}$$

$$\begin{aligned}\mathrm{D}^* &= \frac{32 * N_0\, H_D(0,i)}{32^2\,\alpha_0^2\,E_{c,0}\,\frac{H_D(0,i)^2}{16^2}}, \\ &= \frac{N_0}{32\,\alpha_0^2\,E_{c,0}} \cdot \frac{256}{H_D(0,i)} = D \cdot \frac{256}{H_D(0,i)},\end{aligned}$$

$$\begin{aligned}\mathrm{B}^*(\phi_{c_1}, n_{\tau_1}, \hat{\tau}_1) &= \frac{E_{c,1}\,\alpha_1^2 E[\mathcal{Z}(\phi_{c_1}, n_{\tau_1}, \hat{\tau}_1)|S_1]}{32^2\,T_c^2\,E_{c,0}\alpha_0^2 \cdot \frac{H_D(0,i)^2}{16^2}} \;-\; \frac{E_{c,1}\,\alpha_1^2 E[\mathcal{Z}(\phi_{c_1}, n_{\tau_1}, \hat{\tau}_1)|S_0]}{32^2\,T_c^2\,E_{c,0}\alpha_0^2 \cdot \frac{H_D(0,i)^2}{16^2}} = \\ &= \Big(\frac{E_{c,1}\,\alpha_1^2\,E[\mathcal{Z}(\phi_{c_1}, n_{\tau_1}, \hat{\tau}_1)|S_0]}{2048\,T_c^2\,E_{c,0}\,\alpha_0^2} \cdot \frac{E[\mathcal{Z}(\phi_{c_1}, n_{\tau_1}, \hat{\tau}_1)|S_1]}{2 \cdot E[\mathcal{Z}(\phi_{c_1}, n_{\tau_1}, \hat{\tau}_1)|S_0] \cdot \frac{H_D(0,i)^2}{16^2}}\Big) - \\ &\quad \Big(\frac{E_{c,1}\,\alpha_1^2\,E[\mathcal{Z}(\phi_{c_1}, n_{\tau_1}, \hat{\tau}_1)]}{2048\,T_c^2\,E_{c,0}\,\alpha_0^2} \cdot \frac{1}{2 \cdot \frac{H_D(0,i)^2}{16^2}}\Big) = \\ &= \mathrm{B}(\phi_{c_1}, n_{\tau_1}, \hat{\tau}_1) \cdot \Big[\frac{E[\mathcal{Z}(\phi_{c_1}, n_{\tau_1}, \hat{\tau}_1)|S_1]}{2 \cdot E[\mathcal{Z}(\phi_{c_1}, n_{\tau_1}, \hat{\tau}_1)|S_0] \cdot \frac{H_D(0,i)^2}{16^2}} - \frac{1}{2 \cdot \frac{H_D(0,i)^2}{16^2}}\Big]\end{aligned} \tag{4.36}$$

where Thus, we could write $\mathrm{D}^*, \mathrm{B}^*$ as a function of $\mathrm{D}, \mathrm{B}$, the values of equation 4.3 which are the SNR component and the SIR component respectively. Therefore, assuming that the symbol sent is $S_0$ so the matching is done with respect to $S_0$ and we are computing the error probability of matching the received signal to other sequences, (4.13) can be written as

$$P_{e|S_0} = \sum_{i=1}^{15} \mathrm{Prob}[Y_0 < Y_i] = \sum_{i=1}^{15} Q\Big[ \Big( a_i \, D \, e^{-\chi_0(t)} + \, b_i \, \mathrm{B}(\phi_{c_1}, n_{\tau_1}, \hat{\tau}_1) \, e^{\chi_1(t) - \chi_0(t)} \Big)^{-\frac{1}{2}} \Big] \tag{4.37}$$

where $a_i, b_i$ are real constants for each selected scenario and have the following expressions

$$\begin{aligned} a_i &= \frac{256}{H_D(0,i)}, \\ b_i &= \frac{E[\mathcal{Z}(\phi_{c_1}, n_{\tau_1}, \hat{\tau}_1)|S_i]}{2 \cdot E[\mathcal{Z}(\phi_{c_1}, n_{\tau_1}, \hat{\tau}_1)|S_0] \cdot \frac{H_D(0,i)^2}{16^2}} - \frac{1}{2 \cdot \frac{H_D(0,i)^2}{16^2}} \\ &= \frac{128 \cdot (E[\mathcal{Z}(\phi_{c_1}, n_{\tau_1}, \hat{\tau}_1)|S_i] \, - \, E[\mathcal{Z}(\phi_{c_1}, n_{\tau_1}, \hat{\tau}_1)|S_0])}{H_D(0,i)^2 \, \cdot E[\mathcal{Z}(\phi_{c_1}, n_{\tau_1}, \hat{\tau}_1)|S_0]}, \end{aligned} \tag{4.38}$$

Therefore, since the matching is being done at the symbol level, the expression for the symbol error rate as a function of the received SINR $\gamma(t, \phi_{c_1}, n_{\tau_1}, \hat{\tau}_1)$ is

$$P_{e|S_0} = \sum_{i=1}^{15} Q\Big[ \Big( a_i \, D \, e^{-\chi_0(t)} + \, b_i \, \mathrm{B}(\phi_{c_1}, n_{\tau_1}, \hat{\tau}_1) \, e^{\chi_1(t) - \chi_0(t)} \Big)^{-\frac{1}{2}} \Big] \, = \, \mathrm{R}_s(\chi_0(t), \chi_1(t)), \tag{4.39}$$

where $\mathrm{R}_s(\chi_0(t), \chi_1(t))$ is the symbol error rate (SER, $\mathrm{R_s}$) assuming that the useful transmitted symbol is $S_0$. Thus, the *packet* error rate (PER, $\mathrm{R_p}$) is related to SINR through SER, where $\chi_0(t), \chi_1(t) \in (-\infty, \infty)$. $\mathrm{R_p}(\chi_0(t), \chi_1(t)) \in [0, 1]$ can be expressed as

$$\mathrm{R}_p(\chi_0(t), \chi_1(t)) = 1 \, - (1 \, - \, \mathrm{R}_s(\chi_0(t), \chi_1(t)))^{\frac{\ell_\mathrm{F}}{4}}, \tag{4.40}$$

We can write (4.39) as

$$\begin{aligned} \mathrm{R}_s(\chi_0(t), \chi_1(t)) &= \sum_{i=1}^{15} Q\Big[ \Big( \Omega_i(t, \phi_{c_1}, n_{\tau_1}, \hat{\tau}_1)(\mathrm{D}e^{-\chi_0(t)} + \mathrm{B}(\phi_{c_1}, n_{\tau_1}, \hat{\tau}_1) e^{\chi_1(t) - \chi_0(t)}) \Big)^{-\frac{1}{2}} \Big] \, = \\ &= \sum_{i=1}^{15} Q\Big[ \Big( \Omega_i(t, \phi_{c_1}, n_{\tau_1}, \hat{\tau}_1) \, L(t, \phi_{c_1}, n_{\tau_1}, \hat{\tau}_1) \Big)^{-\frac{1}{2}} \Big] \approx \\ &\approx \sum_{i=1}^{15} Q\Big[ \Big( \psi_i(t, \phi_{c_1}, n_{\tau_1}, \hat{\tau}_1) \, \Gamma \, (t, \phi_{c_1}, n_{\tau_1}, \hat{\tau}_1) \Big) \Big], \end{aligned} \tag{4.41}$$

where $\Gamma\left(t, \phi_{c_1}, n_{\tau_1}, \hat{\tau}_1\right)$ is a Gaussian process with mean $\eta_\Gamma$, variance $\sigma_\Gamma^2$ and autocovariance $c_\Gamma(\tau)$. $\psi_i(t, \phi_{c_1}, n_{\tau_1}, \hat{\tau}_1) = \left(\Omega_i(t, \phi_{c_1}, n_{\tau_1}, \hat{\tau}_1)\right)^{-\frac{1}{2}}$ can be seen as a function of interferer to noise ratio $\frac{\mathrm{B}(\phi_{c_1}, n_{\tau_1}, \hat{\tau}_1)}{D}\, e^{\chi_1(t)}$ and once we find $D$ it becomes a function of the interferer and can be expressed as

$$\psi_i(t, \phi_{c_1}, n_{\tau_1}, \hat{\tau}_1) = \sqrt{\frac{1 + \frac{\mathrm{B}(\phi_{c_1}, n_{\tau_1}, \hat{\tau}_1)}{D}\, e^{\chi_1(t)}}{a_i \; + \; b_i \cdot \frac{\mathrm{B}(\phi_{c_1}, n_{\tau_1}, \hat{\tau}_1)}{D}\, e^{\chi_1(t)}}} = f_i\left(\chi_1(t)\right), \tag{4.42}$$

with $\frac{\mathrm{B}(\phi_{c_1}, n_{\tau_1}, \hat{\tau}_1)}{D}, a_i, b_i$ are know parameters $\forall i$. $\chi_1(t)$ is a Gaussian process with mean $\mu_{\chi_1} = 0$, variance $\sigma_{\chi_1}^2$ and autocovariance $c_{\chi_1}(\tau)$. Since $\frac{\mathrm{B}(\phi_{c_1}, n_{\tau_1}, \hat{\tau}_1)}{D}, a_i, b_i$ are positive for $\forall i$ and $e^{\chi_1(t)}$ is defined in the range $(0, +\infty)$, both nominator and denominator of $\psi_i$ are positive and the denominator can not be zero in that range. Consequently, $\psi_i(t, \phi_{c_1}, n_{\tau_1}, \hat{\tau}_1)$ is a continuous function $\forall i$ with a probability density function expressed as

$$f\left(\psi_i\right) = \sqrt{\frac{2}{\pi}} \frac{\psi_i\, e^{-\frac{\left(ln\left(\frac{D\cdot(1-a_i\,\psi_i^2)}{B\cdot(b_i\,\psi_i^2-1)}\right)-\mu_{\chi_1}\right)^2}{2\,\sigma_{\chi_1}^2}}}{\sigma_{\chi_1}\left(\frac{1-a_i\,\psi_i^2}{b_i\,\psi_i^2-1}\right)} \cdot \frac{(a_i - b_i)}{(b_i\,\psi_i^2 - 1)^2}, \tag{4.43}$$

The proof of this equation can be found in appendix A
From 4.42 and 4.41 we can say that $\mathrm{R}_s(\chi_0(t), \chi_1(t))$ can be also considered as a function of both $\Gamma(t, \phi_{c_1}, n_{\tau_1}, \hat{\tau}_1)$ and $\chi_1(t)$ and written as

$$\mathrm{R}_s(\chi_0(t), \chi_1(t)) = g_s\Big(\chi_1(t), \Gamma(t, \phi_{c_1}, n_{\tau_1}, \hat{\tau}_1)\Big). \tag{4.44}$$

Therefore, the PER could be expressed as

$$\begin{aligned} \mathrm{R}_p\left(\chi_1(t), \Gamma(t, \phi_{c_1}, n_{\tau_1}, \hat{\tau}_1)\right) &= 1 \; - \Big(1 \; - \; g_s\Big(\chi_1(t), \Gamma(t, \phi_{c_1}, n_{\tau_1}, \hat{\tau}_1)\Big)\Big)^{\frac{\ell_\mathrm{F}}{4}} = \\ &= g_p\Big(\chi_1(t), \Gamma(t, \phi_{c_1}, n_{\tau_1}, \hat{\tau}_1)\Big), \end{aligned} \tag{4.45}$$

### 4.1.5 Link Quality Metrics

An unreliable communication link can be characterized by the likelihood of the information losses and by the maximum number of consecutive dropouts [31], which in stochastic framework have a non-negligible probability of occurrence. The PER defined on the presented implicit *analytic* model of SINR encompasses this information, since the probability density function $f_\Gamma(\cdot)$ of the SINR is known and both $\chi_1(t), \Gamma(t, \phi_{c_1}, n_{\tau_1}, \hat{\tau}_1)$ are continuous

functions in the range $(-\infty, +\infty)$, meaning that both $g_s\Big(\chi_1(t), \Gamma(t, \phi_{c_1}, n_{\tau_1}, \hat{\tau}_1)\Big) \in [0, 0.5]$, $g_p\Big(\chi_1(t), \Gamma(t, \phi_{c_1}, n_{\tau_1}, \hat{\tau}_1)\Big) \in [0, 1]$ are continuous monotonically non-increasing. Therefore, by the law of the unconscious statistician and following the reasoning of [100, p. 847] the expected value of the PER, denoted by $\eta_{\mathrm{A}}$, can be obtained as a double integral over two ranges as follows

$$\begin{aligned}\eta_{\mathrm{A}} &= \int_{-\infty}^{+\infty}\int_{-\infty}^{+\infty} g_p\Big(\chi_1(t), \Gamma(t, \phi_{c_1}, n_{\tau_1}, \hat{\tau}_1)\Big) f_{\chi_1,\Gamma}(x, y)\, dx\, dy = \\ &= \int_{-\infty}^{+\infty}\int_{-\infty}^{+\infty} g_p\Big(\chi_1(t), \Gamma(t, \phi_{c_1}, n_{\tau_1}, \hat{\tau}_1)\Big) f_{\Gamma|\chi_1}(y|x)\ f_{\chi_1}(x) dx\, dy,\end{aligned} \tag{4.46}$$

where $f_{\chi_1,\Gamma}(x, y)$ refers to the joint pdf of $\Gamma(t, \phi_{c_1}, n_{\tau_1}, \hat{\tau}_1)$ and $\chi_1(t)$
The variance of PER, indicated by $\sigma^2_{\mathrm{A}}$, can be computed as:

$$\sigma^2_{\mathrm{A}} = \int_{-\infty}^{+\infty}\int_{-\infty}^{+\infty} g_p\Big(\chi_1(t), \Gamma(t, \phi_{c_1}, n_{\tau_1}, \hat{\tau}_1)\Big) f_{\chi_1,\Gamma}(x, y)\, dx\, dy - \eta^2_{\mathrm{A}}. \tag{4.47}$$

In practical applications, the PER is considered negligible when it is smaller than a specified threshold $\varepsilon_{\mathrm{p}}$, which may be as small as the machine epsilon. Since $\mathrm{R_p}(\cdot)$ is a continuous monotonically non-increasing function of $\Gamma(t)$, any value $\upsilon_{\Gamma}$ of the SINR such that $\upsilon_{\Gamma} \geq \upsilon^{\star}_{\Gamma}(\varepsilon_{\mathrm{p}})$, where

$$\upsilon^{\star}_{\Gamma}(\varepsilon_{\mathrm{p}}) \triangleq \min_{\upsilon} \mathrm{R_p}(\upsilon) = \varepsilon_{\mathrm{p}} \tag{4.48}$$

almost surely has PER equal to zero. The value of $\upsilon^{\star}_{\Gamma}(\varepsilon_{\mathrm{p}})$ can be easily computed by one of the standard root-finding algorithms, and the probability of having a non-negligible PER is given by the value of the cumulative distribution function $F_{\Gamma}(\cdot)$ of the $\Gamma(t, \phi_{c_1}, n_{\tau_1}, \hat{\tau}_1)$ in $\upsilon^{\star}_{\Gamma}(\varepsilon_{\mathrm{p}})$. When there is a time correlation, i.e., when $c_{\Gamma}(k\ell_{\mathrm{E}}+1) \neq 0$ for all $k \in \mathbb{N}$, the formal definition of the probability of having a packet error *burst* of length $\ell_{\mathrm{B}}$ relies on the notion of the multivariate normal cumulative distribution function [112]

$$F_{\Gamma_1 \cdots \Gamma_{\ell_{\mathrm{B}}}}(\upsilon \mathbf{1}) \triangleq \frac{1}{\sqrt{|\boldsymbol{\Sigma}|(2\pi)^{\ell_{\mathrm{B}}}}} \int_{-\infty}^{\upsilon-\eta_{\Gamma}} \cdots \int_{-\infty}^{\upsilon-\eta_{\Gamma}} e^{-0.5\mathbf{z}'\boldsymbol{\Sigma}^{-1}\mathbf{z}} dz_1 \cdots dz_{\ell_{\mathrm{B}}},$$

where $\mathbf{1}$ denotes the column vector of the appropriate length with all entries being equal to the scalar 1, $|\cdot|$ indicates the determinant, $'$ symbolizes the operation of transposition, while $\boldsymbol{\Sigma}$ is a symmetric, positive definite covariance matrix, whose entry in position $(i, j)$ is the value of $c_{\Gamma}(\tau)$, for $\tau = (i-j)\ell_{\mathrm{E}}+1$, if $i \neq j$, and $\tau = 0$ otherwise. We observe that $\boldsymbol{\Sigma}$ is banded [112], i.e., it satisfies the condition $c_{\Gamma}(\tau) = 0$ whenever $\tau > l$ for some $l \geq 0$. This special correlation structure of $\boldsymbol{\Sigma}$ allows efficient computation [113] of $F_{\Gamma_1 \cdots \Gamma_{\ell_{\mathrm{B}}}}\big(\upsilon^{\star}_{\Gamma}(\varepsilon_{\mathrm{p}})\mathbf{1}\big)$.

Since the probability of a packet error burst is negligible when it is smaller than a specified threshold $\varepsilon_{\mathrm{B}}$, the largest number of consecutive dropouts with a non-negligible probability of occurrence $\ell^{\star}_{\mathrm{B}}(\varepsilon_{\mathrm{B}},\varepsilon_{\mathrm{p}})$ can be computed iteratively:

$$\begin{aligned}\ell^{\star}_{\mathrm{B}}(\varepsilon_{\mathrm{B}},\varepsilon_{\mathrm{p}}) \triangleq \max_{\ell_{\mathrm{B}}} F_{\Gamma_1\cdots\Gamma_{\ell_{\mathrm{B}}}}\big(\upsilon^{\star}_{\Gamma}(\varepsilon_{\mathrm{p}})\mathbf{1}\big) \text{ subject to}\\ F_{\Gamma_1\cdots\Gamma_{\ell_{\mathrm{B}}}}\big(\upsilon^{\star}_{\Gamma}(\varepsilon_{\mathrm{p}})\mathbf{1}\big)\geq\varepsilon_{\mathrm{B}}.\end{aligned} \tag{4.49}$$

When $l\leq\ell_{\mathrm{E}}$, we have that $F_{\Gamma_1\cdots\Gamma_{\ell_{\mathrm{B}}}}\big(\upsilon^{\star}_{\Gamma}(\varepsilon_{\mathrm{p}})\mathbf{1}\big)=F_{\Gamma}\big(\upsilon^{\star}_{\Gamma}(\varepsilon_{\mathrm{p}})\big)^{\ell_{\mathrm{B}}}$, so it is easy to verify that

$$\ell^{\star}_{\mathrm{B}}(\varepsilon_{\mathrm{B}},\varepsilon_{\mathrm{p}})=\mathrm{ceil}\left(\frac{\ln(\varepsilon_{\mathrm{B}})}{\ln\left(\frac{1}{2}\left(1+\mathrm{erf}\left(\frac{\upsilon^{\star}_{\Gamma}(\varepsilon_{\mathrm{p}})-\eta_{\Gamma}}{\sigma_{\Gamma}\sqrt{2}}\right)\right)\right)}\right), \tag{4.50}$$

where $\mathrm{ceil}(\cdot)$ and $\mathrm{erf}(\cdot)$ are the ceiling and error functions, respectively. The presented closed form expression (4.50) of $\ell^{\star}_{\mathrm{B}}(\varepsilon_{\mathrm{B}},\varepsilon_{\mathrm{p}})$ provides a useful lower bound on its true value (4.49).

In summary, the LQMs characterizing the analytic model of the WirelessHART link are listed in Table 4.1. They will be compared with the LQMs of finite-state abstractions of the analytic model in order to validate these abstractions and provide guidelines on the choice of parameters defining the aforementioned abstractions.

Table 4.1: Analytic LQMs.

| **Link quality metric** | **Notation** |
|---|---|
| The packet error probability (PEP) | $\eta_{\mathrm{A}}$ |
| The PER's variance | $\sigma^2_{\mathrm{A}}$ |
| The maximum number of consecutive dropouts | $\ell^{\star}_{\mathrm{B}}(\varepsilon_{\mathrm{B}},\varepsilon_{\mathrm{p}})$ |

### 4.1.6 Finite-state Markov model

The analytic model of a communication link presented in the previous subsections is defined on a continuous state-space, where the SINR is defined on the set of all ordinary real numbers, namely $\Gamma(t,\phi_{c_1},n_{\tau_1},\hat{\tau}_1)\in(-\infty,+\infty)$. Nevertheless, there are several application scenarios (e.g. decoding in channels with memory, adaptive transmission, as well as modeling of lossy communication link's error bursts) where using a finite number of channel states can be more advantageous [38].

The coarsest abstraction of the analytic model collapses the infinite-dimensional state-space into one state with a representative PEP (given by $\eta_{\mathrm{A}}$), which may be seen as a probability of the packet loss event in the Bernoulli distribution. If random variables are *jointly normal* and uncorrelated, then they are independent: if the autocovariance of the Gaussian process representing the evolution of $\Gamma(t,\phi_{c_1},n_{\tau_1},\hat{\tau}_1)$ has $c_\Gamma(\tau)\approx 0$ for all $\tau > \ell_{\mathrm{E}}$, then the i.i.d. Bernoulli model introduces no conservatism.

In a more accurate finite-state Markov channel abstraction the range of SINR is divided into several consecutive regions, to each of which is associated a certain representative PEP. A region $i$ of the values of SINR is mapped into a state $\mathbf{s}_i$ of the related Markov chain and is delimited by two thresholds $\zeta_i$ and $\zeta_{i+1}$ belonging to the set of extended reals. The steady state probability $\mathbf{p}_i$ of a state $\mathbf{s}_i$ is the probability that the SINR is between thresholds of the region, which is given by

$$\mathbf{p}_i = \int_{\zeta_i}^{\zeta_{i+1}} f_\Gamma(\zeta) d\zeta, \tag{4.51}$$

while the PEP associated to the same state is given by the expected value of the PER within the respective region, i.e.

$$\eta_{\mathrm{M}}^{(i)} = \frac{1}{\mathbf{p}_i} \int_{\zeta_i}^{\zeta_{i+1}} \int_{-\infty}^{+\infty} g_p\Big(\chi_1(t), \Gamma(t,\phi_{c_1},n_{\tau_1},\hat{\tau}_1)\Big) f_{\Gamma/\chi_1}(y/x)\ f_{\chi_1}(x) dx\, dy. \tag{4.52}$$

The TPM of the Markov channel may be obtained from the level crossing rate (LCR) analysis [38]. This analysis considers the number of times per second the SINR crosses each threshold (with the obvious exception of the two thresholds having the values equal to $\pm\infty$) in a downward direction, divided by the average number of symbols per second the SINR falls in the interval associated to state of interest (i.e. $(\mathbf{p}_i/T_s) = 62500\mathbf{p}_i$ for the WirelessHART, [12, p. 49]). In particular, the well known expressions for the LCR analysis of a Gaussian process [114] may be used as follows. Let $\mathrm{R_c}$ denote the rate of *crossing* a certain threshold. Then

$$\mathrm{R_c}(\zeta_i) = \frac{1}{2\pi}\sqrt{\frac{\ddot{c}_\Gamma(0)}{c_\Gamma(0)}}\, e^{-\frac{(\zeta_i-\eta_\Gamma)^2}{2c_\Gamma(0)}},\ \text{with } \ddot{c}_\Gamma(0) \triangleq \frac{d^2 c_\Gamma(\tau)}{d\tau^2}\Big|_{\tau=0}.$$

We remark that since $c_\Gamma(\tau)$ is examined only for $\tau = 0$, the LCR analysis may introduce non-negligible approximation errors and should be used with care. When evolving at the symbol rate, the transition probabilities between the Markov channel's states are denoted by $\Pi_{i\triangleright j}$, $i,j \le N$. In the LCR approach they are approximated as

$$\begin{cases} \Pi_{i\triangleright i+1} \approx \frac{\mathrm{R_c}(\zeta_{i+1})T_s}{\mathbf{p}_i} & \forall\, 1 \le i \le N-1, \\ \Pi_{i\triangleright i-1} \approx \frac{\mathrm{R_c}(\zeta_i)T_s}{\mathbf{p}_i}, & \forall\, 2 \le i \le N, \end{cases} \tag{4.53}$$

where $N$ here is the number of channel's states. Such an approximation is valid under assumptions that the LCR at the chosen thresholds is much smaller than $(P_i/T_s)$ and that the values of SINR during symbol duration time $T_s$ either stay in the same region $i$ or transit to their immediate neighboring regions $i\pm1$. When satisfied, the stated assumptions allow to derive the remaining nonzero transition probabilities as

$$\begin{cases} \Pi_{1\triangleright 1} = 1 - \Pi_{1\triangleright 2} \\ \Pi_{N\triangleright N} = 1 - \Pi_{N\triangleright N-1}, \\ \Pi_{i\triangleright i} = 1 - \Pi_{i\triangleright i-1} - \Pi_{i\triangleright i+1} \quad \text{for} \quad 2 \leq i \leq N-1. \end{cases} \tag{4.54}$$

When the aforementioned assumptions are not satisfied, the channel state transition probabilities should be derived from integrating the joint PDF of the SINR over two consecutive symbol time intervals and over the desired regions [38] as

$$\Pi_{i\triangleright j} = \frac{\int_{\zeta_i}^{\zeta_{i+1}} \int_{\zeta_j}^{\zeta_{j+1}} f_\Gamma(z_{t-1}, z_t)\, dz_{t-1} dz_t}{\mathbf{p}_i}, \tag{4.55}$$

where, from the definition of the autocovariance, the two-dimensional PDF of the Gaussian process $\Gamma(t)$ is

$$f_\Gamma(z_{t-1}, z_t) = \frac{1}{2\pi\sqrt{\sigma_\Gamma^4 - c_\Gamma^2(1)}} \cdot \cdot e^{-\frac{1}{2}\frac{\sigma_\Gamma^2 (z_{t-1}-\eta_\Gamma)^2 + \sigma_\Gamma^2 (z_t - \eta_\Gamma)^2 - 2c_\Gamma(1)(z_{t-1}-\eta_\Gamma)(z_t-\eta_\Gamma)}{\sigma_\Gamma^4 - c_\Gamma^2(1)}}.$$

Thus, thanks to the closed-form expression of $f_\Gamma(z_{t-1}, z_t)$, any transition probability $\Pi_{i\triangleright j}$ can be computed numerically. The associated TPM is denoted by $\mathbf{\Pi}$. It is computed by taking into account the symbol rate, and it is defined as a stochastic $N \times N$ matrix with entries $\Pi_{i\triangleright j}$.

Since the values of $\Pi_{i\triangleright j}$ depend heavily on the choice of the thresholds delimiting the regions of SINR associated to each state of the Markov chain, in the literature on finite-state Markov channel abstractions there are different methods of partitioning the range of SINR, see e.g. [38, 115]. In this thesis we consider two well known approaches for doing such methods of partitioning. The first one consists in choosing $\upsilon_\Gamma^\star(\varepsilon_\mathrm{p})$, that can be computed via (4.48), as the only threshold, obtaining a Markov channel with two modes, namely "good" and "bad". When the channel is in "good" mode of operation, the transmissions occur without any errors, i.e. $\eta_\mathrm{M}^{(\mathrm{g})} \approx 0$ (since its exact value is by construction $\leq \varepsilon_\mathrm{B}$), while in "bad" operational mode the channel has a probability $\eta_\mathrm{M}^{(\mathrm{b})} > 0$ of presenting

Table 4.2: Characterization of an $N$-state Markov channel abstraction.

| **Parameter** | **Notation** |
|---|---|
| The steady state probability | $\mathbf{p}_i$ |
| The associated PEP | $\eta_{\mathrm{M}}^{(i)}$ |
| The thresholds | $\zeta_i$ |
| TPM | $\mathbf{P}$ |

a failure. This model is known as Gilbert channel, see e.g. [38],[39]. In the second approach of partitioning the range of SINR, the thresholds are selected in such a way that the steady state probabilities of being in any state are equal [38],[115], i.e. $\forall i,j \leq N$, $\mathbf{p}_i = \mathbf{p}_j = (1/N)$.

As in case of analytic model of the WirelessHART link, also its finite-state abstraction should evolve at the timescale of the control-related data transmissions, and not at the timescale of individual symbols. Fortunately, the transition probabilities of channel's states in between two control-related data transmissions can be computed simply as $\ell_{\mathrm{E}}$-th power of $\mathbf{\Pi}$, since the considered Markov channel is time-homogeneous and has a finite number of states. We define this new TPM as

$$[p_{ij}]_{i,j=1}^{N} \triangleq \mathbf{P} = \mathbf{\Pi}^{\ell_{\mathrm{E}}}. \tag{4.56}$$

The values of $p_{ij}$ may also be computed directly by integrating the joint PDF of the SNIR over two consecutive packet transmissions and over the desired regions, so we could write

$$p_{ij} = \frac{\int_{\zeta_i}^{\zeta_{i+1}} \int_{\zeta_j}^{\zeta_{j+1}} f_{\Gamma}(z_{t-\ell_{\mathrm{E}}-1}, z_t)\, dz_{t-\ell_{\mathrm{E}}-1} dz_t}{\mathbf{p}_i}. \tag{4.57}$$

In summary, the $N$-state Markov channel abstraction of the wireless link is characterized by the parameters illustrated in Table 4.2, knowing that the first and last thresholds are by construction $\zeta_1 = -\infty$ and $\zeta_{N+1} = +\infty$.

These parameters are used to define the related **Markovian link quality metrics**: the long-run mean PEP of the Markov channel, $\eta_{\mathrm{M}}$, is by construction equal to $\eta_{\mathrm{A}}$ since

$$\eta_{\mathrm{M}} = \sum_{i=1}^{N} \eta_{\mathrm{M}}^{(i)} \mathbf{p}_i = \sum_{i=1}^{N} \int_{\zeta_i}^{\zeta_{i+1}} \int_{-\infty}^{+\infty} g_p\Big(\chi_1(t), \Gamma(t, \phi_{c_1}, n_{\tau_1}, \hat{\tau}_1)\Big) f_{\Gamma/\chi_1}(y/x)\ f_{\chi_1}(x) dx\, dy, \tag{4.58}$$

while its long-run variance, $\sigma_{\mathrm{M}}^2$, is given by

$$\sigma_{\mathrm{M}}^2 = \sum\nolimits_{i=1}^{N} (\eta_{\mathrm{M}}^{(i)})^2 \mathbf{p}_i - \eta_{\mathrm{M}}^2. \tag{4.59}$$

To find the maximal number of consecutive packet *dropouts* with a non-negligible probability of occurrence, denoted by $\ell_{\mathrm{D}}^{\star}$, we rely on the notion of a sojourn time in a given subset of states of a discrete-time Markov process (see [116]). It is defined on a proper subset of all $N$ states of the Markov channel, indicated by $\mathbb{S}_0$, where the packets have a non-negligible error probability, i.e. $\mathbb{S}_0 \triangleq \{\mathbf{s}_i : \eta_{\mathrm{M}}^{(i)} \geq \varepsilon_{\mathrm{p}}\}$. We denote by $\mathbb{S}_1$ the complementary subset of $\mathbb{S}_0$. $\mathbb{S}_1$ should contain at least one element. If all the states of the Markov channel have non-negligible PEP, then the analysis of the sojourn time is possible only after splitting the $N$-th state into two, where the new last state, denoted by $\mathbf{s}_{N+1}$, has $\eta_{\mathrm{M}}^{(N+1)} < \varepsilon_{\mathrm{B}}$. Since $\ell_{\mathrm{D}}^{\star}$ is related to the worst-case analysis, the initial state of the channel is considered to be a state in $\mathbb{S}_0$ with the largest value of the PEP. Therefore, by construction the initial probability distribution vector $\mathrm{v}_0$ has 1 in correspondence of $\mathbf{s}_1$, and 0 everywhere else. The partition $\{\mathbb{S}_0, \mathbb{S}_1\}$ of the state space of the Markov channel induces a decomposition of its TPM $\mathbf{P}$ into four submatrices:

$$\mathbf{P} = \begin{bmatrix} \mathbf{P}_{00} & \mathbf{P}_{01} \\ \mathbf{P}_{10} & \mathbf{P}_{11} \end{bmatrix}, \quad \text{with} \quad \mathbf{P}_{\mathrm{AB}} \triangleq [p_{ij}]_{i,j:i\in\mathbb{S}_{\mathrm{A}},j\in\mathbb{S}_{\mathrm{B}}}, \tag{4.60}$$

where $\mathrm{A}, \mathrm{B} \in \{0, 1\}$. Accordingly, the probability of having $\ell_{\mathrm{D}}$ consecutive dropouts during $k$-th visit of partition $\mathbf{P}_{00}$ is

$$\begin{aligned} \Delta(\ell_{\mathrm{D}}, k) = \mathrm{v}_0 \left( (\mathbb{I} - \mathbf{P}_{00})^{-1} \mathbf{P}_{01} (\mathbb{I} - \mathbf{P}_{11})^{-1} \mathbf{P}_{10} \right)^{k-1} \cdot \\ \cdot \mathbf{P}_{00}^{\ell_{\mathrm{D}}-1} (\mathbb{I}\mathbf{P}_{00}) \mathbf{1}, \end{aligned} \tag{4.61}$$

where $\mathbb{I}$ is the identity matrix of the appropriate size. Then, $\ell_{\mathrm{D}}^{\star}$ is obtained as the solution of the optimization problem

$$\max(\ell_{\mathrm{D}}), \quad \text{subject to} \quad \Delta(\ell_{\mathrm{D}}, k) \geq \varepsilon_{\mathrm{B}}, \ k \geq 0. \tag{4.62}$$

In summary, the Markovian LQMs listed in Table 4.3 can be compared with the LQMs characterizing the analytic model of the radio link (see Table 4.1), permitting us to evaluate and validate this finite-state model of the WirelessHART in straightforward manner.

It is worth mentioning that the wireless needs for industrial applications are significantly different from those required for residential, commercial, or military applications [10]. Many constraints could be taken into consideration such as device cost, system cost, life-cycle cost, reliability, maintainability, consistency, robustness, extensibility, security, coexistence, regulatory restrictions, interconnectability, etc. One method for categorizing the communication needs of industrial applications is classes based on the usage like in

Table 4.3: Markovian LQMs.

| **Link quality metric** | **Notation** |
|---|---|
| The long-run mean PEP | $\eta_{\mathrm{M}}$ |
| The long-run variance of PER | $\sigma^2_{\mathrm{M}}$ |
| The maximal number of consecutive dropouts | $\ell^{\star}_{\mathrm{D}}$ |

[10]. Therefore, according to safety, control and monitoring constraints, there are different classes of communication needs. The ideal link in our plants should satisfy closed loop regulatory control needs so it belongs to "often critical" class. An example of these communication needs is that the average packet reception rate should be at least 0.9999 and the maximum fading length $< 500ms$ [10].

## 4.2 Summary

In this chapter, we found a tractable representation of the explicit analytic model derived in chapter 3. To this aim, we approximated it with another random process (e.g. log-normal process) and then applied moment matching approach to get the signal statistics. We derived the probability of incorrect received packets taking into account both the noise and the interference effect. Then, we introduce the LQMs which allow us to enable accurate representation of the radio link's average and its extreme behavior. By embracing these LQMs, we handle a consistent finite-state Markov link. In the next chapter, we will show on a case study from the automatic control domain how the quality metrics permit to find a high fidelity finite-state abstraction of the analytic channel useful for solving networked control problems.

Chapter 5

# Applying the model

In this chapter, we will apply our model in WNCSs to prove its applicability on different protocols in different scenarios and how it could allow us to improve the stability and thus the overall control performance of a closed loop system. We base on some assumptions to get a simplified yet realistic version of our model [3] and choose WirelessHART as a wireless industrial control protocol subject to different imperfections. Then, we apply this model and examine its relevancy on an inverted pendulum on a cart and we get the results published in [3]. Moreover, we generalize the application to cover other protocols including ISA-100.11a, IEEE 802.15.4e and present a thorough parametric analysis of the wireless link model subject to the effect of a persistent interferer with the variation of different parameters.

## 5.1 Numerical results

We simplify the model by considering some assumptions. First, we assume the transmitted signal of interest is a quadrature phase shift keying (QPSK) direct sequence spread spectrum (DSSS) signal with rectangular pulse. Moreover, we assume that the received signal arrives at the receiver with negligible time offset and phase offset. In particular, for the same scenario of chapter 3 we have the signal received by the reference user

$$y(t) = \sum_{i=0}^{1} \alpha_i e^{\frac{\beta_i(t)}{2}} s_i(t) + w(t), \tag{5.1}$$

where $\alpha_i = 10^{\frac{-\varsigma(d_i)}{10}}$ is the path loss coefficient, $s_i(t)$ is the quadrature phase shift keying (QPSK) direct sequence spread spectrum (DSSS) signal, that could be written as

$$s_i(t) = \sqrt{2P_i}a_i(t)[b_{I,i}(t)\cos(2\pi f_c t) - b_{Q,i}(t)\sin(2\pi f_c t)]\,,$$

with $P_i$ being the transmitted (Tx) power over the $i$-th link, $a_i(t)$ the spreading signal, $b_{j,i}(t)$ the baseband data signal on the in-phase ($j = I$) or quadrature ($j = Q$) component, $f_c$ the center frequency. Notably,

$$a_i(t) = \sum_{l=-\infty}^{+\infty} \bar{a}_{i,l} p_{i,T_c}(t - lT_c), \tag{5.2}$$

$$b_{j,i}(t) = \sum_{m=-\infty}^{+\infty} \bar{b}_{j,i,m} p_{i,T_s}(t - mT_s), \tag{5.3}$$

where $\{\bar{a}_{i,l}\}$ denotes the spreading sequences for the $i$-th link and $\{\bar{b}_{j,i,m}\}$ the binary data sequence for the $i$-th link on the I or Q component. Moreover, $p_{i,T_c}$ and $p_{i,T_s}$ are rectangular pulses with chip duration $T_c$ and symbol duration $T_s$. We assume also a coherent demodulation, allowing $y(t)$ to be decomposed into its $I$ and $Q$ components, $Y_I(t)$ and $Y_Q(t)$.

Then the next step of our simplified modeling framework is to derive an explicit analytic model od SINR

### 5.1.1 Explicit analytic model of SINR

In this case and following [106], the output of the correlation receiver matched to the user signal is given by

$$Y_j(t) = \sum_{i=0}^{1} Y_{j,i}(t) + W_j(t), \tag{5.4}$$

where $Y_{j,i}(t)$ and $W_j(t)$ are the components of $y_i(t)$ and $w(t)$,

$$Y_{j,i}(t) = \alpha_i e^{\frac{\chi_i(t)}{2}} \sqrt{\frac{P_i T_s}{2}} u_{j,i}, \tag{5.5}$$

with $u_{j,i}$ being the $I$ or $Q$ component of the transmitted complex symbol $u_i$, while $\chi_i(t)$ is the same value as in equation 3.17

Thus, the SINR (which will be denoted by $\Gamma$ in logarithmic scale, and by $\gamma$ when using the power value, $\Gamma \triangleq 10\log_{10}(\gamma)$ [dB]) conditioned to PCEs and shadowing, assuming $\sqrt{u_{Q,i}^2 + u_{I,i}^2} = 1$, and after some algebra is

$$\gamma(t) = \frac{\sqrt{Y_{I,0}^2(t)+Y_{Q,0}^2(t)}}{\sqrt{\frac{N_0 T_s}{4}+\mathrm{var}\left\{\sqrt{Y_{I,1}^2(t)+Y_{Q,1}^2(t)}\right\}}}$$
$$= \sqrt{\frac{P_0 e^{\chi_0(t)}\alpha_0^2}{\frac{N_0}{4}+\frac{8}{3G}P_1 e^{\chi_1(t)}\alpha_1^2}}, \tag{5.6}$$

where the expectations are taken with respect to carrier phases, time delays, data symbols but not with respect to random processes vectors $\boldsymbol{\xi}(t) = (\xi_0(t), \xi_1(t))$, $\boldsymbol{\beta}(t) = (\beta_0(t), \beta_1(t))$ [106]. $N_0$ denotes the noise spectral density, $G = WT_s$ is the processing gain, $W$ is the bandwidth, $1/T_s$ is the symbol rate.

The following step of our modeling process is approximating the SINR function with another random process, (e.g. log-normal process) and then apply moment matching approach to get the signal statistics.

### 5.1.2 Implicit analytic model of SINR

Following the same approach of [110] and since the time and phase offsets are negligible so the SINR will be function of just one factor which is the time i.e $\Gamma(t)$. By letting $\Gamma(t) = \mathrm{L}^{-1/2}(t)$, where $\mathrm{L}(t)$ can be expressed as

$$\mathrm{L}(t) = \mathrm{D}e^{-\chi_0(t)} + \mathrm{B}e^{\chi_1(t)-\chi_0(t)}, \tag{5.7}$$

$$\mathrm{D} = \frac{N_0}{4\alpha_0^2 P_0}, \quad \mathrm{B} = \frac{8P_1\alpha_1^2}{3GP_0\alpha_0^2}. \tag{5.8}$$

So, we apply the moment matching technique [110] as follows. Let $Z(t)$ be a Gaussian process with mean $\eta_Z$, variance $\sigma_Z^2$, and autocovariance $c_Z(\tau)$, such that $\mathrm{L}(t) \approx e^{Z(t)}$. Let $\mathrm{E}\{\cdot\}$ denote the mathematical expectation. Then

$$\begin{cases} \mathrm{M}_1 = \mathrm{E}\{\mathrm{L}(t)\} \triangleq \mathrm{E}\{e^{Z(t)}\} = e^{\eta_Z + \frac{1}{2}\sigma_Z^2}, \\ \mathrm{M}_2(\tau) = \mathrm{E}\{\mathrm{L}(t)\mathrm{L}(t+\tau)\} \triangleq \mathrm{E}\{e^{Z(t)+Z(t+\tau)}\} \\ \qquad\quad = e^{2\eta_Z + \sigma_Z^2 + c_Z(\tau)}, \\ \mathrm{M}_2(0) = e^{2\eta_Z + 2\sigma_Z^2}. \end{cases} \tag{5.9}$$

Solving the equations defining $\mathrm{M}_1$, $\mathrm{M}_2(\tau)$ and $\mathrm{M}_2(0)$ in $\eta_Z$, $\sigma_Z^2$ and $c_Z(\tau)$ yields the following expressions:

$$\begin{cases} \eta_Z = 2\ln \mathrm{M}_1 - \frac{1}{2}\ln \mathrm{M}_2(0), \\ \sigma_Z^2 = \ln \mathrm{M}_2(0) - 2\ln \mathrm{M}_1, \\ c_Z(\tau) = \ln\left(\frac{\mathrm{M}_2(\tau)}{\mathrm{M}_1^2}\right). \end{cases} \tag{5.10}$$

Since $\xi_i(t)$ and $\beta_i(t)$ are zero mean independent processes,

$$\begin{cases} \mathrm{M}_1 = \mathrm{D}e^{\frac{1}{2}(\sigma_{\xi_0}^2+\sigma_{\beta_0}^2)} + \mathrm{B}e^{\frac{1}{2}(\sigma_{\xi_1}^2+\sigma_{\beta_1}^2+\sigma_{\xi_0}^2+\sigma_{\beta_0}^2)}, \\ \mathrm{M}_2(\tau) = e^{\sigma_{\chi_0}^2+c_{\chi_0}(\tau)}\Big[\mathrm{D}^2 + 2\mathrm{DB}e^{\frac{1}{2}\sigma_{\chi_1}^2} + \mathrm{B}^2 e^{\sigma_{\chi_1}^2+c_{\chi_1}(\tau)}\Big], \end{cases}$$

where $c_{\chi_i}(\tau) = c_{\xi_i}(\tau) + c_{\beta_i}(\tau)$, $\sigma_{\chi_i}^2 = \sigma_{\xi_i}^2 + \sigma_{\beta_i}^2$, for $i = 0, 1$.

Given the relation between $Z(t)$ and $\mathrm{L}(t)$, few manipulations bring to

$$\Gamma(t) = \kappa Z(t) \quad \text{where} \quad \kappa = -\frac{5}{\ln 10}, \tag{5.11}$$

so that $\Gamma(t)$ is a Gaussian process with mean, variance and autocovariance

$$\begin{cases} \eta_\Gamma = \kappa \eta_Z, \\ \sigma_\Gamma^2 = \kappa^2 \sigma_Z^2, \\ c_\Gamma(\tau) = \kappa^2 c_Z(\tau). \end{cases} \tag{5.12}$$

In the rest of this chapter, we will denote it by $\Gamma(t) \sim \mathcal{N}(\eta_\Gamma, \sigma_\Gamma^2)$, if the relevant values of $c_\Gamma(\tau)$ will be given.

### 5.1.3 Link quality metrics of the analytic model

We follow the same procedure to derive the LQMs with the assumption that the *bit* error ratio (BER, $\mathrm{R_b}$), according to the IEEE 802.15.4-2006 standard [12] which provides the physical layer of WirelessHART, depends only on the power value $\gamma$ of SINR [12, p. 268]. Therefore, the *packet* error rate (PER, $\mathrm{R_p}$) is related to SINR through BER, where $\gamma \in (0, \infty)$, and both $\mathrm{R_b}(\gamma) \in [0, 0.5]$, $\mathrm{R_p}(\gamma) \in [0, 1]$ are continuous monotonically non-increasing

$$\begin{aligned} \mathrm{R_p}(\gamma) &= 1 - (1 - \mathrm{R_b}(\gamma))^{\ell_\mathrm{F}}, \\ \mathrm{R_b}(\gamma) &= \frac{1}{30}\sum\nolimits_{i=2}^{16} (-1)^i \binom{16}{i} e^{\left(20\gamma\frac{1-i}{i}\right)}. \end{aligned} \tag{5.13}$$

Therefore, the expected value of PER 4.46 and its variance 4.47 become

$$\eta_{\mathrm{A}} = \int_{-\infty}^{+\infty} \mathrm{R_p}(10^{\frac{\zeta}{10}}) f_{\Gamma}(\zeta)\, d\zeta, \tag{5.14}$$

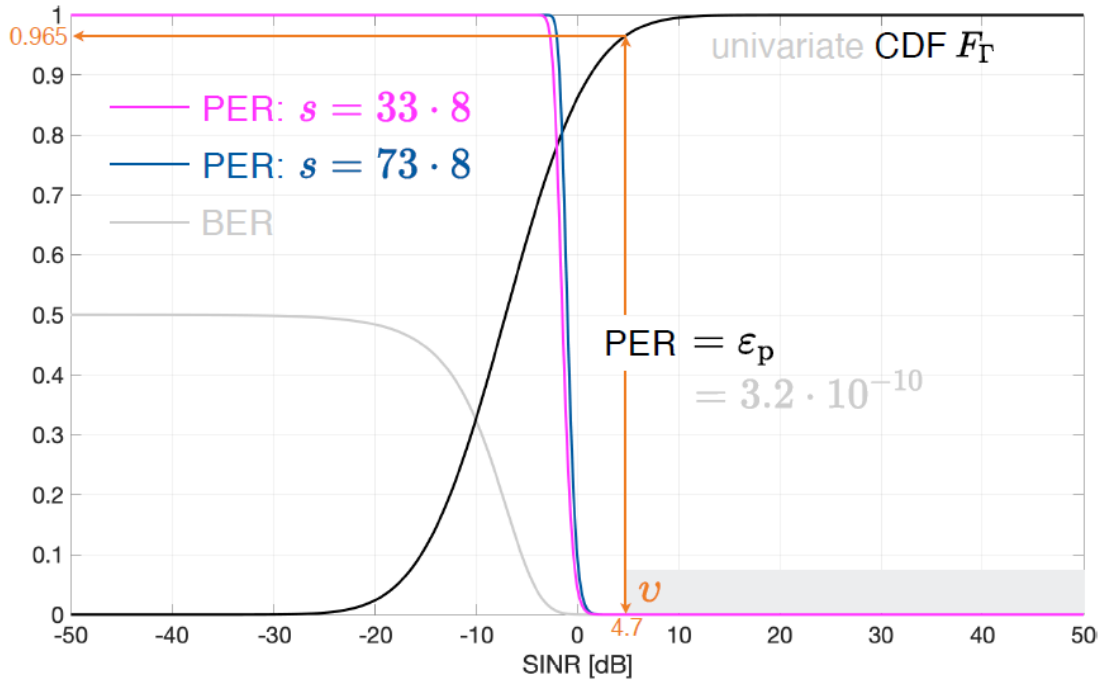


Figure 5.1: Packet error rate as a function of SINR.

$$\sigma_{\mathrm{A}}^2 = \int_{-\infty}^{+\infty} \mathrm{R_p^2}(10^{\frac{\zeta}{10}}) f_{\Gamma}(\zeta)\, d\zeta - \eta_{\mathrm{A}}^2. \tag{5.15}$$

As we said previously, the PER can be considered negligible when it is smaller than a specified threshold $\varepsilon_{\mathrm{p}}$. In particular, let $\nu$ be the threshold value of SINR for which PER $= \varepsilon_{\mathrm{p}}$. The packet error rate is negligible for all values of SINR $\geq \nu$. The probability of having a non-negligible PER is given by univrite comulative distribution function at the threshold $\nu$ i.e. $F_{\Gamma}(\nu)$. Figure 5.1 shows an example of this value where $s$ is the size of a PSDU which determines the packet error probability. This holds true for a single control-related data transmission. For multiple consecutive transmissions, as we said previously, we need to consider multivariate CDF which defines the probability of packet error burst of a certain length. In other words, the probability of a non-negligible PER over multiple consecutive transmissions depends on the time correlation of the link.

Between two consecutive control-related data transmissions the link performs a certain number of evolutions expressed in equation 4.8. In addition, the maximum number of consecutive dropouts will be derived as in equation 4.49 and 4.50.

### 5.1.4 Finite-state Markov model

The finit-state Markov abstraction is derived following the exact steps of our model. The steady state probability $\mathbf{p}_i$ of a state $\mathbf{s}_i$ is given as in equation 4.51. However, considering the assumptions of the simplified version of the model the PEP associated to the same state is given by the expected value of the PER within the respective region, i.e.

$$\eta_{\mathrm{M}}^{(i)} = \frac{1}{\mathbf{p}_i} \int_{\zeta_i}^{\zeta_{i+1}} \mathrm{R_p}(10^{\frac{\zeta}{10}}) f_\Gamma(\zeta)\, d\zeta. \tag{5.16}$$

The TPM of the Markov channel may be obtained using the same LCR analysis under the same assumptions indicated in 4 or by integrating the joint PDF of SINR over two consecutive symbol time intervals and over the required regions as in equation 4.51.

The **Markovian link quality metrics** become: the long-run mean PEP of the Markov channel, $\eta_{\mathrm{M}}$, is by construction equal to $\eta_{\mathrm{A}}$ in 5.14

$$\eta_{\mathrm{M}} = \sum\nolimits_{i=1}^{N} \eta_{\mathrm{M}}^{(i)} \mathbf{p}_i = \sum\nolimits_{i=1}^{N} \int_{\zeta_i}^{\zeta_{i+1}} \mathrm{R_p}(10^{\frac{\zeta}{10}}) f_\Gamma(\zeta)\, d\zeta, \tag{5.17}$$

while its long-run variance, $\sigma_{\mathrm{M}}^2$, is given by

$$\sigma_{\mathrm{M}}^2 = \sum\nolimits_{i=1}^{N} (\eta_{\mathrm{M}}^{(i)})^2 \mathbf{p}_i - \eta_{\mathrm{M}}^2. \tag{5.18}$$

The maximal number of consecutive packet *dropouts* with a non-negligible probability of occurrence, denoted by $\ell_{\mathrm{D}}^{\star}$, can be derived as in chapter 4 to get equation4.62.

## 5.2 Optimal control over a WirelessHART link

To show the importance of the accurate Markov channel model for the WNCSs, we examine the inverted pendulum (on a cart) described in [117], which is controlled remotely over a WirelessHART link presented in the previous section. We model it as a linear stochastic system with intermittent control packets due to the lossy communication channel [33]:

$$x_{k+1} = Ax_k + Bu_k^a + w_k \quad \text{with} \quad u_k^a = \nu_k u_k^c, \tag{5.19}$$

where, $x_k$ is a system state, $u_k^a$ is the control input to the actuator, $A$ and $B$ are state and input matrices of appropriate size, respectively, $u_k^c$ is the desired control input computed by the controller, $w_k$ is Gaussian white process noise (with zero mean and covariance matrix $\Sigma_w$) assumed to be independent from the initial state $x_0$ and from the stochastic variable $\nu_k$, which models the packet loss between the controller and the actuator: if the packet is correctly delivered then $u_k^a = u_k^c$, otherwise if it is lost then the actuator does nothing, i.e., $u_k^a = 0$. We assume full state observation with no measurement noise, and no observation packet loss, so the optimal control must necessarily be a static state feedback and no filter is necessary.

In such a setting we compare the performance of two state feedback optimal controllers, both designed to minimize a cost function, which can be described by

$$J_* = \limsup_{t\to\infty} \frac{1}{t}\mathbb{E}\Big[\sum\nolimits_{k=0}^{t}(x_k^* Q x_k + u_k^{a*} R u_k^a)\Big], \tag{5.20}$$

where $Q \succeq 0$ and $R \succ 0$ are the state and control weighting matrices, respectively. In other words, $Q$ is a positive semi-definite matrix where its eigenvalues could be 0 or positive and $R$ is a positive definite matrix where its eigenvalues are only positive.

The first state-feedback controller is derived in [33], treating $\nu_k$ as i.i.d. Bernoulli random variables. The obtained state-independent controller and the value of the related performance index will be denoted respectively as $K_\star^b, J_\star^b$.

The second controller is the optimal linear quadratic regulator for a MJLS in the presence of one time-step delayed mode observations [40]. It considers $\nu_k$ as a random variable governed by the Markov channel, where the probability of the successful packet delivery is conditioned to the state of the communication link, i.e., $\Pr(\nu_k = 1 \mid \theta_k = \mathbf{s}_i) = \hat{\nu}_i$, while the probability of the packet loss is $\Pr(\nu_k = 0 \mid \theta_k = \mathbf{s}_i) = 1 - \hat{\nu}_i$. The operational modes are observed by the controller via ACKs that are available only after the current decision on the controller gain to apply has been made and sent through the channel, since the actual success of the transmission is not known in advance. We assume that ACKs, and also the communication channel states (measured through SINR), are not received at the controller instantaneously, but become available before the next decision on the control to apply. This means that the state-space representation of the MJLS in closed-loop becomes

$$x_{k+1} = (A + \nu_{\theta_k} B K_{\theta_{k-1}}^c) x_k + w_k \tag{5.21}$$

where $K_{\theta_{k-1}}^c$ is a mode-dependent state-feedback controller, computed as in [40]. The value of the related performance index will be denoted as $J_\star^c$.

To be of any practical use, the system should remain always stable in closed-loop. To check whether the controlled system is actually stable, we adopt the techniques from the theory of discrete-time MJLSs [118]. In particular, we rely on [41], which shows that a MJLS with one time-step delayed mode observations is mean square stable if and only if the spectral radius $\rho$ of the characteristic matrix $\mathbf{\Lambda}$ is smaller than 1, being

$$\mathbf{\Lambda} = \left(\bigodot_{j=1}^{N}\left(\bigoplus_{i=1}^{N} p_{ij}\right)\right)' \otimes \left(\bigodot_{j=1}^{N}(A \otimes A)\right) + \left(\bigodot_{j=1}^{N}\left(\bigoplus_{i=1}^{N} \hat{\nu}_i p_{ij}\right)\right)' \otimes \left(\bigodot_{j=1}^{N}\Big(\big((BK_j)\otimes(BK_j)\big)+\big((BK_j)\otimes A\big)+\big(A\otimes(BK_j)\big)\Big)\right),$$

where, as before, $p_{ij}$ is the probability of transition between the Markov channel's states, $\otimes$ indicates the Kronecker product, $\oplus$ the direct sum, and $\odot$ the horizontal concatenation of two matrices with the same number of rows.

In Section 5.3.3 we will check the stability of the closed-loop system through the computation of $\rho(\mathbf{\Lambda})$, and verify it via a statistical analysis.

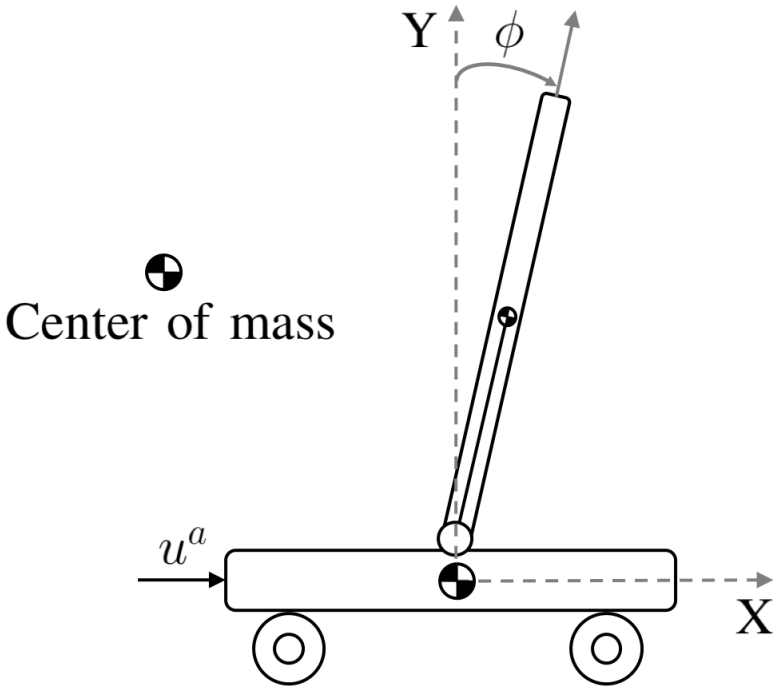


Figure 5.2: The inverted pendulum on a cart.

First, we applied the model on the pendulum on a cart and obtained results published in [3]. In particular, we investigated the following case study.

Table 5.1: parameters of the inverted pendulum on a cart.

| **Parameter** | **Notation** |
|---|---|
| The cart mass | 0.5 kg |
| The pendulum mass | 0.2 kg |
| The inertia about the pendulum mass center | 0.006 kg |
| The distance from the pivot to the mass center | 0.3 m |
| The friction coefficient of the cart | 0.1 N·s / m |

## 5.3 Numerical case study applied on the first model

The parameters of our inverted pendulum shown in Figure 5.2 are summarized in Table 5.1. The state variables are the cart position coordinate x and pendulum's angle from vertical $\phi$, together with respective first derivatives. We are interested in designing a controller that stabilizes the pendulum in up-right position, corresponding to unstable equilibrium point $\mathrm{x}^\star = 0\,\mathrm{m}$, $\phi^\star = 0$ rad, so the system state is defined by $x = \left[\delta\mathrm{x}, \delta\dot{\mathrm{x}}, \delta\phi, \delta\dot{\phi}\right]'$, where $\delta\mathrm{x}(t) = \mathrm{x}(t) – \mathrm{x}^\star$, $\delta\phi(t) = \phi(t) – \phi^\star$. This determines the frame length of the control-related messages: $\ell_\mathrm{F} = 208$ bits. It is assumed that the initial state $x_0$ equals $\left[0, 0, \frac{\pi}{10}, 0\right]'$. The process noise is characterized by the covariance matrix $\Sigma_w = vv'$, with $v = [0.030, 0.100, 0.010, 0.150]'$. To prioritize the goal of maintaining the inverted pendulum in the upright position, we use the following weighting matrices for all the control schemes being compared: $Q = \oplus(1, 0.1, 100, 0.1)$ and $R = 1$, so that the weight associated to $\delta\phi(t)$ is much larger than all other weights. The inverted pendulum on a cart moves in a direction orthogonal to both its remote controller and the transmitter that creates interference. We set the noise figure $F_n$ of the receiver to 23.8 dB (so that its sensitivity is just above $-85$ dBm as required by the standard [9]). Thus, the noise spectral density $N_0 = k_B T_0 F_n$, where $k_B$ is the Boltzmann's constant and $T_0$ is standard noise temperature. The values of other channel parameters used in this case study are summarized in Table 5.2, where $\varepsilon_1$ denotes the machine epsilon, and $\varepsilon_\mathrm{p}$ is the probability of one data packet loss in a century of continuous operation with the sampling time of $T_u$ (measured in seconds).

### 5.3.1 Case 1

The first case describes the scenario, where the minimum update period of the WirelessHART standard is considered for the control application, i.e., $T_u = 0.1\,\mathrm{s}$. The distance between the transmitter-receiver pair of interest, $d_0$, and the distance between the interfering Tx and the reference user, $d_1$, have the values shown in Table 5.2. According to these values, we have $\ell_{\mathrm{E}} = 60$, and the implicit analytic model of the channel is characterized by the Gaussian process described in Table 5.3. We underline that $c_{\Gamma_1}(61) = 0$. This means that at the packet level two consecutive data transmissions are independent, so the i.i.d. Bernoulli distribution is appropriate to model packet losses. The analytic LQMs are also outlined in Table 5.3.

To show the usefulness of the derived link quality metrics, we first construct a three-state Markov model with equiprobable partitioning of the range of SINR, as introduced in Section 4.1.6. Specifically, the range of SINR is partitioned in such a way that the steady state probabilities of being in any state are equal. The related TPM is derived from either LCR analysis via (4.53) and (4.54), or by integrating $f_{\Gamma_1}(z_{t-1}, z_t)$. We have for both approaches that

$$\begin{cases} (\mathbf{p}_i)_{i=1}^{3} = (1/3, 1/3, 1/3)\,, \\ (\zeta_i)_{i=1}^{4} = (-\infty, 3.522, 9.139, \infty)\,, \\ (\eta_{\mathrm{M}}^{(i)})_{i=1}^{3} = \left(0.339, 4.4 \cdot 10^{-9}, 0\right). \end{cases} \tag{5.22}$$

Therefore, from (5.17) and (5.18) we get respectively $\eta_{\mathrm{M}} = 0.113$ and $\sigma_{\mathrm{M}}^2 = 0.026$. TPMs describing the evolution of the Markov channel at the symbol rate, denoted by $\mathbf{\Pi}_i$, and TPMs of the Markov channel evolving at the packet rate, $\mathbf{P}_i$, (with $i = \mathrm{L}$ when the transition probabilities are obtained from the LCR analysis, and $i = \mathrm{I}$ when the integration of $f_{\Gamma_1}(z_{t-1}, z_t)$ is used) are

$$\mathbf{\Pi}_{\mathrm{L}} = \begin{bmatrix} 0.997 & 0.003 & 0 \\ 0.003 & 0.994 & 0.003 \\ 0 & 0.003 & 0.997 \end{bmatrix}, \mathbf{\Pi}_{\mathrm{I}} = \begin{bmatrix} 0.532 & 0.315 & 0.153 \\ 0.3146 & 0.371 & 0.3146 \\ 0.153 & 0.315 & 0.532 \end{bmatrix};$$

$$\mathbf{P}_{\mathrm{L}} = \begin{bmatrix} 0.846 & 0.141 & 0.013 \\ 0.141 & 0.717 & 0.141 \\ 0.013 & 0.141 & 0.846 \end{bmatrix}, \mathbf{P}_{\mathrm{I}} = \begin{bmatrix} 1/3 & 1/3 & 1/3 \\ 1/3 & 1/3 & 1/3 \\ 1/3 & 1/3 & 1/3 \end{bmatrix}.$$

Importantly, the values of $\mathbf{P}_{\mathrm{I}}$ show that at the packet level two consecutive data transmissions are independent, while the structure of $\mathbf{P}_{\mathrm{L}}$ erroneously indicates the correlation

Table 5.2: Parameter values for case study.

| **Parameter** | **Notation** | **Value** | | | **Unit** | **Reference** |
|---|---|---|---|---|---|---|
| | | *Case 1* | *Case 2* | *Case 3* | | |
| Symbol rate | $1/T_s$ | 62.5 | | | ksymb/s | [119] |
| Chip rate | $1/T_c$ | 2 | | | Mchip/s | [119] |
| Channel bandwidth | $W$ | 2 | | | MHz | [12] |
| Users speed | $v_0, v_1$ | 5.37 | | | m/s | Pendulum |
| Shadowing decay dist. | $d_{c_0}, d_{c_1}$ | 9 | | | m | [80] |
| Shadowing std. dev. | $\sigma_{\beta_0}, \sigma_{\beta_1}$ | 2 | | | dB | [120] |
| PCE std. dev. | $\sigma_{e_0}, \sigma_{e_1}$ | 1.5 | | | dB | [110] |
| PCE decorr. time | $\tau_{\xi_0}, \tau_{\xi_1}$ | $1.52 \cdot 10^{-3}$ | | | s | [110] |
| Ref. user Tx power | $P_0$ | 0 | | | dBm | [9] |
| Interf. Tx power | $P_1$ | 10 | | | dBm | [9] |
| Dist. ref. Tx-Rx pair | $d_0$ | 6 | 6 | 10 | m | Indoor: 1–10 m |
| Dist. interf. Tx-Rx pair | $d_1$ | 10 | 10 | 4 | m | |
| Publish data message update period | $T_u$ | 100 | 5 | 5 | ms | [80] [9] |
| Negligible PER threshold | $\varepsilon_{\mathrm{P}}$ | $\frac{1}{(1/T_u)\cdot 3600\cdot 24\cdot 36525}$ | | | scalar | Design choice |
| Negligible packet error burst threshold | $\varepsilon_{\mathrm{B}}$ | $100\varepsilon_1$ | | | scalar | |

Table 5.3: Results of case study.

| | **Parameter** | **Case 1** | **Case 2** | **Case 3** |
|---|---|---|---|---|
| Gaussian process | $\mu$ | 6.331 | 6.331 | -9.061 |
| | $\sigma^2$ | 42.504 | 42.504 | 42.505 |
| | $\ell_{\mathrm{E}}$ | 60 | 3 | 3 |
| | $c_{\Gamma}(1)$ | 19.825 | 19.825 | 19.826 |
| | $c_{\Gamma}(\ell_{\mathrm{E}}+1)$ | 0 | 1.373 | 1.373 |
| Analytic LQMs | $\eta_{\mathrm{A}}$ | 0.113 | 0.113 | 0.871 |
| | $\sigma^2_{\mathrm{A}}$ | 0.087 | 0.087 | 0.098 |
| | $\ell^{\star}_{\mathrm{B}}(\varepsilon_{\mathrm{B}}, \varepsilon_{\mathrm{p}})$ | 36 | 40 | 2270 |
| Gilbert channel abstraction | $\mathbf{p}_i$ | $(0.413, 0.587)$ | $(0.437, 0.563)$ | $(0.986, 0.014)$ |
| | $\eta^{(i)}_{\mathrm{M}}$ | $(0.274, 0)$ | $(0.258, 0)$ | $(0.883, 0)$ |
| | $\zeta_2 = \upsilon^{\star}_{\Gamma}(\varepsilon_{\mathrm{p}})$ | 4.889 | 5.302 | 5.302 |
| | $\mathbf{P}$ | $\begin{bmatrix} 0.413 & 0.587 \\ 0.413 & 0.587 \end{bmatrix}$ | $\begin{bmatrix} 0.454 & 0.546 \\ 0.4246 & 0.575 \end{bmatrix}$ | $\begin{bmatrix} 0.986 & 0.014 \\ 0.9846 & 0.015 \end{bmatrix}$ |
| Markovian LQMs | $\eta_{\mathrm{M}}$ | 0.113 | 0.113 | 0.871 |
| | $\sigma^2_{\mathrm{M}}$ | 0.018 | 0.016 | 0.011 |
| | $\ell^{\star}_{\mathrm{D}}$ | 36 | 40 | 2011 |

between the channel states. Fortunately, the difference in the maximal number of consecutive dropouts helps to discover this mistake, since (for the same values of $\varepsilon_{\mathrm{B}}$, $\varepsilon_{\mathrm{p}}$) we have that $\ell^{\star}_{\mathrm{D_L}} = 441$, $\ell^{\star}_{\mathrm{D_I}} = 77$, while from the application of either (4.49), or (4.50), we have that $\ell^{\star}_{\mathrm{B_1}} = 36$. This discrepancy in the values of $\ell^{\star}_{\mathrm{D}}$ and $\ell^{\star}_{\mathrm{B}}$ also indicates that the simple equiprobable partitioning of the range of SINR is not the best choice, since it does not consider the value of $\upsilon^{\star}_{\Gamma_1}(\varepsilon_{\mathrm{p}})$ in deriving the thresholds $\zeta_i$.

Consequently, we consider also a Gilbert model of the WirelessHART link. Henceforth, we will use only the integration of the joint PDF of the SINR over two consecutive packet transmissions to compute exact values of TPMs $\mathbf{P}$ directly, via (4.57). The characteristics of the obtained Gilbert channel abstraction of the radio link and its LQMs are reported in Table 5.3. Notably, we have that $\ell^{\star}_{\mathrm{D_1}} = 36$, and also $\ell^{\star}_{\mathrm{B_1}} = \ell^{\star}_{\mathrm{B}}(\varepsilon_{\mathrm{B_1}}, \varepsilon_{\mathrm{p}}) = 36$. Therefore, as expected, the Gilbert channel is well suited for studying the maximal number of consecutive dropouts.

It is worth mentioning that the update period used in this case i.e $T_u = 0.1\,\mathrm{s}$ is a bit long to ensure the stability of the real inverted pendulum on a cart. However, we could stabilize it because, as we said before, we approximated the non linear model of the pendulum by the linear one as in [41]. Advanced control methods, such as the model predictive ones or the adaptive methods, could be used to get a better representation of the non linear model.

### 5.3.2 Case 2

The minimum update period $T_u = 0.1\,\mathrm{s}$ of the WirelessHART standard is too slow for several control applications and it makes the wireless link uncorrelated at the packet level. Thus, in view of the continuous development of mobile network technologies that support much higher update rates, we consider $T_u = 0.005\,\mathrm{s}$, i.e. Case 2 in Table 5.2. The characteristics of the implicit analytic model of the radio link and of its finite-state abstraction via Gilbert model are reported in Table 5.3. We notice that the higher update rate does not change the values of $\eta_{\Gamma}$, $\sigma^2_{\Gamma}$, and $c_{\Gamma}(\tau)$, which are computed via (5.12). Accordingly, also the values of $\eta_{\mathrm{A}}$ and $\sigma^2_{\mathrm{A}}$, that are obtained respectively through (5.14) and (5.15), remain the same as before. However, with $\ell_{\mathrm{E}}$ being equal to 3, we have $c_{\Gamma_1}(4) = 1.373$: there is a correlation between the control-related transmissions. Since a smaller value of $\varepsilon_{\mathrm{p}}$ is used in this case, then $\upsilon^{\star}_{\Gamma_2}(\varepsilon_{\mathrm{p}}) = 5.302$. Therefore, the lower bound of $\ell^{\star}_{\mathrm{B_2}}$ computed via (4.50) becomes 39 while its exact value obtained from (4.49) is 40. The associated Gilbert channel, with characteristics and LQMs shown in Table 5.3, is still able

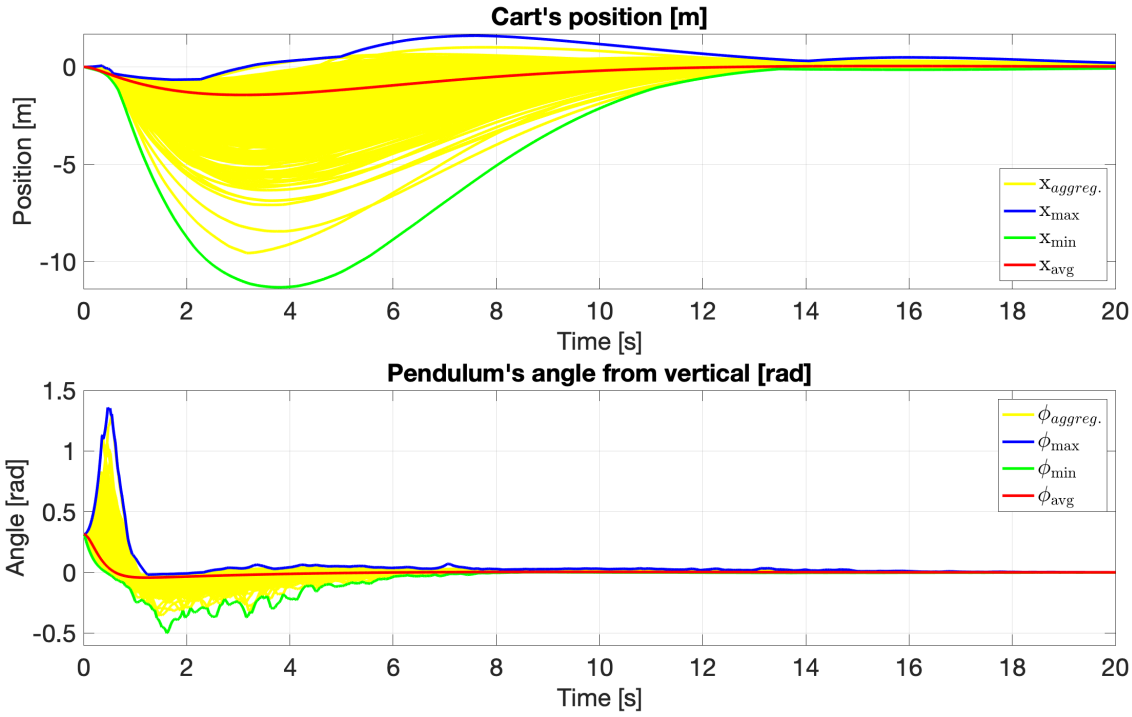


Figure 5.3: Traces of the system's state that are generated under the Markovian control law over the analytic WirelessHART channel.

to closely track the behavior of the analytic model, which is evident from the comparison of the respective LQMs.

### 5.3.3 Case 3

This case shows the real utility of the accurate finite-state Markov channel models in networked control applications. This scenario describes the situation with a sustained jamming activity. The analytic and Gilbert channel abstraction have the values depicted in Table 5.3, where $\ell^{\star}_{\mathrm{B}_3} = 2270$ is computed via (4.49), while its lower bound from (4.50) is 2263. The discrepancy with $\ell^{\star}_{\mathrm{D}_3} = 2011$ is due to the numerical precision of the operations involved in computing (4.61).

We consider the networked control application implemented over this link, and analyze the performance of both the optimal linear quadratic regulation with Bernoulli and Gilbert abstractions of the analytic wireless channel. The state space representation (5.21) of the controlled system linearized about the unstable equilibrium point and discretized with

sampling period $T_u = 0.005\,\mathrm{s}$ is defined by

$$A = \begin{bmatrix} 1 & 0.005 & 0 & 0 \\ 0 & 0.999 & 0.013 & 0 \\ 0 & 0 & 1 & 0.005 \\ 0 & -0.002 & 0.156 & 1 \end{bmatrix}, \; B = \begin{bmatrix} 0 \\ 0.009 \\ 0 \\ 0.023 \end{bmatrix}.$$

The matrix $A$ is unstable, since its eigenvalues are $\mathrm{eig}(A) = (1.028, 1.000, 0.999, 0.972)$. It is easy to verify that $R \succ 0$, $Q \succeq 0$, and the pairs $(A, B)$ and $(A, Q)$ are controllable, so the closed-loop system is asymptotically stable, when $\nu_k = 1$ for all $k$. The critical probability $\nu_c$ for the networked control over Bernulli channel [33] for this system is $0.\mathbf{053}$, so that maximal length of the fading sequence with the probability of occurrence larger than $\varepsilon_{\mathrm{B}}$ is 573, i.e. it is much smaller then 2270. Still, since $\hat{\nu} = 1 - \eta_{\mathrm{A}_3} > \nu_c$, we may try to apply the controller $K^b$ as in [33]. We obtain $K^b = [0.024, -3.252, 255.665, 45.958]$, $J^b_\star = 1.25 \cdot 10^6$. By checking the stability of this controller when applied to a Gilbert channel case, we find out that $\rho(\mathbf{\Lambda}^b) = 1.000065 > 1$, so the system is unstable. If we exploit the information available from the Gilbert channel to construct a MJLS with one time-step delayed mode observations presented at the beginning of this section, we obtain $K^c_1 = [-0.754, -3.668, 114.502, 20.698]$, $K^c_2 = [-0.764, -3.713, 115.912, 20.953]$, so that $J^c_\star = 451.124$. This controller stabilizes the system, since $\rho(\mathbf{\Lambda}^c) = 0.997 < 1$.

It is crucial to highlight that since $\rho(\mathbf{\Lambda}^c)$ is very close to 1 thus it will converge very slowly and if the link condition is worsen, the spectral radius will become greater than 1 and it will not converge. Nevertheless, it can be more robust if we have access to the parameters of the link. Specifically, if we have, for example, higher power thus we have less packet loss and the value of the spectral radius will be further from 1.

To validate the presented results, we have simulated the behavior of the inverted pendulum on a cart, with a remote controller implementing either the Bernoulli, or Markovian control law, and sending the data over the analytic WirelessHART channel. Specifically, we randomly generated 10000 admissible evolutions (each one with 4000 samples accounting for 20s of operation) of the analytic channel, and used them for both control strategies. Since both Bernoulli and Markovian controllers do not consider any constraints on the system states or control inputs, all the physics-related constraints were neglected in our simulations. Figures 5.3 and 5.4 depict statistical results of our simulations: it is evident that Figure 5.3 shows a stable system behavior of the linearized inverted pendulum on a cart when it is governed by the remote Markovian controller, while the behavior of the pendulum controlled remotely by a Bernoulli strategy, that is reported in Figure 5.4, is

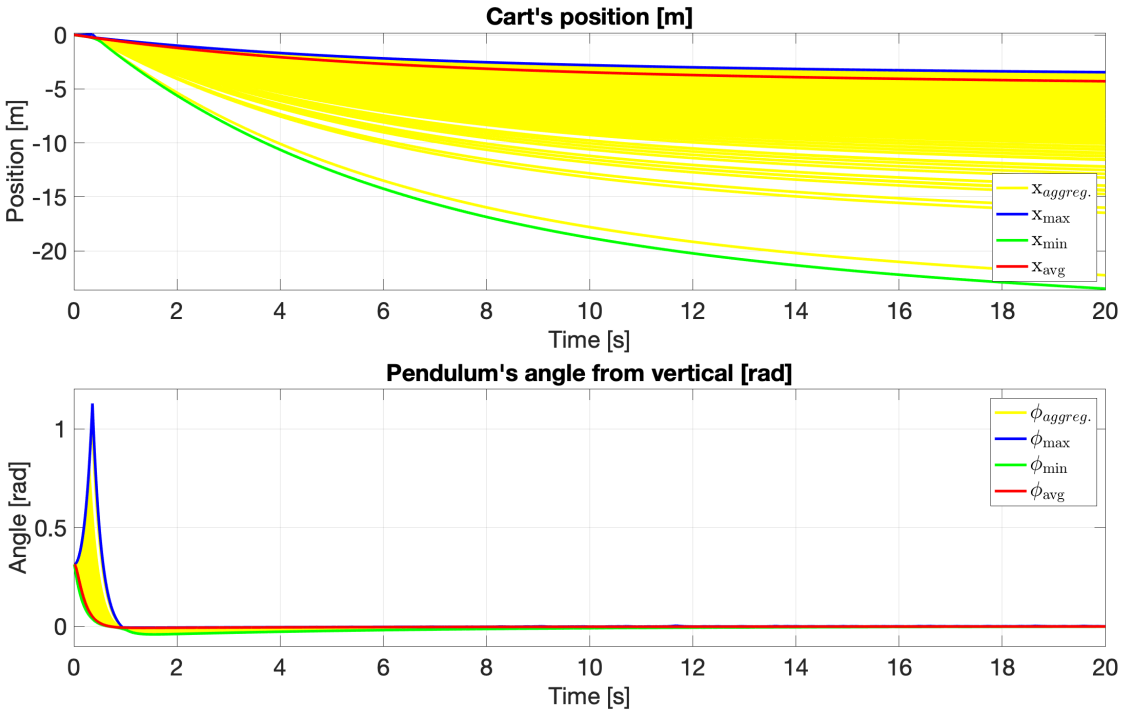


Figure 5.4: Traces of the system's state that are generated under the Bernoulli control law over the same analytic WirelessHART channel.

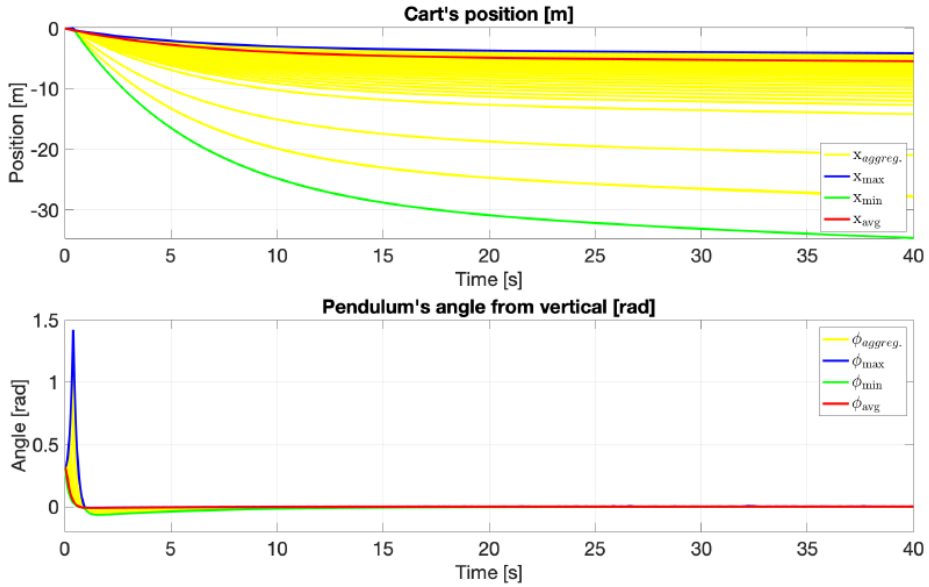


Figure 5.5: Traces of the system's state that are generated under the Bernoulli control law over the same analytic WirelessHART link (special case).

clearly unstable, as it was expected from our analysis of stability conditions based on the spectral radius of the characteristic matrices.

It is worth mentioning that using the sampling period of IEEE 802.15.4e LLDN superframe which is $T_u = 0.01s$ with shorter overhead of LLDN specification thus the size of PSDU is 33 bytes, we have no information loss and with 12 states Markov channel we abstract perfectly the analytic model. Figures 5.5 and 5.6 show for this special case how the inverted pendulum is still stabilizable with accurate Markov control law based on one time step delayed channel state observations while it is unstable using Bernoulli law in such harsh propagation environment.

## 5.4 Parametric analysis of the ideal wireless link and choosing the scenarios for the standards

In order to choose the ideal scenario for industrial standards before the existence in the environment, we set the constraints of the average packet reception rate and the maximum fading length as mentioned in chapter 3. After generalizing the derived model to cover

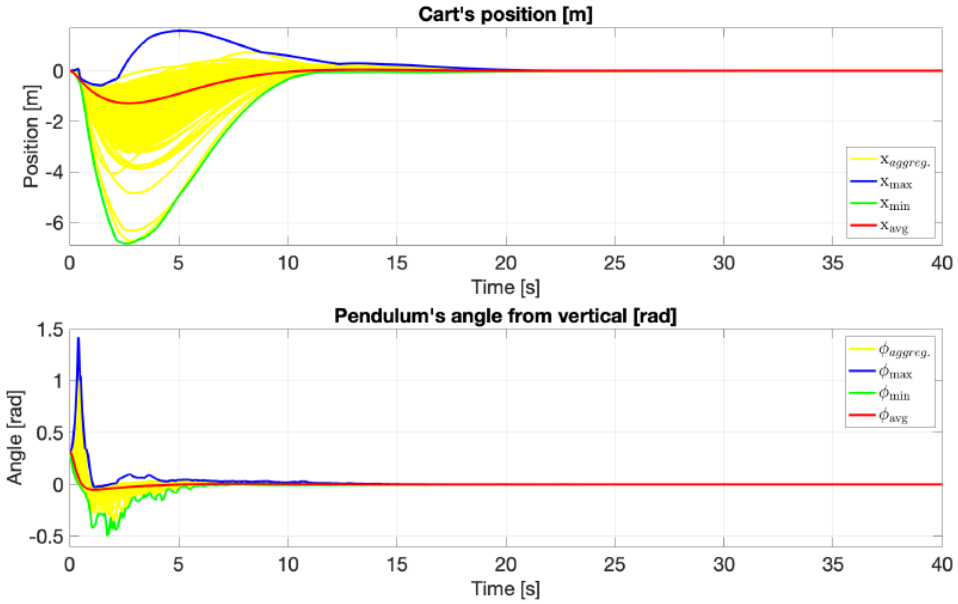


Figure 5.6: Traces of the system's state that are generated under the Markovian control law over the analytic WirelessHART link (special case).

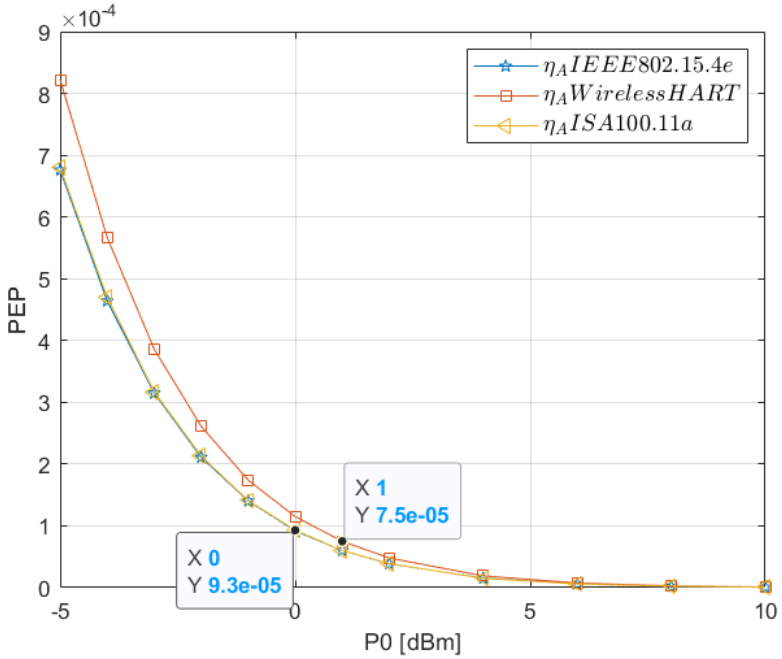


Figure 5.7: The power effect on the PEP.

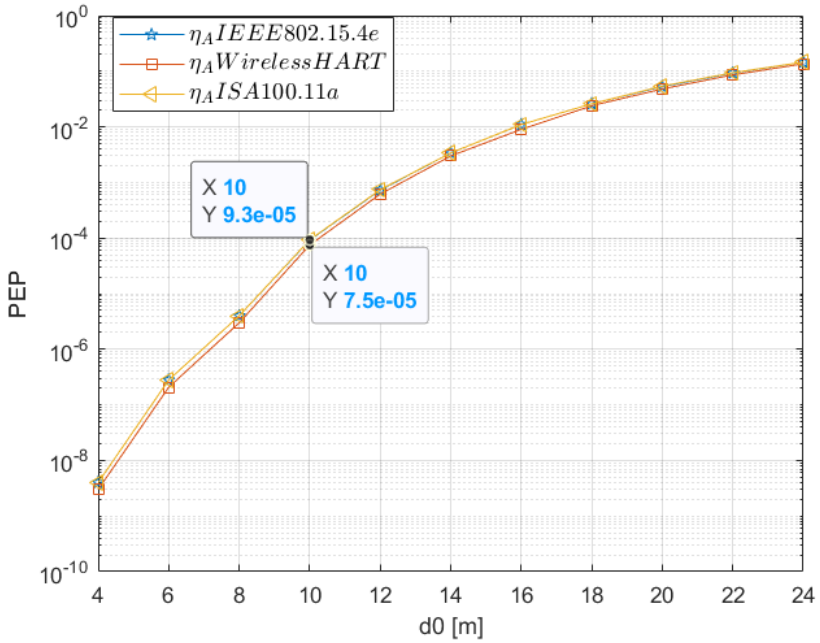


Figure 5.8: The distance effect on the PEP.

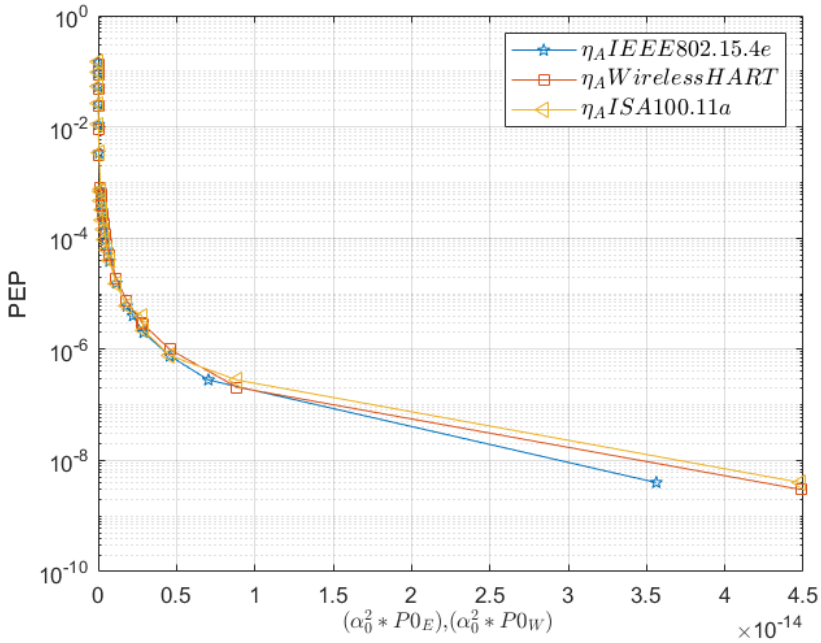


Figure 5.9: The effect of $\alpha^2 * P0$ on the PEP.

Table 5.4: The parameters of the ideal scenario of each standard.

| Parameter | unit | **Standards** | | |
|---|---|---|---|---|
| | | IEEE 802.15.4e | WirelessHART | ISA-100.11a |
| $T_u$ | s | 0.01 | 0.1 | 1/32 |
| $\ell_F$ | octet | 62 | 102 | 63 |
| $P_0$ | dBm | 0 | 1 | 0 |
| $d_0$ | m | 10 | 10 | 10 |
| $\sigma_{\xi_0}$ | dB | $10^{0.15}$ | $10^{0.15}$ | $10^{0.15}$ |
| $\sigma_{\beta_0}$ | dB | 2 | 2 | 2 |
| $\tau_{\xi_0}$ | dB | $1.52 * 10^{-3}$ | $1.52 * 10^{-3}$ | $1.52 * 10^{-3}$ |
| $dc_0$ | m | 6.5 | [3-30] | [3-19] |
| $v_0$ | m/s | 5.37 | 5.37 | 5.37 |
| $\eta_{\mathrm{A}}$ | dB | $0.092 * 10^{-3}$ | $0.075 * 10^{-3}$ | $0.093 * 10^{-3}$ |
| ${\sigma_A}^2$ | dB | $0.06 * 10^{-3}$ | $0.05 * 10^{-3}$ | $0.06 * 10^{-3}$ |
| $\ell^{\star}_{\mathrm{B}}$ | ms | 40 | 400 | 125 |
| $\eta_{\Gamma}$ | dB | 16.4 | 16.9 | 16.4 |
| $\sigma_{\Gamma}$ | dB | 4.61 | 4.61 | 4.61 |
| $c_{\Gamma}(\ell_E)$ | dB | $2e{-}3$ | 0 | $1e{-}15$ |

more standards other than WirelessHART, for example IEEE802.15.4e and ISA-100.11a, we apply a parametric analysis to discuss the effect of different parameters on the stochastic characteristics of the link and the link quality metrics. In order to choose the ideal scenario for each standard we will discuss the effect of the following parameters on the packet error probability and the maximum fading length. These parameters are the power of the device, the distance between the device (transmitter) and the receiver, the logarithmic residual power control error standard deviation, the shadowing correlation standard deviation, the decorrelation time, the device velocity and the decorrelation decay distance. After choosing the following update period and using 6 variables in the plants for each standard i.e. $(T_u = 0.01, 0.1, 1/32)$ s, $(\ell_F = 62, 102, 63)$ octets for IEEE802.15.4e, WirelessHART and ISA-100.11a respectively, we apply a parametric analysis to show the effect of each aforementioned parameter on the chosen constraints.

Table 5.4 shows the selected parameters for the ideal scenario for each standard before

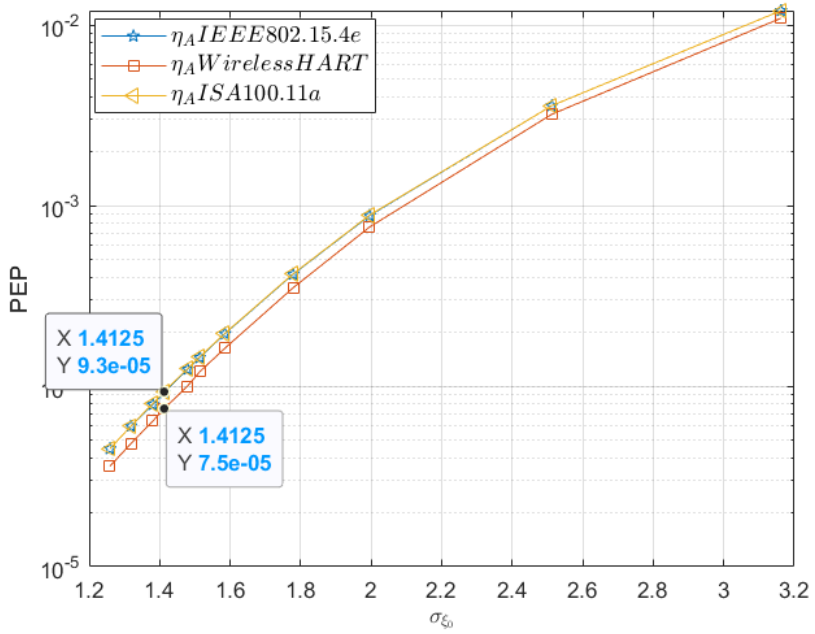


Figure 5.10: The effect of the standard deviation of power control error on the PEP.

the existence of the interferer. In the discussion below, we explain why we choose these parameters.

Power: from equation 5.12 we can analyze the effect of each parameter on the stochastic characteristics of the link by substituting explicitly each variable by its value. If we increase the power of the device the mean of the corresponding Gaussian process will increase. However, the variance and the autocovariance will remain almost constant. The PEP, the PER's variance and the maximum fading length will decrease. Figure 5.7 shows the effect of the power on the link for all the standards. As we see the values of the power in Table 5.4 for each standard fulfill the aforementioned constraints.

Distance: Increasing the distance between the transmitter and the receiver will decrease the mean of the Gaussian process and without any significant effect on its variance and autocovariance. Moreover, increasing the distance, according to 3.11, will decrease the pathloss and as a result it will increase the PEP, PER's variance and the maximum fading length. Figure 5.8 describes the distance effect on PEP. As it is shown the farther the device from the receiver, the greater the PEP and the worse the link. Figure 5.9 shows the effect of the path loss squared per power on the PEP. We notice that the higher this parameter the smaller the PEP.

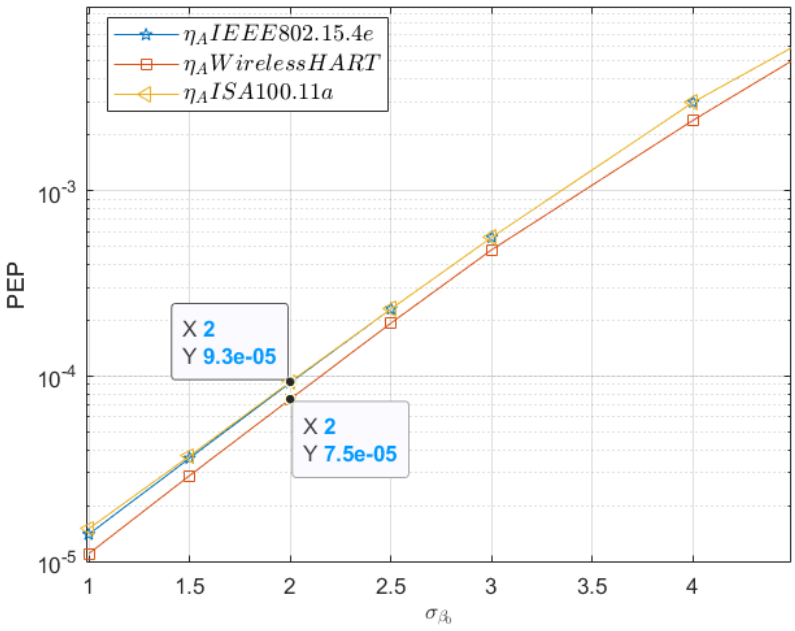


Figure 5.11: The effect of the standard deviation of the shadow correlation on the PEP.

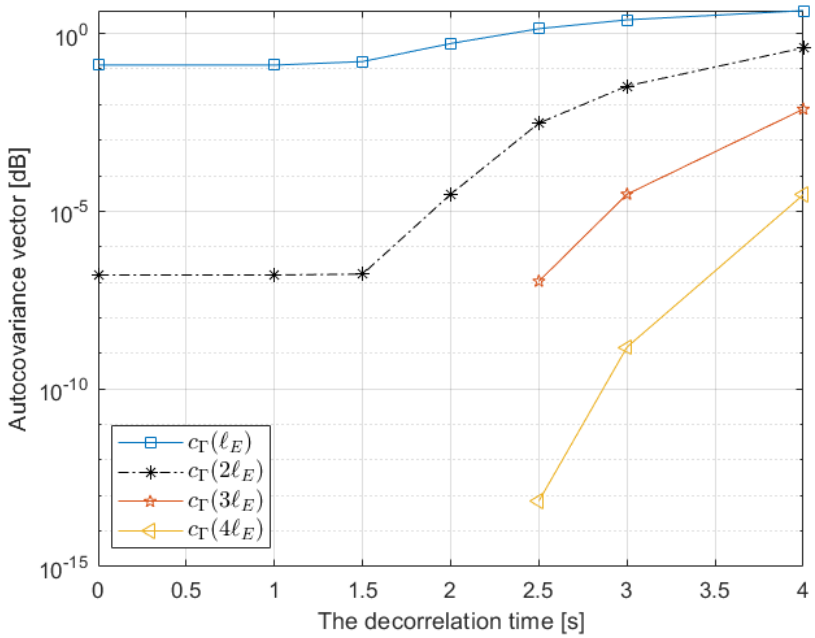


Figure 5.12: The effect of the decorrelation time on the PEP for IEEE 802.15.4e.

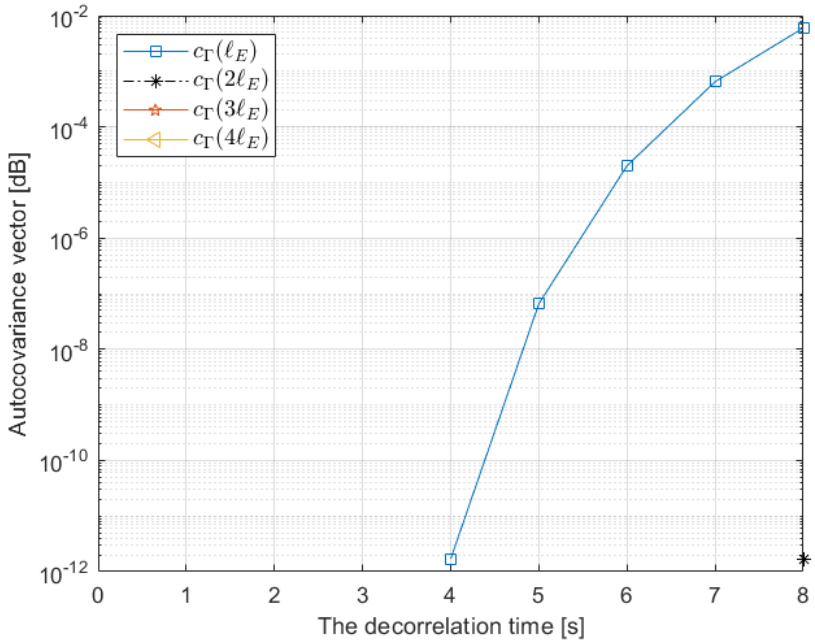


Figure 5.13: The effect of the decorrelation time on the PEP for WirelessHART

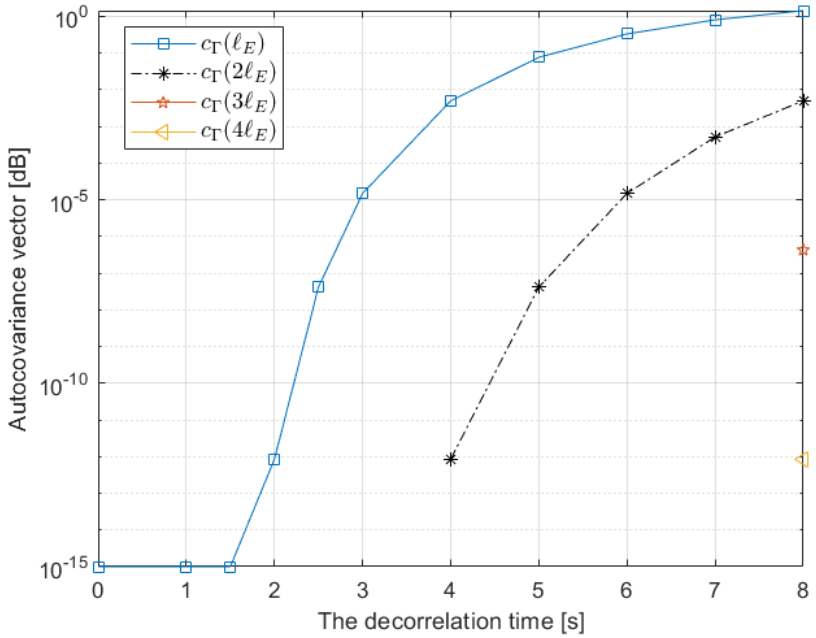


Figure 5.14: The effect of the decorrelation time on the PEP for ISA-100.11a.

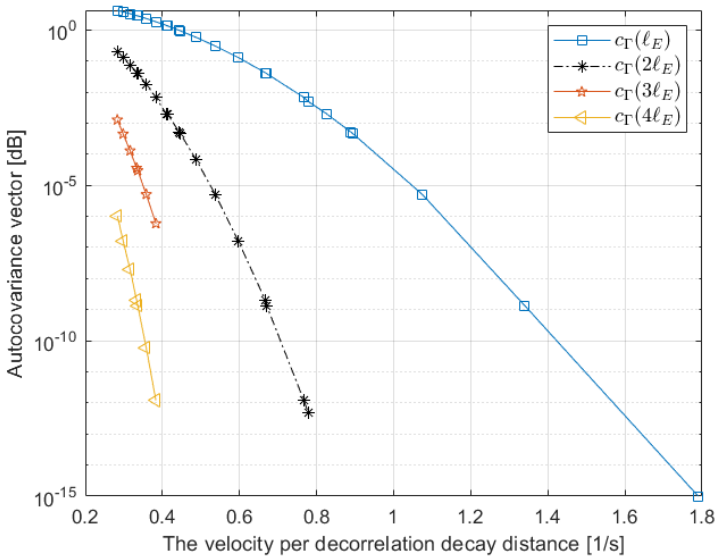


Figure 5.15: The autocovariance vector as a function of velocity per decorrelation decay distance for IEEE 802.15.4e.

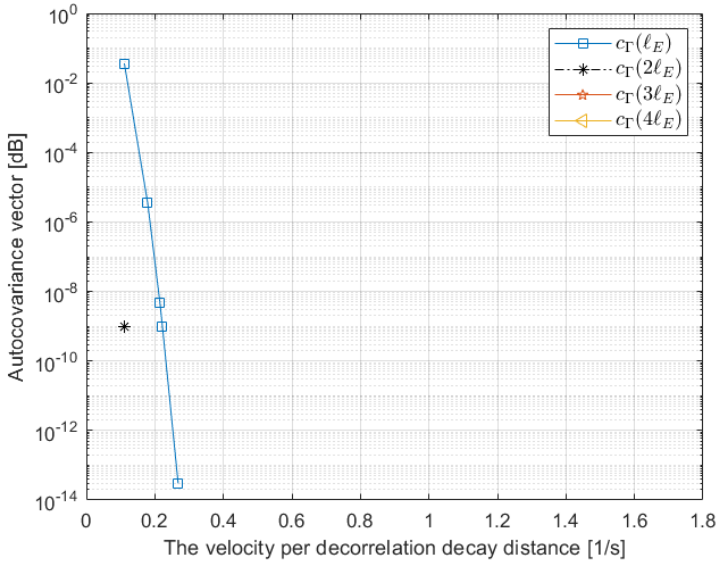


Figure 5.16: The autocovariance vector as a function of velocity per decorrelation decay distance for WirelessHART.

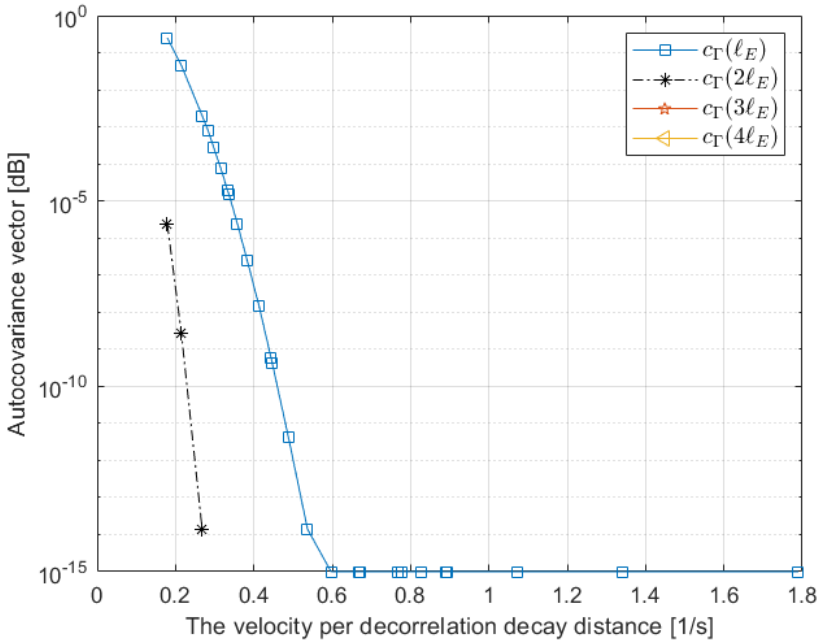


Figure 5.17: The autocovariance vector as a function of velocity per decorrelation decay distance for ISA-100.11a.

The logarithmic residual power control error standard deviation has a logarithmic impact on the stochastic characteristics of the link. Increasing its value will increase the standard deviation of the Gaussian process without any significant change of the mean and the autocovariance. Moreover, it will worsen the whole LQMs. From Table 5.4, Figure 5.10 we ensure that the selected values satisfy our constraints.

The shadowing correlation standard deviation has also a logarithmic effect on the stochastic characteristics of the link where it affects the variance of the Gaussian process and the autocovariance without any significant change of the mean. It will also lower the quality of the LQMs. Figure 5.11 shows the effect of this parameter on the PEP which increases by increasing this parameter.

The decorrelation time will just affect the autocovariance of the Gaussian process, where increasing this time will augment the autocovariance vector, which is a vector containing $c_\Gamma(n\ell_E)$ non zero values, where $n$ is an integer number. Figures 5.12, 5.13, and 5.14 illustrate the effect of this parameter, i.e decorrelation time, on the autocovariance for IEEE802.15.4e, WirelessHART and ISA-100.11a respectively. As we can see from Figure 5.12 that when the decorrelation time is smaller than $1.5s$ the autocovariance is almost constant and when it becomes greater than $1.5s$ then the higher the decorrelation time, the greater the autocovariance. Whereas, the autocovariance vector of WirelessHART and ISA-100.11a in Figures 5.13, and 5.14 for the same value of decorrelation time, for instance $\tau_{\xi_0} = 4\,s$, has just two values comparing to the case of IEEE 802.15.4e. In other words, the packets are less correlated in Figures 5.13, and 5.14 comparing to the parameters of Figure 5.12

The decorrelation decay distance: This distance is used to describe the correlation properties where a short decorrelation distance indicates that the shadow component varies quickly as the object moves and a longer decorrelation distance refers to a slowly shadowing. The decorrelation distance is defined as the distance to which the correlation coefficient has dropped to $e^{-1}$, which is a commonly used value in the literature [81]. It is on the order of the size of the blocking object or cluster of these objects [121]. Therefore, having different scenarios and applications might result in different decorrelation distances. Moreover, increasing the decorrelation decay distance will increase the correlation properties and the autcovariance as it is shown in Figure 5.15 for IEEE802.15.4e which illustrates the autocovariance as a function of velocity per decorrelation decay distance $V_0/d_{c0}$ . The same result idea is obtained for the other two standards as in Figures 5.16 and 5.17.

## 5.5 Parametric analysis of the wireless link models

This section presents the parametric analysis of the wireless link model subject to the effect of a persistent interferer with the variation of its different parameters including the decay decorrelation distance, the sampling time, the power of the interferer, the distance between the interferer-receiver pair, the length of the message, the number of the Markov chain states, the standard deviation of residual power error, the standard deviation of the shadowing correlation, and the decorrelation time.

### 5.5.1 Decay decorrelation distance

We apply a Monte Carlo simulation of the analytic model, the moment matching model and the Markov chain one. The minimum sampling rate of IEEE802.15.4e standard ( $T_u = 0.01s$) [5] is chosen together with other parameters of this standard in Table 5.4. The interferer has the same nature of the useful device and it is $14m$ farther from the receiver. Table 5.5 shows the impact of changing the decorrrelation distance on the characteristics of the channel. The bigger the blocking object, i.e. the longer the decorrelation distance, the longer the autocovariance vector. This imposes an upper bound of the decorrelation decay distance, i.e. the maximum value of this parameter for which the first order Markov chain is able to perfectly represent the stochastic characteristics of the link. Therefore, as shown in Table 5.5 using a value of the shadowing decay distance ( $d_{c1} = 9m$), [80], the first order Markov chain is not able to perfectly abstract the stochastic behavior of the link where $c_\Gamma(2\ell_E) = 2 * 10^{-9} dB$, whereas as long as $d_{c1} <= 6.8m$, a first order Markov chain is sufficient to abstract the behavior of the link. Figure 5.18 displays the autocovariance vector as a function of the decorrelation distance, and therefore it shows the effect of this parameter on choosing the memory of the Markov chain abstraction. We notice from the figure that as long as $d_{c1} <= d_{c0}$ the autocovarince remains almost constant. Moreover, It is clear from this figure that having a large obstructing object that causes $dc >= 14m$ will result in a longer autocovariance vector and thus will require at least a fourth order Markov chain abstraction.

In Table 5.5 $\eta_\Gamma$, $\sigma_\Gamma$, $\eta_{MM}$, $\sigma_{MM}$, $\eta_{MC}$, $\sigma_{MC}$ refer to the mean and the standard deviation of the stochastic process representing the SINR obtained through each of the previously described methods: analytic, moment matching and Markov chain, respectively.

The values of the aforementioned variables obtained through Monte Carlo simulation are reported in Table 5.5. The mean of each solution is thus evaluated and results show that the mean of the moment matching matches the mean of the Gaussian process with an absolute error equals to $2 * 10^{-4}$, and the mean of the Markov chain matches the one of the moment matching with an absolute error of $2.5 * 10^{-4}$, whereas the standard deviation error of the moment matching with respect to the one of the stochastic process is $1.45 * 10^{-3}$. The error of the standard deviation of the Markov chain with respect to its corresponding value of the moment matching is $0.276$. We notice that the last error is larger than the previous errors and this is due to the fact that we have used only four states in this analysis for the Markov chain: increasing the number of states will diminish the error but at the expense of computational complexity. It is worth mentioning that having a slower sampling rate will increase the upper bound of the decorrelation decay distance at which the first order Markov chain is sufficient to perfectly represent the wireless link. For instance, when the update rate is $0.02s$ this upper bound becomes $13.6m$, whereas it is $20.4m$ when the sampling rate is $0.03s$ etc. Moreover, it should be pointed out that changing the decorrelation decay distance will change the quantization levels of SINR values. Moreover, having this interferer at $14m$ far from the receiver will change the LQMs. In particular, the PEP, the PER's variance and the maximum fading length will be increased to $0.5 * 10^{-3}, 0.12 * 10^{-3}, 220ms$ respectively. Therefore, the communication needs are not perfectly satisfied as it was in the ideal scenario without the interferer, especially the PEP. It should be pointed out that if we have the same scenario with the other two standards the first order Markov chain can perfectly abstract the channel for all the values of $d_{c1} = [3 - 20]$ since the probability of the future state depends only on the current state, in other words, the autocovariance vector just contains one value.

### 5.5.2 The interferer power

Different devices in the industrial environment might produce different power. Various effects on the studied link arise while assuming a scenario where the interferer could have different power and at the same distance as in the previous analysis i.e., $d_{c1} = 14m$. First, the higher the power of the interferer, the smaller the mean of the Gaussian process and the smaller the second quantization level after $(-\infty)$ as depicted in Table 5.6 for IEEE802.15.4e. Second, the PEP and the maximum dropouts increase if the power of the interferer increases. Moreover, it is noteworthy that the variance and the autocovariance vector for this scenario will not have a crucial change when changing the power.

Table 5.5: The parametric analysis of the decay decorrelation distance for IEEE802.15.4e.

| **Case** | $d_{c1}$ **[m]** | $\eta_\Gamma$ **[dB]** | $\sigma_\Gamma$ **[dB]** | $\eta_{MM}$ **[dB]** | $\sigma_{MM}$ **[dB]** | $\eta_{MC}$ **[dB]** | $\sigma_{MC}$ **[dB]** | $c_\Gamma(\ell_E)$ **[dB]** | $c_\Gamma(2\ell_E)$ **[dB]** | $c_\Gamma(3\ell_E)$ **[dB]** | $c_\Gamma(4\ell_E)$ **[dB]** |
|---|---|---|---|---|---|---|---|---|---|---|---|
| 1 | 3 | 5.204 | 1.726 | 5.205 | 1.727 | 5.206 | 1.601 | $3.9 * 10^{-6}$ | 0 | 0 | 0 |
| 2 | 4 | 5.203 | 1.724 | 5.203 | 1.725 | 5.204 | 1.601 | $3.9 * 10^{-6}$ | 0 | 0 | 0 |
| 3 | 5 | 5.204 | 1.726 | 5.205 | 1.727 | 5.205 | 1.602 | $3.91 * 10^{-6}$ | 0 | 0 | 0 |
| 4 | 6 | 5.204 | 1.725 | 5.205 | 1.728 | 5.205 | 1.601 | $4.36 * 10^{-6}$ | 0 | 0 | 0 |
| 5 | 6.5 | 5.204 | 1.724 | 5.205 | 1.727 | 5.204 | 1.601 | $7.79 * 10^{-6}$ | 0 | 0 | 0 |
| 6 | 6.8 | 5.204 | 1.725 | 5.204 | 1.727 | 5.204 | 1.602 | $0.015 * 10^{-3}$ | 0 | 0 | 0 |
| 7 | 7 | 5.203 | 1.724 | 5.206 | 1.729 | 5.205 | 1.601 | $0.025 * 10^{-3}$ | $1 * 10^{-15}$ | 0 | 0 |
| 8 | 8 | 5.203 | 1.725 | 5.203 | 1.728 | 5.203 | 1.602 | 0.0003 | $0.96 * 10^{-12}$ | 0 | 0 |
| 9 | 9 | 5.203 | 1.726 | 5.204 | 1.728 | 5.204 | 1.601 | 0.0015 | $0.32 * 10^{-9}$ | 0 | 0 |
| 10 | 10 | 5.207 | 1.727 | 5.206 | 1.728 | 5.203 | 1.602 | 0.005 | $0.02 * 10^{-6}$ | 0 | 0 |
| 11 | 11 | 5.203 | 1.727 | 5.204 | 1.728 | 5.205 | 1.601 | 0.0128 | $0.44 * 10^{-6}$ | 0 | 0 |
| 12 | 12 | 5.206 | 1.726 | 5.206 | 1.727 | 5.203 | 1.602 | 0.026 | $4.5 * 10^{-6}$ | 0 | 0 |
| 13 | 13 | 5.207 | 1.724 | 5.205 | 1.728 | 5.204 | 1.601 | 0.044 | $0.03 * 10^{-3}$ | 0 | 0 |
| 14 | 14 | 5.204 | 1.727 | 5.204 | 1.726 | 5.204 | 1.601 | 0.067 | 0.0001 | $4.9 * 10^{-9}$ | $4 * 10^{-15}$ |
| 15 | 15 | 5.204 | 1.727 | 5.204 | 1.730 | 5.204 | 1.602 | 0.095 | $0.379 * 10^{-3}$ | $0.058 * 10^{-6}$ | $0.34 * 10^{-12}$ |
| 16 | 16 | 5.204 | 1.727 | 5.205 | 1.727 | 5.204 | 1.602 | 0.127 | $0.983 * 10^{-3}$ | $0.435 * 10^{-6}$ | $0.011 * 10^{-9}$ |
| 17 | 17 | 5.207 | 1.727 | 5.204 | 1.725 | 5.205 | 1.603 | 0.16 | 0.0022 | $2.3 * 10^{-6}$ | $0.196 * 10^{-9}$ |
| 18 | 18 | 5.203 | 1.725 | 5.204 | 1.727 | 5.205 | 1.601 | 0.195 | 0.0042 | $0.009 * 10^{-3}$ | $2.19 * 10^{-9}$ |
| 19 | 19 | 5.206 | 1.727 | 5.203 | 1.728 | 5.203 | 1.602 | 0.23 | 0.0073 | $0.031 * 10^{-3}$ | $0.0169 * 10^{-6}$ |
| 20 | 20 | 6.322 | 1.727 | 5.204 | 1.725 | 5.204 | 1.601 | 0.266 | 0.012 | $0.08 * 10^{-3}$ | $0.097 * 10^{-6}$ |

### 5.5.3 Interferer-receiver distance

The impact of the interferer-receiver distance is significant when the interferer is at a closer distance from the receiver with respect to the reference transmitter. The closer the inter-

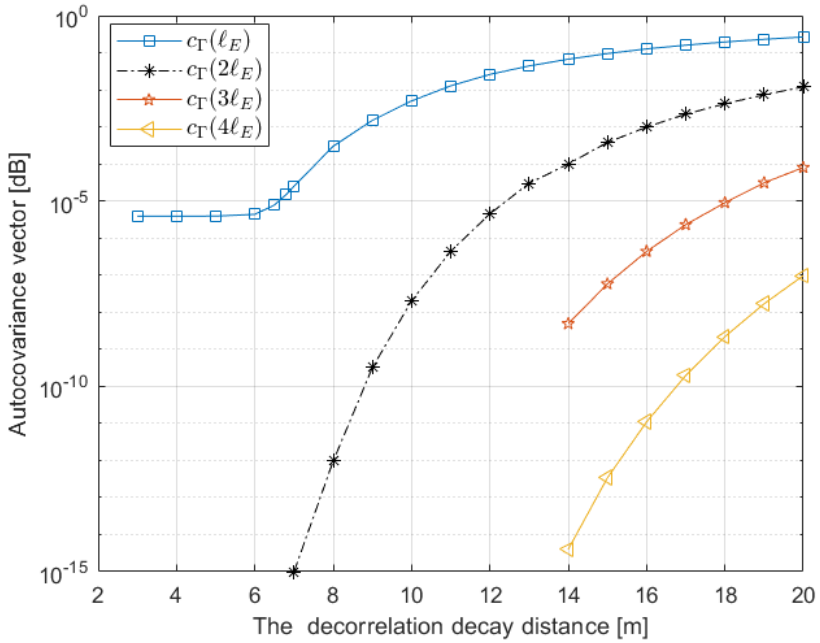


Figure 5.18: The impact of changing $d_{c1}$ on $c_\Gamma(n\ell_E)[dB]$ in IEEE802.15.4e .

Table 5.6: The parametric analysis of the interferer power.

| $P_1$ | $\eta_{MM}$ [dB] | $\sigma_{MM}$ [dB] | $c_\Gamma(\ell_E)$ [dB] | $\eta_A$ [dB] | $\sigma_A$ [dB] | $\ell^\star_{\mathrm{B}}$ [ms] | **Thresholds** |
|---|---|---|---|---|---|---|---|
| 2 | 9.133 | 1.709 | $0.015 * 10^{-3}$ | $0.043 * 10^{-6}$ | $0.021 * 10^{-6}$ | 40 | $7.981, 9.133, 10.286$ |
| 4 | 8.194 | 1.717 | $0.015 * 10^{-3}$ | $0.064 * 10^{-6}$ | $0.052 * 10^{-6}$ | 60 | $7.006, 8.164, 9.322$ |
| 6 | 7.184 | 1.722 | $0.015 * 10^{-3}$ | $7.4 * 10^{-6}$ | $0.93 * 10^{-6}$ | 80 | $6.022, 7.184, 8.346$ |
| 8 | 6.195 | 1.725 | $0.015 * 10^{-3}$ | $0.067 * 10^{-3}$ | $0.012 * 10^{-3}$ | 130 | $5.033, 6.19, 7.360$ |
| 10 | 5.204 | 1.728 | $0.015 * 10^{-3}$ | $0.47 * 10^{-3}$ | $0.12 * 10^{-3}$ | 220 | $4.039, 5.204, 6.369$ |

ferer to the receiver, the longer the maximum dropouts and the higher the PEP. Moreover, we find out that changing the distance of the interferer-receiver pair will change the mean

of the Gaussian process that describes the link. However, the variance and the autocovariance will slightly change. Furthermore, the quantization levels of the states of the Markov chain which describes the channel will change. Fixing the shadowing decorrelation distance to its upper bound, i.e. $d_{c1} = 6.8m$ for IEEE 802.15.4e, and using the transmitter ideal parameters, Table 5.7 demonstrates the influence of changing this distance on the link. As it is reported, the greater the distance between the interferer-receiver pair with respect to the reference transmitter-receiver distance, clearly the less its impact on the channel, so the better the LQMs and the larger the second threshold after $-\infty$. Since the upper bound value of the decorrelation decay distance is exploited, the first order Markov chain is perfectly able to represent the channel: $c_\Gamma(2\ell_E) = 0$ for all values of $d_1$ and the first value of the autocovariance vector will not greatly change.

Table 5.7: The parametric analysis of the interferer-receiver distance.

| $d_1$ | $\eta_{MM}$ [dB] | $\sigma_{MM}$ [dB] | $c_\Gamma(\ell_E)$ [dB] | $\eta_A$ [dB] | $\sigma_A$ [dB] | $\ell_{\mathrm{B}}^{\star}$ [s] | **Thresholds** |
|---|---|---|---|---|---|---|---|
| 6 | $-5.539$ | 1.731 | $0.015 * 10^{-3}$ | 0.992 | 0.0038 | 121172331.04 | $-6.706, -5.539, -4.371$ |
| 8 | $-3.04$ | 1.731 | $0.015 * 10^{-3}$ | 0.856 | 0.077 | 52257.95 | $-4.208, -3.041, -1.873$ |
| 10 | 0.394 | 1.731 | $0.015 * 10^{-3}$ | 0.217 | 0.106 | 31.75 | $-0.773, 0.394, 1.562$ |
| 12 | 3 | 1.730 | $0.015 * 10^{-3}$ | 0.0155 | $6.7e-3$ | 1.16 | $1.837, 3, 4.171$ |
| 14 | 5.204 | 1.728 | $0.015 * 10^{-3}$ | $0.47 * 10^{-3}$ | $0.12 * 10^{-3}$ | 0.22 | $4.039, 5.204, 6.369$ |

### 5.5.4 Sampling rates

The selection of sampling rates is an important issue. It is a joint parameter that affects both channel and control dynamics [1], and as a consequence, needs to be set carefully. In industrial applications, for economic reasons, sampling rates are kept as low as possible, therefore there is more time available for the control algorithm execution. However, the wireless standard used in the WNCS has some limitations on the update rate. In our work [3], we used the WirelessHART standard, which is too slow for several control applications: the packets of the wireless link are always uncorrelated and a Bernoulli abstraction is sufficient to represent the stochastic characteristics of the link. However, several control

applications require a faster sampling rate to meet the growing demands of high reliability and low latency constrains of industrial applications. The IEEE 802.15.4e standard has been released to address the aforementioned issues and support a short update rate $T_u = 10\ ms$ [122], which is more convenient for fast dynamic applications like the inverted pendulum on a cart. Moreover, ISA-10.11a has update periods starting from 1/32 ms increments up to 3600 s [10]. Table 5.8 shows the effect of changing the sampling rate on the stochastic characteristics. Changing the sampling period will not have a major effect on the stochastic characteristics of the wireless link but it has a notable impact on the autocovariance vector as shown in Table 5.8. The shorter the update period, the more correlated the packets are, thus the autocovariance vector would be longer. In particular, choosing the shortest update period of ISA-100.11a would make the packets very correlated and the autocovariance vector would be 128 elements length. Moreover, if we fix the length of the message for this standard and use a longer update period, the maximum fading length will be decreased. Furthermore, from Table 5.8, although the first case satisfies the maximum fading length constraint, it doesn't fulfill the PEP limitation because of the imperfections caused by the interferer. It is worth noting that when the sampling rate is too slow, for instance for our plant is greater or equal to $2s$, the plant is not controllable anymore.

### 5.5.5 The length of the message

There is an argument that the message size should be small to achieve reliable wireless delivery [60, p. 74]. The contention is that, on one hand, the shorter the message, the quicker it will be transmitted hence the less chance that it will be corrupted by noise. On the other hand, it is preferable to combine several commands in one message to enhance throughput. This likewise could improve reliability as sending commands individually will expose each of them to interference. Therefore, the message length ought to be chosen as a trade-off between the reliability and throughput. In addition, the physical frame in each standard is specified. For example, most IEEE 802.15.4 physical layer only support frames of up to 127 bytes (adaptation layer protocols such as 6LoWPAN provide fragmentation schemes to support larger network layer packets). Table 5.9 shows how changing the length of the message would affect the link stochastic characteristics and the LQMs for IEEE 802.15.4e. By changing the command number, which is the key attribute assigned to the variable to be written [13], and changing the number of the variables the mean and variance of the corresponding channel model will not be affected. However, increasing the

Table 5.8: The parametric analysis of the sampling rate.

| $T_u$ [s] | $\ell_F$ [octets] | reference | $\eta_{MM}$ [dB] | $\sigma_{MM}$ [dB] | $c_\Gamma(\ell_E)$ [dB] | $\eta_A$ [dB] | $\sigma_A$ [dB] | $\ell_{\mathrm{B}}^\star$ [ms] |
|---|---|---|---|---|---|---|---|---|
| 0.01 | 62 | [13] | 5.204 | 1.727 | $0.015 * 10^{-3}$ | $0.47 * 10^{-3}$ | $0.12 * 10^{-3}$ | 220 |
| 1/32 | 63 | [10] | 5.204 | 1.727 | $1 * 10^{-15}$ | 0.0005 | 0.00012 | 625 |
| 0.1 | 102 | [13] | 5.204 | 1.727 | $1 * 10^{-15}$ | 0.0007 | 0.00021 | 1900 |
| 0.25 | 102 | [13] | 5.204 | 1.727 | $1 * 10^{-15}$ | 0.0007 | 0.00021 | 1700 |
| 0.5 | 102 | [13] | 5.204 | 1.727 | $1 * 10^{-15}$ | 0.0007 | 0.00021 | 1600 |
| 1 | 102 | [13] | 5.204 | 1.727 | $1 * 10^{-15}$ | 0.0007 | 0.00021 | 1500 |
| 2 | 102 | [13] | The described plant sampled at Ts = 2 s is uncontrolable | | | | | |

number of the variables would render the packets more correlated. Moreover, the LQMs get slightly worse by increasing the length of the message.

### 5.5.6 The number of Markov chain states

Increasing the number of states of the Markov chain will increase the abstraction accuracy. In particular, the mean and variance of the Markov chain will match more precisely the ones of the analytic model. However, at a certain number of Markov chain states, increasing their number will barely improve the model precision at the expense of increasing the complexity. Thus, the number of the Markov chain states has to be chosen as a trade off among the degree of accuracy and complexity. Therefore, according to Table 5.10 if we use 50 Markov chain states we can tolerate $(4 * 10^{-3})$ of an absolute error between the Markov chain stage and the analytic one. Moreover, the number of states that makes the standard deviation of the Markov chain perfectly match the one of the moment matching for the same scenario used in the previous analysis ends up to be 120 states.

Table 5.9: The parametric analysis of the length of the message.

| **Comm. Number** | $\ell_F$ **[octets]** | $\eta_{MM}$ **[dB]** | $\sigma_{MM}$ **[dB]** | $c_\Gamma(\ell_E)$ **[dB]** | $c_\Gamma(2\ell_E)$ **[dB]** | $\eta_A$ **[dB]** | $\sigma_A$ **[dB]** | $\ell^\star_{\mathrm{B}}$ **[ms]** |
|---|---|---|---|---|---|---|---|---|
| 1 | 14 | 5.204 | 1.727 | $1 * 10^{-15}$ | 0 | $0.13 * 10^{-3}$ | $0.015 * 10^{-3}$ | 190 |
| 3 | 18 | 5.204 | 1.727 | $1 * 10^{-15}$ | 0 | $0.16 * 10^{-3}$ | $0.023 * 10^{-3}$ | 200 |
| 3 | 23 | 5.204 | 1.727 | $1 * 10^{-15}$ | 0 | $0.2 * 10^{-3}$ | $0.033 * 10^{-3}$ | 200 |
| 3 | 28 | 5.204 | 1.727 | $1 * 10^{-15}$ | 0 | $0.23 * 10^{-3}$ | $0.043 * 10^{-3}$ | 210 |
| 3 | 33 | 5.204 | 1.727 | $1 * 10^{-15}$ | 0 | $0.28 * 10^{-3}$ | $0.054 * 10^{-3}$ | 210 |
| 9 | 62 | 5.204 | 1.727 | $0.15e - 3$ | 0 | $0.47 * 10^{-3}$ | $0.12 * 10^{-3}$ | 220 |
| 9 | 70 | 5.204 | 1.727 | $0.127 * 10^{-3}$ | $0.047 * 10^{-12}$ | $0.52 * 10^{-3}$ | $0.13 * 10^{-3}$ | 220 |
| 9 | 78 | 5.204 | 1.727 | $0.59 * 10^{-3}$ | $1.081 * 10^{-12}$ | $0.57 * 10^{-3}$ | $0.16 * 10^{-3}$ | 230 |

### 5.5.7 The logarithmic residual power control error standard deviation and the shadowing correlation standard deviation

As we saw the effect of these two parameters on the link and the LQMs, the interferer's parameters affect the channel in the same manner. Thus, the standard deviation of the power control error affects mainly the variance of the Gaussian process and decrease the quality of LQMs. The standard deviation of the shadowing correlation affects the variance, autocovariance and worsen LQMs too as it is depicted in Table 5.11 and Table 5.12.

### 5.5.8 The decorrelation time

As mentioned before, this parameter affects mostly the autocovariance of the Gaussian process where by increasing this time, the packets will be more correlated and a higher order Markov chain model is needed to better abstract the analytic model as shown in Figure 5.19.

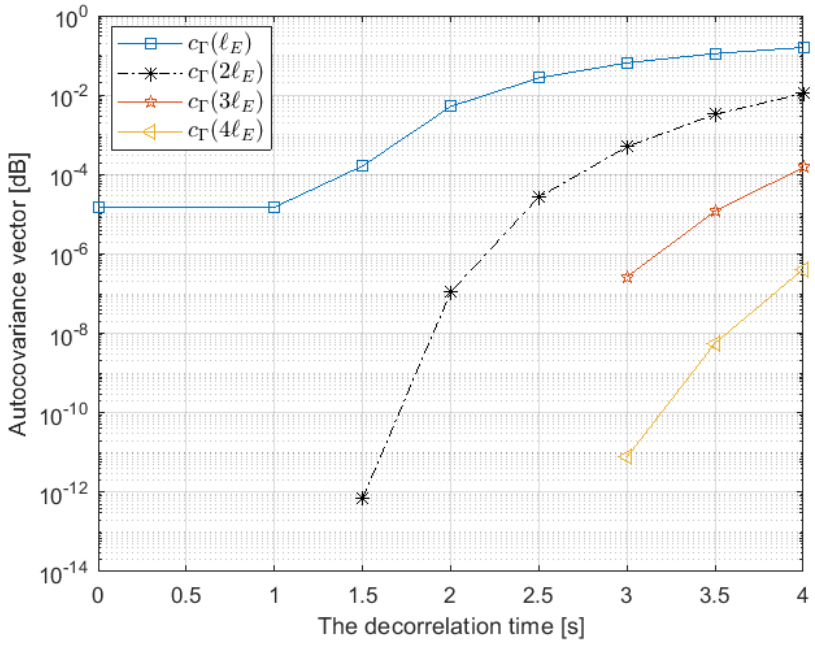


Figure 5.19: The autocovariance vector as a function of decorrelation time of the interferer for IEEE 802.15.4e.

Table 5.10: The parametric analysis of the number of the Markov chain states.

| **States Number** | $\eta_\Gamma$ **[dB]** | $\sigma_\Gamma$ **[dB]** | $\eta_{MM}$ **[dB]** | $\sigma_{MM}$ **[dB]** | $\eta_{MC}$ **[dB]** | $\sigma_{MC}$ **[dB]** |
|---|---|---|---|---|---|---|
| 2 | 5.202 | 1.724 | 5.205 | 1.727 | 5.206 | 1.357 |
| 4 | 5.203 | 1.725 | 5.204 | 1.726 | 5.204 | 1.603 |
| 10 | 5.202 | 1.725 | 5.202 | 1.728 | 5.206 | 1.692 |
| 20 | 5.204 | 1.727 | 5.204 | 1.728 | 5.205 | 1.713 |
| 50 | 5.203 | 1.725 | 5.204 | 1.727 | 5.204 | 1.723 |
| 100 | 5.204 | 1.725 | 5.206 | 1.727 | 5.202 | 1.726 |
| 120 | 5.204 | 1.727 | 5.204 | 1.727 | 5.204 | 1.727 |

Table 5.11: The parametric analysis of the standard deviation of the residual power control error

| $\sigma_{\xi_0}$ | $\eta_{MM}$ **[dB]** | $\sigma_{MM}$ **[dB]** | $c_\Gamma(\ell_E)$ **[dB]** | $\eta_A$ **[dB]** | $\sigma_A$ **[dB]** | $\ell_{\mathrm{B}}^\star$ **[ms]** |
|---|---|---|---|---|---|---|
| $10^{0.14}$ | 5.204 | 1.721 | $0.05 * 10^{-3}$ | $0.46 * 10^{-3}$ | $0.11 * 10^{-3}$ | 220 |
| $10^{0.17}$ | 5.204 | 1.741 | $0.05 * 10^{-3}$ | $0.51 * 10^{-3}$ | $0.13 * 10^{-3}$ | 220 |
| $10^{0.2}$ | 5.204 | 1.764 | $0.05 * 10^{-3}$ | $0.5 * 10^{-3}$ | $0.16 * 10^{-3}$ | 220 |
| $10^{0.3}$ | 5.204 | 1.865 | $0.05 * 10^{-3}$ | $0.95 * 10^{-3}$ | $0.306 * 10^{-3}$ | 230 |
| $10^{0.4}$ | 5.204 | 2.015 | $0.05 * 10^{-3}$ | 0.0018 | 0.0007 | 230 |

It is interesting to mention that the autocovariance vector plays an important role in stability of the system. In particular, when it is all zero we can apply the Bernoulli

Table 5.12: The parametric analysis of the standard deviation of the shadowing correlation.

| $\sigma_{\beta_0}$ | $\eta_{MM}$ **[dB]** | $\sigma_{MM}$ **[dB]** | $c_\Gamma(\ell_E)$ **[dB]** | $c_\Gamma(2\ell_E)$ **[dB]** | $\eta_A$ **[dB]** | $\sigma_A$ **[dB]** | $\ell_{\mathrm{B}}^\star$ **[ms]** |
|---|---|---|---|---|---|---|---|
| 1.5 | 5.204 | 1.597 | $0.01 * 10^{-3}$ | 0 | $0.22 * 10^{-3}$ | $0.11 * 10^{-3}$ | 220 |
| 2 | 5.204 | 1.727 | $0.015 * 10^{-3}$ | 0 | $0.47 * 10^{-3}$ | $0.12 * 10^{-3}$ | 220 |
| 2.5 | 5.204 | 1.882 | $0.022 * 10^{-3}$ | $1 * 10^{-15}$ | 0.001 | $0.16 * 10^{-3}$ | 230 |
| 3 | 5.204 | 2.056 | $0.029 * 10^{-3}$ | $1 * 10^{-15}$ | 0.0021 | $0.306 * 10^{-3}$ | 230 |
| 4 | 5.204 | 2.445 | $0.049 * 10^{-3}$ | $2 * 10^{-15}$ | 0.0071 | 0.0007 | 240 |

controller to control the plant since all packets are independent. However, when it becomes significant at the packet level, so it is not zero, and all the other elements of the vector are zeros then we have to use the first order Markov chain representation which works until a certain point. For a longer autocovariance vector we need a higher order Markov chain or a more complicated ones.

## 5.6 Discussion

As we have seen, our proposed model in this thesis allows us to abstract the link behaviour subject to several imperfections. It permits us to design a controller that guarantees stability and thus improving the control performance of the overall closed loop control system. However, the findings of this study have to be seen in light of some limitations. In particular, our research methodology were based fundamentally on the PHY layer thus network characteristics mainly related to data link layer (e.g. reliability, latency, jitter etc) and mechanisms including scheduling, routing etc, were not taken into account in this study. In other words, our model can abstract the real model under certain conditions in specific scenarios in which these mechanisms could be neglected. For instance, assuming that we use the same frequency we could neglect the need for scheduling. Another example is when the latency of the network is relatively small, i.e in the order of $10^{-6}$ and we

reason that the update period is $T_u = 0.01\,\mathrm{s}$ therefore, the latency could be neglected. On the other hand, if the latency is comparable with $T_u$ so the model is not valid because we are not in the scenario of 1 time step delay anymore. Therefore, the cross-layer view is not considered in our proposed model, and this creates the main limitation which prevents us from implementing the proposed work in real embedded systems. Thus, I have included this further research in my future plan so we can have a more thorough model abstracting the stochastic characteristics of the link and considering several mechanisms.

Moreover, during the derivation of our model we adopted the highly absorbing environments which often eliminate the effect of multipath propagation [92]. Thus, log-normal fading is able to abstract the multipath fading and it is considered as an accepted model to describe the small scale fading in such environments. However, for a more precise model which represent more general industry plants where multipath fading cannot be neglected, our model should be generalised to capture the effect of this fading. Furthermore, the effects of several devices which are existed in the same environment and using different standards than the one used by our network are not taken into account in this model. In addition, since it is a challenge to access real industrial environments our model is not implemented and validated in such environments.

## 5.7 Summary

In this chapter, we used WNCSs to demonstrate our model's applicability to various protocols in various scenarios, as well as how it can help us boosting the reliability and thus the overall control efficiency of a closed loop system. To get a simplified version of our model [3], we made some basic assumptions and chose WirelessHART as a wireless industrial control protocol that is subject to various imperfections. Then we tested the relevance of this simplified model on an inverted pendulum on a cart and publish the findings in [3]. Furthermore, after generalizing the model to include different standards including ISA-100.11a and IEEE 802.15.4e, we presented a detailed parametric study of the wireless link model with the effect of a persistent interferer and various parameter variations. Finally, a discussion on the limitations of our proposed model was carried out.

Chapter 6

# Conclusion and Future work

## 6.1 Conclusion

In this thesis, first, we worked on a systematic derivation of an accurate Markov link model suitable to represent any industrial communication protocol. This model accounts for both channel and control dynamics. The proposed analytic model is derived by taking into account multiple interferers and physical phenomena characterizing a communication link. It matches both average packet error probability and worst case bursty behavior of the accurate analytic model of the link.

We described the late developments of our research on cyber-physical systems co-design for industrial applications. To this aim, we derived the accurate Markov link model simultaneously accounting for path loss, shadow fading, multipath fading, interference and power residual control and test its applicability on different protocols. The presented framework may be useful for the emerging scenarios e.g. URLLC (ultra-reliable and low latency communications). In particular, since the challenges in analysis and co-design of wireless networked control systems are well highlighted by considering wireless industrial control protocols. In this perspective, we presented a mathematical framework for deriving an accurate Markov channel model of a WirelessHART radio link affected by path loss, shadowing, power residual control and persistent interference.

A new contribution was the derivation of SINR according to IEEE 802.15.4 PHY layer standard using a symbol-level matching followed by decoding, and considering the characteristics of the PN sequences, which can be summarized by the Hamming distances between them. After having SINR equation we have found a tractable representation of

the explicit analytic model of SINR. To perform that, we can approximate it with another random process, (e.g. log-normal process) and then apply moment matching approach to get the signal statistics.

We have derived the equation of the symbol error rate taking into account the signal to interference plus noise ratio which is, to the best of our knowledge, a new contribution and no other work has addressed this issue before.

We also introduced link quality metrics that permit us to assess how good a finite-state representation of the radio link is. We have shown on a numerical case study how these metrics are essential for an easy discovering of some pitfalls related to both the choice of the method of partitioning of the range of SINR and the computation of transition probabilities between operational modes of the Markov channel. We have also demonstrated in a formal setting that an accurate Markov model of the WirelessHART link allows us to design a controller that guarantees stability and improves control performance of the closed-loop system, where other approaches based on a simplified channel model fail.

We generalize the work to cover all the following wireless standards (IEEE 802.15.4, WirelessHART, ISA-100.11a and IEEE 804.15.4e). We show that our model is able to abstract the wireless standard radio link subject to channel impairments and interference.

We did a rigorous parametric analysis on the model with the variation of different parameters including the decay decorrelation distance, the sampling time, the power of the interferer, the distance between the interferer-receiver pair, the decorrelaion time, the length of the message, the logarithmic residual power control error standard deviation and the shadowing correlation standard deviation and the number of the Markov chain states.

## 6.2 Future work

Future work concerns generalizing the proposed model to take into account, on one hand, all the physical phenomena mentioned in chapter 3. On the other hand, deriving the model for a more general communication scenario including multiple devices belonging to the same network or to different networks. Therefore, we will model the presence of devices which interfere a certain link as a binary random process that represents their activity status (ON-OFF) as in [106]. Moreover, we aim to compare different SINR partitioning methods for improving the wireless link model.

Furthermore, we are planning to apply the forward error correction (FEC) which improves the reliability by making the transmitter send redundant data which allows the

receiver to recognize just the part of the data that contains no errors. Other data link layer functionalities can be also investigated based on the proposed physical model to check how the model behaves when we include these functionalities. In addition, it could be interesting to analyze the impact of the quantization method used in dividing the range of SINR on the LQMs that are indicators of the channel performance.

Another interesting future work could be trying to improve reliability, latency, jitter and overall control performance by considering scheduling, routing and other mechanisms when we derive model thus, a cross-layer view will be taken into account. Moreover, handling coexistence issues in the ISM unlicensed frequency bands, which are mainly used in industrial automation is also an appealing concern which can be studied later.

# Appendices

Appendix A

# Appendix A

## Proofs of chapter 3

### Derivation of the received signal components

In following we compute each of the terms Let's start with the noise components From 3.31 we obtain

$$W_{I,\ell} = \sqrt{\frac{2}{T_c}} \int_0^{T_s} \mathcal{W}(t)\ \cos(w_c t)\, cos(w_p(t)) \sum_{m=0}^{15} \hat{b}_{I,0,l,m}\, dt, \tag{A.1}$$

Since $W(t)$ is the AWGN with two sided power spectral density Psd $\frac{N_0}{2}$, we have $E[W(t)] = 0 \Rightarrow$

$$E[W_{I,\ell}] = \sqrt{\frac{2}{T_c}} \int_0^{T_s} E[\mathcal{W}(t)]\ \cos(w_c t)\, cos(w_p(t)) \sum_{m=0}^{15} \hat{b}_{I,0,l,m}\, dt = 0, \tag{A.2}$$

We know that

$$\begin{aligned}
\sigma^2[W_{I,\ell}] &= E[W_{I,\ell}^2] - E^2[W_{I,\ell}] = E[W_{I,\ell,m}^2] \\
&= \frac{2}{T_c} \int_0^{T_s} \int_0^{T_s} E[w(t_1)w(t_2)] \cos(w_c t_1) \cos(w_p t_1)\, . \\
&\qquad \sum_{m=0}^{15} \hat{b}_{I,0,l,m}^2\ \cos(w_c t_2) \cos(w_p t_2)\, dt_1 dt_2 \\
&= \frac{2}{T_c} \frac{N_0}{2} \int_0^{T_s} \delta(t_1 - t_2) \cos(w_c t_1) \cos(w_p t_1). \\
&\qquad \sum_{m=0}^{15} \hat{b}_{I,0,l,m}^2\ \cos(w_c t_2) \cos(w_p t_2)\, dt_1 dt_2,
\end{aligned}$$

since $\hat{b}^2_{I,0,l,m} = 1$ and using the trigonometric identities where $\cos^2(\theta) = \frac{1}{2}(1 + \cos(2\theta))$ and $\cos(\theta)\cos(\phi) = \frac{1}{2}(\cos(\theta - \phi) + \cos(\theta + \phi)) \Rightarrow$

$$\begin{aligned}
\sigma^2[W_{I,\ell}] &= \frac{N_0}{T_c}\int_0^{T_s} \cos^2(w_c t)\cos^2(w_p t)dt \\
&= \frac{N_0}{4T_c}\int_0^{T_s} (1+\cos(2w_c t))\,(1+\cos(2w_p t))\,dt \\
&= \frac{N_0}{4T_c}\int_0^{T_s} \Big(1+\cos(2w_c t)+\cos(2w_p t)+cos(2w_p t)\cos(2w_c t)\Big)dt \\
&= \frac{N_0 T_s}{4T_c} + \frac{N_0}{4T_c}\int_0^{T_s} \cos(2w_c t)+\cos(2w_p t)+\frac{1}{2}\cos\left(2(w_p - w_c)t\right) \\
&\qquad\qquad + \frac{1}{2}\cos\left(2(w_p + w_c)t\right)dt \\
&= \frac{N_0 T_s}{4Tc} + \frac{N_0}{4T_c}\Big(\frac{\sin(2w_c t)}{2w_c}\Big|_0^{T_s} + \frac{\sin(2w_p t)}{2w_p}\Big|_0^{T_s} + \frac{\sin\left(2(w_p - w_c)t\right)}{2(w_p - w_c)}\Big|_0^{T_s} + \\
&\qquad\qquad + \frac{\sin\left(2(w_p + w_c)t\right)}{2(w_p + w_c)}\Big|_0^{T_s}\Big) = \frac{N_0 T_s}{4Tc} = \boxed{8\,N_0}\,,
\end{aligned}$$

where $T_s = 32T_c$, $w_c = 2\pi f_c$, $w_p = \frac{2\pi}{T_c}$, $\sin(2((2\pi f_c) \pm (\frac{\pi}{2T_c}))T_s) = 0$ because $\sin(\theta + 2k\pi) = \sin(\theta) \forall k \in \mathbb{Z}$.

The quadrature component of the noise is computed in the same manner i.e starting from 3.35 we get

$$W_{Q,\ell} = \sqrt{\frac{2}{T_c}}\int_0^{T_s} \mathcal{W}(t)\,\sin(w_c t)\,\sin(w_p(t))\sum_{m=0}^{15}\hat{b}_{Q,0,l,m}\,dt, \tag{A.3}$$

Since $E[W(t)] = 0 \Rightarrow$

$$E[W_{Q,\ell,m}] = \sqrt{\frac{2}{T_c}}\int_0^{T_s} E[\mathcal{W}(t)]\,\sin(w_c t)\,\sin(w_p(t))\hat{b}_{Q,0,l,m}\,dt = 0, \tag{A.4}$$

We know that

$$\begin{aligned}\sigma^2[W_{Q,\ell}] &= E[W_{Q,\ell}^2] - E^2[W_{Q,\ell}] = E[W_{Q,\ell,m}^2] \\ &= \frac{2}{T_c}\int_0^{T_s}\int_0^{T_s} E[n(t_1)n(t_2)]\sin(w_c t_1)\sin(w_p t_1)\,. \\ &\qquad\qquad \sum_{m=0}^{15} \hat{b}_{Q,0,l,m}^2 \sin(w_c t_2)\sin(w_p t_2)\,dt_1 dt_2 \\ &= \frac{2}{T_c}\frac{N_0}{2}\int_0^{T_s} \delta(t_1 - t_2)\sin(w_c t_1)\sin(w_p t_1). \\ &\qquad\qquad \sum_{m=0}^{15} \hat{b}_{Q,0,l,m}^2 \sin(w_c t_2)\sin(w_p t_2)\,dt_1 dt_2,\end{aligned}$$

since $\hat{b}_{I,0,l,m}^2 = 1$ and using the trigonometric identities where $\sin^2(\theta) = \frac{1}{2}(1 - \cos(2\theta))$ and $\sin(\theta)\sin(\phi) = \frac{1}{2}(\sin(\theta - \phi) + \sin(\theta + \phi)) \Rightarrow$

$$\begin{aligned}\sigma^2[W_{Q,\ell}] &= \frac{N_0}{T_c}\int_0^{T_s} \sin^2(w_c t)\sin^2(w_p t)dt \\ &= \frac{N_0}{4T_c}\int_0^{T_s} (1 - \sin(2w_c t))\,(1 - \sin(2w_p t))\,dt \\ &= \frac{N_0}{4T_c}\int_0^{T_s} \Big(1 - \sin(2w_c t) - \sin(2w_p t) + \sin(2w_p t)\sin(2w_c t)\Big)dt \\ &= \frac{N_0 T_s}{4T_c} + \frac{N_0}{4T_c}\int_0^{T_s} -\sin(2w_c t) - \sin(2w_p t) + \frac{1}{2}\sin\left(2(w_p - w_c)t\right) \\ &\qquad\qquad + \frac{1}{2}\sin\left(2(w_p + w_c)t\right)dt \\ &= \frac{N_0 T_s}{4Tc} + \frac{N_0}{4T_c}\Big(\frac{\cos(2w_c t)}{2w_c}\Big|_0^{T_s} + \frac{\cos(2w_p t)}{2w_p}\Big|_0^{T_s} - \frac{\cos\left(2(w_p - w_c)t\right)}{2(w_p - w_c)}\Big|_0^{T_s} \\ &\qquad\qquad - \frac{\cos\left(2(w_p + w_c)t\right)}{2(w_p + w_c)}\Big|_0^{T_s}\Big) \approx \frac{N_0 T_s}{4Tc} \approx \boxed{8\,N_0}\,,\end{aligned}$$

The second term equals to $7.6447 * 10^{-20}$ so we could neglect it. Therefore, the variance of the noise can be expressed as

$$\begin{aligned}\sigma^2[W_\ell(t)] &= \sigma^2[W_{I,\ell}] + \sigma^2[W_{Q,\ell}] \\ &\approx 8\,N_0 + 8\,N_0 \approx \boxed{16N_0}\,,\end{aligned}$$

Now let's compute the received SoI components starting from the I-phase component in 3.38 knowing that the received signal is assumed to be synchronized with the transmitted

one so we obtain

$$
\begin{aligned}
Y_{I,0,\ell} = \frac{2}{T_c}\hat{c}_{0,t}\sum_{m=0}^{15}\Bigg(&\int_{2\,(m+32l)\,T_c}^{(2\,(m+32l+1)T_c} \hat{b}^2_{I,0,l,m}\,\cos^2(w_c t)\,cos^2(w_p t)dt \\
&- \int_{2\,(m+32l)\,T_c}^{(2\,(m+32l)+1)T_c} \hat{b}_{I,0,l,m}\hat{b}_{Q,0,l,m-1}\sin(w_c t)\cos(w_c t)\sin(w_p t)\cos(w_p t)dt \\
&- \int_{(2\,(m+32l)+1)T_c}^{2\,(m+32l+1)T_c} \hat{b}_{I,0,l,m}\hat{b}_{Q,0,l,m}\sin(w_c t)\cos(w_c t)\sin(w_p t)\cos(w_p t)dt,\Bigg)
\end{aligned}
\tag{A.5}
$$

Let's examine the three terms separately. The first term and since $\hat{b}^2_{I,0,l,m} = 1$ always we can write

$$
\begin{aligned}
&\frac{2}{T_c}\hat{c}_{0,t}\sum_{m=0}^{15}\int_{2\,(m+32l)\,T_c}^{2\,(m+32l+1)T_c} \hat{b}^2_{I,0,l,m}\cos^2(w_c t)\cos^2(w_p t)dt = \\
&= \frac{32}{4T_c}\hat{c}_{0,t}\sum_{m=0}^{15}\int_0^{2\,T_c}(1+\cos(2w_c t))\,(1+\cos(2w_p t))\,dt = \\
&= \frac{8}{T_c}\hat{c}_{0,t}\int_0^{2T_c}\Big(1+\cos(2w_c t)+\cos(2w_p t)+cos(2w_p t)\cos(2w_c t)\Big)dt = \\
&= \frac{16T_c}{T_c}\hat{c}_{0,t} + \frac{8}{T_c}\hat{c}_{0,t}\int_0^{2T_c}\cos(2w_c t)+\cos(2w_p t)+\frac{1}{2}\cos\left(2(w_p-w_c)t\right) \\
&\qquad\qquad + \frac{1}{2}\cos\left(2(w_p+w_c)t\right)dt = \\
&= 16\,\hat{c}_{0,t} + \frac{8}{T_c}\hat{c}_{0,t}\Bigg(\frac{\sin(2w_c t)}{2w_c}\Bigg|_0^{2T_c} + \frac{\sin(2w_p t)}{2w_p}\Bigg|_0^{2T_c} + \frac{\sin\left(2(w_p-w_c)t\right)}{2(w_p-w_c)}\Bigg|_0^{2T_c} + \\
&\qquad\qquad + \frac{\sin\left(2(w_p+w_c)t\right)}{2(w_p+w_c)}\Bigg|_0^{2T_c}\Bigg) = \boxed{16\,\hat{c}_{0,t}}\,,
\end{aligned}
$$

Now let's compute the following integral using trigonometric functions.

$$
\begin{aligned}
&\int_0^{T_c}\sin(w_c t)\cos(w_c t)\sin(w_p t)\cos(w_p t)dt \\
&= \frac{1}{4}\int_0^{T_c}\sin(2w_c t)\sin(2w_p t)dt \\
&= \frac{1}{8}\int_0^{T_c}\cos\left(2(w_p-w_c)t\right)dt - \frac{1}{8}\int_0^{T_c}\cos\left(2(w_p+w_c)t\right) \\
&= \frac{\sin\left(2(w_p-w_c)t\right)}{16(w_p-w_c)}\Bigg|_0^{T_c} - \frac{\sin\left(2(w_p+w_c)t\right)}{16(w_p+w_c)}\Bigg|_0^{T_c} = \boxed{0}\,,
\end{aligned}
\tag{A.6}
$$

Similarly, we get

$$\int_{T_c}^{2T_c} \sin(w_c t)\cos(w_c t)\sin(w_p t)\cos(w_p t)dt = \boxed{0}, \tag{A.7}$$

Then $\forall\, \ell,\, m \in \mathbb{N} \in 0$ we have that $k = m + 32\ell \in \mathbb{N} \in 0$, so by following the same steps as before for $t \in \{2kT_c,\, (2k+1)T_c,\, 2(k+1)T_c\}$ we obtain $\sin(2((2\pi f_c) \pm (\frac{\pi}{2T_c}))t) = 0$. Thus, $\forall\, \hat{c}_{0,t} \Rightarrow \hat{b}_{I,0,\ell,m},\, \hat{b}_{Q,0,\ell,m},\, \hat{b}_{Q,0,\ell,m-1} \in \{\pm 1\}$ we have that

$$\frac{2}{T_c}\,\hat{c}_{0,t} \sum_{m=0}^{15} \int_{2\,(m+32l)\,T_c}^{(2\,(m+32l)\,+1)T_c} \hat{b}_{I,0,l,m}\hat{b}_{Q,0,l,m-1}\sin(w_c t)\cos(w_c t)\sin(w_p t)\cos(w_p t)dt = \boxed{0}$$

$$\frac{2}{T_c}\,\hat{c}_{0,t} \sum_{m=0}^{15} \int_{2\,(m+32l)\,T_c}^{(2\,(m+32l)\,+1)T_c} \hat{b}_{I,0,l,m}\hat{b}_{Q,0,l,m}\sin(w_c t)\cos(w_c t)\sin(w_p t)\cos(w_p t)dt = \boxed{0},$$

Therefore, we finally conclude that

$$Y_{I,0,\ell,m} = \boxed{16\,\hat{c}_{0,t}}, \tag{A.8}$$

We follow the same steps for computing the quadrature part of the received SoI signal so starting from 3.41 so we obtain

$$\begin{aligned} Y_{Q,0,\ell} = \frac{2}{T_c}\hat{c}_{0,t} \sum_{m=0}^{15} \Bigg( & \int_{(2\,(m+32l)+1)\,T_c}^{2\,(m+32l+1)T_c+T_c} \hat{b}^2_{Q,0,l,m}\,\sin^2(w_c t)\,\sin^2(w_p t) \\ & - \int_{(2\,(m+32l)+1)\,T_c}^{2\,(m+32l+1)T_c} \hat{b}_{Q,0,l,m}\hat{b}_{I,0,l,m}\sin(w_c t)\cos(w_c t)\sin(w_p t)\cos(w_p t)dt \\ & - \int_{2\,(m+32l+1)T_c}^{2\,(m+32l+1)T_c+T_c} \hat{b}_{Q,0,l,m}\hat{b}_{I,0,l,m+1}\sin(w_c t)\cos(w_c t)\sin(w_p t)\cos(w_p t)dt \Bigg), \end{aligned} \tag{A.9}$$

According to A.6 and A.7 we get

$$\begin{aligned} & \frac{2}{T_c}\hat{c}_{0,t} \sum_{m=0}^{15} \int_{(2\,(m+32l)+1)\,T_c}^{2\,(m+32l+1)T_c} \hat{b}_{Q,0,l,m}\hat{b}_{I,0,l,m}\sin(w_c t)\cos(w_c t)\sin(w_p t)\cos(w_p t)dt = \boxed{0} \\ & \frac{2}{T_c}\hat{c}_{0,t} \sum_{m=0}^{15} \int_{2\,(m+32l+1)T_c}^{2\,(m+32l+1)T_c+T_c} \hat{b}_{Q,0,l,m}\hat{b}_{I,0,l,m+1}\sin(w_c t)\cos(w_c t)\sin(w_p t)\cos(w_p t)dt = \boxed{0}, \end{aligned} \tag{A.10}$$

The first term since $\hat{b}^2_{Q,0,\ell,m} = 1$ always we obtain

$$
\begin{aligned}
&\frac{2}{T_c}\hat{c}_{0,t}\sum_{m=0}^{15}\int_{(2\,(m+32l)+1)\,T_c}^{2\,(m+32l+1)T_c+T_c}\hat{b}^2_{Q,0,l,m}\sin^2(w_c t)\sin^2(w_p t)dt = \\
&= \frac{32}{4T_c}\hat{c}_{0,t}\int_0^{2\,T_c}(1-\cos(2w_c t))\,(1-\cos(2w_p t))\,dt = \\
&= \frac{8}{T_c}\hat{c}_{0,t}\int_0^{2T_c}\Big(1-\cos(2w_c t)-\cos(2w_p t)+cos(2w_p t)\cos(2w_c t)\Big)dt = \\
&= \frac{16T_c}{T_c}\hat{c}_{0,t}+\frac{8}{T_c}\hat{c}_{0,t}\int_0^{2T_c}-\cos(2w_c t)-\cos(2w_p t)+\frac{1}{2}\cos\left(2(w_p-w_c)t\right) \\
&\qquad\qquad +\frac{1}{2}\cos\left(2(w_p+w_c)t\right)dt \\
&= 16\,\hat{c}_{0,t}+\frac{8}{T_c}\hat{c}_{0,t}\left(\frac{-\sin(2w_c t)}{2w_c}\bigg|_0^{2T_c}+\frac{-\sin(2w_p t)}{2w_p}\bigg|_0^{2T_c}+\frac{\sin\left(2(w_p-w_c)t\right)}{2(w_p-w_c)}\bigg|_0^{2T_c}+\right. \\
&\qquad\qquad \left.+\frac{\sin\left(2(w_p+w_c)t\right)}{2(w_p+w_c)}\bigg|_0^{2T_c}\right) = \boxed{16\,\hat{c}_{0,t}}\,,
\end{aligned}
$$

Thus, assuming that the received SoI can be written as

$$
Y_0 = \sqrt{Y^2_{I,0,\ell}+Y^2_{Q,0,\ell}} = 16\sqrt{2}\,\hat{c}_{0,t}. \tag{A.11}
$$

## Computing the interferer's I-phase and Q-phase components in four cases

### 1- $0 < \hat{\tau}_1 < T_c$:

In this case we have $Y_{I,1,\ell}/n_{\tau_1} = \frac{2}{T_c}\,\hat{c}_{1,t}(A_1 - B_1)$. Now starting with the $A_1$ and after filtering out $2w_c t$, applying the stochastic analysis and the trigonometric analysis we get

$$
\begin{aligned}
A_1 = \frac{1}{4}\cos(\phi_{c_1}) \sum_{m=0}^{15} \Bigg[ & k_{I,I,0} \int_{2mT_c+\hat{\tau}_1}^{(m+1)2T_c} \cos(\phi_p) + \cos(2w_p t - \phi_p) dt + \\
& k_{I,I,1} \int_{2mT_c}^{2mT_c+\hat{\tau}_1} \cos(\phi_p) + \cos(2w_p t - \phi_p) dt \Bigg], \\
= \frac{1}{4}\cos(\phi_{c_1}) \sum_{m=0}^{15} \Bigg[ & k_{I,I,0} \Bigg( \cos(\phi_p)(2T_c - \hat{\tau}_1) + \int_{2mT_c+\hat{\tau}_1}^{(m+1)2T_c} \Big( \cos(2w_p t)\cos(\phi_p) + \\
& \sin(2w_p t)\sin(\phi_p) \Big) \Bigg) + k_{I,I,1} \Bigg( \cos(\phi_p)(\hat{\tau}_1) + \int_{2mT_c}^{2mT_c+\hat{\tau}_1} \Big( \cos(2w_p t). \\
& \cos(\phi_p) + \sin(2w_p t)\sin(\phi_p) \Big) \Bigg) \Bigg] = \\
= \frac{1}{4}\cos(\phi_{c_1}) \sum_{m=0}^{15} \Bigg[ & k_{I,I,0} \Bigg( \cos(\phi_p)(2T_c - \hat{\tau}_1) + \frac{\cos(\phi_p)}{2w_p} \sin(2w_p t) \Big|_{2mT_c+\hat{\tau}_1}^{(m+1)2T_c} - \\
& - \frac{\sin(\phi_p)}{2w_p} \cos(2w_p t) \Big|_{2mT_c+\hat{\tau}_1}^{(m+1)2T_c} \Bigg) + k_{I,I,1} \Bigg( \cos(\phi_p)(\hat{\tau}_1) + \\
& \frac{\cos(\phi_p)}{2w_p} \sin(2w_p t) \Big|_{2mT_c}^{2mT_c+\hat{\tau}_1} - \frac{\sin(\phi_p)}{2w_p} \cos(2w_p t) \Big|_{2mT_c}^{2mT_c+\hat{\tau}_1} \Bigg) \Bigg] = \\
= \frac{1}{4}\cos(\phi_{c_1}) \Bigg[ & k_{I,I,0} \Bigg( \cos(\phi_p)(2T_c - \hat{\tau}_1) + \frac{\cos(\phi_p)}{2w_p}(-\sin(2\phi_p)) - \\
& - \frac{\sin(\phi_p)}{2w_p}(1 - \cos(2\phi_p)) \Bigg) + k_{I,I,1} \Bigg( \cos(\phi_p)(\hat{\tau}_1) + \\
& \frac{\cos(\phi_p)}{2w_p}(\sin(2\phi_p)) + \frac{\sin(\phi_p)}{2w_p}(1 - \cos(2\phi_p)) \Bigg) \Bigg] = \\
= \frac{1}{4}\cos(\phi_{c_1}) \Bigg[ & \cos(\phi_p) \Big( k_{I,I,0}(2T_c - \hat{\tau}_1) + k_{I,I,1}(\hat{\tau}_1) \Big) + \frac{\sin(\phi_p)}{w_p} \Big( - k_{I,I,0} + k_{I,I,1} \Big) \Bigg]
\end{aligned}
\tag{A.12}
$$

The second part of 3.43 is B1

$$
\begin{aligned}
B_1 &= \frac{1}{2}\sin(\phi_{c_1})\sum_{m=0}^{15}\Bigg[k_{I,Q,0}\int_{(2m+1)T_c+\hat{\tau}_1}^{(m+1)2T_c}\sin(w_pt-\phi_p)\cos(w_pt)dt+ \\
&\qquad + k_{I,Q,1}\int_{2mT_c}^{(2m+1)T_c+\hat{\tau}_1}\sin(w_pt-\phi_p)\cos(w_pt)dt\Bigg], \\
&= \frac{1}{4}\sin(\phi_{c_1})\sum_{m=0}^{15}\Bigg[k_{I,Q,0}\int_{(2m+1)T_c+\hat{\tau}_1}^{(m+1)2T_c}\sin(-\phi_p)+\sin(2w_pt-\phi_p)dt+ \\
&\qquad k_{I,Q,1}\int_{2mT_c}^{(2m+1)T_c+\hat{\tau}_1}\sin(-\phi_p)+\sin(2w_pt-\phi_p)dt\Bigg], \\
&= \frac{1}{4}\sin(\phi_{c_1})\sum_{m=0}^{15}\Bigg[k_{I,Q,0}\Bigg(-\sin(\phi_p)(T_c-\hat{\tau}_1)+\int_{(2m+1)T_c+\hat{\tau}_1}^{(m+1)2T_c}\Big(\sin(2w_pt)\cos(\phi_p)- \\
&\qquad \cos(2w_pt)\sin(\phi_p)\Big)\Bigg)+k_{I,Q,1}\Bigg(-\sin(\phi_p)(T_c+\hat{\tau}_1)+ \\
&\qquad +\int_{2mT_c}^{(2m+1)T_c+\hat{\tau}_1}\Big(\sin(2w_pt)\cos(\phi_p)-\cos(2w_pt)\sin(\phi_p)\Big)\Bigg)\Bigg]= \\
&= \frac{1}{4}\sin(\phi_{c_1})\sum_{m=0}^{15}\Bigg[k_{I,Q,0}\Bigg(-\sin(\phi_p)(T_c-\hat{\tau}_1)+\frac{-\cos(\phi_p)}{2w_p}(\cos(2w_pt))\Big|_{(2m+1)T_c+\hat{\tau}_1}^{(m+1)2T_c}- \\
&\qquad -\frac{\sin(\phi_p)}{2w_p}\sin(2w_pt)\Big|_{(2m+1)T_c+\hat{\tau}_1}^{(m+1)2T_c}\Bigg)+k_{I,Q,1}\Bigg(-\sin(\phi_p)(T_c+\hat{\tau}_1)+ \\
&\qquad \frac{-\cos(\phi_p)}{2w_p}\cos(2w_pt)\Big|_{2mT_c}^{(2m+1)T_c+\hat{\tau}_1}-\frac{\sin(\phi_p)}{2w_p}\sin(2w_pt)\Big|_{2mT_c}^{(2m+1)T_c+\hat{\tau}_1}\Bigg)\Bigg]= \\
&= \frac{1}{4}\sin(\phi_{c_1})\Bigg[k_{I,Q,0}\Bigg(-\sin(\phi_p)(T_c-\hat{\tau}_1)+\frac{-\cos(\phi_p)}{2w_p}(1+\cos(2\phi_p))- \\
&\qquad -\frac{\sin(\phi_p)}{2w_p}(\sin(2\phi_p))\Bigg)+k_{I,Q,1}\Bigg(-\sin(\phi_p)(T_c+\hat{\tau}_1)+ \\
&\qquad \frac{-\cos(\phi_p)}{2w_p}(-\cos(2\phi_p)-1)-\frac{\sin(\phi_p)}{2w_p}(-\sin(2\phi_p))\Bigg)\Bigg]= \\
&= \frac{1}{4}\sin(\phi_{c_1})\Bigg[-\sin(\phi_p)\Big(k_{I,Q,0}(T_c-\hat{\tau}_1)+k_{I,Q,1}(T_c+\hat{\tau}_1)\Big)+ \\
&\qquad +\frac{\cos(\phi_p)}{w_p}\Big(-k_{I,Q,0}+k_{I,Q,1}\Big)\Bigg],
\end{aligned}
$$

The quadrature component of the interferer's received signal 3.61 can be written as $Y_{Q,1,\ell}/n_{\tau_1} = \frac{2}{T_c}\,\hat{c}_{1,t}(C_1 - D_1)$. Now starting with the $C_1$ and after performing the previous steps i.e. filtering out $2w_ct$, applying the stochastic analysis and using trigonometric analysis we get

$$C_1 = \frac{-1}{2}\sin(\phi_{c_1})\sum_{m=0}^{15}\Bigg[k_{Q,I,0}\int_{(2m+1)T_c}^{(m+1)2T_c+\hat{\tau}_1}\sin(w_pt)\cos(w_pt-\phi_p)dt+ \\ + k_{Q,I,-1}\int_{(m+1)2T_c+\hat{\tau}_1}^{(2m+3)T_c}\sin(w_pt)\cos(w_pt-\phi_p)dt\Bigg],$$

$$= \frac{-1}{4}\sin(\phi_{c_1})\sum_{m=0}^{15}\Bigg[k_{Q,I,0}\int_{(2m+1)T_c}^{(m+1)2T_c+\hat{\tau}_1}\sin(\phi_p)+\sin(2w_pt-\phi_p)dt+ \\ k_{Q,I,-1}\int_{(m+1)2T_c+\hat{\tau}_1}^{(2m+3)T_c}\sin(\phi_p)+\sin(2w_pt-\phi_p)dt\Bigg],$$

$$= \frac{-1}{4}\sin(\phi_{c_1})\sum_{m=0}^{15}\Bigg[k_{Q,I,0}\Bigg(\sin(\phi_p)(T_c+\hat{\tau}_1)+\int_{(2m+1)T_c}^{(m+1)2T_c+\hat{\tau}_1}\Big(\sin(2w_pt)\cos(\phi_p)- \\ \cos(2w_pt)\sin(\phi_p)\Big)\Bigg)+k_{Q,I,-1}\Bigg(\sin(\phi_p)(T_c-\hat{\tau}_1)+ \\ +\int_{(m+1)2T_c+\hat{\tau}_1}^{(2m+3)T_c}\Big(\sin(2w_pt)\cos(\phi_p)-\cos(2w_pt)\sin(\phi_p)\Big)\Bigg)\Bigg]=$$

$$= \frac{-1}{4}\sin(\phi_{c_1})\sum_{m=0}^{15}\Bigg[k_{Q,I,0}\Bigg(\sin(\phi_p)(T_c+\hat{\tau}_1)+\frac{-\cos(\phi_p)}{2w_p}(\cos(2w_pt))\Big|_{(2m+1)T_c}^{(m+1)2T_c+\hat{\tau}_1}- \\ -\frac{\sin(\phi_p)}{2w_p}\sin(2w_pt)\Big|_{(2m+1)T_c}^{(m+1)2T_c+\hat{\tau}_1}\Bigg)+k_{Q,I,-1}\Bigg(\sin(\phi_p)(T_c-\hat{\tau}_1)+ \\ \frac{-\cos(\phi_p)}{2w_p}\cos(2w_pt)\Big|_{(m+1)2T_c+\hat{\tau}_1}^{(2m+3)T_c}-\frac{\sin(\phi_p)}{2w_p}\sin(2w_pt)\Big|_{(m+1)2T_c+\hat{\tau}_1}^{(2m+3)T_c}\Bigg)\Bigg]=$$

$$= \frac{-1}{4}\sin(\phi_{c_1})\Bigg[k_{Q,I,0}\Bigg(\sin(\phi_p)(T_c+\hat{\tau}_1)+\frac{-\cos(\phi_p)}{2w_p}(1+\cos(2\phi_p))- \\ -\frac{\sin(\phi_p)}{2w_p}(\sin(2\phi_p))\Bigg)+k_{Q,I,-1}\Bigg(\sin(\phi_p)(T_c-\hat{\tau}_1)- \\ \frac{-\cos(\phi_p)}{2w_p}(-1-\cos(2\phi_p))-\frac{\sin(\phi_p)}{2w_p}(-\sin(2\phi_p))\Bigg)\Bigg]=$$

$$= \frac{-1}{4}\sin(\phi_{c_1})\Bigg[\sin(\phi_p)\Big(k_{Q,I,-1}(T_c-\hat{\tau}_1)+k_{Q,I,0}(T_c+\hat{\tau}_1)\Big)+ \\ + \frac{\cos(\phi_p)}{w_p}\Big(k_{Q,I,-1}-k_{Q,I,0}\Big)\Bigg], \tag{A.13}$$

The second part of 3.61 is $D_1$ and the proof of equation 3.65

$$D_1 = \frac{1}{2}\cos(\phi_{c_1})\sum_{m=0}^{15}\Bigg[k_{Q,Q,0}\int_{(2m+1)T_c+\hat{\tau}_1}^{(2m+3)T_c}\sin(w_pt)\sin(w_pt-\phi_p)dt+ \\ k_{Q,Q,1}\int_{(2m+1)T_c}^{(2m+1)T_c+\hat{\tau}_1}\sin(w_pt)\sin(w_pt-\phi_p)dt\Bigg],$$

$$= \frac{1}{4}\cos(\phi_{c_1})\sum_{m=0}^{15}\Bigg[k_{Q,Q,0}\int_{(2m+1)T_c+\hat{\tau}_1}^{(2m+3)T_c}\Big(\cos(-\phi_p)-\cos(2w_pt-\phi_p)\Big)dt+ \\ k_{Q,Q,1}\int_{(2m+1)T_c}^{(2m+1)T_c+\hat{\tau}_1}\Big(\cos(-\phi_p)-\cos(2w_pt-\phi_p)\Big)dt\Bigg] =$$

$$= \frac{1}{4}\cos(\phi_{c_1})\sum_{m=0}^{15}\Bigg[k_{Q,Q,0}\Bigg(\cos(\phi_p)(2T_c-\hat{\tau}_1)-\int_{(2m+1)T_c+\hat{\tau}_1}^{(2m+3)T_c}\Big(\cos(2w_pt)\cos(\phi_p)+ \\ \sin(2w_pt)\sin(\phi_p)\Big)dt\Bigg)+k_{Q,Q,1}\Bigg(\cos(\phi_p)(\hat{\tau}_1)-\int_{(2m+1)T_c}^{(2m+1)T_c+\hat{\tau}_1}\Big(\cos(2w_pt). \\ \cos(\phi_p)+\sin(2w_pt)\sin(\phi_p)\Big)dt\Bigg)\Bigg] =$$

$$= \frac{1}{4}\cos(\phi_{c_1})\sum_{m=0}^{15}\Bigg[k_{Q,Q,0}\Bigg(\cos(\phi_p)(2T_c-\hat{\tau}_1)-\frac{\cos(\phi_p)}{2w_p}\sin(2w_pt)\Big|_{(2m+1)T_c+\hat{\tau}_1}^{(2m+3)T_c}- \\ -\frac{\Big(-\sin(\phi_p)\Big)}{2w_p}\cos(2w_pt)\Big|_{(2m+1)T_c+\hat{\tau}_1}^{(2m+3)T_c}\Bigg)+k_{Q,Q,1}\Bigg(\cos(\phi_p)(\hat{\tau}_1)- \\ -\frac{\cos(\phi_p)}{2w_p}\sin(2w_pt)\Big|_{(2m+1)T_c}^{(2m+1)T_c+\hat{\tau}_1}-\frac{\Big(-\sin(\phi_p)\Big)}{2w_p}\cos(2w_pt)\Big|_{(2m+1)T_c}^{(2m+1)T_c+\hat{\tau}_1}\Bigg)\Bigg] =$$

$$= \frac{1}{4}\cos(\phi_{c_1})\Bigg[k_{Q,Q,0}\Bigg(\cos(\phi_p)(2T_c-\hat{\tau}_1)-\frac{\cos(\phi_p)}{2w_p}(\sin(2\phi_p))- \\ -\frac{\sin(\phi_p)}{2w_p}(1-\cos(2\phi_p))\Bigg)+k_{Q,Q,1}\Bigg(\cos(\phi_p)(\hat{\tau}_1)- \\ -\frac{\cos(\phi_p)}{2w_p}(-\sin(2\phi_p))+\frac{\sin(\phi_p)}{2w_p}(1-\cos(2\phi_p))\Bigg)\Bigg] =$$

$$= \frac{1}{4}\cos(\phi_{c_1})\Bigg[\cos(\phi_p)\Big(k_{Q,Q,0}(2T_c-\hat{\tau}_1)+k_{Q,Q,1}(\hat{\tau}_1)\Big)+\frac{\sin(\phi_p)}{w_p}\Big(-k_{Q,Q,0}+k_{Q,Q,1}\Big)\Bigg] \tag{A.14}$$

**2-** $T_c < \hat{\tau}_1 < 2T_c$**:** The inphase a quadrature components are respectively $Y_{I,1,\ell}/n_{\tau_1} = \frac{2}{T_c}\hat{c}_{1,t}(A_2-B_2)$, $Y_{Q,1,\ell}/n_{\tau_1} = \frac{2}{T_c}\hat{c}_{1,t}(C_2-D_2)$. $A_2, D_2$ have the same structure of $A_1, D_1$. We derive $B_2, C_2$ as follows. After we filter out $2w_ct$, applying the stochastic analysis and the trigonometric analysis we get

$$\begin{aligned}
B_2 &= \frac{1}{2}\sin(\phi_{c_1})\sum_{m=0}^{15}\Bigg[k_{I,Q,1}\int_{(2m-1)T_c+\hat{\tau}_1}^{(m+1)2T_c}\sin(w_pt-\phi_p)\cos(w_pt)dt+\\
&\qquad + k_{I,Q,2}\int_{2mT_c}^{(2m-1)T_c+\hat{\tau}_1}\sin(w_pt-\phi_p)\cos(w_pt)dt\Bigg],\\
&= \frac{1}{4}\sin(\phi_{c_1})\sum_{m=0}^{15}\Bigg[k_{I,Q,1}\int_{(2m-1)T_c+\hat{\tau}_1}^{(m+1)2T_c}\sin(-\phi_p)+\sin(2w_pt-\phi_p)dt+\\
&\qquad k_{I,Q,2}\int_{2mT_c}^{(2m-1)T_c+\hat{\tau}_1}\sin(-\phi_p)+\sin(2w_pt-\phi_p)dt\Bigg],\\
&= \frac{1}{4}\sin(\phi_{c_1})\sum_{m=0}^{15}\Bigg[k_{I,Q,1}\Bigg(-\sin(\phi_p)(3T_c-\hat{\tau}_1)+\int_{(2m-1)T_c+\hat{\tau}_1}^{(m+1)2T_c}\Big(\sin(2w_pt)\cos(\phi_p)-\\
&\qquad \cos(2w_pt)\sin(\phi_p)\Big)\Bigg)+k_{I,Q,2}\Bigg(-\sin(\phi_p)(-T_c+\hat{\tau}_1)+\\
&\qquad +\int_{2mT_c}^{(2m-1)T_c+\hat{\tau}_1}\Big(\sin(2w_pt)\cos(\phi_p)-\cos(2w_pt)\sin(\phi_p)\Big)\Bigg)\Bigg]=\\
&= \frac{1}{4}\sin(\phi_{c_1})\sum_{m=0}^{15}\Bigg[k_{I,Q,1}\Bigg(-\sin(\phi_p)(3T_c-\hat{\tau}_1)+\frac{-\cos(\phi_p)}{2w_p}(\cos(2w_pt))\Big|_{(2m-1)T_c+\hat{\tau}_1}^{(m+1)2T_c}-\\
&\qquad -\frac{\sin(\phi_p)}{2w_p}\sin(2w_pt)\Big|_{(2m-1)T_c+\hat{\tau}_1}^{(m+1)2T_c}\Bigg)+k_{I,Q,2}\Bigg(-\sin(\phi_p)(-T_c+\hat{\tau}_1)+\\
&\qquad \frac{-\cos(\phi_p)}{2w_p}\cos(2w_pt)\Big|_{2mT_c}^{(2m-1)T_c+\hat{\tau}_1}-\frac{\sin(\phi_p)}{2w_p}\sin(2w_pt)\Big|_{2mT_c}^{(2m-1)T_c+\hat{\tau}_1}\Bigg)\Bigg]=
\end{aligned}$$

$$= \frac{1}{4}\sin(\phi_{c_1})\Bigg[k_{I,Q,1}\Bigg( -\sin(\phi_p)(3T_c-\hat{\tau}_1)+\frac{-\cos(\phi_p)}{2w_p}(1+\cos(2\phi_p))- \\ -\frac{\sin(\phi_p)}{2w_p}(\sin(2\phi_p))\Bigg)+k_{I,Q,2}\Bigg(-\sin(\phi_p)(-T_c+\hat{\tau}_1)+ \\ \frac{-\cos(\phi_p)}{2w_p}(-\cos(2\phi_p)-1)-\frac{\sin(\phi_p)}{2w_p}(-\sin(2\phi_p))\Bigg)\Bigg]= \tag{A.15}$$

$$= \frac{1}{4}\sin(\phi_{c_1})\Bigg[-\sin(\phi_p)\Big(k_{I,Q,1}(3T_c-\hat{\tau}_1)+k_{I,Q,2}(-T_c+\hat{\tau}_1)\Big)+ \\ +\frac{\cos(\phi_p)}{w_p}\Big(-k_{I,Q,1}+k_{I,Q,2}\Big)\Bigg],$$

$$C_2 = \frac{-1}{2}\sin(\phi_{c_1})\sum_{m=0}^{15}\Bigg[k_{Q,I,0}\int_{2mT_c+\hat{\tau}_1}^{(2m+3)T_c}\sin(w_pt)\cos(w_pt-\phi_p)dt+ \\ +k_{Q,I,1}\int_{(2m+1)T_c}^{2mT_c+\hat{\tau}_1}\sin(w_pt)\cos(w_pt-\phi_p)dt\Bigg],$$

$$= \frac{-1}{4}\sin(\phi_{c_1})\sum_{m=0}^{15}\Bigg[k_{Q,I,0}\int_{2mT_c+\hat{\tau}_1}^{(2m+3)T_c}\sin(\phi_p)+\sin(2w_pt-\phi_p)dt+ \\ k_{Q,I,1}\int_{(2m+1)T_c}^{2mT_c+\hat{\tau}_1}\sin(\phi_p)+\sin(2w_pt-\phi_p)dt\Bigg],$$

$$= \frac{-1}{4}\sin(\phi_{c_1})\sum_{m=0}^{15}\Bigg[k_{Q,I,0}\Bigg(\sin(\phi_p)(3T_c-\hat{\tau}_1)+\int_{2mT_c+\hat{\tau}_1}^{(2m+3)T_c}\Big(\sin(2w_pt)\cos(\phi_p)- \\ \cos(2w_pt)\sin(\phi_p)\Big)dt\Bigg)+k_{Q,I,1}\Bigg(\sin(\phi_p)(-T_c+\hat{\tau}_1)+ \\ +\int_{(2m+1)T_c}^{2mT_c+\hat{\tau}_1}\Big(\sin(2w_pt)\cos(\phi_p)-\cos(2w_pt)\sin(\phi_p)\Big)dt\Bigg)\Bigg]=$$

$$= \frac{-1}{4}\sin(\phi_{c_1})\sum_{m=0}^{15}\Bigg[k_{Q,I,0}\Bigg(\sin(\phi_p)(3T_c-\hat{\tau}_1)+\frac{-\cos(\phi_p)}{2w_p}(\cos(2w_pt))\Big|_{2mT_c+\hat{\tau}_1}^{(2m+3)T_c}- \\ -\frac{\sin(\phi_p)}{2w_p}\sin(2w_pt)\Big|_{2mT_c+\hat{\tau}_1}^{(2m+3)T_c}\Bigg)+k_{Q,I,1}\Bigg(\sin(\phi_p)(-T_c+\hat{\tau}_1)+ \\ \frac{-\cos(\phi_p)}{2w_p}\cos(2w_pt)\Big|_{(2m+1)T_c}^{2mT_c+\hat{\tau}_1}-\frac{\sin(\phi_p)}{2w_p}\sin(2w_pt)\Big|_{(2m+1)T_c}^{2mT_c+\hat{\tau}_1}\Bigg)\Bigg]=$$

$$= \frac{-1}{4}\sin(\phi_{c_1})\Bigg[k_{Q,I,0}\Bigg(\sin(\phi_p)(3T_c-\hat{\tau}_1)+\frac{-\cos(\phi_p)}{2w_p}(-1-\cos(2\phi_p))- \\ -\frac{\sin(\phi_p)}{2w_p}(-\sin(2\phi_p))\Bigg)+k_{Q,I,1}\Bigg(\sin(\phi_p)(-T_c+\hat{\tau}_1)+ \\ \frac{-\cos(\phi_p)}{2w_p}(1+\cos(2\phi_p))-\frac{\sin(\phi_p)}{2w_p}(\sin(2\phi_p))\Bigg)\Bigg]= \tag{A.16}$$

$$= \frac{-1}{4}\sin(\phi_{c_1})\Bigg[\sin(\phi_p)\Big(k_{Q,I,0}(3T_c-\hat{\tau}_1)+k_{Q,I,}(-T_c+\hat{\tau}_1)\Big)+ \\ +\ \frac{\cos(\phi_p)}{w_p}\Big(k_{Q,I,0}-k_{Q,I,1}\Big)\Bigg],$$

## 3- $\hat{\tau}_1 = T_c$:

In this case $Y_{I,1,\ell}/n_{\tau_1} = \frac{2}{T_c}\,\hat{c}_{1,t}(A_3-B_3)$, $Y_{Q,1,\ell}/n_{\tau_1} = \frac{2}{T_c}\,\hat{c}_{1,t}(C_3-D_3)$. We follow the same approach to derive $A_3, B_3, C_3, D_3$.

$$A_3 = \frac{1}{4}\cos(\phi_{c_1})\sum_{m=0}^{15}\Bigg[k_{I,I,0}\int_{(2m+1)T_c}^{(m+1)2T_c}\cos(\phi_p)+\cos(2w_pt-\phi_p)dt+ \\ k_{I,I,1}\int_{2mT_c}^{(2m+1)T_c}\cos(\phi_p)+\cos(2w_pt-\phi_p)dt\Bigg],$$

$$= \frac{1}{4}\cos(\phi_{c_1})\sum_{m=0}^{15}\Bigg[k_{I,I,0}\Bigg(\cos(\phi_p)T_c+\int_{(2m+1)T_c}^{(m+1)2T_c}\Big(\cos(2w_pt)\cos(\phi_p)+ \\ \sin(2w_pt)\sin(\phi_p)\Big)\Bigg)+k_{I,I,1}\Bigg(\cos(\phi_p)\,T_c+\int_{2mT_c}^{(2m+1)T_c}\Big(\cos(2w_pt)\cdot \\ \cos(\phi_p)+\sin(2w_pt)\sin(\phi_p)\Big)\Bigg)\Bigg]=$$

$$= \frac{1}{4}\cos(\phi_{c_1})\sum_{m=0}^{15}\Bigg[k_{I,I,0}\Bigg(\cos(\phi_p)T_c+\frac{\cos(\phi_p)}{2w_p}\sin(2w_pt)\Big|_{(2m+1)T_c}^{(m+1)2T_c}- \\ -\frac{\sin(\phi_p)}{2w_p}\cos(2w_pt)\Big|_{(2m+1)T_c}^{(m+1)2T_c}\Bigg)+k_{I,I,1}\Bigg(\cos(\phi_p)\,T_c+ \\ \frac{\cos(\phi_p)}{2w_p}\sin(2w_pt)\Big|_{2mT_c}^{(2m+1)T_c}-\frac{\sin(\phi_p)}{2w_p}\cos(2w_pt)\Big|_{2mT_c}^{(2m+1)T_c}\Bigg)\Bigg]=$$

$$
\begin{aligned}
&= \frac{1}{4}\cos(\phi_{c_1})\Bigg[k_{I,I,0}\Bigg(\cos(\phi_p)\,T_c + \frac{\cos(\phi_p)}{2w_p}(0) - \\
&\qquad - \frac{\sin(\phi_p)}{2w_p}(1+1)\Bigg) + k_{I,I,1}\Bigg(\cos(\phi_p)\,T_c + \\
&\qquad \frac{\cos(\phi_p)}{2w_p}(0) - \frac{\sin(\phi_p)}{2w_p}(-1-1)\Bigg)\Bigg] = \\
&= \frac{1}{4}\cos(\phi_{c_1})\Bigg[\cos(\phi_p)\,T_c\Big(k_{I,I,0} + k_{I,I,1}\Big) + \frac{\sin(\phi_p)}{w_p}\Big(-k_{I,I,0} + k_{I,I,1}\Big)\Bigg]
\end{aligned}
\tag{A.17}
$$

$$
\begin{aligned}
B_3 &= \frac{1}{2}\sin(\phi_{c_1})\sum_{m=0}^{15}\Bigg[k_{I,Q,1}\int_{2mT_c}^{(m+1)2T_c}\sin(w_p t - \phi_p)\cos(w_p t)dt\Bigg] = \\
&= \frac{1}{4}\sin(\phi_{c_1})\sum_{m=0}^{15}\Bigg[k_{I,Q,1}\int_{2mT_c}^{(m+1)2T_c}\sin(-\phi_p) + \sin(2w_p t - \phi_p)dt\Bigg] = \\
&= \frac{1}{4}\sin(\phi_{c_1})\sum_{m=0}^{15}\Bigg[k_{I,Q,1}\Bigg(-\sin(\phi_p)2T_c + \int_{2mT_c}^{(m+1)2T_c}\Big(\sin(2w_p t)\cos(\phi_p) - \\
&\qquad \cos(2w_p t)\sin(\phi_p)\Big)\Bigg)\Bigg] = \\
&= \frac{1}{4}\sin(\phi_{c_1})\sum_{m=0}^{15}\Bigg[k_{I,Q,1}\Bigg(-\sin(\phi_p)\,2T_c + \frac{-\cos(\phi_p)}{2w_p}(\cos(2w_p t))\Big|_{2mT_c}^{(m+1)2T_c} - \\
&\qquad - \frac{\sin(\phi_p)}{2w_p}\sin(2w_p t)\Big|_{2mT_c}^{(m+1)2T_c}\Bigg)\Bigg] = \\
&= \frac{1}{4}\sin(\phi_{c_1})\Bigg[k_{I,Q,1}\Bigg(-\sin(\phi_p)2\,T_c + \frac{-\cos(\phi_p)}{2w_p}(0) - \frac{\sin(\phi_p)}{2w_p}(0)\Bigg)\Bigg] \\
&= \frac{-T_c}{2}\;k_{I,Q,1}\;\sin(\phi_{c_1})\sin(\phi_p),
\end{aligned}
\tag{A.18}
$$

$$
\begin{aligned}
C_3 &= \frac{-1}{2}\sin(\phi_{c_1})\sum_{m=0}^{15}\left[k_{Q,I,0}\int_{(2m+1)T_c}^{(2m+3)T_c}\sin(w_pt)\cos(w_pt-\phi_p)dt\right] = \\
&= \frac{-1}{4}\sin(\phi_{c_1})\sum_{m=0}^{15}\left[k_{Q,I,0}\int_{(2m+1)T_c}^{(2m+3)T_c}\sin(\phi_p)+\sin(2w_pt-\phi_p)dt\right] = \\
&= \frac{-1}{4}\sin(\phi_{c_1})\sum_{m=0}^{15}\left[k_{Q,I,0}\Bigg(\sin(\phi_p)\,2T_c+\int_{(2m+1)T_c}^{(2m+3)T_c}\Big(\sin(2w_pt)\cos(\phi_p)- \right. \\
&\qquad \left.\cos(2w_pt)\sin(\phi_p)\Big)\Bigg)\right] = \\
&= \frac{-1}{4}\sin(\phi_{c_1})\sum_{m=0}^{15}\left[k_{Q,I,0}\Bigg(\sin(\phi_p)\,2T_c+\frac{-\cos(\phi_p)}{2w_p}(\cos(2w_pt))\Big|_{(2m+1)T_c}^{(2m+3)T_c} \right. \\
&\qquad \left.-\frac{\sin(\phi_p)}{2w_p}\sin(2w_pt)\Big|_{(2m+1)T_c}^{(2m+3)T_c}\Bigg)\right] = \\
&= \frac{-1}{4}\sin(\phi_{c_1})\left[k_{Q,I,0}\left(\sin(\phi_p)2\,T_c+\frac{-\cos(\phi_p)}{2w_p}(0)-\frac{\sin(\phi_p)}{2w_p}(0)\right)\right] = \\
&= \frac{-T_c}{2}\,k_{Q,I,0}\,\sin(\phi_{c_1})\sin(\phi_p),
\end{aligned}
\tag{A.19}
$$

$$
\begin{aligned}
D_3 &= \frac{1}{2}\cos(\phi_{c_1})\sum_{m=0}^{15}\left[k_{Q,Q,0}\int_{(m+1)2T_c}^{(2m+3)T_c}\sin(w_pt)\sin(w_pt-\phi_p)dt+ \right. \\
&\qquad \left. k_{Q,Q,1}\int_{(2m+1)T_c}^{(m+1)2T_c}\sin(w_pt)\sin(w_pt-\phi_p)dt\right], \\
&= \frac{1}{4}\cos(\phi_{c_1})\sum_{m=0}^{15}\left[k_{Q,Q,0}\int_{(m+1)2T_c}^{(2m+3)T_c}\Big(\cos(-\phi_p)-\cos(2w_pt-\phi_p)\Big)dt+ \right. \\
&\qquad \left. k_{Q,Q,1}\int_{(2m+1)T_c}^{(m+1)2T_c}\Big(\cos(-\phi_p)-\cos(2w_pt-\phi_p)\Big)dt\right] = \\
&= \frac{1}{4}\cos(\phi_{c_1})\sum_{m=0}^{15}\left[k_{Q,Q,0}\Bigg(\cos(\phi_p)\,T_c-\int_{(m+1)2T_c}^{(2m+3)T_c}\Big(\cos(2w_pt)\cos(\phi_p)+ \right. \right. \\
&\qquad \left. \sin(2w_pt)\sin(\phi_p)\Big)dt\Bigg)+k_{Q,Q,1}\Bigg(\cos(\phi_p)(T_c)-\int_{(2m+1)T_c}^{(m+1)2T_c}\Big(\cos(2w_pt). \right. \\
&\qquad \left. \left. \cos(\phi_p)+\sin(2w_pt)\sin(\phi_p)\Big)dt\Bigg)\right] =
\end{aligned}
$$

$$
\begin{aligned}
&= \frac{1}{4}\cos(\phi_{c_1})\sum_{m=0}^{15}\Bigg[k_{Q,Q,0}\Bigg(\cos(\phi_p)T_c - \frac{\cos(\phi_p)}{2w_p}\sin(2w_pt)\Big|_{(m+1)2T_c}^{(2m+3)T_c} - \\
&\qquad - \frac{\Big(-\sin(\phi_p)\Big)}{2w_p}\cos(2w_pt)\Big|_{(m+1)2T_c}^{(2m+3)T_c}\Bigg) + k_{Q,Q,1}\Bigg(\cos(\phi_p)\,T_c - \\
&\qquad - \frac{\cos(\phi_p)}{2w_p}\sin(2w_pt)\Big|_{(2m+1)T_c}^{(m+1)2T_c} - \frac{\Big(-\sin(\phi_p)\Big)}{2w_p}\cos(2w_pt)\Big|_{(2m+1)T_c}^{(m+1)2T_c}\Bigg)\Bigg] = \\
&= \frac{1}{4}\cos(\phi_{c_1})\Bigg[k_{Q,Q,0}\Bigg(\cos(\phi_p)\,T_c - \frac{\cos(\phi_p)}{2w_p}(0) + \frac{\sin(\phi_p)}{2w_p}(-1-1)\Bigg) + \\
&\qquad + k_{Q,Q,1}\Bigg(\cos(\phi_p)\,T_c - \frac{\cos(\phi_p)}{2w_p}(0) + \frac{\sin(\phi_p)}{2w_p}(1+1)\Bigg)\Bigg] = \\
&= \frac{1}{4}\cos(\phi_{c_1})\Bigg[\cos(\phi_p)\,T_c\Big(k_{Q,Q,0} + k_{Q,Q,1}\Big) + \frac{\sin(\phi_p)}{w_p}\Big(-k_{Q,Q,0} + k_{Q,Q,1}\Big)\Bigg]
\end{aligned}
\tag{A.20}
$$

## 4- $\hat{\tau}_1 = 2\,T_c$:

In this case $Y_{I,1,\ell}/n_{\tau_1} = \frac{2}{T_c}\,\hat{c}_{1,t}(A_4 - B_4)$, $Y_{Q,1,\ell}/n_{\tau_1} = \frac{2}{T_c}\,\hat{c}_{1,t}(C_4 - D_4)$. We follow the same approach to derive $A_4, B_4, C_4, D_4$.

$$
\begin{aligned}
A_4 &= \frac{1}{4}\cos(\phi_{c_1})\sum_{m=0}^{15}\Bigg[k_{I,I,1}\int_{2mT_c}^{(m+1)2T_c}\cos(\phi_p) + \cos(2w_pt - \phi_p)dt\Bigg] = \\
&= \frac{1}{4}\cos(\phi_{c_1})\sum_{m=0}^{15}\Bigg[k_{I,I,1}\Bigg(\cos(\phi_p)\,2T_c + \int_{2mT_c}^{(m+1)2T_c}\Big(\cos(2w_pt)\cos(\phi_p) + \\
&\qquad \sin(2w_pt)\sin(\phi_p)\Big)dt\Bigg)\Bigg] = \\
&= \frac{1}{4}\cos(\phi_{c_1})\sum_{m=0}^{15}\Bigg[k_{I,I,1}\Bigg(\cos(\phi_p)\,2T_c + \frac{\cos(\phi_p)}{2w_p}\sin(2w_pt)\Big|_{2mT_c}^{(m+1)2T_c} - \\
&\qquad - \frac{\sin(\phi_p)}{2w_p}\cos(2w_pt)\Big|_{2mT_c}^{(m+1)2T_c}\Bigg)\Bigg] = \\
&= \frac{1}{4}\cos(\phi_{c_1})\Bigg[k_{I,I,1}\Bigg(\cos(\phi_p)\,2T_c + \frac{\cos(\phi_p)}{2w_p}(0) - \frac{\sin(\phi_p)}{2w_p}(1-1)\Bigg)\Bigg] = \\
&= \frac{T_c}{2}\,k_{I,I,1}\,\cos(\phi_{c_1})\cos(\phi_p),
\end{aligned}
\tag{A.21}
$$

$$
\begin{aligned}
B_4 = \frac{1}{2}\sin(\phi_{c_1}) \sum_{m=0}^{15} \Bigg[ & k_{I,Q,1} \int_{(2m+1)T_c}^{(m+1)2T_c} \sin(w_p t - \phi_p)\cos(w_p t)dt + \\
& + k_{I,Q,2} \int_{2mT_c}^{(2m+1)T_c} \sin(w_p t - \phi_p)\cos(w_p t)dt \Bigg], \\
= \frac{1}{4}\sin(\phi_{c_1}) \sum_{m=0}^{15} \Bigg[ & k_{I,Q,1} \int_{(2m+1)T_c}^{(m+1)2T_c} \sin(-\phi_p) + \sin(2w_p t - \phi_p)dt + \\
& k_{I,Q,2} \int_{2mT_c}^{(2m+1)T_c} \sin(-\phi_p) + \sin(2w_p t - \phi_p)dt \Bigg], \\
= \frac{1}{4}\sin(\phi_{c_1}) \sum_{m=0}^{15} \Bigg[ & k_{I,Q,1} \Bigg( -\sin(\phi_p)\, T_c + \int_{(2m+1)T_c}^{(m+1)2T_c} \Big( \sin(2w_p t)\cos(\phi_p) - \\
& \cos(2w_p t)\sin(\phi_p) \Big) dt \Bigg) + k_{I,Q,2} \Bigg( -\sin(\phi_p)\, T_c + \\
& + \int_{2mT_c}^{(2m+1)T_c} \Big( \sin(2w_p t)\cos(\phi_p) - \cos(2w_p t)\sin(\phi_p) \Big) dt \Bigg) \Bigg] = \\
= \frac{1}{4}\sin(\phi_{c_1}) \sum_{m=0}^{15} \Bigg[ & k_{I,Q,1} \Bigg( -\sin(\phi_p)\, T_c + \frac{-\cos(\phi_p)}{2w_p} (\cos(2w_p t)) \Big|_{(2m+1)T_c}^{(m+1)2T_c} - \\
& - \frac{\sin(\phi_p)}{2w_p} \sin(2w_p t) \Big|_{(2m+1)T_c}^{(m+1)2T_c} \Bigg) + k_{I,Q,2} \Bigg( -\sin(\phi_p)\, T_c + \\
& \frac{-\cos(\phi_p)}{2w_p} \cos(2w_p t) \Big|_{2mT_c}^{(2m+1)T_c} - \frac{\sin(\phi_p)}{2w_p} \sin(2w_p t) \Big|_{2mT_c}^{(2m+1)T_c} \Bigg) \Bigg] = \\
= \frac{1}{4}\sin(\phi_{c_1}) \Bigg[ & k_{I,Q,1} \Bigg( -\sin(\phi_p)\, T_c + \frac{-\cos(\phi_p)}{2w_p} (1+1) - \\
& - \frac{\sin(\phi_p)}{2w_p} (0) \Bigg) + k_{I,Q,2} \Bigg( -\sin(\phi_p)\, T_c + \\
& \frac{-\cos(\phi_p)}{2w_p} (-1-1) - \frac{\sin(\phi_p)}{2w_p} (0) \Bigg) \Bigg] = \\
= \frac{1}{4}\sin(\phi_{c_1}) \Bigg[ & -\sin(\phi_p)\, T_c \Big( k_{I,Q,1} + k_{I,Q,2} \Big) + \frac{\cos(\phi_p)}{w_p} \Big( -k_{I,Q,1} + k_{I,Q,2} \Big) \Bigg],
\end{aligned}
\tag{A.22}
$$

$$
\begin{aligned}
C_4 = \frac{-1}{2}\sin(\phi_{c_1}) \sum_{m=0}^{15} \Bigg[ & k_{Q,I,0} \int_{(m+1)2T_c}^{(2m+3)T_c} \sin(w_p t)\cos(w_p t - \phi_p)dt + \\
& + k_{Q,I,1} \int_{(2m+1)T_c}^{(m+1)2T_c} \sin(w_p t)\cos(w_p t - \phi_p)dt \Bigg], \\
= \frac{-1}{4}\sin(\phi_{c_1}) \sum_{m=0}^{15} \Bigg[ & k_{Q,I,0} \int_{(m+1)2T_c}^{(2m+3)T_c} \sin(\phi_p) + \sin(2w_p t - \phi_p)dt + \\
& k_{Q,I,1} \int_{(2m+1)T_c}^{(m+1)2T_c} \sin(\phi_p) + \sin(2w_p t - \phi_p)dt \Bigg], \\
= \frac{-1}{4}\sin(\phi_{c_1}) \sum_{m=0}^{15} \Bigg[ & k_{Q,I,0} \Bigg( \sin(\phi_p)\, T_c + \int_{(m+1)2T_c}^{(2m+3)T_c} \Big( \sin(2w_p t)\cos(\phi_p) - \\
& \cos(2w_p t)\sin(\phi_p) \Big) dt \Bigg) + k_{Q,I,1} \Bigg( \sin(\phi_p)\, T_c + \\
& + \int_{(2m+1)T_c}^{(m+1)2T_c} \Big( \sin(2w_p t)\cos(\phi_p) - \cos(2w_p t)\sin(\phi_p) \Big) dt \Bigg) \Bigg] = \\
= \frac{-1}{4}\sin(\phi_{c_1}) \sum_{m=0}^{15} \Bigg[ & k_{Q,I,0} \Bigg( \sin(\phi_p)\, T_c + \frac{-\cos(\phi_p)}{2w_p} (\cos(2w_p t)) \Big|_{(m+1)2T_c}^{(2m+3)T_c} - \\
& - \frac{\sin(\phi_p)}{2w_p} \sin(2w_p t) \Big|_{(m+1)2T_c}^{(2m+3)T_c} \Bigg) + k_{Q,I,1} \Bigg( \sin(\phi_p)\, T_c + \\
& + \frac{-\cos(\phi_p)}{2w_p} \cos(2w_p t) \Big|_{(2m+1)T_c}^{(m+1)2T_c} - \frac{\sin(\phi_p)}{2w_p} \sin(2w_p t) \Big|_{(2m+1)T_c}^{(m+1)2T_c} \Bigg) \Bigg] = \\
= \frac{-1}{4}\sin(\phi_{c_1}) \Bigg[ & k_{Q,I,0} \Bigg( \sin(\phi_p)\, T_c + \frac{-\cos(\phi_p)}{2w_p}(-1-1) - \frac{\sin(\phi_p)}{2w_p}(0) \Bigg) \\
& + k_{Q,I,1} \Bigg( \sin(\phi_p)\, T_c + \frac{-\cos(\phi_p)}{2w_p}(1+1) - \frac{\sin(\phi_p)}{2w_p}(0) \Bigg) \Bigg] = \qquad \text{(A.23)} \\
= \frac{-1}{4}\sin(\phi_{c_1}) \Bigg[ & \sin(\phi_p)\, T_c \Big( k_{Q,I,0} + k_{Q,I,1} \Big) + \frac{\cos(\phi_p)}{w_p} \Big( k_{Q,I,0} - k_{Q,I,1} \Big) \Bigg],
\end{aligned}
$$

$$
\begin{aligned}
D_4 &= \frac{1}{4}\cos(\phi_{c_1})\sum_{m=0}^{15}\left[k_{Q,Q,1}\int_{(2m+1)T_c}^{(2m+3)T_c}\sin(w_p t)\sin(w_p t-\phi_p)dt\right] = \\
&= \frac{1}{4}\cos(\phi_{c_1})\sum_{m=0}^{15}\left[k_{Q,Q,1}\int_{(2m+1)T_c}^{(2m+3)T_c}\cos(\phi_p)-\cos(2w_p t-\phi_p)dt\right] = \\
&= \frac{1}{4}\cos(\phi_{c_1})\sum_{m=0}^{15}\left[k_{Q,Q,1}\left(\cos(\phi_p)\,2T_c-\int_{(2m+1)T_c}^{(2m+3)T_c}\Big(\cos(2w_p t)\cos(\phi_p)+\right.\right. \\
&\qquad\left.\left.\sin(2w_p t)\sin(\phi_p)\Big)dt\right)\right] = \\
&= \frac{1}{4}\cos(\phi_{c_1})\sum_{m=0}^{15}\left[k_{Q,Q,1}\left(\cos(\phi_p)\,2T_c-\frac{\cos(\phi_p)}{2w_p}\sin(2w_p t)\Big|_{(2m+1)T_c}^{(2m+3)T_c}-\right.\right. \\
&\qquad\left.\left.-\frac{\sin(\phi_p)}{2w_p}\cos(2w_p t)\Big|_{(2m+1)T_c}^{(2m+3)T_c}\right)\right] = \\
&= \frac{1}{4}\cos(\phi_{c_1})\left[k_{Q,Q,1}\left(\cos(\phi_p)\,2T_c-\frac{\cos(\phi_p)}{2w_p}(0)-\frac{\sin(\phi_p)}{2w_p}(-1+1)\right)\right] = \\
&= \frac{T_c}{2}\,k_{Q,Q,1}\,\cos(\phi_{c_1})\cos(\phi_p),
\end{aligned}
\tag{A.24}
$$

# The expected value of the random variable $k_{j_0,j_1,n_{\tau_1}}$

To prove equation 3.54 let's have some examples with different $j_0, j_1, n_{\tau_1}$. First of all let's calculate the $E[k_{I,I,0}]$ for example we go back to Table 3.2 and we substitute $\nu_{n_{\tau_1}}(i)), m_{n_{\tau_1}}(i)$ by their values.

$$
\begin{aligned}
E[k_{I,I,0}] &= \sum_i \frac{1}{256}(16-2\nu_{n_{\tau_1}}(i))*m_{n_{\tau_1}}(i) = \frac{1}{256}\Big(\Big(16-2\cdot 6\Big)\cdot 4+ \\
&\quad+\Big(16-2\cdot 12\Big)\cdot 6+\Big(16-2\cdot 0\Big)\cdot 2+\Big(16-2\cdot 8\Big)\cdot 4\Big) = \\
&= \frac{1}{256}\Big(16-48+32+0\Big) = 0
\end{aligned}
\tag{A.25}
$$

$$
\begin{aligned}
E[k_{I,I,1}] = \sum_i \frac{1}{256}(16 - 2\nu_{n_{\tau_1}}(i)) * m_{n_{\tau_1}}(i) = \frac{1}{256}\Bigg( \Big(16 - 2\cdot 5\Big)\cdot\ 16 + \\
+ \Big(16 - 2\cdot 6\Big)\cdot\ 32 + \Big(16 - 2\cdot 7\Big)\cdot\ 48 + \Big(16 - 2\cdot 8\Big)\cdot\ 64 + \\
+ \Big(16 - 2\cdot 9\Big)\cdot\ 48 + \Big(16 - 2\cdot 10\Big)\cdot\ 32 + \Big(16 - 2\cdot 11\Big)\cdot\ 16\Bigg) = \\
= \frac{1}{256}\Big(96 + 128 + 96 + 0 - 96 - 128 - 96\Big) = 0
\end{aligned}
\tag{A.26}
$$

let's assume $j_0 = I$, $j_1 = Q$, $n_{\tau_1} = 5$ so the Hamming distance matrix would be $HD_n(\mathrm{i},\mathrm{j})|5 =$

$$
= \begin{bmatrix}
12 & 10 & 10 & 10 & 10 & 10 & 10 & 12 & 9 & 11 & 11 & 11 & 11 & 11 & 11 & 9 \\
9 & 7 & 7 & 7 & 7 & 7 & 7 & 9 & 6 & 8 & 8 & 8 & 8 & 8 & 8 & 6 \\
10 & 8 & 8 & 8 & 8 & 8 & 8 & 10 & 7 & 9 & 9 & 9 & 9 & 9 & 9 & 7 \\
8 & 6 & 6 & 6 & 6 & 6 & 6 & 8 & 5 & 7 & 7 & 7 & 7 & 7 & 7 & 5 \\
8 & 6 & 6 & 6 & 6 & 6 & 6 & 8 & 5 & 7 & 7 & 7 & 7 & 7 & 7 & 5 \\
8 & 6 & 6 & 6 & 6 & 6 & 6 & 8 & 5 & 7 & 7 & 7 & 7 & 7 & 7 & 5 \\
12 & 10 & 10 & 10 & 10 & 10 & 10 & 12 & 9 & 11 & 11 & 11 & 11 & 11 & 11 & 9 \\
10 & 8 & 8 & 8 & 8 & 8 & 8 & 10 & 7 & 9 & 9 & 9 & 9 & 9 & 9 & 7 \\
7 & 5 & 5 & 5 & 5 & 5 & 5 & 7 & 4 & 6 & 6 & 6 & 6 & 6 & 6 & 4 \\
11 & 9 & 9 & 9 & 9 & 9 & 9 & 11 & 8 & 10 & 10 & 10 & 10 & 10 & 10 & 8 \\
9 & 7 & 7 & 7 & 7 & 7 & 7 & 9 & 6 & 8 & 8 & 8 & 8 & 8 & 8 & 6 \\
11 & 9 & 9 & 9 & 9 & 9 & 9 & 11 & 8 & 10 & 10 & 10 & 10 & 10 & 10 & 8 \\
11 & 9 & 9 & 9 & 9 & 9 & 9 & 11 & 8 & 10 & 10 & 10 & 10 & 10 & 10 & 8 \\
11 & 9 & 9 & 9 & 9 & 9 & 9 & 11 & 8 & 10 & 10 & 10 & 10 & 10 & 10 & 8 \\
7 & 5 & 5 & 5 & 5 & 5 & 5 & 7 & 4 & 6 & 6 & 6 & 6 & 6 & 6 & 4 \\
9 & 7 & 7 & 7 & 7 & 7 & 7 & 9 & 6 & 8 & 8 & 8 & 8 & 8 & 8 & 6
\end{bmatrix}
$$

Therefore, we can write

$$
\begin{aligned}
E[k_{I,Q,5}] = \sum_i \frac{1}{256}(16 - 2\nu_{n_{\tau_1}}(i)) * m_{n_{\tau_1}}(i) = \frac{1}{256}\Bigg( \Big(16 - 2\cdot 5\Big)\cdot\ 18 + \\
+ \Big(16 - 2\cdot 6\Big)\cdot\ 36 + \Big(16 - 2\cdot 7\Big)\cdot\ 44 + \Big(16 - 2\cdot 8\Big)\cdot\ 44 + \Big(16 - 2\cdot 9\Big)\cdot \\
46 + \Big(16 - 2\cdot 10\Big)\cdot\ 40 + \Big(16 - 2\cdot 11\Big)\ + 20\Big(16 - 2\cdot 12\Big)\cdot\ 4\Bigg) = \\
= \frac{1}{256}\Big(108 + 144 + 88 + 0 - 88 - 160 - 120 - 32\Big) = 0
\end{aligned}
\tag{A.27}
$$

And so on for $\forall j_0, j_1, n_{\tau_1}$.

## The expected value of $\cos^2(\phi_{c_1})$ and $\sin^2(\phi_{c_1})$

$$
\begin{aligned}
E[\cos^2(\phi_{c_1})] &= \frac{1}{2\pi}\int_0^{2\pi} \cos^2(\phi_{c_1})\, 1_{[0,2\pi]}\, \phi_{c_1}\, d\phi_{c_1} = \\
&= \frac{1}{2\pi}\int_0^{2\pi} \frac{1}{2} + \frac{1}{2}\cos(2\phi_{c_1}) d\phi_{c_1} = \\
&= \frac{1}{4\pi}\Big(2\pi + \frac{1}{2\phi_{c_1}}\sin(2\phi_{c_1})\Big|_0^{2\pi}\Big) = \frac{1}{2}, \\
E[\sin^2(\phi_{c_1})] &= \frac{1}{2\pi}\int_0^{2\pi} \sin^2(\phi_{c_1})\, 1_{[0,2\pi]}\, \phi_{c_1}\, d\phi_{c_1} = \\
&= \frac{1}{2\pi}\int_0^{2\pi} \frac{1}{2} - \frac{1}{2}\cos(2\phi_{c_1}) d\phi_{c_1} = \\
&= \frac{1}{4\pi}\Big(2\pi - \frac{1}{2\phi_{c_1}}\sin(2\phi_{c_1})\Big|_0^{2\pi}\Big) = \frac{1}{2},
\end{aligned}
$$

## The proof of probability density function of $\psi_i$

Starting from the derived closed form expression of $\psi_i$, equation 4.42 and assuming that $Z_1 = e^{\chi_1(t)}$ we can write $\psi_i$ as a function of $Z_1$ as

$$
\psi_i(t, \phi_{c_1}, n_{\tau_1}, \hat{\tau}_1) = \sqrt{\frac{1 + \frac{\mathrm{B}(\phi_{c_1}, n_{\tau_1}, \hat{\tau}_1)}{D}\, e^{\chi_1(t)}}{a_i \; + \; b_i \cdot \frac{\mathrm{B}(\phi_{c_1}, n_{\tau_1}, \hat{\tau}_1)}{D}\, e^{\chi_1(t)}}} = g(Z_1), \tag{A.28}
$$

We know that $Z_1$ has a log-normal distribution with a zero-mean $\mu_{\chi_1} = 0$ and standard deviation $\sigma_{\chi_1}$ thus, applying the fundamental transformation law of probabilities **cite** we obtain

$$
f\left(\psi_i\right) = \frac{f\left(Z_1\right)}{\left|g^{'}(Z_1)\right|}\Bigg|_{Z_1 = g^{-1}(\psi_i)}, \tag{A.29}
$$

where $|g^{'}(Z_1)|$ is the absolute value of the derivative of $\psi_i$ function, $g^{-1}(\psi_i)$ is the inverse function of $\psi_i$. In other words, we need to get benefit of the know probability density function of $Z_1$ in obtaining the pdf of $\psi_i$. First, we know that the pdf of the log-normal distributed variable $Z_1$ can be expressed as

$$
f\left(Z_1\right) = \frac{1}{Z_1 \sigma_{\chi_1}\sqrt{2\,\pi}} \cdot e^{-\frac{\left(ln(Z_1) - \mu_{\chi_1}\right)^2}{2\,\sigma_{\chi_1}^2}}, \tag{A.30}
$$

The inverse function of $\psi_i$ can be expressed as

$$Z_1 = g^{-1}(\psi_i) = \frac{D}{B}\left(\frac{1 - a_i\psi_i^2}{b_i\psi_i^2 - 1}\right), \tag{A.31}$$

Now we calculate the derivative $g^{'}(Z_1)$ as follows

$$\begin{aligned} g^{'}(Z_1) = \frac{d\,\psi_i}{d\,Z_1} = \frac{d}{dZ1}\left(\frac{1 + \frac{\mathrm{B}(\phi_{c_1}, n_{\tau_1}, \hat{\tau}_1)}{D} Z_1}{a_i \; + \; b_i \cdot \frac{\mathrm{B}(\phi_{c_1}, n_{\tau_1}, \hat{\tau}_1)}{D} eZ_1}\right)^{\frac{1}{2}} = \\ = \frac{1}{2}\left(\frac{1 + \frac{\mathrm{B}(\phi_{c_1}, n_{\tau_1}, \hat{\tau}_1)}{D} Z_1}{a_i \; + \; b_i \cdot \frac{\mathrm{B}(\phi_{c_1}, n_{\tau_1}, \hat{\tau}_1)}{D} Z_1}\right)^{\frac{-1}{2}} \cdot \frac{\frac{B}{D}\,(a_i + b_i\frac{B}{D}\,Z_1) - b_i \cdot \frac{B}{D}(1 + \frac{B}{D}\,Z_1)}{(a_i + b_i\frac{B}{D}\,Z_1)^2} = \\ = \frac{1}{2}\left(\frac{1 + \frac{\mathrm{B}(\phi_{c_1}, n_{\tau_1}, \hat{\tau}_1)}{D} Z_1}{a_i \; + \; b_i \cdot \frac{\mathrm{B}(\phi_{c_1}, n_{\tau_1}, \hat{\tau}_1)}{D} Z_1}\right)^{\frac{-1}{2}} \cdot \frac{B(a_i - b_i)}{D(a_i + b_i\frac{B}{D}\,Z_1)^2}, \end{aligned} \tag{A.32}$$

Therefore, by substituting the values of A.30 and A.32 in A.29 we get

$$f\,(\psi_i) = \frac{e^{-\frac{\left(ln(Z_1) - \mu_{\chi_1}\right)^2}{2\,\sigma_{\chi_1}^2}}}{\sigma_{\chi_1}\sqrt{2\pi}} 2\,\psi_i \cdot \left.\frac{D(a_i + b_i\frac{B}{D}\,Z_1)^2}{B(a_i - b_i)}\right|_{Z_1 = g^{-1}(\psi_i)}, \tag{A.33}$$

After some algebra we get

$$f\,(\psi_i) = \sqrt{\frac{2}{\pi}}\frac{\psi_i\, e^{-\frac{\left(ln\left(\frac{D\cdot(1 - a_i\,\psi_i^2)}{B\cdot(b_i\,\psi_i^2 - 1)}\right) - \mu_{\chi_1}\right)^2}{2\,\sigma_{\chi_1}^2}}}{\sigma_{\chi_1}\left(\frac{1 - a_i\,\psi_i^2}{b_i\,\psi_i^2 - 1}\right)} \cdot \frac{(a_i - b_i)}{(b_i\,\psi_i^2 - 1)^2}, \tag{A.34}$$

and this is the equation 4.43.

Appendix B

# Appendix B

## Used Industrial standards overview

We can identify any Industrial standard as a set of criteria through an industry relating to the standard elaborating and performing operations in its respective fields of production. In other words it is the generally accepted requirements followed by the members of an industry. It provides an orderly and systematic formulation, adoption, or application of standards used in a particular industry or sector of the economy. Industry standards vary from one industry to another.

Industry standards facilitate global as well as domestic competitiveness. It is a crucial tool for developing and meeting industry goals. For Example in the automotive industry, tire sizes and durability must fall within a standardized range. Standardization serves as a quality check for any industry. Since the challenges in analysis and co-design of WNCSs

Table B.1: Differences between short range communication protocols of interest.

| | WirelessHART | ISA-100.11a | IEEE 802.15.4e |
|---|---|---|---|
| Data rates | 250 kbit/s | 250 kbit/s | various, [54] |
| Channel hopping | Time slot based | Time slot based<br>Slow, [123] | Time slot based |
| Modulation | DSSS QPSK | DSSS OQPSK | DSSS OQPSK |
| Frequency | 2.4 GHz | 2.4 GHz | 2.4 GHz |
| Symbols | 16-ary orthogonal | 16-ary orthogonal | 16-ary orthogonal |

are best explained by considering wireless industrial control protocols (WICPs). In our thesis, we focused on short range WICPs. In particular, we focused on WirelessHART, ISA-100.11a, and IEEE 802.15.4e. In this appendix, we will review the most important characteristics of the aforementioned standards used in our analysis. Table B.1 summarizes some differences of the protocols of interest.

# WirelessHART

WirelessHART it is considered to be the first open standard for WSNs specific targeted for industrial automation, [60]. It is an extension of HART communication protocol. WirelessHART network consists of several elements as it is depicted in Figure B.1field devices that could work as sensor or actuators [8]. These devices can route the packets in the network by routers. There might be also mobile devices used by the engineers or workers. Access points which connect the wireless network to the gateway, adapters to link wired HART devices to wireless ones, a security manager that could be established in the gateway device or in a separate form, a redundant gateway which works as a viaduct to the host applications and there might included a single network manager that could be also inside the gateway device or outside. One way of scaling up this network to service more wireless devices and achieving higher data rate by using multiple access points over a single backbone [8] as shown in Figure B.2.

WirelessHART standard is IEC 62591 standard which does several functionalities in five OSI layers as shown in Figure B.3.

Its application layer protocol support publishing at cyclical process data with update period from $(0.1, 0.25, 0.5, 1, 2, 4, 8, 16, 32, 60, 3600)$s [9]. The device publishes the structured data using information service report service. The data is communicated as a structure variable identified by publish command number [13] as reported in Table B.2.

It transmits from $1-8$ variables and requires from 5 to 69 octets. The protocol overhead is between $49-73$ bytes and it is constrained by maximal size of physical service data 127 bytes. The number of octets added by each layer and the payload is illustrated in Figure B.4.

The physical layer specification relies on the standard 802.15.4-2011 [14, p. 151] and they are reported in Table B.3.

Medium Access Control (MAC) layer is based on a centrally managed mesh network Time Division Multiple Access (TDMA) and channel hopping providing collision free de-

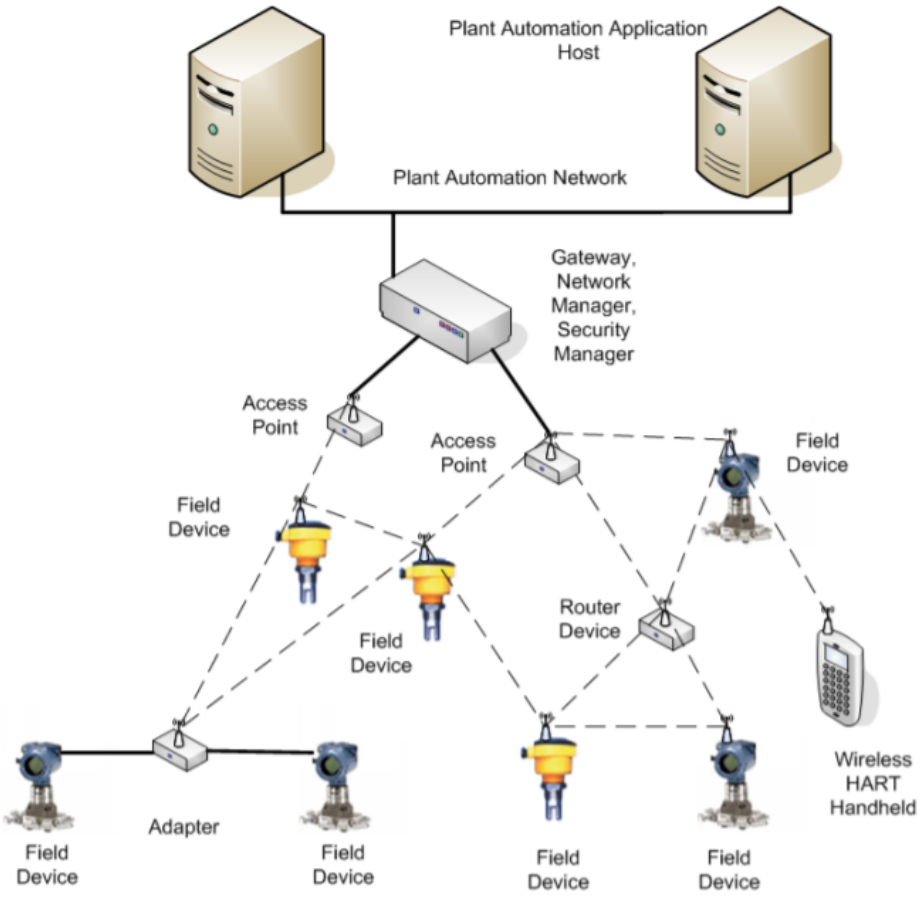


Figure B.1: WirelessHART architecture [8].

Table B.2: Published command numbers of the variables [13, p. 37].

| Command Number | Device Application Services | Number of Variables | Number of Octets |
|---|---|---|---|
| 1 | Read primary variable | 1 | 5 |
| 2 | Read loop current and percent of range | 2 | 8 |
| 3 | Read dynamic variables and loop current | 2-5 | 9, 14, 19, 24 |
| 9 | Read device variables with status | 1-8 | 13, 21, 29, ..., 69 |
| 48 | Read additional device status | Device Status | 4, 9 - 20 |

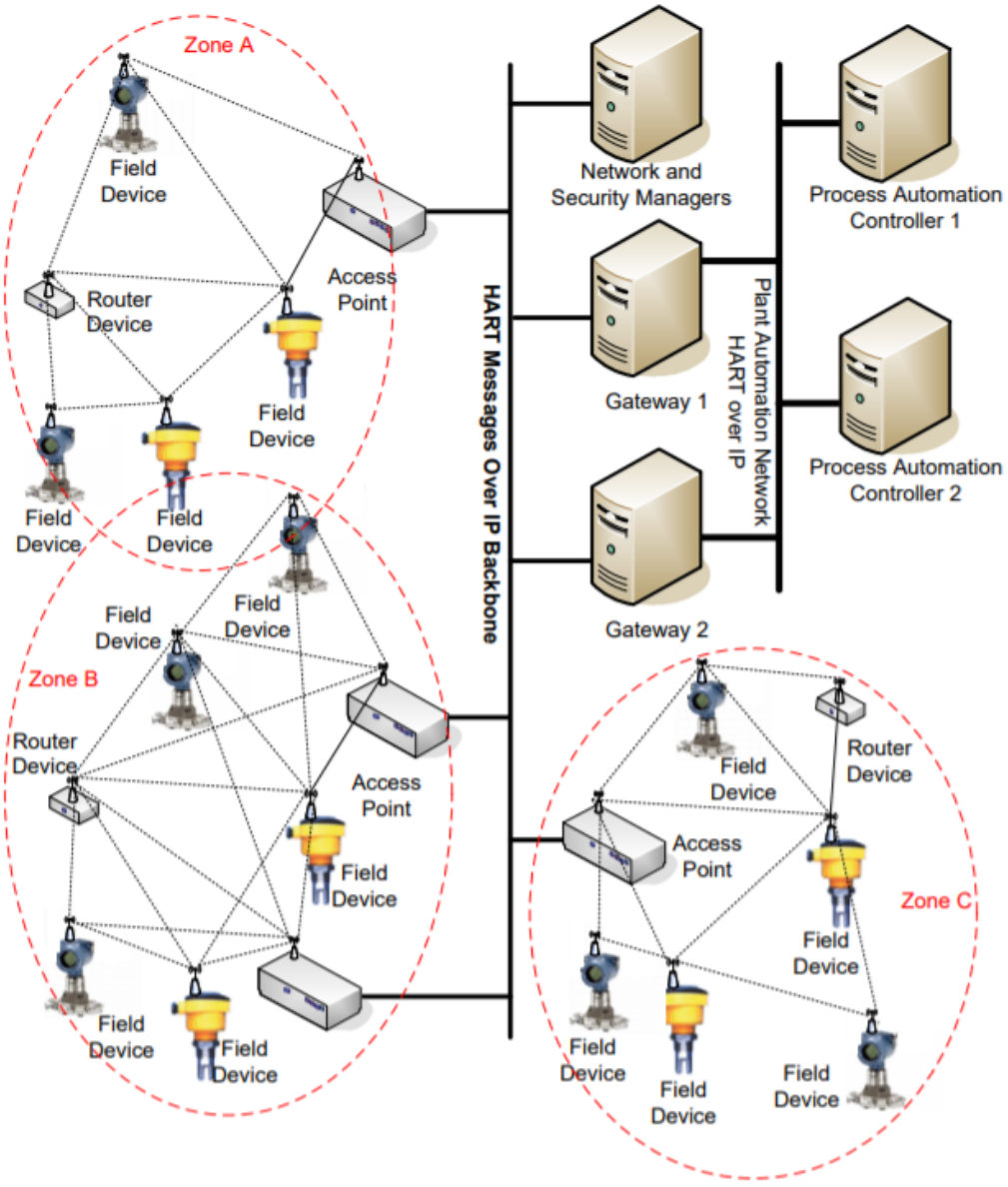


Figure B.2: Utilizing a single backbone to connect multiple access points [8].

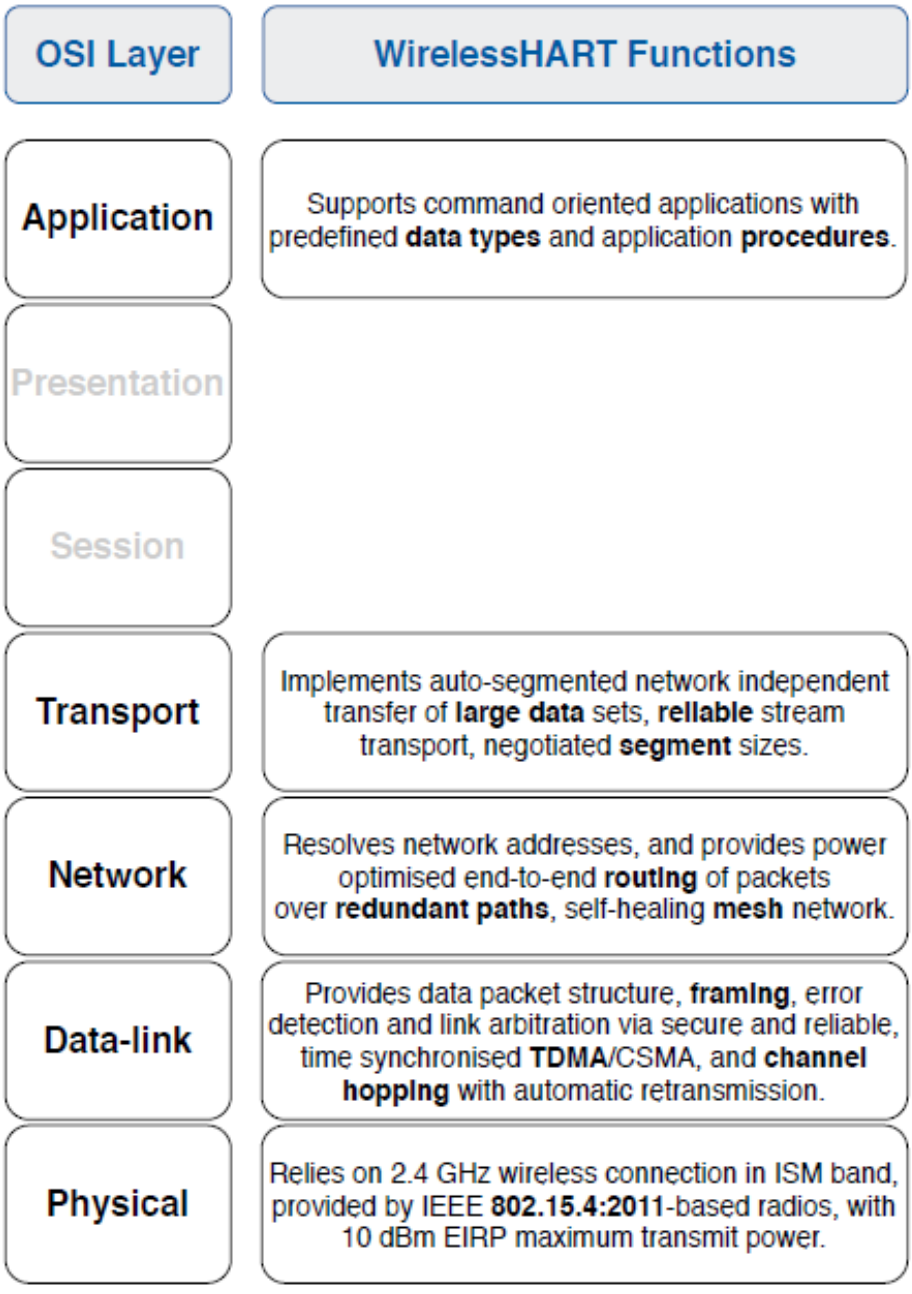


Figure B.3: The function of OSI layers of WirelessHART [9].

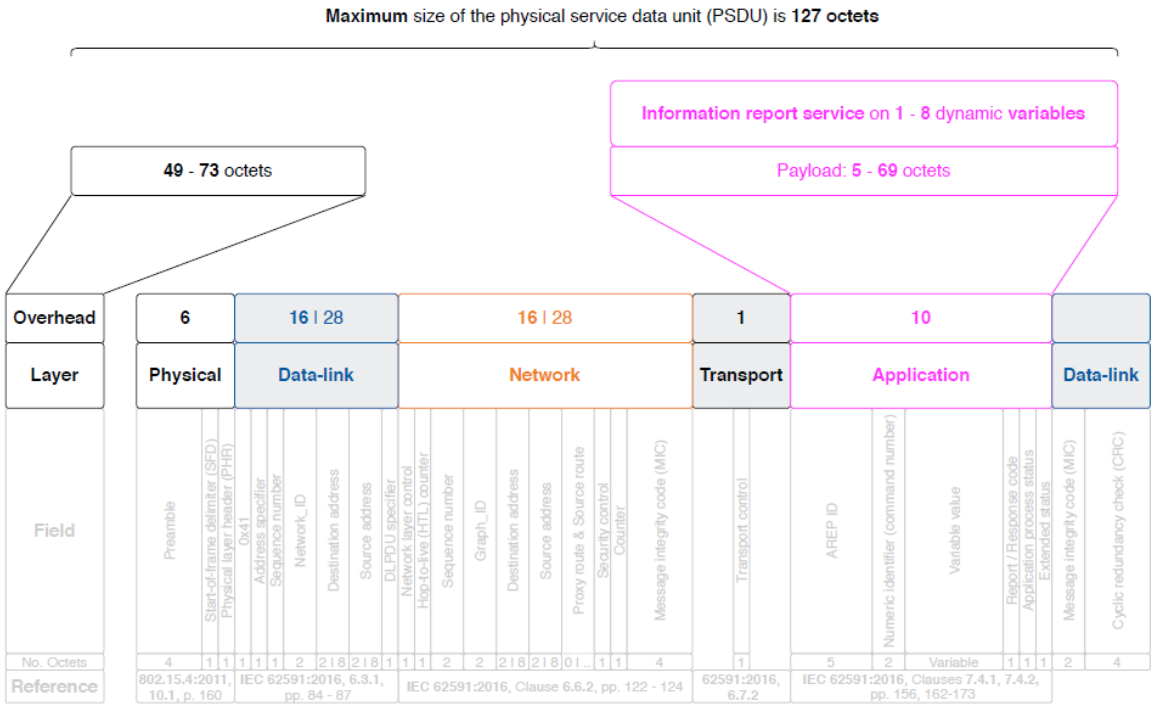


Figure B.4: WirelessHART Protocol Data Unite (PDU).

Table B.3: The physical layer specifications of WirelessHART [9, p. (370-373)], [14, p. 151].

| Physical Layer Specification | Value |
|---|---|
| Operating frequency | 2 450 MHz band |
| Assigned channels | 15 (from 11 to 25) |
| Transmit power | 10 dBm ±3 dB in equivalent isotropic radiated power (EIRP) |
| Output power control | Programmable from -10 dBm to +10 dBm EIRP within ±4 dBm error |
| Receiver sensitivity | -85 dB or better |
| CCA | Clear channel assessment (CCA) mode can be enabled / disabled |
| Data unit size constraint | Maximum size of the physical service data unit (PSDU) is 127 octets Octets |
| Modulation | Offset quadrature phase-shift keying (O-QPSK) |
| Symbols | 16-ary orthogonal |
| Symbol rate | 62.5 ksymbol/s |

terministic communications on dedicated links [9]. It uses carrier-sense multiple access (CSMA) protocol on shared links. The link transaction occurs during one time slot with transmitting of one Downlink Protocol Data Unit (DLPDU) followed by an ACK. Slot timing is defined in [54]. The slot period is 10ms which is the duration of the shortest standard super-frame in IEEE 802.15.4e low latency deterministic network (LLDN). It requires star topology, meaning that it has shortened frame control (1-octet MAC header), short time slots and ACK frames. It is worth saying that sampling with periods as short as 10ms is suitable for factory automation.

# ISA-100.11a

ISA-100.11a is the major competitor of WirelessHART and it shares many similar features with WirelessHART, [61]. This standard was developed by the International Society of Automation (ISA) [124]. It provides reliable and secure wireless operation for different control applications whether they are open loop or closed loop. It could be used also for non-critical monitoring, alerting, supervisory control, open loop control, and closed loop control applications [10].

ISA-100.11a network structure assimilates WirelessHART's structure to some extent. Figure B.5 depicts the communication areas addressed by this standard. As we can see from Figure B.5 the network consists of the following elements. The D subnet which is a collection of wirelessly connected field devices and some of them can work as routers, the backbone could be any other network which interface with the plant's network, a transit subnet which composed of infrastructure devices on a backbone like gateways, security managers, system managers and backbone routers. A field D-subnet with a backbone D-subnet are connected by a backbone router and a backbone subnet with a plant subnet are linked by gateway.

ISA-100.11a is IEC 62734 standard which performs different functions in five OSI layers as it is shown in Figure B.6.

The ISA-100.11a application layer protocol supports publishing of cyclic processed data. The supported values for the update period are 1/32ms increments up to 3600s. The publish service for this standard is a unicast service used to update data periodically/ aperiodically from a single publication source in a single access point (AP) to (at most) a single subscriber destination. Native communication in this standard supports both native protocol and encapsulation of legacy protocols via tunneling. Native published communi-

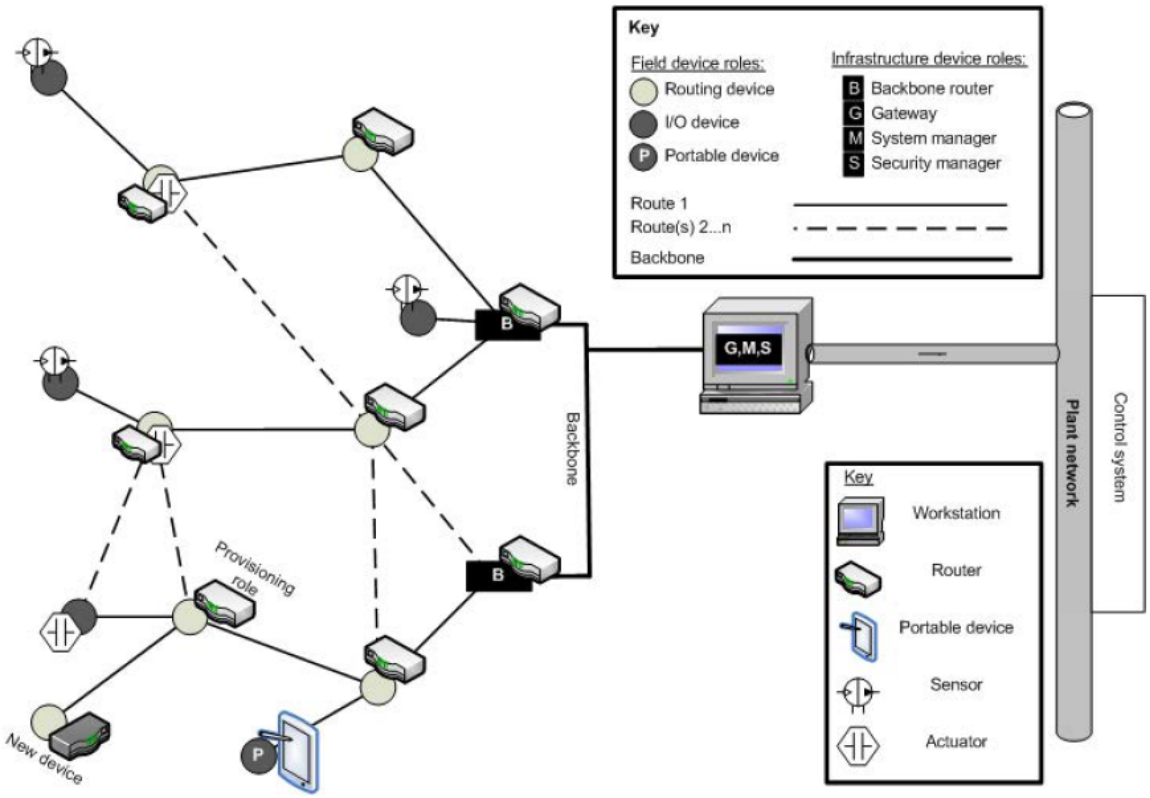


Figure B.5: ISA-100.11a architecture [10].

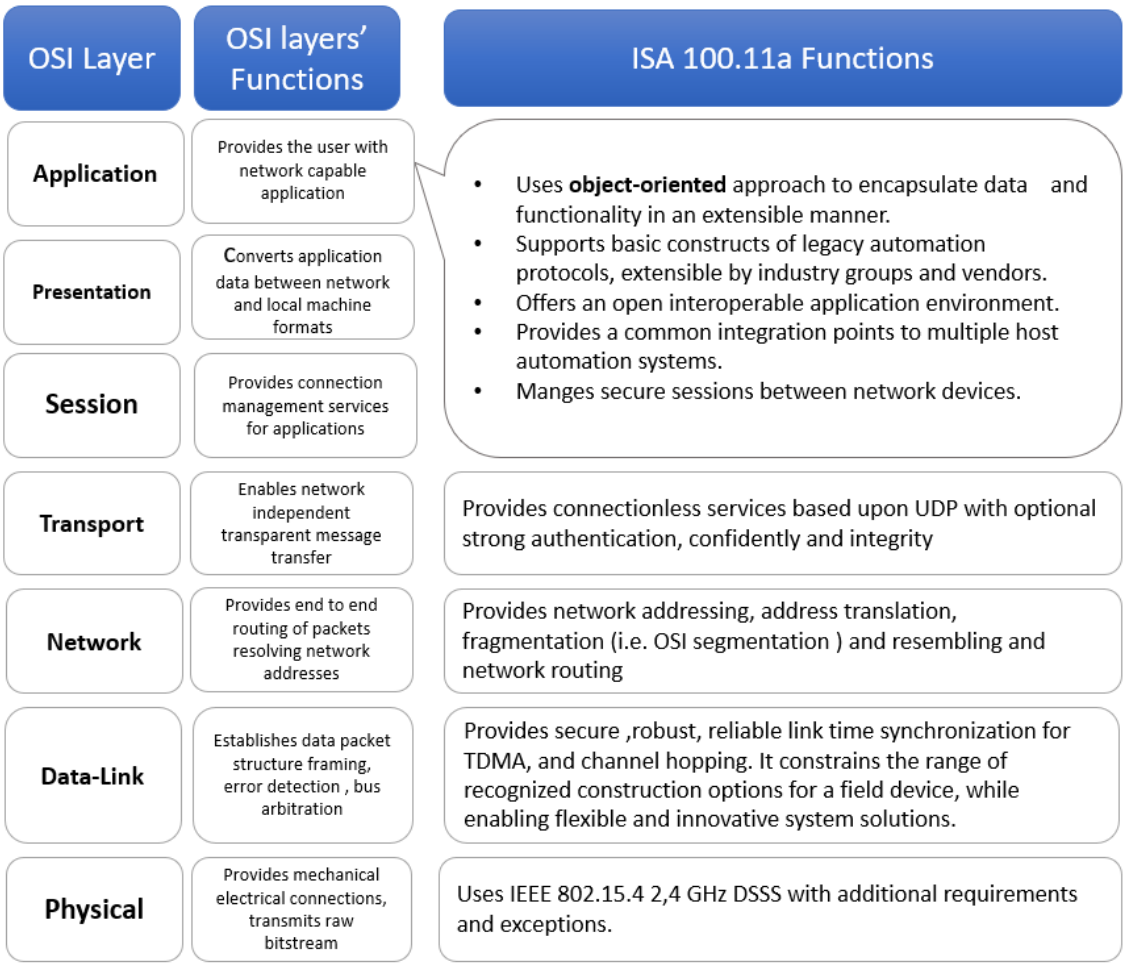


Figure B.6: ISA-100.11a architecture [10].

cation includes a freshness indicator to enable the subscriber to determine whether or not a value has changed [10]. The construct of the information to be conveyed via publication could be one of three constructs: native individual value, native sequence of values, non-native data which is an information being tunneled via a publication service. More in details, the single native value has the data structure as follows [10]

- Freshness value sequence number: it is present when the data structure information that indicates the structure of the data is a native individual value. it indicates the freshness of the data.
- Individual analog value and status: it is present if the native individual value is analog. It contains standard value status indicating the quality of the value and the analog value itself.
- Individual digital value and status: this parameter is present when the native individual value is digital. As the analog value and status this parameter contains standard status denoting to the quality of that digital value and the digital value itself.

The sequence of native values has the following structure [10]

- Publishing content version: it is present if the publication is for native sequence data. It guarantees the harmonious interpretation of published data by the subscriber.
- List of publish data: it represents the list of data conveyed via the publish service.
- Status and analog value.
- Status and digital value.

The last two parameters contain the same elements which the single native data contains. Finally, the non native data to publish is conveyed as a string of octets.

In order to support both native and non-native data, the application layer uses the object-oriented approach to encapsulate the data (attributes) and functionalities in a consistent manner. Moreover, objects are also defined to address the process industry needs [10]. The unified field object defined in this standard can be analog input object, analog output object, binary input object, or binary output object. The attributes of these objects are described in tables (287, 290, 293, 296) in [10] respectively. Figures B.7, B.8 show the object diagrams of the ISA-100.11a standard's analog and digital objects respectively and the coding rule for the native publish service.

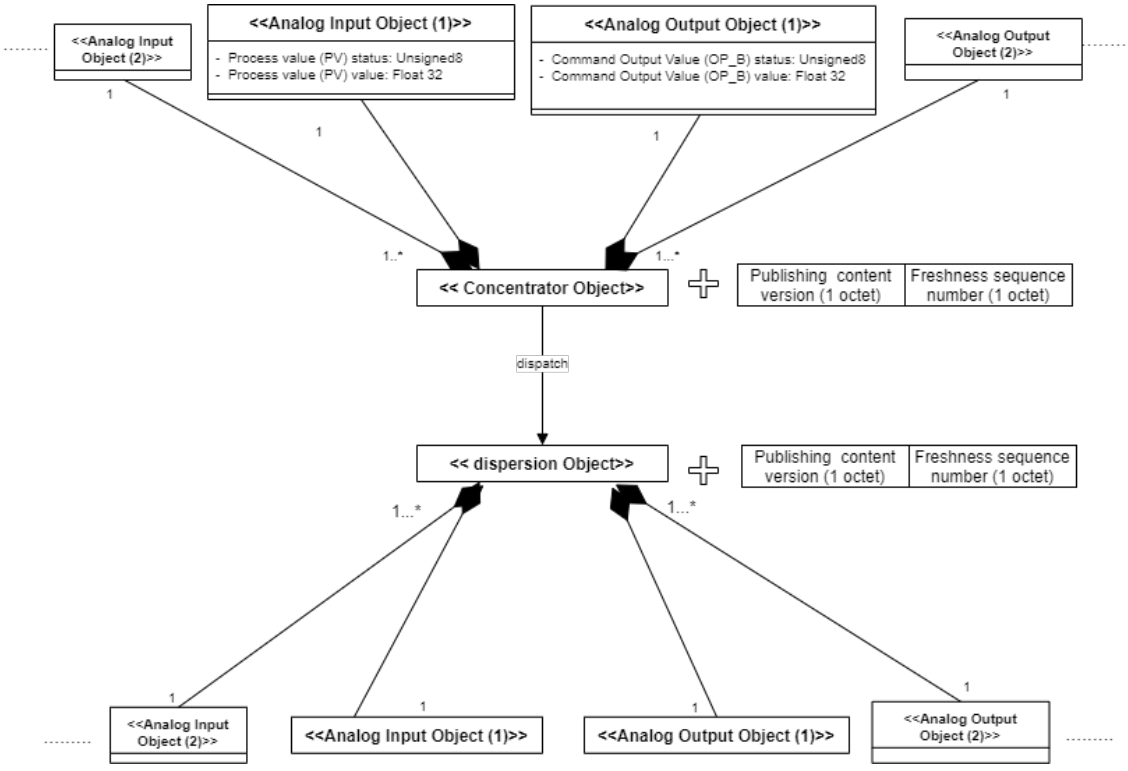


Figure B.7: Analog objects diagram.

Specifically, as we see in the figures, a collection of data from several objects in one User Application Process (UAP) is gathered in the concentrator object. The attributes of this object is illustrated in Table 256 in [10]. A UAP may have zero or more concentrator objects. After collecting the data from different objects in a particular concentrator object, the native publish service is coded according to the following coding rule. The data is added to 1 octet of the publishing content version which indicates the structure of the data and one octet of freshness sequence number which manifests if the data value has been changed or not. Therefore, according to the object diagram, the payload would be $(5 \cdot N) + 2$ octets for analog (input/output) objects and $(2 \cdot N) + 2$ octets for digital (input/output) objects where $N$ is the number of the objects collected in the concentrator object. At the receiver side, the attributes of the concentrator object is matched to the corresponding list of attributes of the dispersion object. This object specifies how to parse the published content of a concentrator object. Multiple dispersion user objects should be used if multiple disassemblies are needed [10].

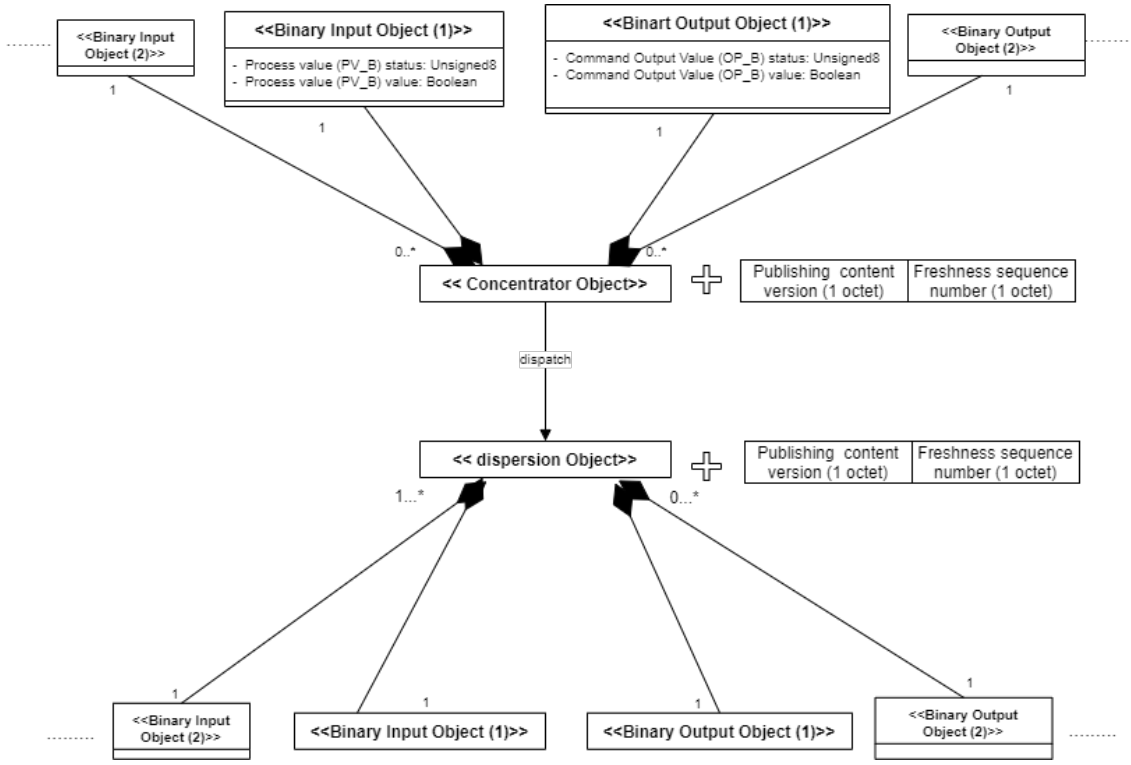


Figure B.8: Digital objects diagram.

Each layer of the standard add a certain number of octets to the header as it is shown in Table B.4. As we see from the Table B.4 the header can be uncompressed or compressed

Table B.4: Number of octets added by each layer of ISA 100.11a standard to the compressed and uncompressed header.

| Layer | Compressed header | Uncompressed header |
|---|---|---|
| Physical | 6 | 6 |
| Data Link | $17-34$ | $19-64$ |
| Network | 1\|2..6 | 40 |
| Transport | 5\|6 | 11\|12 |
| Application | 2\|3\|4 | 2\|3\|4 |

to get some advantages of compressing including reducing the packet loss and improved interactive response time. Thus, the header can be either $31-57$ octets in the case of compressed header or $78-127$ octets in the case of uncompressed header as it is shown in Figure B.9.

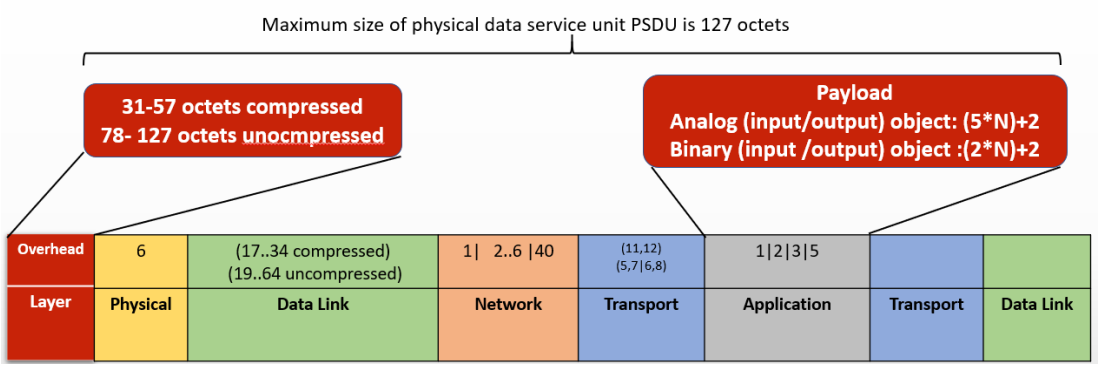


Figure B.9: Physical Service Data Unite (PSDU) structure of ISA-100.11a.

The physical layer characteristics are summarized in the Table B.5 Indeed, ISA-100.11a is based on the IEEE 802.15.4 physical layer and its MAC layer assumes TDMA communication but with a configurable slot size on a super frame base. Channel blacklisting and three options for channel hopping are also described. On the other hand, it does not provide for backward compatibility with other industrial standards, focusing instead on improving flexibility and adaptability.

Table B.5: The physical layer specifications of ISA-100.11a [10], [14, p. 151].

| Physical Layer Specification | Value |
|---|---|
| Operating frequency | 2 450 MHz band |
| Assigned channels | 15 (from 11 to 25) |
| Transmit power | It is determined according to the operation mode [10, p.861] |
| Output power control | It depends on the country code [10, p. 363] |
| Receiver sensitivity | -85 dB or better |
| CCA | Clear channel assessment (CCA) mode can be enabled / disabled |
| Data unit size constraint | Maximum size of the physical service data unit (PSDU) is 127 octets Octets |
| Modulation | DSSS QPSK Modulation |
| Symbols | 16-ary orthogonal |
| Symbol rate | 62.5 ksymbol/s |

# IEEE 802.15.4e

The standard IEEE 802.15.4 is for low rate, power, and cost Personal Area Networks (PANs) where PAN coordinator is responsible of managing the network. The PAN coordinator is also in charge of the communication between nodes. The standard defines two channel access models. The first one uses the duty cycle to manage the power and is called Beacon enabled mode as it is shown in Figure B.10.

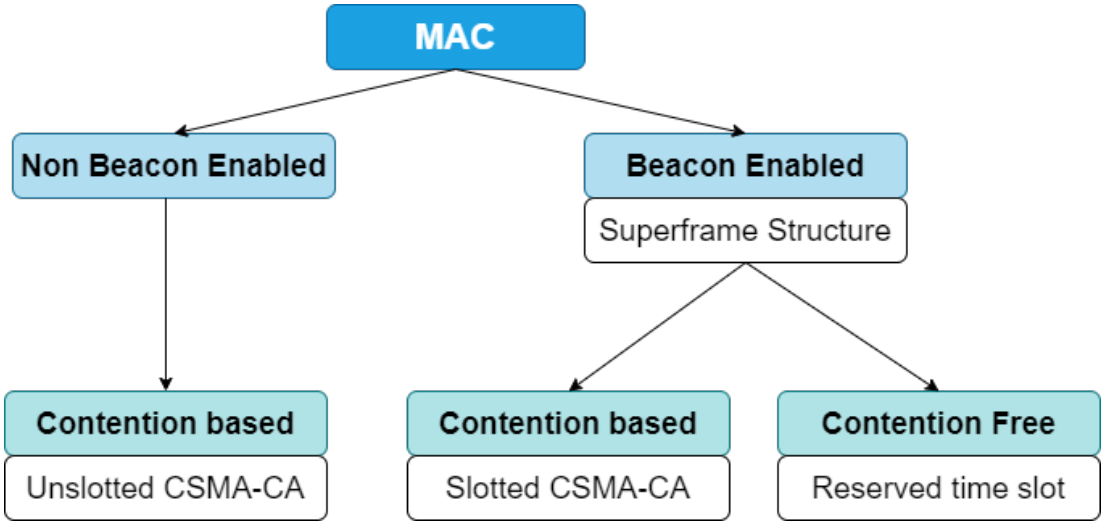


Figure B.10: Behavioral modes of IEEE 802.15.4 MAC layer [11].

It uses superframe structure bounded by beacons [125] as illustrated in Figure B.11. The superframe is divided into active period and inactive period. During the active period

the communication between nodes occur through the PAN coordinator they are associated with. Furthermore, the active period can be divided to Contention Access Period (CAP) and a Contention Free Period (CFP). CAP is the period where the channel access occurs by the slotted CSMA-CA algorithm and CFP is the period for the communication in TDMA mode using Guaranteed time slots (GTS) which are pre assigned to nodes [125]. On the other hand, non beacon enabled mode uses an unslotted CSMA-CA algorithm to access the channel and there is no superframe and nodes are always active.

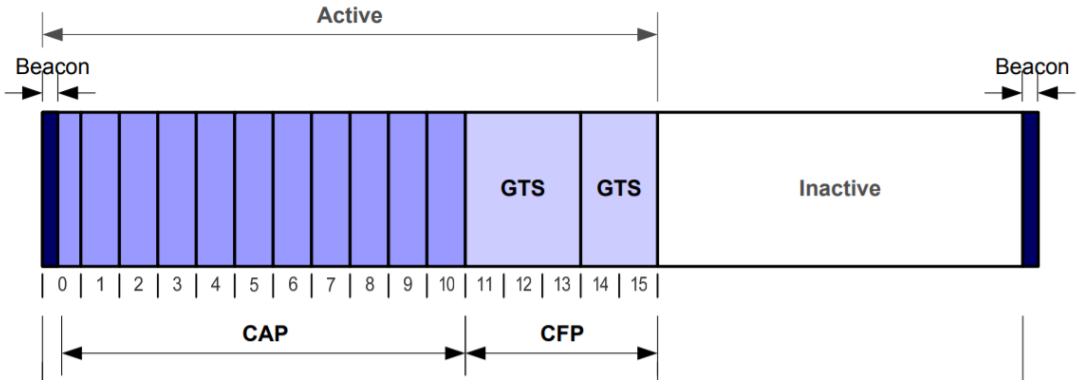


Figure B.11: Beacon enabled mode of IEEE 802.15.4 MAC layer [11].

IEEE 802.15.4 is not suitable for high reliable and low latency requirements because its MAC suffer from some limitations which are investigated in the literature. In particular, since MAC layer in both BE and NBE modes uses CSMA-CA thus on one hand, the maximum delay can not be bounded and as a result it can not be used for application where low latency and a certain delay is required. On the other hand, CSMA-CA does not guarantee high reception rate. Moreover, since IEEE 802.15.4 does not use the frequency hopping to mitigate the interference and fading like the case of WirelessHART, for example, the channel is more prone to these imperfections. Furthermore, using multihop topology in BE mode imposes complex beacon scheduling and synchronization mechanism requirement [15].

In order to overcome with these limitations an extension of this standard was developed in 2012 which is IEEE 802.15.4e. This new version overcomes the restrictions of the IEEE 802.15.4 MAC layer inserting some mechanisms including slotted access, multi-channel communication and frequency hopping [5]. In addition, it provides several functions improvements including mechanisms like offering low energy for energy efficient applications, exchanging information at the MAC layer, enhanced beacon for better resilience, flexible frame mechanism for several MAC operations, feedback on the channel quality mechanism

Table B.6: TSCH, DSME and LLDN's main features [15].

| | TSCH | DSME | LLDN |
|---|---|---|---|
| Beacons | Yes (Enhanced Beacons) | Yes (Enhanced Beacons) | Yes |
| Time Organization | Periodic Slotframe:<br>-Arbitrary number of timeslots<br>-Dedicated and shared timeslots | Periodic Multisuperframe:<br>- Rigid structure<br>- Recurring CAPs and CFPs | Periodic Superframe:<br>-3 transmission states<br>-management, uplink, bidirectional timeslots<br>-intended for short timeslots (< 1 ms) |
| Channel Access | Time Slotted (dedicated timeslots)<br>-TSCH CSMA-CA (shared timeslots) | Contention-based (during CAPs)<br>-Time Slotted (during CFPs) | Time Slotted (dedicated timeslots)<br>-LLDN CSMA-CA (shared timeslots) |
| Topologies | Star, tree, mesh | Star, tree, mesh | Only star |
| Multichannel mechanisms | Channel hopping | Channel hopping<br>Channel adaptation | No |
| Timeslot Scheduling Mechanism | Not specified | Distributed GTS Allocation | Centralized |
| Group ACKs | No | Yes | Yes |
| Network Synchronization | Frame/Ack-based Synchronization | On Enhanced Beacon Reception | On Beacon Reception |

and fast association mechanism for low latency applications [11]. It introduced several new behavior modes and Table B.6 [15] describes the main features of each of these modes.

Authors in [5] provided a description summary of these modes. More in detail, the advantages of frequency hopping for higher reliability against interference, time slotted access for boosting the throughput of traffic free links to send data, and multi channel for changing packets simultaneously between more nodes are combined in the medium access protocol which is called Time Slotted Channel Hopping (TSCH). it includes almost all the functionalities defined in the WirelessHART DLL [62]. On the other hand, Deterministic and Synchronous Multichannel Extension (DSME) is developed to support stringent timeliness and reliability requirements imposed by industrial automation. it increases the number of GTS slots and channels in the BE mode of IEEE 802.15.4 standard. it depends on a collection of IEEE 802.15.4 superframes called multi-superframe to access the channel. Since DSME uses the distributed beacon scheduling and slot allocation it does not suffer from single point of failure [5]. However, this is done at the expense of

high complexity. Low Latency Deterministic Network (LLDN) is designed for low latency industrial applications. Differently from TSCH and DSME it is designed only for star topology where 20 sensor nodes send data to a central sink every 10 ms. In order to be used for a very latency applications it provides some features to decease the transmissions and processing time. In particular, the MAC frame and header is designed shorter than in the ones of TSCH and DSME, it starts transmitting even before the beginning of the time slot and it uses a group Acknowledgment (Ack) feature.

In addition IEEE 802.15.4e provides a short identification of two more modes. First, Asynchronous multi-channel adaptation (AMCA) is suitable for applications applied on a large area where the communication between different nodes is not always guaranteed. AMCA relies on asynchronous multi-channel adaptation and can be used only in non Beacon-Enabled PANs [15]. Any sender device can change asynchronously its dedicated channel to the designated listening channel of the receiver device, in order to send the packets and can announce that by broadcasting a message to all other physical channels. Second, Radio Frequency Identification Blink (BLINK) which is used for announcing the ID of the node to other nodes in the network to indicate its existence.

# Bibliography


[1] A. Alrish, Y. Zacchia Lun, A. DInnocenzo, and F. Santucci, "Work in progress: Systematic derivation of accurate analytic markov channel models for industrial control," in *IEEE Int. Workshop Factory Commun. Syst. (WFCS)*, May 2019, pp. 1–4.

[2] Y. Zacchia Lun, A. Alrish, C. Rinaldi, A. DInnocenzo, and F. Santucci, "Accurate radio link modeling and its impact on wireless networked control systems design," 2021, the paper will be submitted soon to IEEE Transactions on Control Systems Technology.

[3] Y. Zacchia Lun, C. Rinaldi, A. Alrish, A. DInnocenzo, and F. Santucci, "On the impact of accurate radio link modeling on the performance of wirelesshart control networks," in *IEEE INFOCOM 2020 - IEEE Conference on Computer Communications*, 2020, pp. 2430–2439.

[4] BCG, "Embracing industry 4.0 and rediscovering growth," https://www.bcg.com/it-it/capabilities/operations/embracing-industry-4.0-rediscovering-growth, 2019.

[5] P. Park, S. C. Ergen, C. Fischione, C. Lu, and K. H. Johansson, "Wireless network design for control systems: A survey," *IEEE Commun. Surveys Tut.*, vol. 20, no. 2, pp. 978–1013, 2018.

[6] A. Goldsmith, *Wireless Communications*. Cambridge University Press, 2005.

[7] D. W. Matolak, "Air-ground channel characterization," https://www.icao.int/safety/FSMP/MeetingDocsFSMP/20WG-F33/Presentations/FSMP-WGF33-01_AGChanModeling_Submitted_28Aug2015.pdf, August 2015, accessed: 2021/03/17.

[8] *A comparison of Wirelesshart and Isa100.11a*, Emerson Process Management, Tech, Rep, 2012.

[9] BSI Standards Publication BS EN 62591:2016, *Industrial communication networks – Wireless communication network and communication profiles – WirelessHART™*, it is identical to IEC 62591:2016.

[10] "Industrial networks – wireless communication network and communication profiles – isa 100.11a," IEC - International Electrotechnical Commission, International Standard IEC 62734, 10 2014.

[11] D. W. Matolak, "Ieee 802.15.4e standard a building block for the internet of relevant things," http://info.iet.unipi.it/~anastasi/talks/2016-MST.pdf, May 2016, accessed: 2021/03/20.

[12] IEEE Std 802.15.4™-2006, *Standard for Information technology – Local and metropolitan area networks – Specific requirements – Part 15.4: Wireless MAC and PHY Specifications for Low-Rate WPANs.*

[13] BSI Standards Publication BS EN 61158-5-20-2014, *Industrial communication networks – Fieldbus specifications – Part 5-20: Application layer service definition Type 20 elements™*, it is identical to IEC 61158-5-20-2014.

[14] IEEE standard association, *IEEE Standard for Local and metropolitan area networks – Part 15.4: Low-Rate Wireless Personal Area Networks LR-WPANs™.*

[15] D. De Guglielmo, S. Brienza, and G. Anastasi, "Ieee 802.15.4e: A survey," *Computer Communications*, vol. 88, pp. 1 – 24, 2016. [Online]. Available: http://www.sciencedirect.com/science/article/pii/S0140366416301980

[16] W. P. M. H. Heemels and N. Van De Wouw, *Stability and stabilization of networked control systems.* Springer, London, 2010.

[17] C. Lu, A. Saifullah, B. Li, M. Sha, H. Gonzalez, D. Gunatilaka, C. Wu, L. Nie, and Y. Chen, "Real-time wireless sensor-actuator networks for industrial cyber-physical systems," *Proc. IEEE*, vol. 104, no. 5, pp. 1013–1024, May 2016.

[18] E. Gökalp, U. Şener, and P. E. Eren, "Development of an assessment model for industry 4.0: Industry 4.0-mm," in *Software Process Improvement and Capability*

*Determination*, A. Mas, A. Mesquida, R. V. O'Connor, T. Rout, and A. Dorling, Eds. Cham: Springer International Publishing, 2017, pp. 128–142.

[19] A. Martinelli, A. Mina, and M. Moggi, "The Enabling Technologies of Industry 4.0: Examining the Seeds of the Fourth Industrial Revolution," Laboratory of Economics and Management (LEM), Sant'Anna School of Advanced Studies, Pisa, Italy, LEM Papers Series 2019/09, Apr. 2019. [Online]. Available: https://ideas.repec.org/p/ssa/lemwps/2019-09.html

[20] A. Gilchrist, *Industry 4.0: The Industrial Internet of Things*, 1st ed. USA: Apress, 2016.

[21] Dataflair, "How IoT works – 4 main components of iot system," https://data-flair.training/blogs/how-iot-works/, 2018.

[22] Y. Lu, "Cyber physical system (cps)-based industry 4.0: A survey," *Journal of Industrial Integration and Management*, vol. 02, no. 03, p. 1750014, 2017. [Online]. Available: https://app.dimensions.ai/details/publication/pub.1092583322

[23] N. Boulila, "Cyber-physical systems and industry 4.0: Properties, structure, communication, and behavior," Siemens AG, Tech. Rep., apr 2019.

[24] H. Kagermann, W. Wahlster, and J. Helbig, "Recommendations for implementing the strategic initiative industrie 4.0 – securing the future of german manufacturing industry," acatech – National Academy of Science and Engineering, München, Final Report of the Industrie 4.0 Working Group, apr 2013. [Online]. Available: http://forschungsunion.de/pdf/industrie_4_0_final_report.pdf

[25] M. Wollschlaeger, T. Sauter, and J. Jasperneite, "The future of industrial communication: Automation networks in the era of the Internet of Things and Industry 4.0," *IEEE Ind. Electron. Mag.*, vol. 11, no. 1, pp. 17–27, 2017.

[26] Won-jong Kim, Kun Ji, and A. Ambike, "Networked real-time control strategies dealing with stochastic time delays and packet losses," in *Proceedings of the 2005, American Control Conference, 2005.*, 2005, pp. 621–626 vol. 1.

[27] A. Willig, K. Matheus, and A. Wolisz, "Wireless technology in industrial networks," *Proc. IEEE*, vol. 93, no. 6, pp. 1130–1151, 2005.

[28] A. Ahlén, J. Akerberg, M. Eriksson, A. J. Isaksson, T. Iwaki, K. H. Johansson, S. Knorn, T. Lindh, and H. Sandberg, "Toward wireless control in industrial process automation: A case study at a paper mill," *IEEE Control Syst. Mag.*, vol. 39, no. 5, pp. 36–57, 2019.

[29] A. Sikora and V. F. Groza, "Coexistence of IEEE 802.15.4 with other systems in the 2.4 GHz-ISM-Band," in *IEEE Instrum. Meas. Technol. Conf.*, vol. 3, May 2005, pp. 1786–1791.

[30] S. Zacharias, T. Newe, S. O'Keeffe, and E. Lewis, "A lightweight classification algorithm for external sources of interference in IEEE 802.15.4-based wireless sensor networks operating at the 2.4 GHz," *Int. J. Distrib. Sensor Netw.*, vol. 10, no. 9, pp. 1–24, 2014.

[31] J. P. Hespanha, P. Naghshtabrizi, and Y. Xu, "A survey of recent results in networked control systems," *Proc. IEEE*, vol. 95, no. 1, pp. 138–162, 2007.

[32] W. M. H. Heemels, A. R. Teel, N. van de Wouw, and D. Nesic, "Networked control systems with communication constraints: Tradeoffs between transmission intervals, delays and performance," *IEEE Trans. Autom. Control*, vol. 55, no. 8, pp. 1781–1796, 2010.

[33] L. Schenato, B. Sinopoli, M. Franceschetti, K. Poolla, and S. S. Sastry, "Foundations of control and estimation over lossy networks," *Proc. IEEE*, vol. 95, no. 1, pp. 163–187, 2007.

[34] V. Gupta, A. F. Dana, J. P. Hespanha, R. M. Murray, and B. Hassibi, "Data transmission over networks for estimation and control," *IEEE Trans. Autom. Control*, vol. 54, no. 8, pp. 1807–1819, 2009.

[35] M. Pajic, S. Sundaram, G. J. Pappas, and R. Mangharam, "The wireless control network: a new approach for control over networks," *IEEE Trans. Autom. Control*, vol. 56, no. 10, pp. 2305–2318, 2011.

[36] R. Maben, S. Luca, P. Alexandre, and J. Mikael, "Networked estimation under contention-based medium access," *International journal of robust and nonlinear control*, vol. 20, no. 2, pp. 140–155, 2010.

[37] D. Felix, Z. Tingting, and G. Mikael, "End-to-end reliability-aware scheduling for wireless sensor networks," *IEEE Transactions on Industrial Informatics*, vol. 12, no. 2, pp. 758–767, 2016.

[38] P. Sadeghi, R. Kennedy, P. Rapajic, and R. Shams, "Finite-state Markov modeling of fading channels – a survey of principles and applications," *IEEE Signal Process. Mag.*, vol. 25, no. 5, pp. 57–80, 2008.

[39] A. P. Gonçalves, A. R. Fioravanti, and J. C. Geromel, "Markov jump linear systems and filtering through network transmitted measurements," *Signal Process.*, vol. 90, no. 10, pp. 2842–2850, 2010.

[40] I. Matei, N. C. Martins, and J. S. Baras, "Optimal linear quadratic regulator for Markovian jump linear systems, in the presence of one time-step delayed mode observations," *IFAC Proc.*, vol. 41, no. 2, pp. 8056–8061, 2008, 17th IFAC World Congr.

[41] Y. Zacchia Lun and A. D'Innocenzo, "Stabilizability of Markov jump linear systems modeling wireless networked control scenarios," in *IEEE Conf. Decision Control (CDC)*, 2019, pp. 5766–5772, also available on arXiv at https://arxiv.org/abs/1907.12403.

[42] A. Gonzalez-Ruiz, A. Ghaffarkhah, and Y. Mostofi, "Characterization and modeling of wireless channels for networked robotic and control systems - a comprehensive overview," in *2009 IEEE/RSJ International Conference on Intelligent Robots and Systems*, 2009, pp. 4849–4854.

[43] G. De Guglielmo, F. Restuccia, G. Anastasi, M. Conti, and S. K. Das, "Accurate and efficient modeling of 802.15.4 unslotted csma/ca through event chains computation," *IEEE Transactions on Mobile Computing*, vol. 15, no. 12, pp. 2954–2968, 2016.

[44] V. Díez, A. Arriola, I. Val, and M. Velez, "Reliability evaluation of point-to-point links based on ieee 802.15.4 physical layer for iwsan applications," *AEU - International Journal of Electronics and Communications*, vol. 113, p. 152967, 2020. [Online]. Available: https://www.sciencedirect.com/science/article/pii/S1434841119308866

[45] T. Olofsson, A. Ahlén, and M. Gidlund, "Modeling of the fading statistics of wireless

sensor network channels in industrial environments," *IEEE Transactions on Signal Processing*, vol. 64, no. 12, pp. 3021–3034, 2016.

[46] J. Nikonowicz, A. Mahmood, E. Sisinni, and M. Gidlund, "Noise power estimators in ism radio environments: Performance comparison and enhancement using a novel samples separation technique," *IEEE Transactions on Instrumentation and Measurement*, vol. 68, no. 1, pp. 105–115, 2019.

[47] F. Barac, M. Gidlund, and T. Zhang, "Clap: Chip-level augmentation of ieee 802.15.4 phy for error-intolerant wsn communication," in *2015 IEEE 81st Vehicular Technology Conference (VTC Spring)*, 2015, pp. 1–7.

[48] M. Wilhelm, V. Lenders, and J. B. Schmitt, "On the reception of concurrent transmissions in wireless sensor networks," *IEEE Transactions on Wireless Communications*, vol. 13, no. 12, pp. 6756–6767, 2014.

[49] M. Wilhelm, V. Lenders, and J. Schmitt, "An analytical model of packet collisions in ieee 802.15.4 wireless networks," TU Kaiserslautern, Kaiserslautern, Germany, Tech. Rep. WLS13, Aug. 2013. [Online]. Available: https://disco.cs.uni-kl.de/discofiles/publicationsfiles/WLS13.pdf

[50] C. Gezer, A. Zanella, and R. Verdone, "An analytical model for the performance analysis of concurrent transmission in ieee 802.15.4," *Sensors (Basel, Switzerland)*, vol. 14, no. 3, pp. 5622–5643, March 2014. [Online]. Available: https://europepmc.org/articles/PMC4004011

[51] U. Pešović and P. Planinšič, "Error probability model for ieee 802.15.4 wireless communications in the presence of co-channel interference," *Physical Communication*, vol. 25, pp. 43–53, 2017. [Online]. Available: https://www.sciencedirect.com/science/article/pii/S1874490717300927

[52] U. Pešović, "Error probability model for ieee 802.15.4 wireless transmission with co-channel interference and background noise," Ph.D. dissertation, University of Maribor, sep 2016.

[53] D. Chen, M. Nixon, and A. Mok, *WirelessHART™*. Springer, 2010.

[54] "Ieee standard for local and metropolitan area networks–part 15.4: Low-rate wireless personal area networks (lr-wpans) amendment 1: Mac sublayer," *IEEE Std 802.15.4e-2012 (Amendment to IEEE Std 802.15.4-2011)*, pp. 1–225, 2012.

[55] "Ieee standard for information technology–telecommunications and information exchange between systems - local and metropolitan area networks–specific requirements - part 11: Wireless lan medium access control (mac) and physical layer (phy) specifications amendment 2: Sub 1 ghz license exempt operation," *IEEE Std 802.11ah-2016 (Amendment to IEEE Std 802.11-2016, as amended by IEEE Std 802.11ai-2016)*, pp. 1–594, 2017.

[56] *3GPP low power wide area technologies*, GSMA, London, UK, Rep, 2016.

[57] M. Condoluci, G. Araniti, T. Mahmoodi, and M. Dohler, "Enabling the iot machine age with 5g: Machine-type multicast services for innovative real-time applications," *IEEE Access*, vol. 4, pp. 5555–5569, 2016.

[58] *The cellular network operator enabling the INternet of Things*, Sigfox, Labége, France, Rep, 2015.

[59] "Lorawan specification. v1. 1," https://lora-alliance.org/sites/default/files/2018-04/lorawantm_specification_-v1.1.pdf, 2017, accessed: 02/07/2020.

[60] D. Chen, *WirelessHART : real-time mesh network for industrial automation.* New York London: Springer, 2010.

[61] S. Petersen and S. Carlsen, "Wirelesshart versus isa100.11a: The format war hits the factory floor," *IEEE Ind. Electron. Mag.*, vol. 5, no. 4, pp. 23–34, Dec. 2011.

[62] D. Chen, M. Nixon, S. Han, A. K. Mok, and X. Zhu, "Wirelesshart and ieee 802.15.4e," in *2014 IEEE International Conference on Industrial Technology (ICIT)*, 2014, pp. 760–765.

[63] B. Victor, A. M. Shahwaiz, L. Elena, and G. Eduard, "Ieee 802.11ah: A technology to face the iot challenge." *Sensors (Basel, Switzerland)*, vol. 16, no. 11, 2016.

[64] L. Alliance, "A technical overview of lora and lorawan," Tech. Rep., 2015, white Paper.

[65] L. Vinicius, E. Mark, G. Konstantinos, and R. Alejandro, "Model-free design of control systems over wireless fading channels," sep 2020, IEEE TRANSACTIONS ON SIGNAL PROCESSING (SUBMITTED).

[66] B. Demirel, A. Ramaswamy, D. E. Quevedo, and H. Karl, "Deepcas: A deep reinforcement learning algorithm for control-aware scheduling," *IEEE Control Systems Letters*, vol. 2, no. 4, pp. 737–742, 2018.

[67] A. S. Leong, A. Ramaswamy, D. E. Quevedo, H. Karl, and L. Shi, "Deep reinforcement learning for wireless sensor scheduling in cyber physical systems," *Automatica*, vol. 113, p. 108759, 2020. [Online]. Available: https://www.sciencedirect.com/science/article/pii/S0005109819306223

[68] D. Baumann, J.-J. Zhu, G. Martius, and S. Trimpe, "Deep reinforcement learning for event-triggered control," in *In Proceedings of the 57th IEEE International Conference on Decision and Control (CDC)*, December 2018, pp. 943–950.

[69] A. Redder, A. Ramaswamy, and D. E. Quevedo, "Deep reinforcement learning for scheduling in large-scale networked control systems," *IFAC-PapersOnLine*, vol. 52, no. 20, pp. 333–338, 2019, 8th IFAC Workshop on Distributed Estimation and Control in Networked Systems NECSYS 2019. [Online]. Available: https://www.sciencedirect.com/science/article/pii/S2405896319320300

[70] M. Eisen, M. M. Rashid, D. Cavalcanti, and A. Ribeiro, "Control-aware scheduling for low latency wireless systems with deep learning," 2019.

[71] M. Eisen, C. Zhang, L. F. O. Chamon, D. D. Lee, and A. Ribeiro, "Learning optimal resource allocations in wireless systems," *IEEE Transactions on Signal Processing*, vol. 67, no. 10, pp. 2775–2790, May 2019. [Online]. Available: http://dx.doi.org/10.1109/TSP.2019.2908906

[72] F. Liang, C. Shen, W. Yu, and F. Wu, "Towards optimal power control via ensembling deep neural networks," 2019.

[73] S. Petersen and S. Carlsen, "Wirelesshart versus isa100.11a: The format war hits the factory floor," *IEEE Industrial Electronics Magazine*, vol. 5, no. 4, pp. 23–34, 2011.

[74] M. S. Miah, M. Rahman, T. K. Godder, B. Singh, and M. Parvin, "Performance comparison of awgn , flat fading and frequency selective fading channel for wireless communication system using 4 qpsk," 2011.

[75] K. Manju, Y. Tilotma, Y. Pooja, s. P. K, and S. Dinesh, "Comparative study of path loss models in different environments," *International Journal of Engineering Science and Technology (IJEST)*, vol. 3, no. 4, apr 2011.

[76] "Ieee standard definitions of terms for antennas," *IEEE Std 145-1993*, pp. 1–32, 1993.

[77] T. Rappaport, *Wireless communications – Principles and practice, 2nd Edition.* Prentice Hall, 2001.

[78] M. C. Jeruchim, P. Balaban, and K. S. Shanmugan, *Simulation of Communication Systems: Modeling, Methodology and Techniques*, 2nd ed. USA: Kluwer Academic Publishers, 2000.

[79] T. Rappaport, *Wireless communications: Principles and practice*, 2nd ed., ser. Prentice Hall communications engineering and emerging technologies series. Prentice Hall, 2002, includes bibliographical references and index.

[80] A. Goldsmith, *Wireless Communications.* CUP, 2005.

[81] N. Jaldén, P. Zetterberg, B. Ottersten, A. Hong, and R. Thoma, "Correlation properties of large scale fading based on indoor measurements," in *IEEE Wireless Commun. Netw. Conf. (WCNC)*, 2007, pp. 1894–1899.

[82] A. Seetharam, J. Kurose, D. Goeckel, and G. Bhanage, "A Markov chain model for coarse timescale channel variation in an 802.16e wireless network," in *IEEE Conf. Comput. Commun. (INFOCOM)*, 2012, pp. 1800–1807.

[83] J. Salo, L. Vuokko, H. M. El-Sallabi, and P. Vainikainen, "An additive model as a physical basis for shadow fading," *IEEE Transactions on Vehicular Technology*, vol. 56, no. 1, pp. 13–26, 2007.

[84] F. Graziosi, L. Fuciarelli, and F. Santucci, "Second order statistics of the SIR for cellular mobile networks in the presence of correlated co-channel interferers," in *IEEE Veh. Technol. Conf. (VTC)*, vol. 4, 2001, pp. 2499–2503.

[85] A. Abdi and M. Kaveh, "A comparative study of two shadow fading models in ultrawideband and other wireless systems," *IEEE Transactions on Wireless Communications*, vol. 10, no. 5, pp. 1428–1434, 2011.

[86] D. Pimienta-del Valle, L. Mendo, J. M. Riera, and P. Garcia-del Pino, "Indoor los propagation measurements and modeling at 26, 32, and 39 ghz millimeter-wave frequency bands," *Electronics*, vol. 9, no. 11, 2020. [Online]. Available: https://www.mdpi.com/2079-9292/9/11/1867

[87] S. Sun, T. A. Thomas, T. S. Rappaport, H. Nguyen, I. Z. Kovacs, and I. Rodriguez, "Path loss, shadow fading, and line-of-sight probability models for 5g urban macro-cellular scenarios," in *2015 IEEE Globecom Workshops (GC Wkshps)*, 2015, pp. 1–7.

[88] S. Yoo, S. Cotton, P. Sofotasios, and S. Freear, "Shadowed fading in indoor off-body communication channels: A statistical characterization using the $\kappa$ $\mu$ $\gamma$ composite fading model," *IEEE Transactions on Wireless Communications*, vol. 15, no. 8, pp. 5231 – 5244, aug 2016, this work is licensed under a Creative Commons Attribution 3.0 License. For more information, see http://creativecommons.org/licenses/by/3.0/.

[89] K. Zhang, B. Li, X. Tang, D. Wang, and L. Wei, "Path loss measurement and modeling for industrial environment," in *2019 IEEE 20th International Conference on High Performance Switching and Routing (HPSR)*, 2019, pp. 1–5.

[90] E. Tanghe, W. Joseph, L. Verloock, L. Martens, H. Capoen, K. V. Herwegen, and W. Vantomme, "The industrial indoor channel: large-scale and temporal fading at 900, 2400, and 5200 mhz," *IEEE Transactions on Wireless Communications*, vol. 7, no. 7, pp. 2740–2751, 2008.

[91] B. Sklar, "Rayleigh fading channels in mobile digital communication systems .i. characterization," *IEEE Communications Magazine*, vol. 35, no. 7, pp. 90–100, 1997.

[92] F. Barac, M. Gidlund, and T. Zhang, "Scrutinizing bit-and symbol-errors of IEEE 802.15.4 communication in industrial environments," *IEEE Trans. Instrum. Meas.*, vol. 63, no. 7, pp. 1783–1794, 2014.

[93] I. S. of Automation, *Wireless Systems for Industrial Automation: Process Control and Related Applications : ISA-100.11a-2009.* ISA, 2009. [Online]. Available: https://books.google.it/books?id=2UTljgEACAAJ

[94] A. Sikora and V. F. Groza, "Coexistence of ieee802.15.4 with other systems in the 2.4

ghz-ism-band," in *2005 IEEE Instrumentationand Measurement Technology Conference Proceedings*, vol. 3, 2005, pp. 1786–1791.

[95] N. Laboratories, "Co-existence of ieee 802.15.4 at 2.4 ghz application note," NXP Laboratories, Sheffield, UK, Tech. Rep., 2013.

[96] S. Shin, H. Park, and W. Kwon, "Packet error rate analysis of ieee 802.15.4 under saturated ieee 802.11b network interference," *IEICE Trans. Commun.*, vol. 90-B, pp. 2961–2963, 2007.

[97] S. Y. Shin, H. S. Park, S. Choi, and W. H. Kwon, "Packet error rate analysis of zigbee under wlan and bluetooth interferences," *IEEE Transactions on Wireless Communications*, vol. 6, no. 8, pp. 2825–2830, 2007.

[98] K. Yu, F. Barac, M. Gidlund, J. øAkerberg, and M. Björkman, "A flexible error correction scheme for ieee 802.15.4-based industrial wireless sensor networks," in *2012 IEEE International Symposium on Industrial Electronics*, May 2012, pp. 1172–1177.

[99] T. Vayssade, F. Azaïs, L. Latorre, and F. Lefévre, "Low-cost digital test solution for symbol error detection of rf zigbee transmitters," *IEEE Transactions on Device and Materials Reliability*, vol. 19, no. 1, pp. 16–24, 2019.

[100] Proakis, *Digital Communications 5th Edition.* McGraw Hill, 2007.

[101] F. Barac, M. Gidlund, and T. Zhang, "Scrutinizing bit- and symbol-errors of ieee 802.15.4 communication in industrial environments," *IEEE Transactions on Instrumentation and Measurement*, vol. 63, no. 7, pp. 1783–1794, 2014.

[102] F. Graziosi, L. Fuciarelli, and E. Santucci, "Second order statistics of the sir for cellular mobile networks in the presence of correlated co-channel interferers," in *IEEE VTS 53rd Vehicular Technology Conference, Spring 2001. Proceedings (Cat. No.01CH37202)*, vol. 4, 2001, pp. 2499–2503 vol.4.

[103] F. Santucci and F. Graziosi, "Power allocation in a multimedia CDMA wireless system with imperfect power control," in *IEEE Int. Conf. Commun. (ICC)*, vol. 3, 1999, pp. 1668–1672.

[104] D. Shengchen, Q. Hua, K. Kai, and X. Weidong, "A robust demodulator for OQPSK – DSSS system," *Circuits, Systems, and Signal Processing*, jan 2015.

[105] M. A. Zubair, A. K. Nain, J. Bandaru, P. Rajalakshmi, and U. B. Desai, "Reconfigurable dual mode ieee 802.15.4 digital baseband receiver for diverse iot applications," in *2016 IEEE 3rd World Forum on Internet of Things (WF-IoT)*, 2016, pp. 389–394.

[106] F. Santucci, G. Durastante, F. Graziosi, and C. Fischione, "Power allocation and control in multimedia CDMA wireless systems," *Telecommun. Syst.*, vol. 23, no. 1–2, pp. 69–94, 2003.

[107] R. Elsas, J. Hoebeke, D. Van Leemput, A. Shahid, G. Daneels, J. Famaey, and E. De Poorter, "Intra-network interference robustness : an empirical evaluation of ieee 802.15.4-2015 sun-ofdm," *ELECTRONICS*, vol. 9, no. 10, p. 21, 2020. [Online]. Available: http://dx.doi.org/10.3390/electronics9101691

[108] F. Ferrari, M. Zimmerling, L. Thiele, and O. Saukh, "Efficient network flooding and time synchronization with glossy," in *Proceedings of the 10th ACM/IEEE International Conference on Information Processing in Sensor Networks*, 2011, pp. 73–84.

[109] Y. Wang, Y. Liu, Y. He, X. Li, and D. Cheng, "Disco: Improving packet delivery via deliberate synchronized constructive interference," *IEEE Transactions on Parallel and Distributed Systems*, vol. 26, no. 3, pp. 713–723, 2015.

[110] C. Fischione, F. Graziosi, and F. Santucci, "Approximation for a sum of On-Off log-normal processes with wireless applications," *IEEE Trans. Commun.*, vol. 55, no. 9, pp. 1822–1822, Sept. 2007.

[111] M. Di Renzo, F. Graziosi, and F. Santucci, "Approximating the linear combination of log-normal rvs via pearson type iv distribution for uwb performance analysis," *IEEE Transactions on Communications*, vol. 57, no. 2, pp. 388–403, 2009.

[112] A. Genz and F. Bretz, *Computation of multivariate normal and t probabilities*, ser. Lecture Notes Statist. Springer, 2009, vol. IE.

[113] Z. I. Botev, "The normal law under linear restrictions: simulation and estimation via minimax tilting," *J. Roy. Statistical Soc.: Series B (Statistical Methodology)*, vol. 79, no. 1, pp. 125–148, 2017.

[114] G. L. Stüber, *Principles of mobile communication.* Springer, 2017.

[115] J. G. Ruiz, B. Soret, M. C. Aguayo-Torres, and J. T. Entrambasaguas, "On finite state Markov chains for Rayleigh channel modeling," in *Wireless Commun., Veh. Technol., Inf. Theory Aerosp. Electron. Syst. Technol. (Wireless VITAE)*, 2009, pp. 191–195.

[116] G. Rubino and B. Sericola, "Sojourn times in finite Markov processes," *J. Appl. Probability*, vol. 26, no. 4, pp. 744–756, 1989.

[117] G. F. Franklin, J. D. Powell, and A. Emami-Naeini, *Feedback control of dynamic systems*, 6th ed. Prentice Hall, 2009.

[118] O. L. V. Costa, M. D. Fragoso, and R. P. Marques, *Discrete-time Markov jump linear systems*. Springer, 2005.

[119] HART Communication Foundation document number HCF_SPEC-065, *2.4 GHz DSSS O-QPSK Physical Layer Specification*, Sept. 2007.

[120] S. Yao and E. Geraniotis, "Optimal power control law for multimedia multirate CDMA systems," in *IEEE Veh. Technol. Conf. (VTC)*, vol. 1. IEEE, 1996, pp. 392–396.

[121] A. Goldsmith, *Wireless Communications*. USA: Cambridge University Press, 2005.

[122] "Ieee standard for local and metropolitan area networks–part 15.4: Low-rate wireless personal area networks (lr-wpans)," *IEEE Std 802.15.4-2011 (Revision of IEEE Std 802.15.4-2006)*, pp. 1–314, Sep. 2011.

[123] D. Christin, P. S. Mogre, and M. Hollick, "Survey on wireless sensor network technologies for industrial automation: The security and quality of service perspectives." *Future Internet*, no. 2, pp. 96–125, 2010.

[124] International society of Automation ISA. [Online]. Available: http://www.isa.org/

[125] D. De Guglielmo, G. Anastasi, and A. Seghetti, *From IEEE 802.15.4 to IEEE 802.15.4e: A Step Towards the Internet of Things*. Cham: Springer International Publishing, 2014, pp. 135–152. [Online]. Available: https://doi.org/10.1007/978-3-319-03992-3_10